

KOMUNIKÁCIE

C O M M U N I C A T I O N S

SCIENTIFIC LETTERS OF THE UNIVERSITY OF ŽILINA

Volume 27

JOURNAL FOR SCIENCES IN TRANSPORT



UNIVERSITY
OF ŽILINA



4/2025



UNIVERSITY OF ŽILINA
EDIS-Publishing House
UNIZA

EDIS-Publishing House of the University of Žilina (UZ) is one of the University of Žilina's constituents. The beginning of its existence dates back to 1990. In the course of its work, the publishing house has published more than 5 000 titles of book publications, especially university textbooks, scientific monographs, scripts, prose, but also enriched the book market with titles of regional, children's and popular literature.

Students and professional public have the opportunity to purchase published titles in the „Selling Study Literature“ directly on the premises of the University of Žilina, in the EDIS shop or upon order on a „cash on delivery“ basis. All published titles are available at: www.edis.uniza.sk.



EDIS-Publishing House of the University of Žilina offers book titles in English

Lenka Černá, Jozef Daniš

**APPLICATION OF COST CALCULATIONS
IN THE TARIFF POLICY FORMATION
IN RAILWAY TRANSPORT**

ISBN 978-80-554-1391-4 Price 7.61 €

Eva Nedeliaková, Jana Sekulová

**EVALUATION OF QUALITY
IN RAILWAY TRANSPORT**

ISBN 978-554-1272-6 Price 8.00 €

Martin Bugaj

AEROMECHANICS 1

ISBN 978-80-554-1675-5 Price 14.50 €

Anna Tomová

**ECONOMICS OF AIR NAVIGATION
SERVICES**

ISBN 978-80-554-0905-4 Price 14.30 €

Marica Mazurek

**MODELS OF BRANDING AND THEIR
APPLICATION**

ISBN 978-80-554-1705-9 Price 9.00 €

Jozef Melcer

DYNAMICS OF STRUCTURES

ISBN 978-80-554-1698-4 Price 19.00 €

Jozef Gašparík et al.

RAILWAY TRAFFIC OPERATION

ISBN 978-80-554-1281-8 Price 15.80 €

Tetiana Hovorushchenko et.al.

**CD - INTELLIGENT INFORMATION-
ANALYTICAL TECHNOLOGIES...**

ISBN 978-80-554-1729-5 Price 3.50 €

*Karol Matiaško, Michal Kvet,
Marek Kvet*

**CD - PRACTICES FOR DATABASE
SYSTEMS**

ISBN 978-80-554-1397-6 Price 2.20 €

*Michal Kvet, Karol Matiaško,
Štefan Toth*

**USB - PRACTICAL SQL FOR ORACLE
CLOUD**

ISBN 978-80-554-1880-3 Price: 11,30 €

Veronika Valašková,

Daniela Kucharová

USB - STATICS OF STRUCTURES 3

ISBN 978-80-554-1826-1 Price: 8,90 €

Michal Kvet, Karol Matiaško, Marek Kvet

**USB - BECOME EXPERT IN MYSQL
PRACTICES FOR DATABASE SYSTEMS
IN MYSQL**

ISBN 978-80-554-1786-8 Price 13.50 €

*Michal Kvet, Alenka Baggia,
Monika Borkovcová, Diana Mudrinič,
Frane Urem*

E-book - Environmental Data Analysis

ISBN 978-80-554-2145-2 Price 0,00 €

Michal Kvet

E-book – Become master in SQL

ISBN 978-80-554-2132-2 Price 0,00 €

EDIS-Publishing House UNIZA

Univerzitná 8215/1,
010 26 Žilina,
Slovakia

e-mail: edis_objednavky@uniza.sk, edis@uniza.sk
www.edis.uniza.sk

A - OPERATION AND ECONOMICS IN TRANSPORT

- CARPOOLING IN TRANSPORT IN TODAY'S ICT - BASED ECONOMY** **A48**
P. Wiączek, I. Sitak, A. Novák Sedláčková, A. Novák, M. Bugaj

B - MECHANICAL ENGINEERING IN TRANSPORT

- METHODOLOGY FOR ASSESSING THE KEY OPERATIONAL EFFICIENCY INDICATORS FOR REMOVAL AND SHUNTING OPERATIONS OF SHUNTING LOCOMOTIVES** **B250**
G. Bakyt, A. Makhanova, M. Mussabekov, G. Ashirbayev, M. Zhamankulov, K. Sarsenov, A. Mussabekova

- ALGORITHM FOR MAKING THE OPTIMAL DECISION FOR FURTHER OPERATION OF FREIGHT CARS** **B261**
A. Kadyrov, P. Baigozhina, A. Kukesheva, I. Marat, A. Karsakova

C - ELECTRICAL ENGINEERING IN TRANSPORT

- EVALUATION OF SILICONE CARBIDE MOSFET DRIVING CIRCUIT PERFORMANCE** **C53**
V. Švárna, M. Frivaldský

- DETECTION OF SELECTED REGULATORY TRAFFIC SIGNS USING COMMON DASHBOARD CAMERA** **C61**
D. Koniar, L. Hargaš, M. Danko

- MODELLING OF DYNAMIC STATES OF FIVE-PHASE INDUCTION MOTOR** **C70**
P. Záskalický, D. Perduková, J. Kaňuch

D - CIVIL ENGINEERING IN TRANSPORT

- MODELLING THE EQUIVALENCY FACTOR OF E-RICKSHAW UNDER HETEROGENEOUS TRAFFIC CONDITIONS** **D102**
A. A. Khan, S. Dass

E - MANAGEMENT SCIENCE AND INFORMATICS IN TRANSPORT

- GEOLOCATION OF DEVICES IN LOW-POWER WIDE-AREA LORA NETWORK** **E46**
L. Zemko, D. Hroš, A. Valach, M. Galinski, P. Čičák



This is an open access article distributed under the terms of the Creative Commons Attribution 4.0 International License (CC BY 4.0), which permits use, distribution, and reproduction in any medium, provided the original publication is properly cited. No use, distribution or reproduction is permitted which does not comply with these terms.

CARPOOLING IN TRANSPORT IN TODAY'S ICT - BASED ECONOMY

Paulina Wiączek¹, Iryna Sitak², Alena Novák Sedláčková³, Andrej Novák^{3,*}, Martin Bugaj³

¹Department of Economics and Finance, Faculty of Law and Social Sciences, Jan Kochanowski University of Kielce, Kielce, Poland

²Department of Management, Institute of Economics, Management and International Business, National Technical University "Kharkiv Polytechnic Institute", Kharkiv, Ukraine

³Faculty of Operation and Economics of Transport and Communications, University of Zilina, Zilina, Slovakia

*E-mail of corresponding author: andrej.novak@fpedas.uniza.sk

Paulina Wiączek 0000-0002-3630-5020,
Alena Novak Sedlackova 0000-0003-3719-2555,
Martin Bugaj 0000-0001-7205-855X

Iryna Sitak 0000-0002-1146-5730,
Andrej Novak 0000-0001-9567-5104,

Resume

The purpose of this research was, among other things, to show that the carpooling model can be regarded as a manifestation of collective intelligence and a response to the crisis of sustainability in today's ICT-based economy, which makes carpooling services a cheaper alternative to transportation services provided by other modes of transport: train and bus. The main research problem is contained in the question: How do collective intelligence and the tenets of sustainability influence the popularity of carpooling and the lower cost of carpooling services, compared to those provided by other forms of transportation? The critical literature analysis method, the comparison method and the statistical method, among others: the Mann Whitney U test and the Kruskal Wallis ANOVA test, were used in implementation of the study.

Article info

Received 11 March 2025

Accepted 22 July 2025

Online 30 September 2025

Keywords:

carpooling
collective intelligence
sustainability
technological innovation
travel model
transportation
transportation economics

Available online: <https://doi.org/10.26552/com.C.2025.052>

ISSN 1335-4205 (print version)

ISSN 2585-7878 (online version)

1 Introduction

In the context of the development of renewable energy in Poland, the integration of technology and infrastructure plays a crucial role in forming a sustainable energy system. Poland is actively developing various sectors of renewable energy, including wind, solar, bioenergy, hydropower, and geothermal energy. This is driven by both national ambitions to reduce the carbon emissions and commitments to the European Union. At the same time, the electrical engineering sector provides critical support for this transition by developing infrastructure for the generation, storage, and distribution of renewable energy. Special attention is given to the creation of smart grids, which allow the efficient integration of various sources of renewable energy into the national grid.

One important aspect of this transformation is the development of electric vehicles (EV) and the supporting infrastructure, which has significant potential to reduce

reliance on fossil fuels in the transportation sector. In this context, carpooling, or the shared use of cars, acquires new dimensions through the use of electric vehicles, which reduce the environmental footprint of travel. The electrical engineering sector facilitates this process by developing the charging stations, fast-charging technologies, and energy management systems that ensure efficient resource use.

Today, transportation is becoming easier and more accessible to everyone, among other things, through the implementation of innovations into economic and social life, as well as the ongoing evolution of technology, which can be seen in almost every area of human activity [1].

With the development and acceptance of the sharing economy, the popularity of mobile Internet technology, and the application of innovative technologies in many cities, online services and platforms have emerged to facilitate carpooling services. Online carpooling platforms can effectively match unfamiliar drivers and passengers in terms of both time and routes, enabling

the large-scale carpooling to develop [2]. Carpooling is thus an informal form of shared rides for example among commuters [3-4].

Carpooling with EVs is also supported by the development of platforms for finding fellow travellers and optimizing routes, which reduces overall energy consumption and enhances the efficiency of transportation systems. Poland, aiming to become a leader in renewable energy, actively attracts European funds and investments to implement projects that contribute to reducing the greenhouse gas emissions and enhancing energy security. Meanwhile, the government is implementing various policy measures, including subsidies and tax incentives, to stimulate investment in renewable energy and electric transport. The development of these areas creates a synergistic effect, where innovations in one sector support and strengthen others, ensuring the sustainable and environmentally responsible development of the country.

The purpose of this research was to define what the carpooling is and demonstrate that the carpooling model can be seen as a manifestation of collective intelligence and a response to the sustainability crisis in today's ICT-based economy. This makes carpooling services a cheaper alternative to transportation services provided by other means of transport: train and bus.

The main research problem was defined in the form of the following question: "How do collective intelligence and the assumptions of sustainable development influence the popularity of carpooling and the lower cost of carpooling transportation compared to transportation provided by other means of transport?"

The authors posed three problem questions, which supplement the main problem formulated above.

1. How does smart grid integration affect the functioning of carpooling?
2. What is the carpooling phenomenon and what are its possibilities for the development of transport services?
3. How does carpooling influence the development of the concept of sustainable development?

To achieve the main objective of the research and solve the problem posed, the authors used an analysis of the cost of travel by three means (forms) of transportation: via the BlaBlaCar service, by Intercity train and by available bus service from one voivodeship city, i.e. Wrocław, to the other 17 voivodeship cities in Poland in the period before the Covid-19 pandemic (2017-2018) and after the pandemic (2023 - March 2024).

In the implementation of the study, the method of critical analysis of the literature, the comparative method and the statistical method were used, including Mann Whitney U test and Kruskal Wallis ANOVA test. The choice of research methodology was not random; it was an arrangement of specific stages of the research procedure. One should agree with Czakon [5], an authority on research methodology in Poland, that classical research methods include observation, critical

analysis of the literature, text analysis, and statistical research. The method used was triangulation, which, according to Ziolo [6]; "refers to the situation when a study uses several research methods in one study or different research techniques within one method. By using different research methods, triangulation increases the cognitive possibilities in relation to the studied phenomena". Authors made a deliberate choice of such research methods primarily because of the limited information and databases. The deliberate selection of research methods made it possible to supplement, deepen and confirm the existing state of knowledge.

2 Electricity industry in Poland

Poland is actively developing its electrical engineering sector, focusing on the implementation of innovative technologies and the creation of smart grids. Smart grids enable real-time monitoring and management of energy flows, which is crucial for stable energy supply in the face of growing demand and the instability of traditional energy sources. These grids make it possible to optimize the use of electricity, minimize losses, and improve the quality of energy supply.

The innovative technologies being implemented in Poland's electrical engineering sector include the development of new energy storage solutions, such as advanced battery systems, as well as the development of infrastructure for electric vehicles. In recent years, significant attention has also been given to demand management technologies, which allow for more efficient regulation of electricity consumption according to its availability and cost. Smart grids enable balancing energy production and consumption in real-time, contributing to the stability and reliability of energy supply. Additionally, they enhance the security of the power grid and provide the capability for rapid response to emergency situations.

The integration of smart grids and carpooling represents a synergistic advancement towards a more sustainable and efficient energy and transportation system. Smart grids, which are advanced electrical grids enhanced with communication, automation, and IT systems, enable the real-time monitoring and management of energy production, distribution, and consumption. Those grids are pivotal in integrating renewable energy sources, such as solar and wind, into the energy network, ensuring a stable and reliable supply despite the intermittent nature of these sources. By optimizing energy flows and enabling demand-response mechanisms, smart grids facilitate the efficient use of renewable energy, reduce peak loads, and enhance the overall resilience of the energy system.

Carpooling, on the other hand, is an effective strategy to reduce traffic congestion, lower carbon emissions, and decrease individual transportation costs. When

integrated with electric vehicles (EVs) and supported by smart grid infrastructure, carpooling can achieve even greater environmental and economic benefits. Smart grids play a crucial role in this integration by providing the necessary infrastructure for widespread EV charging. They ensure that the increased demand for electricity from EVs can be met sustainably by optimizing the charging times and locations based on grid conditions and renewable energy availability.

Moreover, the smart grids can support the implementation of advanced carpooling platforms that use data analytics and real-time information to optimize routes and match passengers efficiently. These platforms can leverage smart grid data to recommend the best times and locations for charging EVs used in carpooling, thereby minimizing wait times and maximizing the use of renewable energy. Additionally, vehicle-to-grid (V2G) technology, enabled by smart grids, allows EVs to feed stored energy back into the grid during the peak demand periods, further stabilizing the energy supply and providing an additional revenue stream for carpooling participants.

The interplay between smart grids and carpooling also encourages the adoption of sustainable mobility solutions. As smart grids facilitate the reliable and efficient use of renewable energy, they make the operation of EVs more economical and environmentally friendly. This, in turn, promotes the use of EVs in carpooling, amplifying the reduction in greenhouse gas emissions and reliance on fossil fuels. Furthermore, policy measures and incentives, such as subsidies for EV purchases and investments in smart grid technology, can accelerate the adoption of both smart grids and carpooling, fostering a holistic approach to sustainable urban mobility and energy management.

Improvement of battery technology for EVs is another key area where the electrical engineering sector enhances efficiency and range, critical for ensuring the effectiveness of carpooling. Additionally, intelligent transportation systems, evolving within the electrical engineering sector, incorporate communication, navigation, and autonomous vehicle technologies, which also contribute to optimizing carpooling processes. These systems enable effective vehicle management and energy savings.

3 Carpooling - characteristics of the model of today's ICT-based economy

A critical analysis of the literature allows to conclude that carpooling, as a mode of the so-called social travel, has not yet received sufficient attention. Undoubtedly, the lack of analysis and research results of this phenomenon, despite its many different advantages, is an important factor limiting the consideration of this model from the perspective of scientific theory and practice. This is an important limitation, if only because carpooling in many

cities is promoted as the so-called green transportation, allowing to reduce transport congestion, improve the natural environment [7-8], shaping a sustainable and healthy transportation policy, but also a model that has an impact on health, which is affected by air emissions and greenhouse gases as a consequence of excessive transport traffic [9]. Carpooling is also one of the most representative initiatives to promote the responsible use of private vehicles [10].

In a broad sense, carpooling refers to shared car trips between people with similar destinations [11-12]. According to Minet et al., a carpooling system typically involves riding in a car taking into account the sharing of travel/travel costs. A carpooling service requires finding people with similar travel schedules and routes, but it can also include matching preferences in terms of listening to radio stations, smoking, or gender [13].

Carpooling is one of the many alternatives to commuting, etc., promoted by transportation policies to reduce the number of vehicles on the road. It became popular during World War II, mainly because of the need to cope with oil and tires shortages, as well as the need to conserve resources for the war. Carpooling was also popular in the 1970s, when the motive for its spread was to reduce oil consumption during the oil crisis [14]. It thus became an important trend in the transportation services market. Carpooling was also a response to driving restrictions and was also promoted during the 2008 Beijing Olympics.

Carpooling gained popularity after the emergence of the Internet and mobile technologies. These applications, after becoming more widespread and popular in the 1930s and 1970s, have gained in importance again, and in the last decade or so the carpooling has grown in scale and number of users [15-16].

Nowadays, carpooling is a part of mobility management policies due to the issue of sustainable transportation, among other things, including the many opportunities it brings. These include:

- reduction in kilometers travelled,
 - reduction in fuel consumption,
 - reduction of pollution, including, besides the other things, the negative impact of air pollution [17-18],
 - contribution to reducing the carbon footprint,
 - reduction of traffic congestion and problems related to finding a parking space [19],
 - reduction in traffic congestion and noise nuisance,
 - reduction of social inequalities that arise when the poor perceive that transportation services are increasingly unavailable to this social group [20-23].
- As the study of the correlation between the socio-demographic characteristics and usage elements show, lower-income users are more likely to be passengers, while the higher-income users carpool mainly as drivers [24].

All of these policies of sustainable mobility and demand management for transport and its services are implemented to use the transport system to meet

lifestyle needs [25-26].

Indeed, carpooling is a so-called “potential new path to sustainability” and “sustainable lifestyles” [27].

Other benefits of the carpooling model include reducing the number of cars on the road while reducing traffic jams, emissions and noise, as well as saving time, parking space and accidents. Carpooling is also an opportunity to socialize and reduce the stress of commuting [28]. According to the study, carpooling also affects the social sphere, including the development of human capital, allowing people to make social connections and engage in various social activities [29].

The aforementioned attributes and advantages of carpooling are also accompanied by certain disadvantages, limitations and obstacles. These include the necessity to ensure passenger safety, suboptimal mobility matching and the requirement for time flexibility. In addition, a common aspect of the aforementioned obstacles may also be an implicit psychological barrier that makes carpooling less attractive [30].

In addition, the vague and flexible nature of carpooling (e.g., no fixed stops, the possibility of making detours) may hinder the acceptance of carpooling in society [31]. In addition to the traditional concept of carpooling, the literature also encounters the term “casual carpooling” (also known as “slugging”), which reflects a type of informal carpooling of an ad hoc nature. According to the terminology, these are impromptu carpools with three or more people commuting in a configuration of one driver and two or more passengers. Such shared rides usually take place in or near public transportation centers generally in the morning (less often in the evening), when those interested in this particular mode of transportation enjoy commuting to a common place of employment [32].

4 The development of carpooling vs. collective intelligence and the sustainability

Collective intelligence is the kind of collective action that uses the knowledge and work of its users to provide data to an application and improve its usability. Popular examples of collective intelligence are applications labelled Web 2.0., based on which online platforms facilitate collaboration and information sharing among users. Taking collective intelligence as a fundamentally different way of looking at how applications are used, they can support interactions of a social and economic nature, as well as facilitate decision-making. While until recently most traditional applications have focused on improving productivity, today's approach to collective intelligence is based on using the intelligence of groups of people to enable greater productivity and better decision-making [33].

The main principles of collective intelligence are based on two main aspects: collective problem solving and the wisdom of the crowd. Collective problem-solving

generally concerns the optimal design of communication networks in organizations and determines the results of problem-solving through information efficiency. The wisdom of the crowd, on the other hand, indicates that the average response of a large group of novices may be more accurate than the opinions of individual experts [34].

The spread of simple and easy-to-use technologies that allow users to interact and design web applications without programming skills has led to previously unknown amounts of user-generated content [35].

Digital platforms offer the potential to bring people and knowledge together like never before. Initiatives that use digital platforms to focus and activate large groups of people and their knowledge to address challenges in all areas of social and economic life are emerging in increasing numbers [36]. One example of the solution described is shared smart mobility, which is reflected in carpooling. It corresponds to a form of sustainable mobility. This happens when it combines three categories of benefits compared to traditional mobility and transportation:

- economic (e.g., sharing ownership and maintenance costs);
- environmental (e.g., reducing negative externalities, traffic congestion, greenhouse gas emissions and noise),
- social-ethical (better accessibility, higher well-being and quality of life, social inclusion) [37].

According to Gandia et al [38] “smart mobility is characterized by the desire to inject more flexibility into travel, to discover new modes of transportation and sharing experiences. It offers the opportunity to eliminate entry barriers into the mobility market, whether economic (a one-way ticket) or technological variables (for example, smartphone use). It is the desire to propose sustainable mobility in the sense of submitting eco-innovations that reduce environmental impacts (less pollution, and zero tickets) or social consequences (disabled access) and that promote equality of territories (inclusiveness)”.

5 Carpooling, train and bus trips between selected cities in Poland in 2017-2018 and 2023- 2024 - survey results

Montenero [39] reports that online platforms are transforming transport because they create new multilateral markets that connect transport providers (often non-professionals) and passengers in ways that generate new network effects and distribute them among ecosystem participants. Experiences of carpooling show that transport platforms can multiply traditional resource sharing and even replace mass transport modes such as rail and buses.

BlaBlaCar, which is one of the most popular carpooling platforms in Europe, is a platform that

enables communication, negotiation and especially cooperation between users. This form of user activity is regarded as a manifestation of collective intelligence, based on the principles of collective problem-solving and the wisdom of the crowd, but is also an example of a tool that can support sustainable development and respond to its crisis.

The carpooling model, developed and implemented by users through BlaBlaCar, has emerged primarily because its use in the economy is considered to be competitive in terms of price with traditional transport models: rail and bus. The study covered carpooling transportation by BlaBlaCar, rail and bus between Wrocław and other voivodeship cities in Poland in 2017-2018 (i.e., before the Covid-19 pandemic) and in 2023-2024 (i.e., after the pandemic).

In Figure 1, box plots show average ticket prices on individual routes between Wrocław and other voivodeship cities in Poland in two periods: 2017-2018 and 2023-2024. This visualization not only confirms the overall increase in prices but also highlights greater variability in fare levels, which may reflect differences in demand intensity, vehicle availability, or platform usage patterns between regions. Comparing the two periods, one can see a clear increase in ticket prices on individual routes between Wrocław and other voivodeship cities of Poland, but one can also note an increase in the variation of ticket prices on individual routes, as indicated by the width of the box and whiskers. In the first period of

2017-2018, the highest ticket prices were recorded on the Wrocław - Białystok route (by an average of about PLN 91.30; EUR 21.46) and on the Wrocław - Gdańsk route (by PLN 83.20; EUR 19.56), while in the second period, i.e. 2023-2024, the highest fare prices were on the Wrocław - Lublin route (by an average of about PLN 121.9; EUR 28.65) and on the Wrocław - Białystok route (PLN 108.80; EUR 25.57), as well as on the Wrocław - Olsztyn route (the average price in the period under review was about PLN 108.00; EUR 25.39).

In addition, it was checked whether there were statistical differences in average travel costs during the periods studied. The Mann Whitney U test was used for the study, and the tests were conducted at the significance level of $\alpha = 0.05$ (see Table 1). The study found that in most trips between Wrocław and other voivodeship cities in Poland, the differences were statistically significant $p < \alpha$. The exceptions were the routes from Wrocław to Białystok $p > \alpha$ ($p = 0.1110$), from Wrocław to Bydgoszcz $p > \alpha$ (0.9245), from Wrocław to Olsztyn $p > \alpha$ ($p = 0.0742$) and from Wrocław to Toruń $p > \alpha$ ($p = 0.3111$). The price increase (change) was not statistically significant. In other cases, the test showed significant differences in average travel costs (ticket prices).

Figure 2 shows the average ticket prices with regard to the means of transport grouped by the analyzed periods 2017-2018 and 2023-2024. It is evident that while the bus and carpooling prices have increased

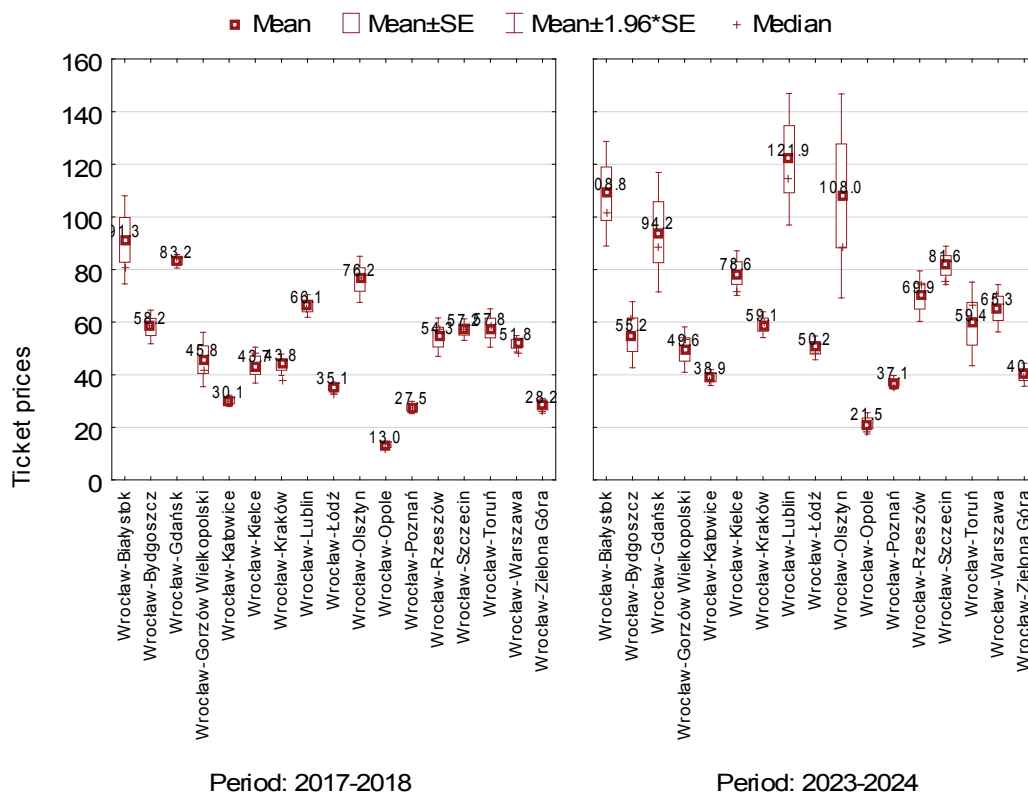


Figure 1 Average travel costs on selected routes between Wrocław and other voivodeship cities in Poland in 2017-2018 and 2023-2024, based on [40] and data from [41], [42] and [43]

Table 1 Results of Mann Whitney U test, based on [40] and data from [41], [42] and [43]

	2017-2018						2023-2024						p-value
	N	Me	Average	σ	Min	Max	N	Me	Average	σ	Min	Max	
Wroclaw-Bialystok	7	81	91.3	22.6	69	122	9	102.0	108.8	30.4	47.0	140.0	0.1110
Wroclaw-Bydgoszcz	14	58	58.2	12.1	36	71.5	9	61.0	55.2	19.2	14.0	70.0	0.9245
Wroclaw-Gdansk	14	84.5	83.2	4.8	71	89	10	88.5	94.2	36.6	23.0	155.0	0.6385
Wroclaw-Gorzow Wielkopolski	27	42	45.8	27.4	25	177	15	53.0	49.6	17.1	15.0	70.0	0.0139*
Wroclaw-Katowice	39	30	30.1	7.0	15	43	24	37.2	38.9	7.7	20.0	54.0	0.0000***
Wroclaw-Kielce	19	48	43.7	15.2	6	64	17	72.0	78.6	17.8	60.0	130.0	0.0000***
Wroclaw-Krakow	35	38	43.8	12.3	30	78	24	59.5	59.1	12.3	35.0	86.0	0.0000***
Wroclaw-Lublin	17	65	66.1	9.1	48	85.5	15	115.0	121.9	49.5	53.6	245.0	0.0000***
Wroclaw-Lodz	31	33	35.1	5.9	28	53.45	20	48.1	50.2	10.3	39.0	80.0	0.0000***
Wroclaw-Olsztyn	13	77	76.2	16.1	48	122	5	88.0	108.0	44.2	68.0	175.0	0.0742
Wroclaw-Opole	31	12	13.0	3.5	11	29	15	18.0	21.5	7.9	9.0	39.5	0.0000***
Wroclaw-Poznan	31	27	27.5	6.7	14	46.95	25	35.0	37.1	6.7	27.0	53.0	0.0000***
Wroclaw-Rzeszow	16	57.5	54.3	14.9	16	83	8	74.1	69.9	13.9	39.9	82.0	0.0146***
Wroclaw-Szczecin	19	57	57.2	9.1	42	77	17	75.0	81.6	15.4	61.2	105.0	0.0000***
Wroclaw-Torun	9	59	57.8	11.2	36	73	8	67.0	59.4	22.9	17.0	84.0	0.3111
Wroclaw-Warszawa	31	48	51.8	8.9	36	75	23	71.0	65.3	22.0	15.0	92.0	0.0005***
Wroclaw-Zielona Gora	36	26.5	28.2	8.5	12	47.5	17	39.0	40.0	9.2	20.0	60.0	0.0000***
all groups	389	40	43.6	21.6	6	177	261	58.0	61.6	32.6	9.0	245.0	

considerably, the average costs of rail travel remained relatively stable or even slightly decreased, which may indicate different pricing strategies or levels of subsidy. In this case, it is also possible to observe an increase in prices for each means of transport grouped

by the studied periods. From the data included in Figure 2, it is clear that the average prices in the analyzed periods increased for BlaBlaCar and bus trips, while they slightly decreased for train trips (i.e., Intercity).

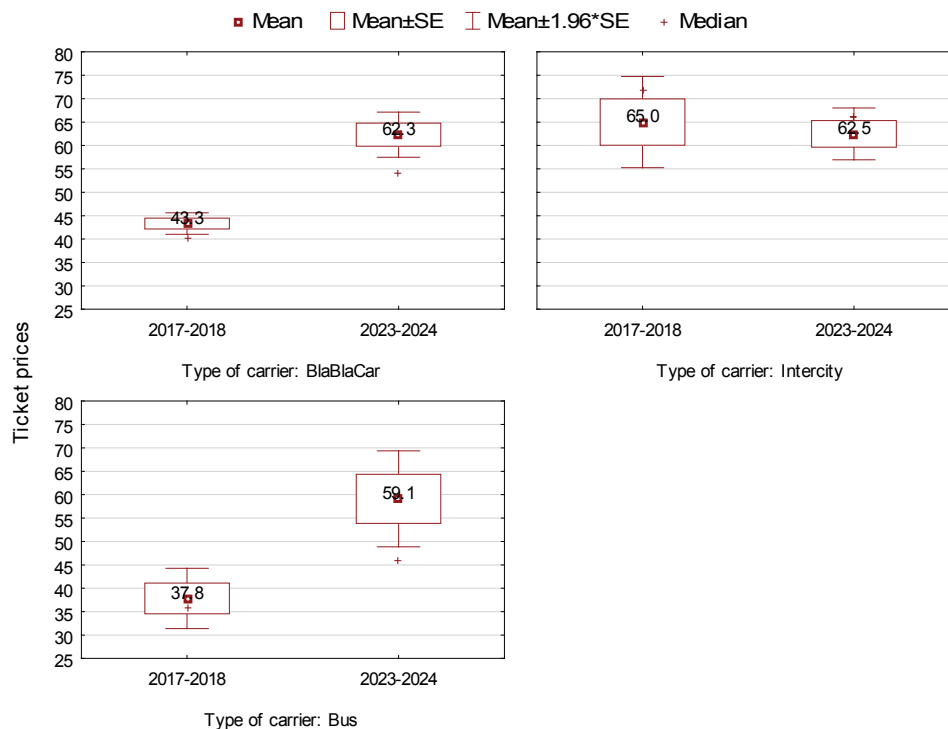
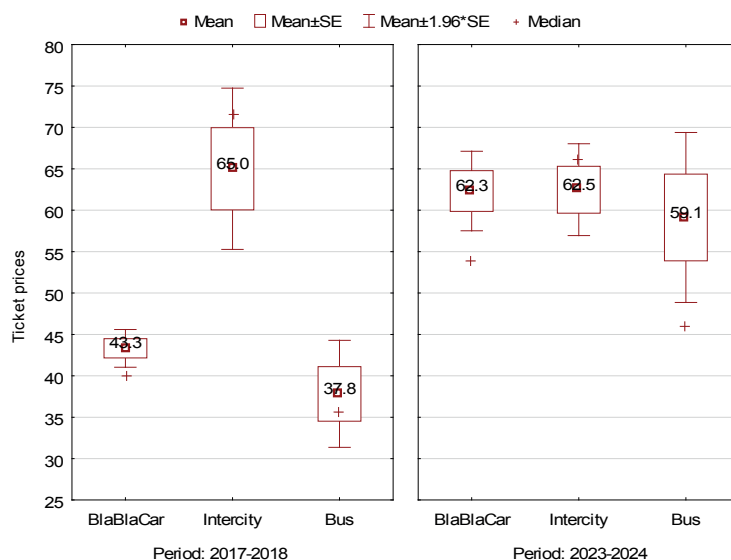


Figure 2 Average cost of travel by selected means of transport: BlaBlaCar, rail, and bus between Wroclaw and other voivodeship cities by period under study, based on [40] and data from [41], [42] and [43]

Table 2 Results of the Mann Whitney U test, based on [40] and data from [41], [42] and [43]

	2017-2018						2023-2024						p-value
	N	Me	Average	σ	Min	Max	N	Me	Average	σ	Min	Max	
BlaBlaCar	347	40	43.3	21.6	11	177	169	54	62.3	31.9	16	245	0.0000***
PKP Intercity	12	71.6	65.0	17.2	29	85.5	32	66.2	62.5	16.0	19.6	88	0.5067
bus journeys	30	19	37.8	18.1	6	78	60	45.9	59.1	40.6	8.9	174.9	0.0358*

**Figure 3** Comparison of average ticket prices between Wrocław and other voivodeship cities in Poland within each carrier group: BlaBlaCar, train trips and bus trips in 2017-2018 and 2023-2024, based on [40] and data from [41], [42] and [43]

It was checked whether the differences in the average costs of a ride between Wrocław and other voivodeship cities were statistically significant in the studied periods in each group of carriers. Mann-Whitney U-test was used for the study and a significance level of $\alpha = 0.05$ was adopted. The analysis showed that statistically significant differences in ticket prices occurred for BlaBlaCar rides $p < \alpha$ ($p = 0.0000$) and bus rides $p < \alpha$ ($p = 0.0358$). In contrast, differences in the cost of rail travel (i.e., Intercity) were not statistically significant.

Analyzing the data, it can be seen that the average prices of rides for BlaBlaCar increased during the periods studied: in 2017-2018 the average was PLN 43.3 (EUR 10.18) and the median PLN 40 (EUR 9.40), while in the period 2023-2024 the average price rose to PLN 62.3 (EUR 14.64) and the median PLN 54 (EUR 12.69). Bus rides also recorded an average increase in fare prices, and the differences were statistically significant, as well, $p < \alpha$ ($p = 0.0358$). In 2017-2018, the average was PLN 37.8 (EUR 8.88) and the median was PLN 19 (EUR 4.46), while in the 2023-2024 period, the average price rose to PLN 59.1 (EUR 13.89) and the median to PLN 45.9 (EUR 10.79) (see Table 2).

Figure 3 shows the average ticket prices by different means of transport for the two periods studied: 2017-2018 and 2023-2024. The narrowing of price differences between the carriers in the latter period suggests

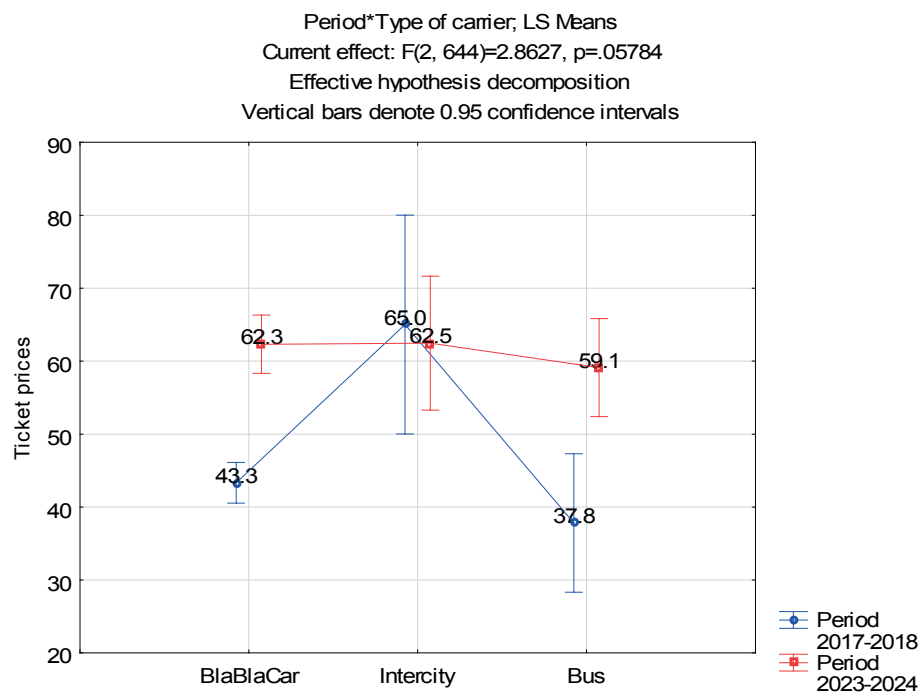
increasing competition and convergence of perceived value among transport modes, especially between the carpooling and buses. A wide variation was noted in 2017-2018. The lowest ticket prices were for bus transportation – PLN 37.8 (EUR 8.88) and for BlaBlaCar transportation – PLN 43.3 (EUR 10.18), while the highest average prices were for Intercity rail transportation (average PLN 65; EUR 15.28). In 2023-2024, the average prices of BlaBlaCar rides, train rides and bus rides equalized.

Thus, it was tested whether the differences in average fare prices between Wrocław and other voivodeship cities are statistically significant between different carriers: BlaBlaCar, rail transport (Intercity) and bus rides in the studied periods of 2017-2018 and 2023-2024. The Kruskal Wallis ANOVA test was used for the study. The test was conducted at the significance level of $\alpha = 0.05$. The test shows that the differences in 2017-2018 between the three studied carriers were statistically significant $p < \alpha$ ($p = 0.0011$). In the period 2023-2024, prices showed no statistically significant differences between carriers $p > \alpha$ ($p = 0.0536$) (see Table 3).

It was also tested whether the type of carrier (BlaBlaCar, Intercity train rides and bus rides) and the study periods (2017-2018 and 2023-2024) had simultaneous effects on fare levels. ANOVA analysis for factorial arrangements was used for the analysis. The study shows that both the study period and the type of carrier together have an impact on the transportation

Table 3 Results of Kruskal Wallis ANOVA test, based on [40] and data from [41], [42] and [43]

		BlaBlaCar	PKP Intercity	bus journeys	p-value
2017-2018	N	347	12	30	0.0011
	Me	40	71.6	19	
	Average	43,3	65	37.8	
	σ	21,6	17.2	18.1	
	Min	11	29	6	
	Max	177	85.5	78	
2023-2024	N	169	32	60	0.0536
	Me	54	66.2	45.9	
	Average	62.3	62.5	59.1	
	σ	31.9	16	40.6	
	Min	16	19.6	8.9	
	Max	245	88	174.9	

**Figure 4** Interaction graph between carrier type (BlaBlaCar, train rides and bus transfers) and period (2017-2018, 2023-2024) and ticket prices, based on [40] and data from [41], [42] and [43]

costs, $p < \alpha$ ($p = 0.0578$). The results are shown in an interaction figure (see Figure 4).

The results of the survey indicate that in most of the surveyed trips between Wrocław and other voivodeship cities in Poland in 2017-2018 and 2023-2024, trips provided by the carpooling model were cheaper than trips by rail and bus. The BlaBlaCar service, permanently supported by users and maintaining its growth momentum, can therefore be a manifestation of collective intelligence in today's high-tech economy. It is also an example of a service-application that fits into the concept of sustainable development and responds to the needs of modern society.

6 Summary

Carpooling is a model of shared travel that fits into the area of the so-called green transport, aiming, among other things, to protect the environment and reduce the so-called congestion in transport, i.e. traffic congestion. The model also corresponds to assumptions of the concept of sustainable development, which means that the implementation of trips through this model can contribute to the achievement of economic, social and environmental goals. This is expressed, among other things, in the generally lower cost of carpooling trips relative to the cost of trips made by train and bus, the

reduction of negative environmental impacts, as well as the building of a community and a certain carpooling culture among users who form the described model. The stated goal of this research has been reached. The authors have shown that the carpooling model is regarded as a manifestation of shared intelligence and is a response to the crisis of sustainability in today's ICT-based economy. Carpooling services are a cheaper alternative to transportation services provided by other means of transport.

A critical analysis of the literature, as well as the results of the study, made it possible to solve the main research problem. Collective intelligence and the assumptions of sustainable development influence the popularity of carpooling and the lower costs of carpooling services compared to those provided by other means of transport due to, among other things, the typically social nature of the service, its co-creation and development, based on the assumptions of the wisdom of the crowd and collective problem-solving, and the promotion and implementation of goals of an ecological and environmental nature. From the point of view of economics and management, the carpooling model is generally regarded as a cheaper alternative in travel to other forms and means of transport.

The authors also solved specific problems. Regarding the first specific research problem, it was noted that the integration of smart grids affects the operation of carpooling, and the expression of this integration can be: new models based on smart solutions, as well as their application in mass transportation, also enabling shared transportation.

In response to the second research problem, it was recognized that the carpooling phenomenon is not only a model, a way or a tool, but a lifestyle for the younger generation and an opportunity to strengthen social ties, as well. Carpooling also offers opportunities for the development of transportation services due to the sharing of travel costs, the convenience of travel and the reduction of transportation congestion.

In response to the last specific problem, it was shown that carpooling can help to strengthen the sustainability effect in the local as well as national economy. This finding is supported by, among other things, lower travel costs, strengthening social relations and creating green patterns.

The results of the conducted study allow to formulate the following conclusions:

1. The carpooling model is one of the important models of the modern economy, with its roots in the 1930s and based on information and communication technologies.
2. Carpooling is an important model and form of traveling in the 21st century from the point of view of price competitiveness and non-economic attractiveness, allowing the achievement of various economic and environmental goals and objectives.
3. Carpooling is a source of competitive advantage

and can be an important alternative to traditional modes of travel and/or movement.

4. Carpooling can be considered as a solution typical of collective intelligence, based on the principles of cooperation, partnership, creativity and the creation of new value.
5. The implementation of the carpooling model by drivers and passengers contributes to strengthening the assumptions of ecology, the so-called "green economy" and its community nature within the concept of sustainable development.

Potential barriers to the wider adoption of carpooling beyond the costs and sustainability include limited or no trust in fellow travellers, concerns about travel safety, the lack of universally accepted carpooling regulations, and changing trends in travel and increasing trends in carpooling. Electrical engineering - is a field of technology and science that deals with issues related to the generation, processing (transformation), transmission, distribution, storage and use of electricity. Areas of scientific interest in electrical engineering include electrical machinery and equipment, their construction, operation, management including in the field of electrical transportation. Engineering, including electrical engineering, has been the subject of scientific discussion for a long time. For example, F. A von Hayek and G. K. Myrdal in 1974 [44] received the Nobel Prize for their analysis of the interdependence of economic and social factors. In electrical engineering they follow the thinking of these Nobel laureates "preferences or subjective evaluations of individuals" are decisive. These views were developed in Japanese descriptive economics." They state that the needs of electrical engineering are determined by the subjective needs of stakeholders and consumers. A similar trend is reflected in the views of another Nobel Prize winner in 1987 - R. M. Solow [44], who proclaimed that technology, (including electrical engineering) is the most significant factor in economic development. According to Solow [44], the real source of growth of economies is the innovative activity of the entrepreneur. Carpooling, as a system that makes the passenger car similar and compatible with mass transportation, through the use of electric cars, is based on electric engineering solutions and fits into the strategic structure of these solutions in the future. Carpooling, as a concept or model for the behavior of individuals, fits into today's problems of sustainable transportation, where the electric engineering solutions would be a challenge. This is a contemporary new area of scientific research. In transportation, electrical engineering has applications in: electric vehicle installations, including electric multiple units, catenary, linear motor-driven railroads, magnetic railroads, electrical equipment of ships (including submarines and torpedoes) and other vessels (including electric aircraft). It should be stressed that the main connection between carpooling and the electrical engineering industry is at three levels.

The authors recognized that carpooling is a complex

and multifaceted topic, closely tied to various areas of socio-economic life. Despite its economic and environmental benefits, the widespread adoption of carpooling continues to face significant challenges, including behavioral barriers, such as lack of trust in strangers, concerns about punctuality and personal safety, and the desire for personal space. Those issues must be addressed for carpooling to achieve broader public acceptance. Looking ahead, future research and development should consider both the technological and human aspects of carpooling. On the technological side, advances, such as artificial intelligence, real-time data analytics, IoT-enabled infrastructure, and smart solutions (e.g., smart cities), offer promising opportunities to improve the efficiency, safety, and user-friendliness of carpooling platforms. The experience of digital transformation in other transport domains - such as smart parking systems at airports - demonstrates the potential of such tools to enhance accessibility and streamline operations. Applying similar principles to carpooling could lead to more robust, flexible, and attractive services. At the same time, further research should focus on the psychological and behavioral dimensions that influence user adoption. This includes exploring issues of trust, privacy, flexibility, and perceived safety through the mixed-method approaches, such as combining survey data with in-depth interviews or behavioral experiments, to gain a deeper understanding of user preferences and motivations.

From a broader perspective, the development of carpooling must also account for the dynamic economic and social landscape. In light of customers' growing tendency to reduce expenses - including those related to travel - and the increasing emphasis on environmental sustainability, carpooling models must evolve to reflect

changing user expectations and societal needs. This includes adapting to new labor market models, the pervasive implementation of ICT tools, and emerging cyber threats [45].

To support this evolution, the authors recommend the following:

- Introduce clear and appropriate legal frameworks at national and international levels to regulate the rights and obligations of participants, cost-sharing methods, and consequences of legal violations.
- Develop carpooling models that facilitate efficient and transparent communication between travellers and expand accessibility to a broader audience.
- Design business models that align with the principles of sustainable development, integrating economic, social, and ecological dimensions.

By addressing both technological opportunities and behavioral challenges, and by supporting development through robust legal and institutional frameworks, carpooling can continue to evolve into a viable, sustainable, and widely accepted mode of transportation.

Acknowledgements

The authors received no financial support for the research, authorship and/or publication of this article.

Conflicts of interest

The authors declare that they have no known competing financial interests or personal relationships that could have appeared to influence the work reported in this paper.

References

- [1] FETNI, M. L. Development of a mobile application for carpooling the elderly. GRIN Verlag, 2018/2019.
- [2] LIU, X., TITHERIDGE, H., YAN, X., WANG, R., TAN, W., CHEN, D., ZHANG, J. A passenger-to-driver matching model for commuter carpooling: case study and sensitivity analysis. *Transportation Research Part C: Emerging Technologies* [online]. 2020, **117**, 102702. ISSN 0968-090X, eISSN 1879-2359. Available from: <https://doi.org/10.1016/j.trc.2020.102702>
- [3] PARK, Y., CHEN, N., AKAR, G. Who is interested in carpooling and why: the importance of individual characteristics, role preferences and carpool markets. *Transportation Research Record: Journal of the Transportation Research Board* [online]. 2018, **2672**(8). ISSN 0361-1981, eISSN 2169-4052. Available from: <https://doi.org/10.1177/0361198118756883>
- [4] TEAL, R. F. Carpooling: who, how and why. *Transportation Research Part A: General* [online]. 1987, **21**(3), p. 203-214. ISSN 0191-2607. Available from: [https://doi.org/10.1016/0191-2607\(87\)90014-8](https://doi.org/10.1016/0191-2607(87)90014-8)
- [5] CZAKON, W. *Fundamentals of research methodology in management sciences / Podstawy metodologii badan w naukach o zarzadzaniu* (in Polish). Warszawa: Wolters Kluwer business, 2016. ISBN 978-83-264-9327-0.
- [6] ZIOLO, M. *Sustainable finance / Finanse zrownowazone* (in Polish). Warsaw: PWE, 2020. ISBN 978-83-208-2406-3.
- [7] HUANGA, K., LIU, Z., KIM, I., ZHANGA, Y., ZHU, T. Analysis of the influencing factors of carpooling schemes. *IEEE Intelligent Transportation Systems Magazine* [online]. 2019, **11**(3), p. 200-208. ISSN 1939-1390, eISSN 1941-1197. Available from: <https://doi.org/10.1109/IMITS.2019.2919550>
- [8] DEWAN, K., AHMAD, I. Carpooling: a step to reduce congestion (a case study of Delhi). *Engineering Letters*. 2017, **14**, p. 1-6. eISSN 1816-0948.

- [9] DINESH, S., REJIKUMAR, G., SISODIA, G. S. An empirical investigation into carpooling behaviour for sustainability. *Transportation Research Part F: Traffic Psychology and Behaviour* [online]. 2021, **77**, p. 181-196. ISSN 1369-8478, eISSN 1873-5517. Available from: <https://doi.org/10.1016/j.trf.2021.01.005>
- [10] ARTEAGA SANTOS, M. A., MENDEZ SANTOS, C., MARTINEZ, S. I., CASTAN ROCHA, J. A., MENCHACA, J. L., TERAN VILLANUEVA, J. D., TREVINO BERRONES, M. G., PEREZ COBOS, J., CASTAN ROCHA, E. A comparison of machine learning techniques in the carpooling problem. *Journal of Computer and Communications*. 2020, **8**(12), p. 159-169. ISSN 2327-5219, eISSN 2327-5227. Available from: <https://doi.org/10.4236/jcc.2020.812015>
- [11] AGUILERA, A., PIGALLE, E. The future and sustainability of carpooling practices. An identification of research challenges. *Sustainability* [online]. 2021, **13**(21), 11824. eISSN 2071-1050. Available from: <https://doi.org/10.3390/su132111824>
- [12] MINETT, P., PEARCE, J. Estimating the energy consumption impact of casual carpooling. *Energies* [online]. 2011, **4**(1), p. 126-139. eISSN 1996-1073. Available from: <https://doi.org/10.3390/en4010126>
- [13] KELLEY, K. L. Casual carpooling - enhanced. *Journal of Public Transportation* [online]. 2007, **10**(4), p. 119-130. ISSN 1077-291X, eISSN 2375-0901. Available from: <http://doi.org/10.5038/2375-0901.10.4.6>
- [14] FRIMAN, M., LATTMAN, K., OLSSON, L. E. Carpoolers' perceived accessibility of carpooling. *Sustainability* [online]. 2020, **12**(21), 8976. eISSN 2071-1050. Available from: <https://doi.org/10.3390/su12218976>
- [15] JULAGASIGORN, P., BANOMYONG, R., GRANT, D. B., VARADEJSATITWONG, P. What encourages people to carpool? A conceptual framework of carpooling psychological factors and research propositions. *Transportation Research Interdisciplinary Perspectives* [online]. 2021, **12**, p. 1-12. eISSN 2590-1982. Available from: <https://doi.org/10.1016/j.trip.2021.100493>
- [16] LI, R., LIU, Z., ZHANG, R. Studying the benefits of carpooling in an urban area using automatic vehicle identification data. *Transportation Research Part C: Emerging Technologies* [online]. 2018, **93**, p. 367-380. ISSN 0968-090X, eISSN 1879-2359. Available from: <https://doi.org/10.1016/j.trc.2018.06.012>
- [17] SHAHEEN, S., COHEN, A., BAYEN, A. The benefits of carpooling [online]. Published Web Location, 2018. p. 1-32. Available from: <https://doi.org/10.7922/G2DZ06GF>
- [18] NAGARE, D. B., MORE, K. L., TANWAR, N. S., KULKARNI, S. S., GUNDA, K. C. Dynamic carpooling application development on android platform. *International Journal of Innovative Technology and Exploring Engineering (IJITEE)* [online]. 2013, **2**(3), p. 136-139. eISSN 2278-3075.
- [19] LIBRINO, F., RENDA, M. E., SANTI, P., MARTELLI, F., RESTA, G., DUARTE, F., RATTI, C., ZHAO, C. Home-work carpooling for social mixing. *Transportation* [online]. 2020, **47**, p. 2671-2701. ISSN 0049-4488, eISSN 1572-9435. Available from: <https://doi.org/10.1007/s11116-019-10038-2>
- [20] MATERNA, M., SLUSNY, R., KOVACIKOVA, K. Air carriers' innovative competitive strategies as part of the hybridization of business models. *Transportation Research Procedia* [online]. 2024, **81**, p. 58-66. ISSN 2352-1457, eISSN 2352-1465. Available from: <https://doi.org/10.1016/j.trpro.2024.11.007>
- [21] KNAPEN, L., BEN-ARROYO HARTMAN, I., KEREN, D., UL-HAQUE YASAR, A., CHO, S., BELLEMANS, T., JANSSENS, D., WETS, G. Scalability issues in optimal assignment for carpooling. *Journal of Computer and System Sciences* [online]. 2015, **81**(3), p. 568-584. ISSN 0022-0000, eISSN 1090-2724. Available from: <https://doi.org/10.1016/j.jcss.2014.11.010>
- [22] CHOA, S., -UL-HAQUE YASARA, A., KNAPENA, L., BELLEMANS, T., JANSSENS, D., WETS, G. A conceptual design of an agent-based interaction model for the carpooling application. *Procedia Computer Science* [online]. 2012, **10**, p. 801-807. eISSN 1877-0509. Available from: <https://doi.org/10.1016/j.procs.2012.06.103>
- [23] COINDREAU, M. A., GALLAY, O., ZUFFEREY, N. Vehicle routing with transportable resources: using carpooling and walking for on-site services. *European Journal of Operational Research* [online]. 2019, **279**(3), p. 996-1010. ISSN 0377-2217, eISSN 1872-6860. Available from: <https://doi.org/10.1016/j.ejor.2019.06.039>
- [24] SHAHEEN, S., STOCKER, A., MUNDLER, M. Online and app-based carpooling in France: analyzing users and practices - a study of BlaBlaCar. In: *Disrupting mobility. Lecture notes in mobility* [online]. MEYER, G., SHAHEEN S. (Eds.). Cham: Springer, 2017. ISBN 978-3-319-51601-1, eISBN 978-3-319-51602-8, p. 181-196. Available from: https://doi.org/10.1007/978-3-319-51602-8_12
- [25] VANOUTRIVE, T., VAN DE VIJVER, E., VAN MALDEREN, L., JOURQUIN, B., THOMAS, I., VERHETSEL, A., WITLOX, F. What determines carpooling to workplaces in Belgium: location, organisation, or promotion? *Journal of Transport Geography* [online]. 2012, **22**, p. 77-86. ISSN 0966-6923, eISSN 1873-1236. Available from: <https://doi.org/10.1016/j.jtrangeo.2011.11.006>
- [26] GUIDOTTI, R., SASSI, A., BERLINGERIO, M., PASCALE, A., GHADDAR, B. Social or green? A data-driven approach for more enjoyable carpooling. In: *IEEE 18th International Conference on Intelligent Transportation Systems: proceedings* [online]. IEEE. 2015. eISBN 978-1-4673-6596-3, ISSN 2153-0009, eISSN 2153-0017, p. 842-847, Available from: <https://doi.org/10.1109/ITSC.2015.142>

- [27] BACHMANN, F., HANIMANN, A., ARTHO, J., JONAS, K. What drives people to carpool? Explaining carpooling intention from the perspectives of carpooling passengers and drivers. *Transportation Research Part F: Traffic Psychology and Behaviour* [online]. 2018, **59**(A), p. 260-268. ISSN 1369-8478, eISSN 1873-5517. Available from: <https://doi.org/10.1016/j.trf.2018.08.022>
- [28] BEN-ARROYO HARTMAN, I., KEREN, D., DBAI, A. A., COHEN, E., KNAPEN, L., -UL-HAQUE YASAR, A., JANSSENS, D. Theory and practice in large carpooling problems. *Procedia Computer Science* [online]. 2014, **32**, p. 339-347. eISSN 1877-0509. Available from: <https://www.mdpi.com/2071-1050/12/22/9587>
- [29] KOFI CHARLES, K., KLINE, P. Relational costs and the production of social capital: evidence from carpooling. *The Economic Journal* [online]. 2006, **116**(511), p. 581-604. ISSN 0013-0133, eISSN 1468-0297. Available from: <https://doi.org/10.1111/j.1468-0297.2006.01093.x>
- [30] BERLINGERIO, M., GHADDAR, B., GUIDOTTI, R., PASCALE, A., SASSI, A. The GRAAL of carpooling: GReen and sociAL optimization from crowd-sourced data. *Transportation Research Part C: Emerging Technologies* [online]. 2017, **80**, p. 20-36. ISSN 0968-090X, eISSN 1879-2359. Available from: <https://doi.org/10.1016/j.trc.2017.02.025>
- [31] HUANG, H., BUCHER, D., KISSLING, J., WEIBEL, R., RAUBAL, M., HUANG, H., BUCHER, D., KISSLING, J., WEIBEL, R., RAUBAL, M. Multimodal route planning with public transport and carpooling. *IEEE Transactions on Intelligent Transportation Systems* [online]. 2019, **20**(9), p. 3513-3525. ISSN 1524-9050, eISSN 1558-0016. Available from: <https://doi.org/10.1109/TITS.2018.2876570>
- [32] SHAHEEN, S. A., CHAN, N. D., GAYNOR, T. Casual carpooling in the San Francisco Bay area: understanding user characteristics, behaviors, and motivations. *Transport Policy* [online]. 2016, **51**, p. 165-173. ISSN 0967-070X, eISSN 1879-310X. Available from: <https://doi.org/10.1016/j.tranpol.2016.01.003>
- [33] GREGG, D. G. Designing for collective intelligence. *Communications of the ACM* [online]. 2010, **53**(4), p. 134-138. ISSN 0001-0782, eISSN 1557-7317. Available from: <https://doi.org/10.1145/1721654.1721691>
- [34] CENTOLA, D. The network science of collective intelligence. *Trends in Cognitive Sciences* [online]. 2022, **26**(11), p. 923-941. ISSN 1364-6613, eISSN 1879-307X. Available from: <https://doi.org/10.1016/j.tics.2022.08.009>
- [35] LEIMEISTER, J. M. Collective intelligence. *Business and Information Systems Engineering* [online]. 2010, **2**, p. 245-248. ISSN 2363-7005, eISSN 1867-0202. Available from: <https://doi.org/10.1007/s12599-010-0114-8>
- [36] BULTEAU, J., FEUILLET, T., DANTAN, S. Carpooling and carsharing for commuting in the Paris region: a comprehensive exploration of the individual and contextual correlates of their uses. *Travel Behaviour and Society* [online]. 2019, **16**, p. 77-87. ISSN 2214-367X, eISSN 2214-3688. Available from: <https://doi.org/10.1016/j.tbs.2019.04.007>
- [37] MULGAN, G. Artificial intelligence and collective intelligence: the emergence of a new field. *AI and Society* [online]. 2018, **33**, p. 631-632. ISSN 0951-5666, eISSN 1435-5655. Available from: <https://doi.org/10.1007/s00146-018-0861-5>
- [38] GANDIA, R., ANTONIALLI, F., NICOLAI, I., SUGANO, J., OLIVEIRA, J., OLIVEIRA, I. Casual carpooling: a strategy to support implementation of mobility-as-a-service in a developing country. *Sustainability* [online]. 2021, **13**(5), 2774. eISSN 2071-1050. Available from: <https://doi.org/10.3390/su13052774>
- [39] MONTENERO, J. J. Regulating transport platforms: the case of carpooling in Europe. In: *The governance of smart transportation systems. The Urban Book Series*. FINGER, M., AUDOUIN, M. (Eds.). Cham: Springer, 2019. ISBN 978-3-319-96525-3, eISBN 978-3-319-96526-0.
- [40] WIACZEK, P. The access economy and the sharing economy: an example of transport business/Gospodarka dostępu i gospodarka dzielenia się na przykładzie działalności przewozowej (in Polish). Unpublished doctoral dissertation. Warsaw: Warsaw School of Economics, 2019.
- [41] BlaBlaCar (2017, 2018, 2023, 2024) [online]. Available from: www.blablacar.pl
- [42] PKP, Polish state railways / PKP, Polskie koleje państwowe (in Polish) [online]. (2017, 2018, 2023, 2024). Available from: www.pkp.pl
- [43] e-podroznik (in Polish) (2017, 2018, 2023, 2024) [online]. Available from: www.e-podroznik.pl e-podroznik
- [44] GRZYWACZ, W. *Economists and economic systems / Ekonomisci i systemy ekonomiczne* (in Polish). Szczecin: PTE, 2005. ISBN 83-87249-51-3.
- [45] KOVACIKOVA, K., NOVAK, A., KOVACIKOVA, M., NOVAK SEDLACKOVA, A. Smart parking as a part of smart airport concept. *Transportation Research Procedia* [online]. 2022, **65**, p. 70-77. ISSN 2352-1457, eISSN 2352-1465. Available from: <https://doi.org/10.1016/j.trpro.2022.11.009>



This is an open access article distributed under the terms of the Creative Commons Attribution 4.0 International License (CC BY 4.0), which permits use, distribution, and reproduction in any medium, provided the original publication is properly cited. No use, distribution or reproduction is permitted which does not comply with these terms.

METHODOLOGY FOR ASSESSING THE KEY OPERATIONAL EFFICIENCY INDICATORS FOR REMOVAL AND SHUNTING OPERATIONS OF SHUNTING LOCOMOTIVES

Gabit Bakyt^{1,*}, Aizhan Makhanova¹, Murat Mussabekov¹, Galymzhan Ashirbayev¹, Malik Zhamankulov¹, Kuantkhan Sarsenov², Aisha Mussabekova³

¹Mukhametzhan Tynyshpayev ALT University, Almaty, Kazakhstan,

²D. Serikbayev East Kazakhstan Technical University, Ust-Kamenogorsk, Kazakhstan,

³Management University, Almaty, Kazakhstan,

*E-mail of corresponding author: gaba_b@bk.ru

Gabit Bakyt 0009-0009-8454-6791,

Galymzhan Ashirbayev 0000-0002-7044-9968

Resume

The problem dealt with in this article is the methodology of the key performance indicators (KPI) evaluation of shunting locomotives operation when performing hauling and shunting work. The main parameters affecting the efficiency of rolling stock operation are described, including performance, fuel efficiency and locomotive utilization rate. The algorithm of KPI calculation is proposed, based on the analysis of operational data and statistical methods is proposed. According to the analysis of the trend in cargo transportation over the past 3 years, the need to develop a methodology for evaluating the key performance indicators of shunting work is justified. A comparative analysis of various approaches to assessing the operational performance of locomotives is carried out, their advantages and disadvantages are revealed. Practical recommendations for improving the operational performance of rolling stock are described.

Article info

Received 10 March 2025

Accepted 22 July 2025

Online 8 September 2025

Keywords:

shunting locomotive
operational efficiency
key indicators
railway transport
fuel efficiency

Available online: <https://doi.org/10.26552/com.C.2025.048>

ISSN 1335-4205 (print version)

ISSN 2585-7878 (online version)

1 Introduction

The railway transport is one of the key elements of the transport system, ensuring efficient logistics of freight and passenger traffic. Shunting locomotives, which perform outbound and shunting operations, play a special role in the functioning of a railway hub. Their operational efficiency has a direct impact on station capacity, freight handling speed and overall operating costs. In this regard, the development of a methodology for assessing the key performance indicators (KPI) for shunting locomotives is an urgent task.

The real conditions of the present show that fuel efficiency of old diesel locomotives does not meet modern requirements and affects the economic performance of the operating depot, so the efficiency of fuel utilization and control of fuel consumption is a priority for the locomotive owning companies [1].

Modern railway transport operating conditions require the introduction of technologies to increase

productivity and reduce costs. Traditional methods for assessing the efficiency of shunting locomotives often do not take into account all factors affecting their operation, such as fuel consumption, idle time, capacity utilisation rate and operating costs. Therefore, it is necessary to develop a more accurate KPI evaluation methodology to make informed management decisions.

It is known that about 65-70% of shunting locomotives produced in the 90s of the last century are still in operation on the railways and industrial enterprises of Kazakhstan and the countries of the Commonwealth of Independent States (CIS). These locomotives are not equipped with modern means of remote monitoring of fuel consumption, and the installation of these means requires a large investment. Therefore, for these locomotives, it is necessary to develop a suitable and adapted method for evaluating the operational efficiency of shunting locomotives, taking into account both the technical condition and economic performance.

The issues of shunting locomotives operation

efficiency assessment are studied by many researchers. in the works [2-5] were considered approaches to the analysis of fuel efficiency and locomotive utilizations factor. in studies [1, 5-7] mathematical models for shunting operation optimization were proposed. However, most of the existing methodologies focus on individual aspects of efficiency without providing a comprehensive approach to analyzing operational parameters. In this paper a methodology that combines various indicators into a single evaluation system is proposed.

The purpose of the study was to develop a methodology for assessing the key performance indicators of shunting locomotives when performing outbound and shunting work. To achieve this goal, the following objectives were set [5]:

- Analysis of existing methods for assessing the operating efficiency of shunting locomotives;
- Identification of key factors affecting KPIs;
- Development of an algorithm for calculating KPIs taking into account operational data;
- Formulation of recommendations to improve the efficiency of shunting locomotive operation.

The scientific novelty of the study lies in the development of a comprehensive approach to assessing the operational efficiency of shunting locomotives, taking into account both technical and economic indicators. Unlike the existing methods, the proposed approach includes automated analysis of operational data and allows optimizing the operation of the locomotive fleet taking into account various operating conditions. The results obtained can be used by transport companies and

railway transport operators to improve the efficiency of shunting locomotives.

2 Materials and methods

Implementation of strategic plans, as well as control over the technological chain of operations, the implementation of which should be achieved in a fairly short period of time and at the lowest costs is a complex and serious process for the organization.

To achieve these goals, the key performance indicators (KPI) are created, which allow to evaluate and analyze the flow of technological processes, to optimize them, to coordinate the actions of personnel and subdivisions [4, 6].

The use of KPIs in managing the production activities of an enterprise makes it possible to [4]:

- improve technological processes;
- quantify all types of activities;
- pay special attention to performance indicators that are necessary to obtain significant operational characteristics.

The use of KPIs makes it possible to consolidate the results of various measurements used in the organization's activities of the so-called key KPIs. Continuous monitoring of the work processes and characteristics assigned to the enterprise complicates the analysis of the results achieved, while the use of KPI indicators is the most effective, their values can be used to analyze the tendency of changes in various

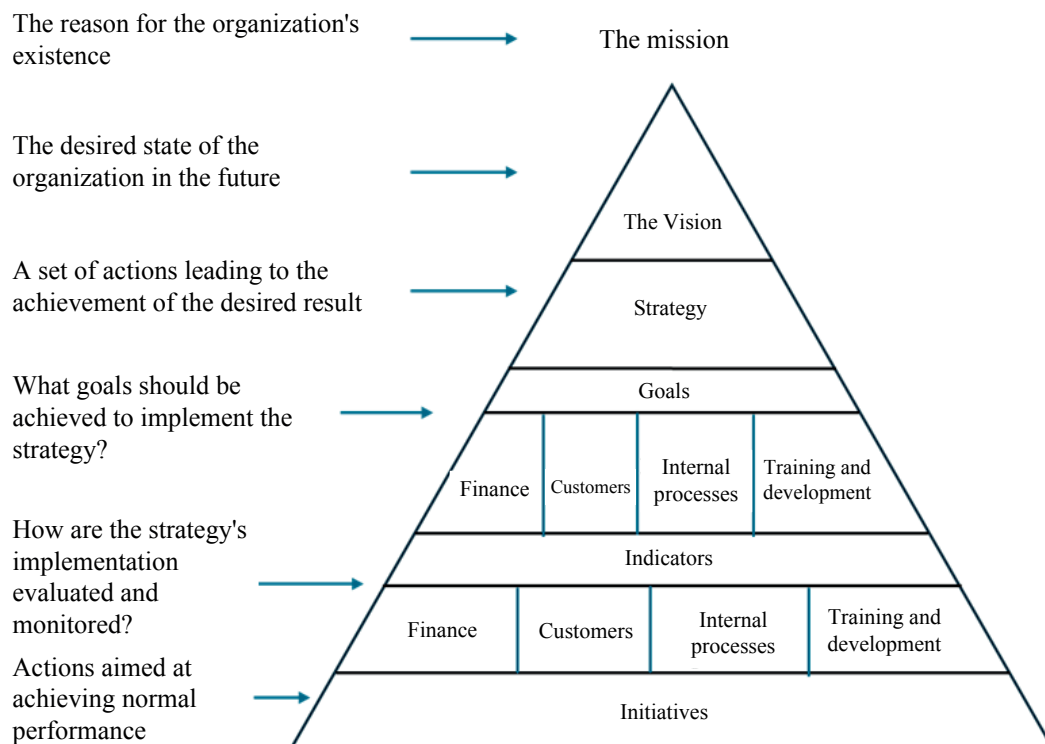


Figure 1 Diagram of a balanced scorecard

production units within the enterprise with different sets of KPI indicators that can be used together for continuous monitoring of the business goals assigned to the enterprise [5]. The implementation and use of the KPIs is a tool that enables an organization to evaluate its business processes, as well as strategy implementation. A diagram of a balanced scorecard is shown in Figure 1.

Thus, the KPI system is linked to the strategic goals of the organization. The KPI system is most relevant in business process management. To develop and use KPIs in an organization, it is necessary to define a list of goals that it wants to achieve.

Shunting locomotives play an important role in ensuring the efficient functioning of railway transport, carrying out work on sorting wagons, transporting goods and forming trains. One of the key factors of their operation is the analysis of the tendency of traffic volumes and fuel consumption, which makes it possible to optimize costs and increase the efficiency of railway junctions [7].

The analysis of the volume of transportation by shunting locomotives includes an assessment of the number of wagons handled, the volume of goods transported and the intensity of shunting work. In recent years, there have been trends towards an increase or decrease in traffic volumes, due to a number of factors [6]:

- Changing the structure of cargo flows;
- Optimizing the operation of railway stations;
- Seasonal fluctuations in freight traffic.

The statistical methods of data analysis are used to assess the development of transportation, which make it possible to identify the key trends and predict the further development of shunting operations.

The results of the analysis of the ratio between the traffic volumes and fuel consumption make it possible to evaluate the efficiency of using shunting locomotives. It is important to take into account the efficiency of the locomotive, which shows how efficiently the fuel is used when performing shunting work. Optimization of operating modes and routing can help to reduce specific fuel consumption while increasing traffic volumes.

On non-public railway access roads [8]:

- train work is performed by 3 pairs of TEM2 diesel locomotives, where each pair consists of 3 interconnected locomotives;
- the removal work is performed by 1 coupling of 2 coupled TEM2 diesel locomotives.

Shunting operations are performed by 8 single TEM18 diesel locomotives.

The total number of diesel locomotives involved in all types of work is 19 TEM2 and TEM18.

Figure 2 shows the histogram of traffic volume changes for 2022-2024 performed by the non-public railway stations.

The train operation is carried out by 3 interconnected diesel locomotives (spark), with a weight of 126 tons per locomotive, the total weight of 3 is 378 tons. This is an additional mass to the weight of the train, therefore, the values of traffic volumes by year are shown both without taking into account the weight of diesel locomotives and with taking into account the same [4, 8].

The results of the analysis of traffic tendency in the period 2022-2024 show that in [9]:

- 2023 traffic volumes decreased by 4.4% compared to 2022;
- traffic volume amounted to 12,132,543 tons, and exceeded the indicator of 2023 (9,606,583 t) by 26.3%.

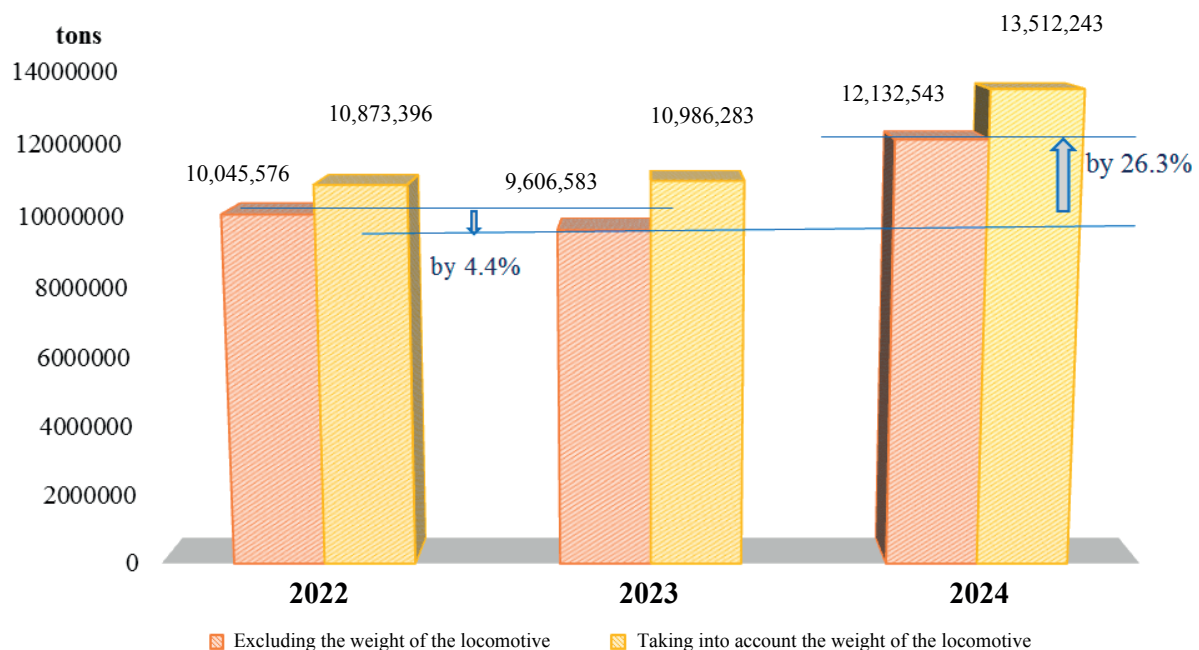


Figure 2 Histogram of traffic volume changes for 2022-2024

The main factors contributing to the decline in traffic volumes in 2023 relative to 2022 are the post-crisis state of the economy.

Changes in the tendency of transportation volumes contributed to a similar change in fuel consumption development (Figure 3).

Thus, in train operation, the fuel consumption by train locomotives in 2023 decreased by 6.6% compared

to 2022, while in 2024 it increased by 30.2% compared to 2023.

At the same time, the total fuel consumption for all types of work (train, export and shunting) in 2024 increased by 22.5% compared to 2023.

Figure 4 shows the tendency of changes in the specific fuel consumption of diesel locomotives during the transportation process.

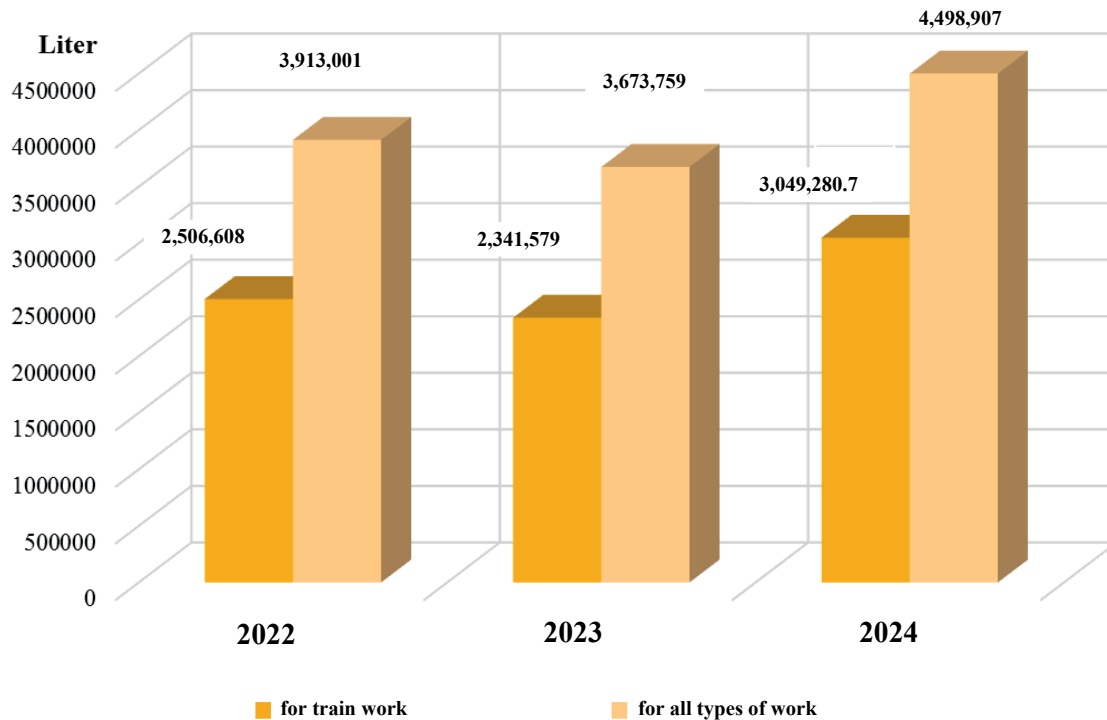


Figure 3 Tendency of changes in fuel consumption by diesel locomotives in 2022-2024

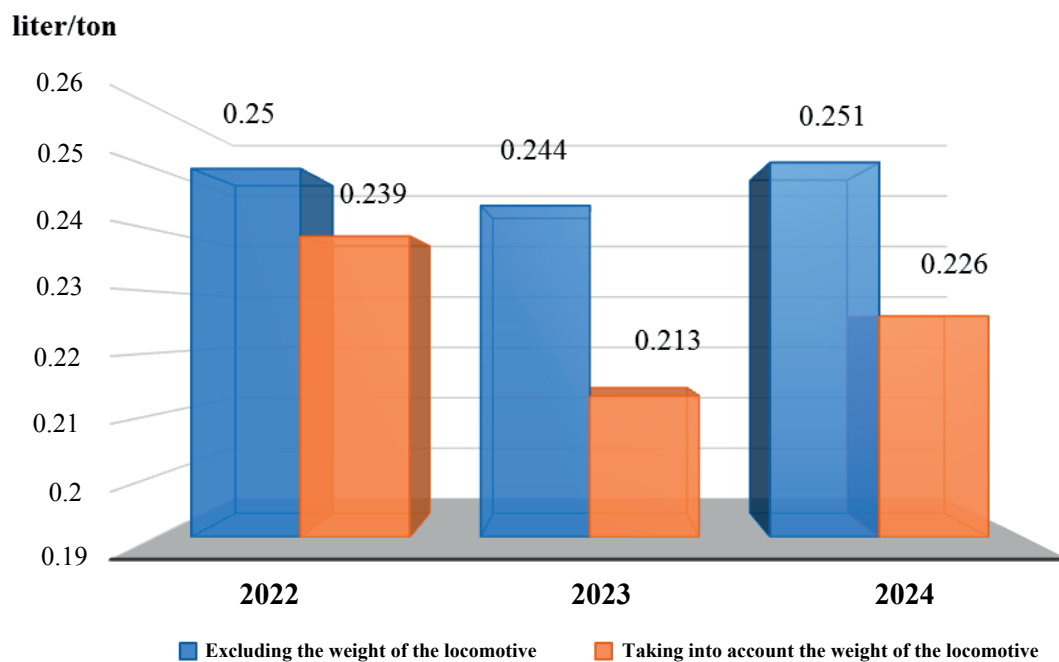


Figure 4 Tendency of changes in the specific fuel consumption of diesel locomotives for the transportation process

The specific fuel consumption of diesel locomotives for all types of work: train, export, shunting, in 2024 amounted to 0.371 liters /ton, which is 2.9% better than the value of the specific consumption in 2023 (0.382 liters / ton).

The amount of fuel savings is $(0.382 - 0.371) = 0.011$ liters/ton $\cdot 12,132,543$ tons = 133,458 liters, i.e., it has a positive trend.

The specific fuel consumption of train locomotives in 2024 was 0.251 liters/ton, which is 2.9% worse than the value of the specific consumption in 2023 (0.244 liters/ton). The amount of fuel overspending is: $(0.244 - 0.251) = -0.007$ l/t $\cdot 12,132,543$ t = 84,928 liters - negative tendency.

For example, train operation of non-public railway sidings is carried out on sections of station A - station B is 95km long. Freight trains are exchanged between the non-public railway sidings and mainline networks at the stations adjacent to station B. An analysis of the operation of railway sidings over 10 years shows that the average number of 4-6 pairs of trains per day. Moreover, the average mass of odd-numbered trains departing from station A is (4000-6000) tons, and the average mass of even-numbered trains receiving railway sidings is (1500-3000) tons. This is due to the specifics of the operation of railway sidings, arriving trains are mainly empty wagons for loading the goods of the owner [1, 7].

The purpose of the timing observations is to obtain the initial data for the development and establishment of time standards for a full turn of the locomotive at the station A - station B.

The procedure for conducting time-lapse observations, filling out time-lapse records and analyzing the results was carried out in accordance with specially developed requirements.

The photochronometric observations included taking photographs and recording every second the operating

time of the diesel generator set of the locomotive at a certain position of the driver's controller (the driver's handle) used by the train driver.

The development of time standards was carried out by an analytical and research method, according to which the standards were established based on the analysis of the results of observation (timekeeping) of the normalized operation performance. Control trips were carried out on technically serviceable diesel locomotives with the involvement of experienced drivers [10].

The time limit was set by the analytical and research method based on the analysis of data obtained as a result of direct observation of the operating time of diesel locomotives at specific positions of the driver's controller in specific conditions.

According to the technical condition, the railway tracks allow trains weighing 6,000 tons and above to operate at an acceptable speed of 70 km/h.

The main factor affecting the fuel consumption is the speed of the train.

During experimental trips, the possibility of reaching speeds within the permissible limits on this section was checked.

Thus, as a result of time-lapse observations, the total travel time of diesel locomotives with a train on the site was determined [10].

The driver did not use the 8th position of the driver's controller practically, due to the danger of failure of diesel locomotives. The average net speed of the train along the section was 32 km/h. Fuel consumption was determined based on the design data of diesel locomotives. The conformity check was carried out on rheostat tests of diesel locomotives. The traction characteristics and fuel consumption according to the positions of the driver's controller are shown in Figure 5 and in Table 1.

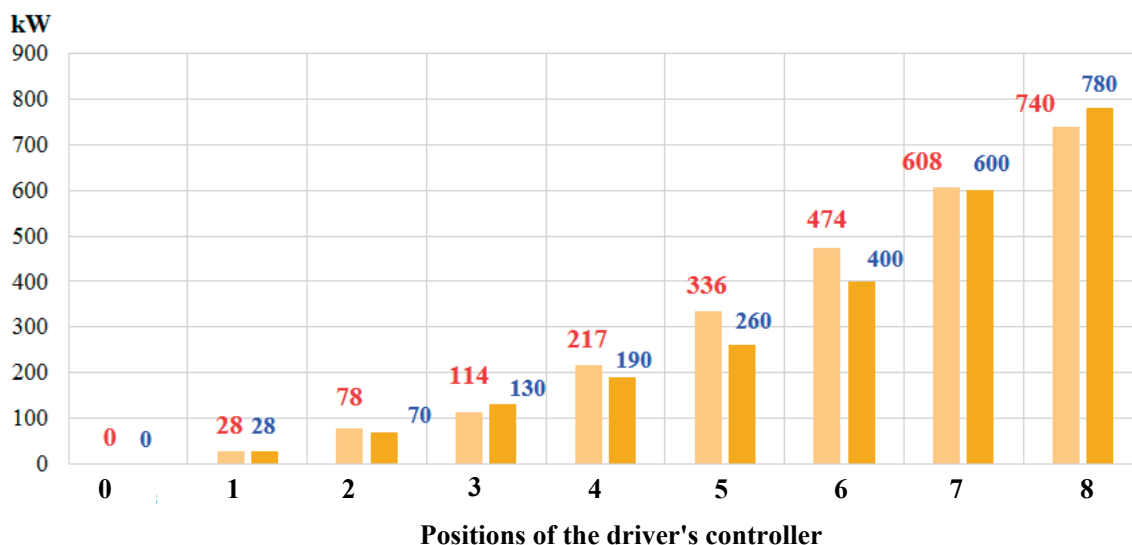
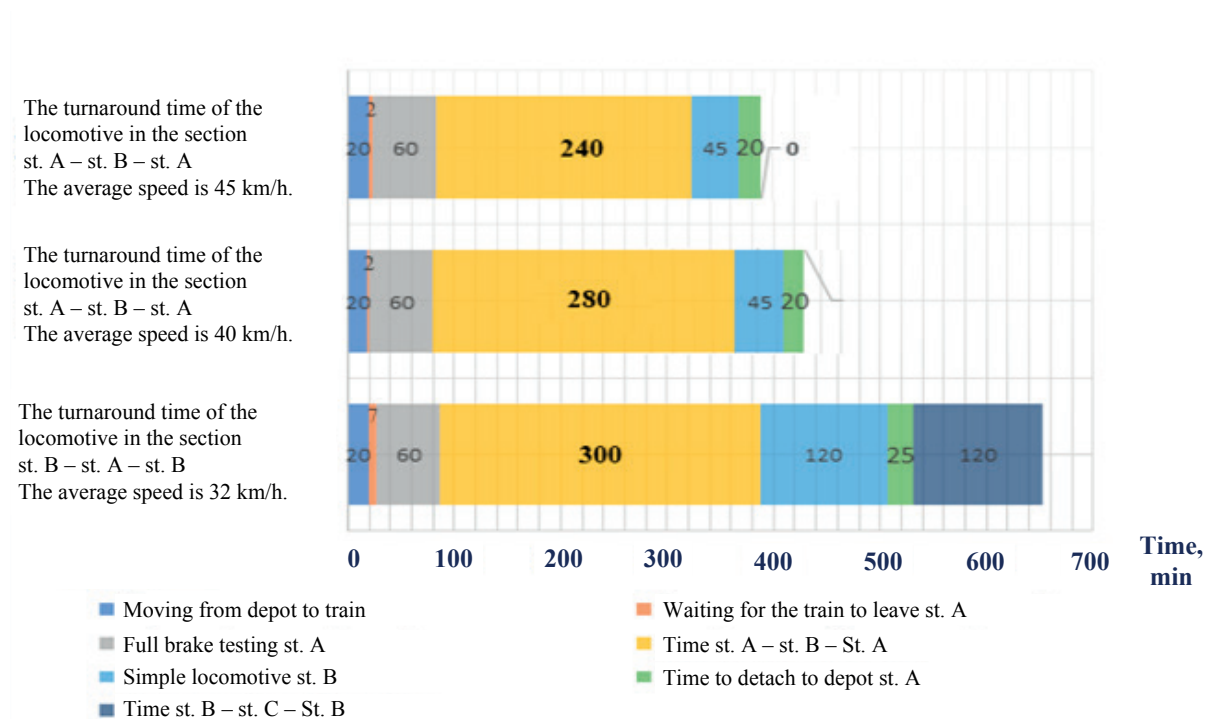


Figure 5 Traction characteristics of the TEM2 (TEM18) diesel locomotive

Table 1 Fuel consumption by the positions of the locomotive driver TEM2 (TEM18) controller

Number of the position of the driver's controller	Fuel consumption (rheostatic)	Power	
		Rheostatic	Passport information
	kg/min	kW	
0 (idling)	0.16	-	-
1	0.19	28	28
2	0.27	78	70
3	0.52	114	130
4	0.76	217	190
5	1.04	336	260
6	1.6	474	400
7	2.4	608	600
8	3.4	740	780



Designations: Station A - Almaty-1 station and Station B - Aksengir Station, Station C - Chemolgan Station

Figure 6 Duration of required regulatory operations.

Figure 6 shows the effect of the average speed of movement on the time of full rotation of diesel locomotives with trains in a given section of circulation.

3 Results and discussions

Currently, there are over 600 non-public railway access roads in Kazakhstan [8], owned by enterprises and organizations of various forms of ownership in

metallurgy, mining, coal, oil production and processing, machine-building and other sectors of the economy.

The infrastructure, complexes of structures, devices and technical means of many non-public railway access roads allow them to provide all types of transportation process.

The transportation activities of the railway access roads of Kazakhstan are carried out by means of diesel traction, consisting mainly of old shunting locomotives TEM2, TEM18.

On railway sidings, diesel locomotives are used in shunting operations related to performing a wide range of different operations for sorting wagons, forming and disbanding trains, feeding and cleaning wagons to cargo loading and unloading fronts, and other shunting operations in accordance with the technological process of the sidings.

The specifics of the operation of shunting locomotives are very different from the operation of diesel locomotives operating in the mainline mode. There are many more factors that combine to make it difficult to determine the actual fuel consumption of a particular locomotive [9].

The system of accounting for the operation of diesel locomotives when using them for shunting operations allows to set the time periods during which a particular locomotive was in motion or standing. However, this is not enough to understand the usefulness and effectiveness of its use [11].

The parking of a diesel locomotive can be caused by various reasons or form part of its shunting operation.

A locomotive can move with a full-fledged train, with several cars, or travel in reserve. In all the cases, it is impossible to determine how efficiently a locomotive is being used based on such a formal feature.

Consequently, the indicators, successfully used to account for and determine the efficiency of diesel locomotives in train operation, are not informative enough when assessing its effectiveness in shunting.

On railway access roads, the movement pattern of diesel locomotives during the shunting operations is almost the same, but the time spent on performing these operations and the power used for the corresponding positions of the locomotive driver's controller may be different. The power depends on the adjustment of the diesel generator set of a particular locomotive, the experience of the driver, etc. Various operational and climatic factors also have a significant impact.

To assess the efficiency of using a particular diesel locomotive, it is important to know the fuel consumption at the positions of the driver's controller used during shunting operations.

Knowing the costs of each individual maneuver and the number of movements (half-trips) during a shift, it is not difficult to determine the total fuel costs for performing shunting work by a diesel locomotive.

Therefore, the main criteria for the efficiency of using a diesel locomotive to perform the shunting work are: time to perform operations and fuel consumption [12].

The TEM2 and TEM18 locomotives are of old construction, they are not equipped with built-in technical means of accounting for fuel consumption, therefore, the amount of fuel in the tank of the locomotive is monitored visually by the driver according to the measuring glass on the fuel tank or fuel rail with a scale of division equal to 250 liters. Accounting for fuel consumption per shift of locomotive operation is carried out by the difference in the amount of fuel in the tank of the locomotive at the

beginning and end of the shift.

It should be noted that currently there are many companies that offer the installation of automatic fuel consumption monitoring and metering systems on diesel locomotives. At the same time, the main motive for installing flow meters on old diesel locomotives is to prevent unauthorized fuel discharge by railway workers.

Basically, these systems came from motor transport, differing in measurement principles and, consequently, costs, they poorly take into account large volumes of fuel tanks, the profile of the path, warming up, seasonality of work - determining consumption rates, etc.

In addition, the installation of fuel consumption monitoring and metering systems on old diesel locomotives may face significant problems, depending on the technical characteristics and structure of a particular locomotive model.

The main problems that may arise are [10]:

- 1) Lack of compatibility - old diesel locomotives have outdated control systems that are sometimes incompatible with modern types of fuel flow meters. Therefore, their installation will require modernization or replacement of control systems;
- 2) Unavailability or lack of spare parts - factories that produced old diesel locomotives could stop producing or supporting spare parts. This makes it difficult to obtain the necessary components for installing flow meters;
- 3) Technical limitations during installation - the structures of old diesel locomotives have limited space for installing new equipment, and this will create difficulties in integrating flow meters.
- 4) Required changes to the locomotive - the installation of new equipment may require changes to the design of the locomotive, for example, the addition of additional cables, sensors, etc. This may require careful design and engineering work;
- 5) The need for certifications - in some cases, the installation of new equipment may require review and certification by regulatory authorities. This may include compliance with safety standards and environmental regulations.

In general, the actual fuel consumption of a diesel locomotive per shift can be represented as the sum of fuel consumption over periods of operation in load mode and at idle [4]:

$$G_{act, shift} = \sum (G_j \cdot \Delta\tau_j + g_i \cdot \Delta\tau_i), \quad (1)$$

where: G_j - fuel consumption at the j -th position of the driver's controller, kg/min;

$\Delta\tau_j$ - operating time of the locomotive at the j -th position, min;

g_i - fuel consumption of a diesel locomotive at idle, kg/min;

$\Delta\tau_i$ - diesel engine idling time, min.

As can be seen from Equation (1), the amount of fuel consumption depends on the operating time

of the locomotive at the j -th position of the driver's controller and idling, therefore, the main indicator to be normalized is the duration of shunting operations.

The time standards for preparatory and final operations, which determine the duration of maneuvering operations for a certain time, are obtained analytically, regulated and introduced into regulatory and reference documents [12].

It should be noted that in many ways, the time standards for shunting operations used in railway transport were established in the 50-70 years of the 20th century and do not correspond to modern operating conditions of railway rolling stock and modern train handling technologies.

It should also be noted that the analytical methods for calculating the time for maneuvering operations described in different sources have both common features and differences.

For example, in [13] it was proposed to set the time limit for sorting the composition by the expression:

$$\tau_c = A \cdot q + B \cdot n, \quad (2)$$

From Equation (2):

$$\tau_c = 1.2(A \cdot q \cdot k_q + B \cdot n \cdot k_n) k_{cur} + \tau_{set} \quad (3)$$

where: A and B - constant coefficients, depending on the method of maneuvering, min/uncoupling;

q, n - the number of uncoupling and wagons in the train, respectively;

k_q, k_n - coefficients of repeated sorting of uncouples and wagons;

k_{cur} - a coefficient that takes into account the increase in sorting time when the exhaust track is located in curves with a small radius of repeated sorting of uncouples and wagons;

τ_{set} - time to settle the wagons, min.

The equation, used to determine the duration of maneuver operations, reads:

$$\tau_{det} = 0.06 \cdot L_{tr} / v_{tr}, \quad (4)$$

where: L_{tr} - travel route length, km;

v_{tr} - travel speed, km/h.

The above expressions represent linear dependences for determining the time for sorting Equation (2) and Equation (3), and the time for performing shunting operations in Equation (4) on the number of detaches and wagons in the train, the length of the route and the speed of movement of the locomotive.

However, for the same conditions, they can give different values of the time norms, and to establish a constant average value of the norm, it is necessary to conduct long-term field and computational studies.

The working conditions of the non-public access roads differ from those of the main railway transport networks, both in terms of technical equipment and

staff, as well as in operating technology.

Since the main activity of non-public access roads is the performance of the same type of cargo operations, the establishment of time standards for shunting operations based on time-lapse observations is much easier. It allows to obtain average technological standards for shunting work that take into account the actual features and conditions inherent in specific access roads and specific types of diesel locomotives used.

The value of the standard operating time of a locomotive per shift is established experimentally based on the timing of shunting operations by a serviceable locomotive under the control of a qualified engineer [11]:

$$\tau_{st.shift} = 12 - (\tau_{shift.ch.} + \tau_{lunch} + \tau_{wait.time}), \quad (5)$$

where: 12 - total shift time, h;

τ_{lunch} - lunch time, 1 h;

$\tau_{shift.ch.}$ - the time of acceptance and delivery of diesel locomotives by locomotive crews is 0.5 h;

$\tau_{wait.time}$ - the waiting time for work is set experimentally based on the rhythm of the access roads, h.

The operating time of the locomotive at the appropriate positions of the driver's controller, indicating this position and idling mode, is taken from the timing data of observations of shunting operations.

The value of the fuel consumption rate per shift [11]:

$$G_{cons.rate\ shift} = G_{act.fuel\ cons.} / \tau_{act.time.shift} \cdot \tau_{st.shift} \quad (6)$$

where: $\tau_{act.time.shift}$ and $G_{act.fuel\ cons.}$ - respectively, the actual operating time of the locomotive and the actual fuel consumption per shift.

$\tau_{st.shift}$ - the standard operating time of a diesel locomotive per shift, established based on the timing studies.

Total actual fuel consumption per shift $G_{act.fuel\ cons.}$ consists of their fuel consumption at the positions of the driver's controller, which were used by the driver when performing shunting work and idling when the locomotive was waiting for work and the designated parking areas of the locomotive (lunch, shifts of locomotive crews). To determine the consumption of diesel fuel at the appropriate positions of the driver's controller, the fuel consumption per kilowatt (1 kW) of diesel power is determined during the rheostatic tests of the locomotive. This figure is then multiplied by the locomotive's power at the driver's controller position and the operating time at that position.

The amount of fuel overspending (burnout) - $\Delta G_{fuel\ over.}$:

$$\Delta G_{fuel\ over.} = G_{act.shift} - G_{cons.rate.shift} \cdot \tau_{st.shift} \quad (7)$$

The amount of downtime:

$$\Delta \tau_{dt} = \tau_{stand.m.} - \tau_{act.m.} \quad (8)$$

$$\Sigma G_{cons.m.} = \Sigma G_{cons.shift} / \Sigma \tau_{act.time} \cdot \tau_{st.shift} \quad (9)$$

where: $\Sigma G_{cons.shift}$ - fuel consumption by locomotives per shift, l;
 $\Sigma \tau_{act.time}$ - actual working time per shift, h;
 $\tau_{stand.m.}$ - the established standard of the locomotive's working hours per shift (month);
 $\tau_{act.m.}$ - the actual working time of the locomotive per shift (month).

The actual specific fuel consumption is:

$$KPI = \tau_{act.} / \tau_{stand.} \quad (10)$$

Thus, the assessment of key performance indicators (KPIs) for the removal and shunting operation of shunting locomotives is an important tool for operational efficiency management. To form a KPI system, the following parameters must be taken into account [13-15]:

- Locomotive performance - the number of wagons handled per shift;
- Fuel efficiency - specific fuel consumption per unit of work performed (ton-km or wagon-hour);

- Locomotive utilization factor - the ratio of operating time under load to the total operating time;
- The average speed of shunting work is an indicator that affects the throughput of nodes;
- Locomotive downtime - waiting time without performing useful work;
- The volume of cargo transported is the total weight of cargo moved as part of shunting operations.

To create a KPI, it is recommended to use the developed monitoring methodology, which allows to collect and analyze data in real time [16-17]. This makes it possible to quickly identify bottlenecks in the operation of shunting locomotives and make informed decisions to optimize their operation. Examples of KPIs for export and shunting operations are given in Tables 2 and 3.

Regular data monitoring, the use of modern analysis methods and the introduction of a continuous monitoring system can not only reduce fuel costs but increase the productivity of the shunting locomotive fleet, as well.

Table 2 Examples of KPIs for export and shunting work

Estimated performance of locomotives		Values Norms	Units of measurement
Operating hours of shunting and hauling locomotives	Shift change (delivery and acceptance of the locomotive) - $\tau_{st.shift}$	1	h
	Lunch - τ_{lunch}	1	
	Waiting for work - $\tau_{wait.time}$	2 (acceptable)	
	per shift $\tau_{st.shift} = 12 - (\tau_{shift.ch.} + \tau_{lunch} + \tau_{wait.time})$	10 - 8	
	per day $\tau_{day} = 2 \cdot \tau_{st.shift}$	20 - 16	
	per month $\Sigma \tau_{stand.m.} = 30.4 \cdot \tau_{day}$	$\Sigma \tau_{stand.m.} = 486.4 \div 600.8$	
The amount of downtime		$\Delta \tau_{dt} = \tau_{stand.m.} - \tau_{act.m.}$	
Fuel consumption of shunting and hauling locomotives	$\Sigma G_{cons.m.} = \Sigma G_{act.m.} / \Sigma \tau_{act.time} \cdot \Sigma \tau_{act.m.}$ where: $\Sigma G_{act.m.}$ - fuel consumption by locomotives per month,; $\Sigma \tau_{act.m.}$ - the actual working hours per month, h.	$\Sigma G_{cons.m.}$	l
The amount of fuel overspending		$\Delta G_{fuel.over} = \Sigma G_{act.m.} - \Sigma G_{cons.m.}$	$\Delta G_{fuel.over}$

Table 3 Standard and actual time values for shunting and removal work

Estimated indicator	Designation of the indicator	Units of measurement	Established norms, indicators	Measurement limit of the indicator value		
REMOVAL AND SHUNTING WORK						
The degree of underworking of the locomotives' time	$KPI = \tau_{act.m.} / \tau_{stand.m.}$	-	$\tau_{stand.m.}$ - the established standard of the locomotive's working hours per shift (month);	1 ÷ 0.8	0.8 ÷ 0.75	< 0.75
The amount of downtime	$\Delta\tau_{dt}$	h	$\tau_{act.m.}$ - the actual working time of the locomotive per shift (month);	$\Delta\tau_m = \tau_{stand.m.} - \tau_{act.m.}$		
The amount of inefficient fuel consumption	$\Delta G_{fuel.over}$	l	$G_{idle} = 0.18$ kg/min - fuel consumption at idle	$\Delta G_{fuel.over} = \Delta\tau_m \cdot G_{idle}$		

4 Conclusions

The KPI value eliminates the problem of fuel losses, which are often associated with inappropriate spending and unauthorized fuel discharge.

Efficient use of fuel helps to reduce operating costs and environmental impact.

As a result of this study, the following conclusions were obtained:

- The development and implementation of a key performance indicators (KPIs) system requires careful planning, integration of appropriate tools and resources, as well as continuous monitoring and updating. If implemented correctly, such a system can significantly increase the efficiency of using locomotives and ensure the optimal functioning of railway sidings.
- The expediency of developing and applying this technique lies in its economic efficiency, that is, there is no need to install a fuel flow meter with the appropriate financial costs for their purchase, installation and debugging, eliminating the problems of structural incompatibilities of old diesel locomotives and fuel consumption monitoring and accounting systems.
- Based on the data of timing studies, it is possible to develop more efficient plans and schedules for the

movement of shunting locomotives. This helps to reduce fuel costs, reduce time delays and increase overall productivity

- The development of accounting methods based on time - based research contributes to the introduction of new technologies and methods, which can make the company more competitive and attractive to investors.

Thus, increasing efficiency and reducing costs will contribute to improving the financial performance of the company and its overall stability in the market.

Acknowledgements

This research has been/was/is funded by the Science Committee of the Ministry of Science and Higher Education of the Republic of Kazakhstan (Grant No. AP22688234).

Conflicts of interest

The authors declare that they have no known competing financial interests or personal relationships that could have appeared to influence the work reported in this paper.

References

- [1] ZHANG, Y., LEI, D., LI, X., FU, Y. The analysis of shunting locomotives' operating efficiency based on Gray-Dea. *Research Journal of Applied Sciences, Engineering and Technology* [online]. 2013, **5**(5), p. 1720-1725. ISSN 2040-7459, eISSN 2040-7467. Available from: <https://doi.org/10.19026/rjaset.5.4927>
- [2] ADLBRECHT, J.-A., HUTTLER, B., ZAZGORNIK, J., GRONALT, M. The train marshalling by a single shunting engine problem. *Transportation Research Part C: Emerging Technologies* [online]. 2015, **58**(A), p. 56-72. ISSN 0968-090X, eISSN 1879-2359. Available from: <https://doi.org/10.1016/j.trc.2015.07.006>
- [3] KUZNETSOV, V., KARDAS-CINAL, E., GOLEBIEWSKI, P., LIUBARSKYI, B., GASANOV, M., RIABOV, I., KONDRATIEVA, L., OPALA, M. Method of selecting energy-efficient parameters of an electric asynchronous traction motor for diesel shunting locomotives - case study on the example of a locomotive series ChME3. *Energies* [online]. 2022, **15**(1), 317. eISSN 1996-1073. Available from: <https://doi.org/10.3390/en15010317>
- [4] BOSI, T., BIGI, F., D'ARIANO, A., VITI, F., PINEDA-JARAMILLO, J. Optimal management of full train load services in the shunting yard: a comprehensive study on shunt-in shunt-out policies. *Computers and Industrial Engineering* [online]. 2024, **188**, 109865. ISSN 0360-8352, eISSN 1879-0550. Available from: <https://doi.org/10.1016/j.cie.2023.109865>
- [5] MUSSABEKOV, M., BAKYT, G., OMIRBEK, A., BRUMERCIKOVA, E., BUKOVA, B. Shunting locomotives fuel and power resources decrease. *MATEC Web of Conferences* [online]. 2017, **134**, 00041. eISSN 2261-236X. Available from: <https://doi.org/10.1051/mateconf/201713400041>
- [6] BOYSEN, N., EMDE, S., FLIEDNER, M. The basic train makeup problem in shunting yards. *OR Spectrum* [online]. 2016, **38**, p. 207-233. ISSN 0171-6468, eISSN 1436-6304. Available from: <https://doi.org/10.1007/s00291-015-0412-0>
- [7] WANG, D., ZHAO, J., PENG, Q. Optimizing the loaded train combination problem at a heavy-haul marshalling station. *Transportation Research Part E: Logistics and Transportation Review* [online]. 2022, **162**, 102717. ISSN 1366-5545, eISSN 1878-5794. Available from: <https://doi.org/10.1016/j.tre.2022.102717>
- [8] MURALI, P., ORDONEZ, F., M. DESSOUKY, M. Modeling strategies for effectively routing freight trains through complex networks. *Transportation Research Part C: Emerging Technologies* [online]. 2016, **70**, p. 197-213. ISSN 0968-090X, eISSN 1879-2359. Available from: <https://doi.org/10.1016/j.trc.2015.08.022>

- [9] ABDULLAYEV, S., TOKMURZINA-KOBERNYAK, N., ASHIRBAYEV, G., BAKYT, G., IZBAIROVA, A. Simulation of spring-friction set of freight car truck, taking into account track profile. *International Journal of Innovative Research and Scientific Studies* [online]. 2024, **7**(2), p. 755-763. eISSN 2617-6548. Available from: <https://doi.org/10.53894/ijirss.v7i2.2883>
- [10] CORMAN, F., MARRA, A., PACCIARELLI, D., SAMA, M. Integrating train scheduling and delay management in real-time railway traffic control. *Transportation Research Part E: Logistics and Transportation Review* [online]. 2017, **105**, p. 213-239. ISSN 1366-5545, eISSN 1878-5794. Available from: <https://doi.org/10.1016/j.tre.2016.04.007>
- [11] REICHMANN, M., HIMMELBAUER, G. S., WAGNER, A., ZAJICEK, J., STADLMANN, B., WANCURA, H., FURIAN, N., VOSSNER, S. Introducing the concept of grades of automation for shunting operations. *Journal of Rail Transport Planning and Management* [online]. 2025, **33**, 100500. ISSN 2210-9706, eISSN 2210-9714. Available from: <https://doi.org/10.1016/j.jrtpm.2024.100500>
- [12] KALEM, A., TADIC, S., KRSTIC, M., CABRIC, N., BRANKOVIC, N. Performance evaluation of railway infrastructure managers: a novel hybrid fuzzy MCDM model. *Mathematics* [online]. 2024, **12**, 1590. eISSN 2227-7390. Available from: <https://doi.org/10.3390/math12101590>
- [13] ABDYKADYROV, A., MARXULY, S., BAIKENZHEYEVA, A., BAKYT, G., ABDULLAYEV, S., KUTTYBAYEVA, A. E. Research of the process of ozonation and sorption filtration of natural and anthropogenically polluted waters. *Journal of Environmental Management and Tourism* [online]. 2023, **14**(3), p. 811-822. eISSN 2068-7729. Available from: [https://doi.org/10.14505/jemt.v14.3\(67\).20](https://doi.org/10.14505/jemt.v14.3(67).20)
- [14] LYSENKO, N., KUZNETSOVA, A., KUZNETSOV, S. On the issue of efficiency of shunting diesel locomotives at cargo terminals. *World of Transport and Transportation* [online]. 2020, **18**(1), p. 170-183. ISSN 1992-3252. Available from: <https://doi.org/10.30932/1992-3252-2020-18-170-183>
- [15] ABDULLAYEV S., BAKYT G., TOKTAMYSSOVA A., ASHIRBAYEV G., BAUBEKOV Y., IMASHEVA G. Determination of parameters of upper assembly of current collector when it interacts with contact suspension. *Vibroengineering Procedia* [online]. 2024, **54**, p. 279-284. ISSN 2345-0533, eISSN 2538-8479. Available from: <https://doi.org/10.21595/vp.2024.23917>
- [16] WANG, D., ZHAO, J., PENG, Q. Optimizing the loaded train combination problem at a heavy-haul marshalling station. *Transportation Research Part E: Logistics and Transportation Review* [online]. 2022, **162**, 102717. ISSN 1366-5545, eISSN 1878-5794. Available from: <https://doi.org/10.1016/j.tre.2022.102717>
- [17] JAEHN, F., RIEDER, J., WIEHL, A. Single-stage shunting minimizing weighted departure times. *Omega* [online]. 2015, **52**, p. 133-141. ISSN 0305-0483, eISSN 1873-5274. Available from: <https://doi.org/10.1016/j.omega.2014.11.001>



This is an open access article distributed under the terms of the Creative Commons Attribution 4.0 International License (CC BY 4.0), which permits use, distribution, and reproduction in any medium, provided the original publication is properly cited. No use, distribution or reproduction is permitted which does not comply with these terms.

ALGORITHM FOR MAKING THE OPTIMAL DECISION FOR FURTHER OPERATION OF FREIGHT CARS

Adil Kadyrov, Perizat Baigozhina, Aliya Kukesheva, Imanov Marat, Akbope Karsakova*

Abylkas Saginov Karaganda Technical University NPJSC, Karaganda, Kazakhstan

*E-mail of corresponding author: karsakova84@mail.ru

Adil Kadyrov 0000-0001-7071-2300,
Aliya Kukesheva 0000-0002-3063-5870,
Akbope Karsakova 0009-0005-0305-6741

Perizat Baigozhina 0000-0002-8583-3292,
Imanov Marat 0000-0002-7963-5417,

Resume

The article deals with the methodology of selecting the optimal decision for the maintenance and operation of freight cars.

The statistics of failures for the main units of freight cars has been collected. A hypothesis has been proposed about the method of selecting a decision based on the optimality criterion, i.e. the maximum profit. The optimality criterion is the difference between the income and the costs and is the function of the frequency of certain operations on each of the car units.

An algorithm has been developed that allows for the effective optimization of the processes of operating, repairing, and writing-off the cars, ensuring an increase in the competitiveness of rail transport due to the rational use of resources and optimization (reduction) of costs.

Article info

Received 6 May 2025

Accepted 25 July 2025

Online 16 September 2025

Keywords:

freight car
decision-making algorithm
optimality criterion
profit maximization
probability of failure
failure rate
failure-free operation

Available online: <https://doi.org/10.26552/com.C.2025.049>

ISSN 1335-4205 (print version)

ISSN 2585-7878 (online version)

1 Introduction

Rail freight transport plays the key role in global logistics due to its cost-effectiveness and ability to transport large volumes over long distances. In recent years, there has been a significant increase in demand for freight cars, especially in such countries as India, China, the United States and Russia [1].

The increase in demand for cars is caused by the global economic recovery, the growth in trade and industrial production. In addition, the strict environmental standards and the desire to reduce carbon emissions have contributed to the transition from road to rail transport in several regions [2]. This has strengthened the position of rail freight as an environmentally friendly and cost-effective mode of transportation.

The global freight car market growth forecast presented in the SCI Verkehr report (2024) indicates an annual increase of 2.6% until 2028 [3].

The growth in demand for freight cars in the railway industry of Kazakhstan is caused by several key factors that are related to the economic, infrastructural and geographical features of the country: increasing

the volume of exports of raw materials, developing the transit potential, depreciation of the existing rolling stock, investments in the railway infrastructure modernization, the growth of agricultural production, and increasing the volume of domestic transportation.

The data of analytical research show that the rolling stock fleet of Kazakhstan owned by state railways has decreased by half, while the fleet of private companies has increased more than sevenfold. Private companies need an approach to operation that leads to increased profits [4].

A significant portion of the current rolling stock has been in operation for more than 10-15 years. This causes a high level of wear and tear and an increase in maintenance costs [5-6]. A significant portion of the cars that have been in operation for over 25 years require either major repairs or write-offs, which leads to additional costs and possible disruptions in transportation.

Before each trip, freight cars undergo mandatory maintenance, including checking their main components and mechanisms [7-11].

Modern diagnostic technologies are used to identify faults: thermal imagers, acoustic systems

and automated control systems [12-18]. However, it is necessary to develop and to implement methods of predicting the condition of cars. The existing forecast methods, including extrapolation, expert assessments and modelling, have a number of limitations [19-20]. As researchers note, such approaches do not completely eliminate the risk of malfunctions and emergency situations.

The main difficulties of the freight car market are related to high capital expenditures for servicing and upgrading the fleet [20-21]. Despite advances in diagnostics and maintenance, the issues of increasing reliability of cars remain relevant. This requires developing the new systems for predicting the technical condition of cars, which will reduce downtime and increase operational efficiency.

The hypothesis of the study is the possibility of increasing profitability of car operation by optimizing the decision for technical maintenance, repair and their operation, taking into account the costs of various activities and the relative frequency of failures.

The aim of the work was to develop and to justify the methodology of optimizing the processes of operating, repairing and writing-off the cars, aimed at increasing their reliability and economic efficiency.

The main criterion for assessing the effectiveness of the proposed methodology is profit maximization,

which emphasizes its importance for increasing the competitiveness of rail transport.

The scientific novelty consists in the development of an algorithm graph for making an optimal decision for the operation of freight cars based on the probabilistic analysis of failures and economic efficiency.

The practical significance lies in the possibility of minimizing the costs of servicing the cars, increasing reliability of their operation and optimizing the use of resources.

2 Materials and methods

The use of the criteria approach to selecting the optimal decision for the operation of railway rolling stock (freight cars) can significantly improve the efficiency of operation. Based on this assumption, the analysis of gondola cars as the most popular and widely used type of freight cars was carried out [22]. Their versatility and significant share in the total wagon fleet determine the feasibility of selecting this object for research.

The proposed hypothesis forms the methodology that, despite being focused on gondola cars, can be adapted to any type of railway rolling stock, which significantly expands its scope of application and confirms its versatility.

Table 1 Collected statistical data of the availability and repair of faulty freight cars (F. CA-31)

No.	Car No.	Year of manufacturing	Last repair type			Time of admission to the faulty ones		Time of dispatch for repair	
			Marking stamp	Date	Fault code	Date	Time	Date	Time
1	53788485	1990	608	09.01.2020	445	22.04.2013	5h 41min.	26.04.2023	20:55
2	94752219	1988	1181	21.05.2018	571	12.01.2020	6h 42min.	15.02.2020	07:08
3	53784518	1991	608	30.11.2019	571	12.01.2020	18h 19min.	14.01.2021	02:37
4	24023988	1975	721	06.01.2017	570	17.01.2020	15h 59min.	22.01.2020	22:36
5	94752912	1988	1181	19.01.2018	571	04.02.2020	16h 45min.	15.02.2020	07:08
6	94305364	1988	697	16.07.2017	571	04.02.2020	16h 45min.	16.02.2020	10:45
7	94343217	2008	698	03.03.2018	572	10.02.2020	17h 55min.	17.02.2020	01:53
8	94283850	2011	612	16.02.2018	572	10.02.2020	17h 55min.	17.02.2020	01:53
9	60262052	2005	691	30.04.2016	572	12.02.2020	23h 20min.	17.02.2020	01:55
10	60259587	2010	745	09.04.2018	572	12.02.2020	2h 50min.	13.02.2020	04:20
11	50256239	1980	697	29.12.2016	570	14.02.2020	12h 03min.	28.02.2020	06:50
12	57302887	1986	697	13.12.2016	570	14.02.2020	12h 03min.	28.02.2020	06:50
13	62217567	1985	220	27.02.2017	571	15.02.2020	11h 10min.	21.02.2020	06:50
14	52052693	2011	1016	20.07.2017	572	28.02.2020	13h 15min.	02.02.2020	23:54
15	24344442	1989	692	10.03.2017	570	01.03.2020	02h 10min.	02.03.2020	23:54
16	63912646	1998	695	15.10.2018	571	07.03.2020	21h 50min.	21.03.2020	05:18
17	94504404	2009	900	29.10.2017	572	09.03.2020	02h 05min.	11.03.2020	12:35
18	60358983	2005	220	22.10.2018	572	13.03.2020	12h 35min.	13.03.2020	13:05
19	28025104	2006	720	25.11.2017	107	13.03.2020	04h 25min.	17.03.2020	07:59
20	55303788	2010	341	22.06.2017	572	15.03.2020	04h 57min.	18.03.2020	07:40
21	90887647	1979	608	19.02.2019	571	28.03.2020	22h 55min.	05.04.2020	06:09

At the first stage of the research work, a summary of statistical information of freight car defects was carried out, based on the data for the period from 2022 to 2024. The main sources of information were the automated wagon fleet database (AWFDB), the automated system for operational management of transportation at the road level (ASONM), and the book of records of the presence and repair of faulty wagons of the freight fleet (form of Carriage accounting-31 (F.CA-31)) [23-24]. The information of freight cars uncoupled for repair work is presented in Table 1.

When analyzing the data on faulty freight cars, parameters recording the technical condition and repair history of the rolling stock were used. Here is provided an explanation of some columns, such as “brand” and “malfunction code” indicated in Table 1.

Brand is a conventional designation (digital or alphanumeric code) assigned to a car by a repair enterprise or depot where the last major or depot repair was performed.

Malfunction code is a numeric identifier corresponding to the classifier of typical failures and defects of freight cars included in the Commonwealth of Independent States (CIS), as well as Latvia, Lithuania and Estonia. Each code reflects a certain type of technical malfunction. For example, code 445 may mean wear of the side frame, 571 - an axle crack, 570 - a defect in the car body, etc [25]. During the study, certificates (Appendix A) of various forms were requested for each freight car, which made it possible to determine the number of times the car was uncoupled, when it was sent for repairs during its service life, the year the car was manufactured, the manufacturer of the car, etc.

When analyzing the data of defective freight cars, the parameters were used that provided the technical condition and the repair history of the rolling stock.

Here is an explanation of some of the columns, such as the “a stamp” and “fault code” listed in Table 1.

The stamp is a symbol (a numeric or an alphanumeric code) assigned to a car by a repair company or depot where the last major or depot repairs were performed [26].

Additionally, the Karaganda operational wagon depot of the NC KTZh JSC (Republic of Kazakhstan) collected the information of the technical condition of wagons and their operation for the period 2022-2024 at the Karaganda branch of the railway.

The analysis of the presented data revealed the most common types of freight car malfunctions and the main components that cause their uncoupling for routine uncoupling repairs (RUR). Based on the collected information, the classification of malfunctions was performed, including the following units: wheel pairs, automatic brake equipment, automatic coupling devices, body, etc.

As an example, Figure 1 shows in detail the main types of malfunctions (deformations) of the gondola car body.

The faults of covered cars include damage to the roof (a, b), weakening or absence of doors (c, d, e), presence of holes, cracks and dents in the skin (e, g, h, i), damage to the floor with holes (k), as well as malfunction or absence of locking devices (l, m) (Figure 2).

The collected data of the Karaganda operational wagon depot of the NC KTZh JSC (Republic of Kazakhstan) are presented in graphic form, which made it possible to visualize the share of each category of faults (Figure 3).

The analysis of the data for 2022-2024 shows that in 2023, the number of faulty cars uncoupled for repairs increased significantly compared to 2022. Uncoupling for trailer equipment increased by 993 units, for the body by 3,106 units, and for the “other” categories by 1,321 units.

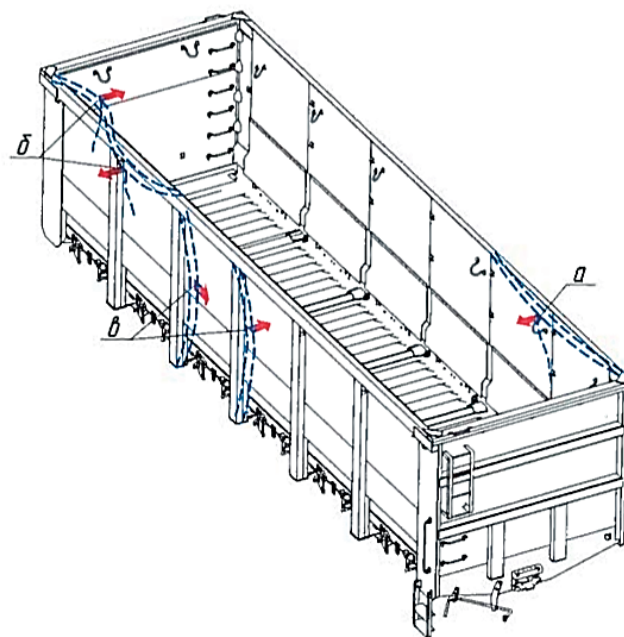


Figure 1 Types of deformations of gondola car bodies: a - widening of the body; b - body skew; c - deflection, dent of pillars

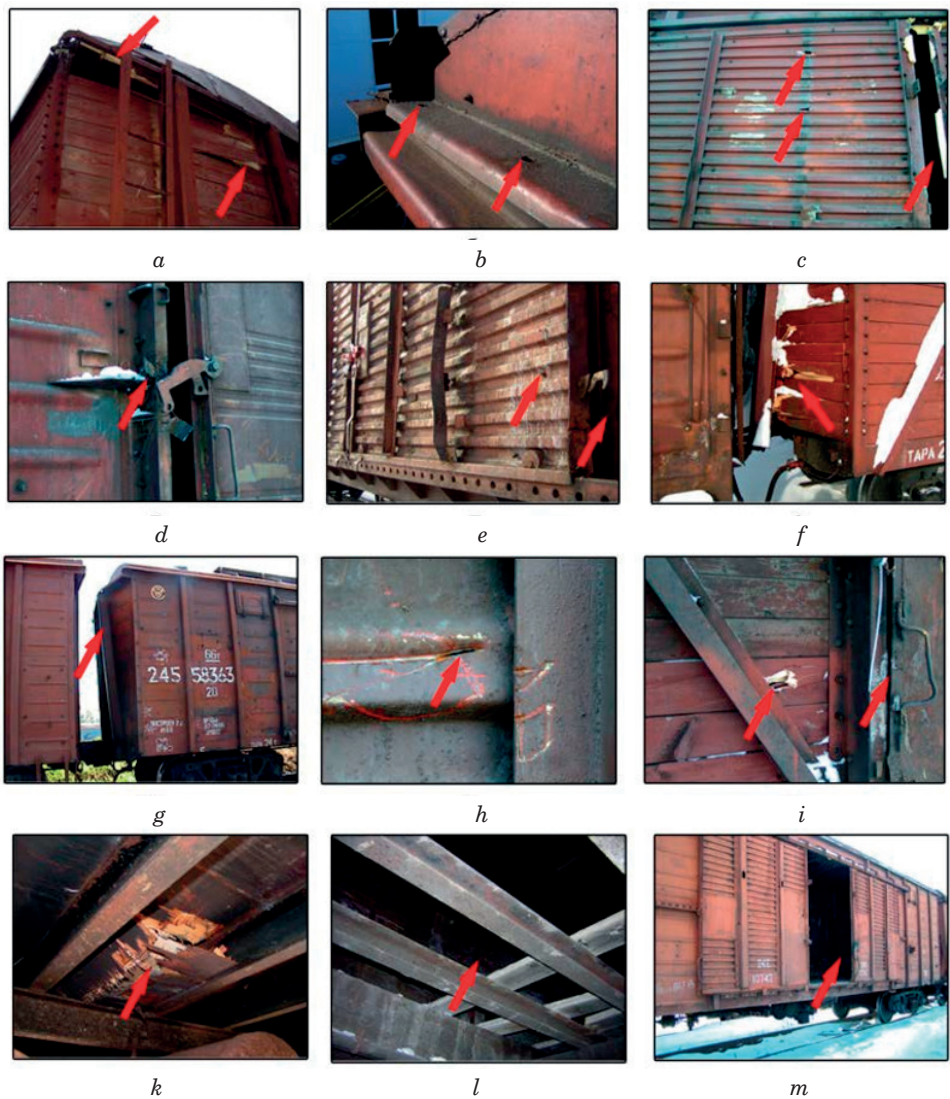


Figure 2 Main types of covered cars faults

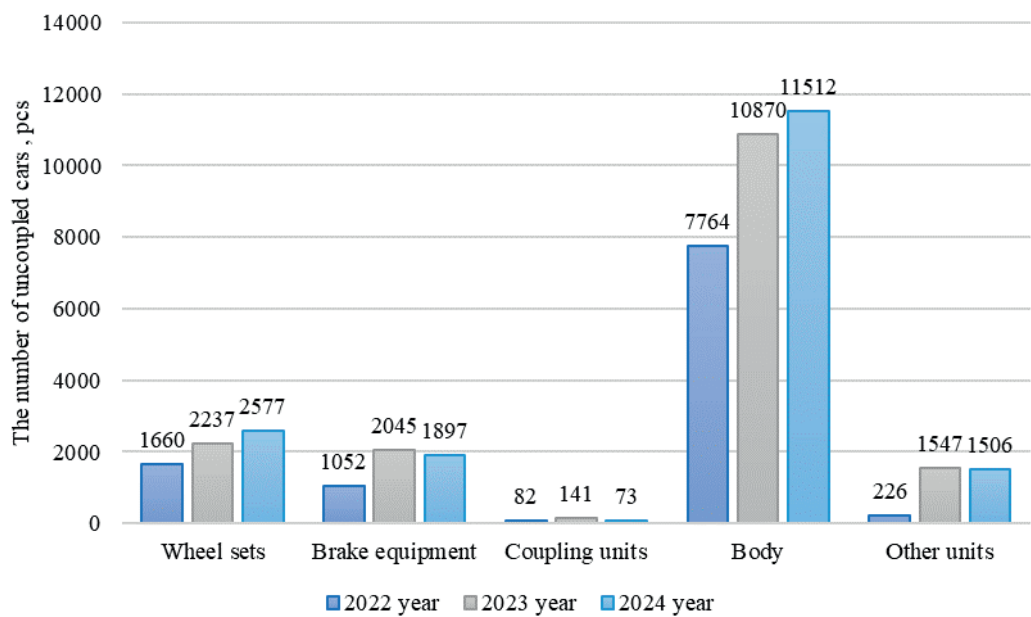


Figure 3 Number of technically faulty cars uncoupled at the technical maintenance points (TMP) of the Karaganda branch (Republic of Kazakhstan) in 2022-2024

Significant growth was also observed for wheel sets and automatic coupling devices.

In 2024, the situation changed, as the number of uncoupling decreased for some units, but for critical elements such as wheel sets and the body, the growth continued by 340 and 642 units, respectively. This indicates that the problem remains relevant and requires the adoption of correct, effective measures.

Statistics confirm the need for an optimal selection of decision-making on the operation of freight cars. To correctly select the decision, it is necessary to develop a decision-making algorithm. A graph of the algorithm for making a decision on the operation of a freight car has been developed. The algorithm is presented in Figure 4 and is implemented using the example of gondola cars, the most universal and popular type of freight cars, which are widely used in various types of transportation and also make up the largest share in the car fleet of the Republic of Kazakhstan (42.6%) [27].

The algorithms for choosing the optimal solution for wheelsets, car brakes, bodywork, and the other components and parts are similar to the algorithm for maintenance of auto couplers. For the sake of brevity, these graphs are given in appendix B.

The graph defines a sequence of steps for selecting

the optimal scenario based on the technical condition of the car and economic indicators. Changes in economic conditions, associated with the fact that most of the car fleet is privately owned, made it possible to formulate the optimality criterion as the maximum profit. To establish the maximum optimality criterion, it is necessary to analyze the costs of repairs and potential income from further operation of the freight car.

To make the optimal decision on further operation of the freight car, a detailed analysis of its condition is carried out, which begins with a technical inspection upon arrival or during the formation of a train at the technical maintenance points (TMP) of the station. As a part of the initial inspection, the condition of the main units is assessed. Based on the inspection results, the degree of wear and tear and the need for repair are determined. Then, a decision is made to put the car in for repair in accordance with one of the three key rules of technical maintenance given in Table 2.

The graph includes the following main scenarios:

- initial inspection of the technical condition of the car: assessment of the units (wheel pairs, trailer equipment, automatic coupling devices, body and other elements) and determination of the degree of wear and the need for repair;

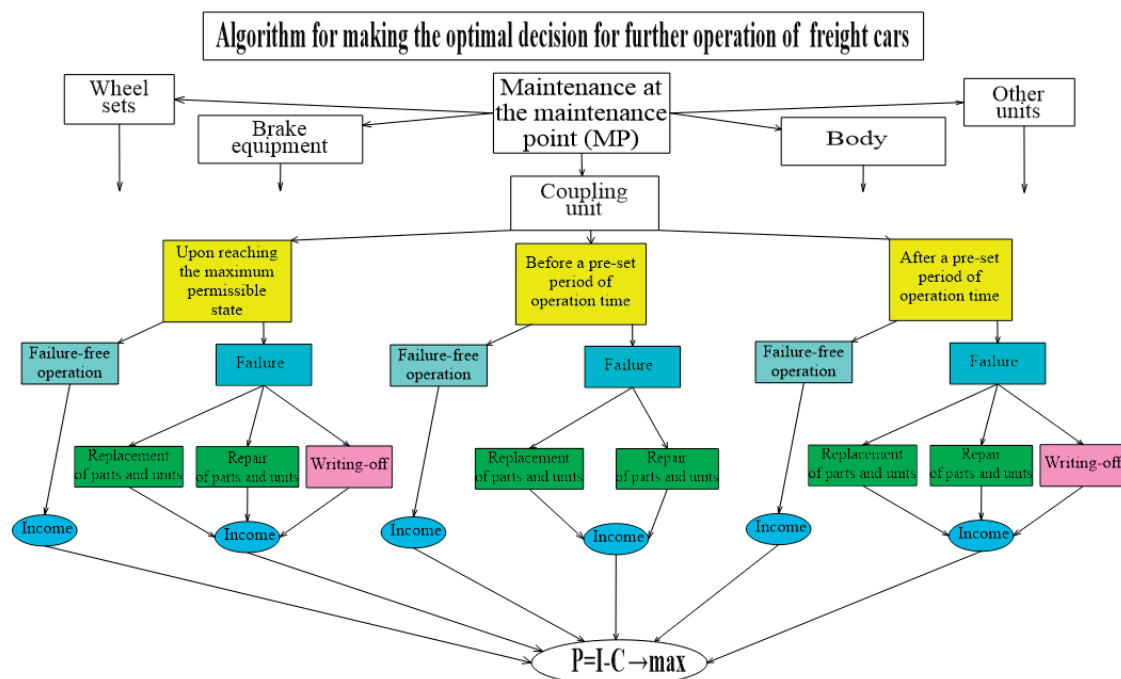


Figure 4 The decision-making algorithm for the further operation of the freight car

Table 2 Freight car technical maintenance guidelines [28-29]

No.	Technical maintenance rule	Description
1	Limit state rule	Repairs are carried out when a unit or part reaches a set wear limit or technical condition.
2	Calendar term rule	Maintenance and repairs are carried out after a predetermined period of time, regardless of the condition of the car.
3	Mean time between failures rule	Repairs are carried out upon the occurrence of a malfunction or complete failure of a unit or part.

- decision making based on the condition of the units: the malfunction is not critical, i.e. the car is allowed for further operation with minimal costs. A moderate malfunction is possible, which requires routine repairs, after which the car is returned to operation, or a critical malfunction, when the car is subject to major repairs or write-off;
- assessment of the economic feasibility of repairs: comparison of the repair costs to the projected income from the remaining service life of the car. If the repair is justified, then the repair work is carried out and the car is returned to operation. If the repair is unprofitable, it is necessary to consider options for writing off the car or selling it on the secondary market;
- optimization of the decision based on the income and cost analysis: selection of the scenario with the maximum profit, if the income from operation exceeds the costs of repairs and maintenance, the car remains in operation.

3 Decision-making algorithm

1. The car undergoes a technical inspection, worn-out wheel sets are identified.
2. The costs of their replacement and the potential income from operating the car after repair are analyzed.
3. If the replacement of parts or units will cost an amount comparable to the income from operation, a decision is made to repair.
4. If the repair costs exceed the income, the car is written off.

Selecting the optimality criteria depends on the priorities and goals, as well as on the specifics of the activities, external conditions. Depending on the goals and conditions of operation, various criteria can be selected. In the case, to assess the efficiency of operating freight cars, the key criterion is profit maximization.

The profit maximization is the main indicator of the economic efficiency of any transport system in the context of modern commodity-money relations. The basis of this approach is the objective function of the optimality criterion, aimed at achieving maximum profit at minimum costs. Profit maximization is the difference between income from operation and the sum of all the costs:

$$\max(P) = I_{rso} - \sum C_i; \quad (1)$$

where $\sum C_i$ consists of the following:

C_{repl} are costs for replacing units and parts;

C_{rep} are costs for repairing units and parts;

C_{wof} are costs for writing-off the car loss of residual resource;

$\max(P)$ is the maximum profit;

I_{rso} is the income from the rolling stock operation (or form

selling its units and parts when written-off) per unit of time or run.

To make an optimal decision, it is necessary to meet the optimality condition that consists of maximizing the profits, while minimizing costs, which allows selecting the most profitable option for the operation, repair or decommissioning of rolling stock:

$$C_{opt} = \min(\sum C_j) \text{ at this } I_{rso} - \sum C_i; \quad (2)$$

This condition means that the minimum costs should ensure a positive income from further operation of the car.

Efficient management of freight car operation requires analyzing the probabilities of failures and failure-free operation of their main units. These are the key indicators to predict the repair costs, to assess reliability of the system and to make informed decisions aimed at increasing the economic efficiency of rolling stock operation.

To analyze the economic efficiency of car operation and to develop an optimal decision-making algorithm, an example of calculating the probabilities of failures for the main units of the rolling stock is given. The analysis is based on statistical data from the Karaganda branch of the railway (Republic of Kazakhstan) for 2023, presented in Figures 1, 2. Based on these data, as well as on the given formulas, the probabilities of failures are included in the calculation of profits and costs. This allows determining the optimal decision-making algorithm for further operation of the rolling stock.

The probability of a unit or system failure shows the frequency of malfunctions over a certain period of time. It is determined based on the statistical data that allow predicting which units require more attention. It is calculated using the formula:

$$F(t) = 1 - e^{-\lambda t}; \quad (3)$$

where λ is the failure rate;

t is the operation time.

The uptime $P(t)$ probability reflects the ability of a component to function without failure for a given period. The higher this probability, the lower the repair and replacement costs. It is determined by the formula:

$$F(t) = e^{-\lambda t}; \quad (4)$$

where λ is the failure rate;

t is the unit operation time.

Determining the probability of failure is directly related to the processing of large volumes of statistical data, which in some cases can be complicated. In this study, to simplify the calculations, the failure rate (relative failure frequency) was used, which allows for a high-precision reflection of the share of failures of each unit relative to the total number of recorded faults. This approach ensures sufficient reliability of the results and

allows for their effective integration into subsequent analysis of the operational reliability of rolling stock.

The failure rate (λ) characterizes the frequency of failures per unit of operating time:

$$\lambda = \frac{n_i}{N \cdot t}; \quad (5)$$

where $n_{i \text{ fail}}$ is the number of failures of a certain i -th unit $n_{i \text{ fail unit}}$;

$n_{1 \text{ fail unit}}$ is the total number of wheel set failures per year;

$n_{2 \text{ fail unit}}$ is the total number of brake equipment failures per year;

$n_{3 \text{ fail unit}}$ is the total number of the coupling unit failures per year;

$n_{4 \text{ fail unit}}$ is the total number of the body failures per year;

$n_{5 \text{ fail unit}}$ is the total number of the other units failures per year;

N is the total number of the processed cars;

t is the tile of operation (the year time).

The calculated failure rates, failure probabilities and failure-free operation probabilities serve as the basis for assessing the economic efficiency of car operation. Those indicators are included in the calculation of profits and maintenance costs, which allows making informed decisions on optimizing operation and repair processes. This approach allows developing an optimal decision-making algorithm aimed at reducing costs and increasing reliability of car operation.

The current state of operation or downtime of cars is taken into account by introducing the existence coefficient (α_i). This coefficient reflects the current operating status of each unit or rolling stock as a whole:

- if the car is idle on the tracks without work, the existence coefficient $\alpha_i = 1$;
- if the car is in operation, the existence coefficient $\alpha_i = 0$.

The calculation formula is as follows:

$$P > I - \alpha_0 \cdot C_{id} - \sum_{i=1}^5 \alpha_i \cdot p(t)_i \cdot 3i; \quad (6)$$

where I is the income from the rolling stock operation (tg);

α_0 is the existence coefficient of the idle costs;

C_{id} is the idle costs (tg);

α_i is the existence coefficient of the costs for repairing units (if the repair was made, $\alpha_i = 1$, if not, $\alpha_i = 0$);

$p(t)_i$ is the failure-free operation of the unit i ;

C_i is the costs for repairing or replacing unit i .

In this case, Equation (6) has the form:

$$\begin{aligned} P > I - \alpha_0 \cdot C_{ip} - \alpha_1 \cdot p(t)_1 \cdot C_1 + \\ &+ \alpha_2 \cdot p(t)_2 \cdot C_2 + \alpha_3 \cdot p(t)_3 \cdot C_3 + \\ &+ \alpha_4 \cdot p(t)_4 \cdot C_4 + \alpha_5 \cdot p(t)_5 \cdot C_5; \end{aligned} \quad (7)$$

where I is the income from the rolling stock operation (tg);

α_0 is the existence coefficient of the idle costs;

C_i is the idle costs (tg);

α_1 is the factor of necessity to repair wheel sets (if repair was made, $\alpha - 1$, if not, $\alpha - 0$);

α_2 is the factor of necessity to repair brake equipment (if repair was made, $\alpha - 1$, if not, $\alpha - 0$);

α_3 is the factor of necessity to repair coupling units (if repair was made, $\alpha - 1$, if not, $\alpha - 0$);

α_4 is the factor of necessity to repair the body (if repair was made, $\alpha - 1$, if not, $\alpha - 0$);

α_5 is the factor of necessity to repair the other units (if repair was made, $\alpha - 1$, if not, $\alpha - 0$);

$p(t)_1$ is the probability of failure-free operation of the wheel set;

$p(t)_2$ is the probability of failure-free operation of the brake equipment;

$p(t)_3$ is the probability of failure-free operation of the coupling units;

$p(t)_4$ is the probability of failure-free operation of the body;

$p(t)_5$ is the probability of failure-free operation of the other units;

C_1 is costs for repair or replacement of a wheel set;

C_2 is costs for repair or replacement brake equipment;

C_3 is costs for repair or replacement coupling units;

C_4 is costs for repair or replacement of the body;

C_5 is costs for repair or replacement of the other units.

The novelty of the proposed dependences in Equations (6) and (7) is the introduction of the existence coefficient of costs, which can be equal to 0 or 1. The introduction of this coefficient allows combining all the existing decision options into one formula.

The probability addition is used if the failure of one unit itself leads to the failure of the entire system. This is typical for a series connection of elements, where the failure of any unit causes the failure of the entire car.

For a freight car, it is logical to apply the probability addition formula, since the failure of even one critical unit (brakes or wheel pairs) makes operation impossible and unsafe.

$$P_{car} = 1 - \prod_{i=1}^n (1 - P_i), \quad (8)$$

where P_{car} is the probability of failure of the whole system (car);

P_i is the probability of failure of each unit;

n is the total number of units.

If the failure of any of the car systems (brakes, wheel sets or body) leads to the failure of the car as a whole, then this formula is suitable.

4 An example of selecting the optimal decision for maintenance and operation of freight cars

To calculate the failure rate, the data on the number of cars processed per year is required. Figure 5 shows the quantitative indicators of cars processed at maintenance points (MP) for the Karaganda branch of the railway (Republic of Kazakhstan).

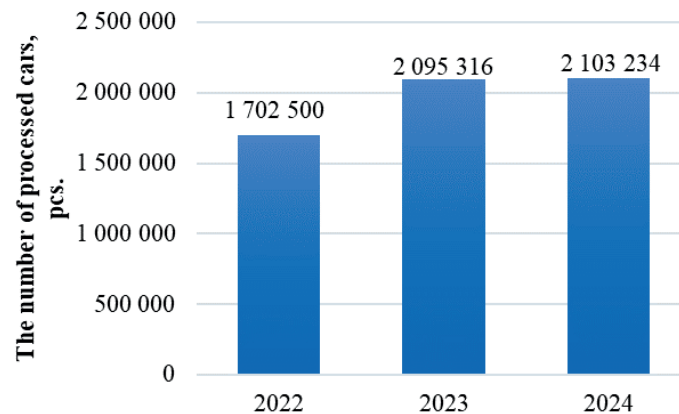


Figure 5 The number of processed cars at the Karaganda branch of the road for 2022-2024

Table 3 Failure rate (λ) for units

No.	Unit	Failure rate (λ) for 2022	Failure rate (λ) for 2023	Failure rate (λ) for 2024
1	Wheel sets	0.000975	0.001067	0.001225
2	Brake equipment	0.000618	0.000976	0.000902
3	Coupling devices	0.000048	0.000067	0.000035
4	Body	0.004562	0.005188	0.005472
5	Other	0.000133	0.000738	0.000716

Table 4 Failure probability ($q(t)$) for units

No.	Unit	Failure probability ($q(t)$) for 2022	Failure probability ($q(t)$) for 2023	Failure probability ($q(t)$) for 2024
1	Wheel sets	0.6843	0.7022	0.7340
2	Brake equipment	0.4661	0.6017	0.5874
3	Coupling devices	0.0491	0.0626	0.0344
4	Body	0.9822	0.9934	0.9952
5	Other	0.1074	0.5077	0.5057

Table 5 Failure-free operation probability ($p(t)$)

No.	Unit	Failure-free operation probability ($p(t)$) for 2022	Failure-free operation probability ($p(t)$) for 2023	Failure-free operation probability ($p(t)$) for 2024
1	Wheel sets	0.3157	0.2978	0.2660
2	Brake equipment	0.5339	0.3983	0.4126
3	Coupling devices	0.9509	0.9374	0.9656
4	Body	0.0178	0.0066	0.0048
5	Other	0.8926	0.4923	0.4943

The calculation of the failure rate (λ), failure probability ($q(t)$) and failure-free operation probability ($p(t)$) for the units was made based on the data presented in Figures 1 and 2 for 2023, in accordance with the data given in Tables 3, 4 and 5.

The highest failure probability is for the car body (0.9934), which indicates its high wear and tear and the need for regular maintenance. The wheel pairs and brake equipment also require special attention, as their

failure probability is 0.7022 and 0.3017, respectively. At the same time, automatic coupling devices have demonstrated the highest reliability (0.0626), which makes them the least expensive to operate.

Calculation of the costs is done for each unit by substituting the conditional values according to Table 6:

1. For the wheel sets:

$$\alpha_1 \cdot p(t)_1 \cdot C_1 = 1 \cdot 0.2978 \cdot 313 = 93.2 \text{ Euro};$$

Table 6 Initial data for calculations

Parameter	Value, Euro
Income (I)	2 083
Idle costs (C_{id})	417
Repair costs	
Wheel sets (C_1)	313
Brake equipment (C_2)	208
Coupling units (C_3)	104
Body (C_4)	625
Other units (C_5)	146
Failure probability (v_i)	
Wheel sets (v_1)	0.133
Brake equipment (v_2)	0.121
Coupling units (v_3)	0.008
Body (v_4)	0.646
Other units (v_5)	0.092
Existence coefficients (α_i)	
Cost existence coefficients (α_0)	1
Wheel sets (α_1)	1
Brake equipment (α_2)	0
Coupling units (α_3)	0
Body (α_4)	1
Other units (α_5)	1

2. For the brake equipment:
 $\alpha_2 \cdot p(t)_2 \cdot C_2 = 0 \cdot 0.3983 \cdot 208 = 0$ Euro;
 3. For the coupling units:
 $\alpha_3 \cdot p(t)_3 \cdot C_3 = 0 \cdot 0.9374 \cdot 104 = 0$ Euro;
 4. For body:
 $\alpha_4 \cdot p(t)_4 \cdot C_4 = 1 \cdot 0.0066 \cdot 625 = 4.13$ Euro;
 5. For the other units:
 $\alpha_5 \cdot p(t)_5 \cdot C_5 = 1 \cdot 0.4923 \cdot 146 = 71.89$ Euro;
- The total costs for repair:
 $93.2 + 0 + 0 + 4.13 + 71.89 = 169.22$ Euro.
- The probable profit:
 $P = 2083 - 1 \cdot 147 - 169.22 = 2083 - 417 - 169.22 = 1496.78$ Euro.
- Calculation of the total failure probability is done according to Equation (9):

$$P_{car} = 1 - [0.2978 \cdot 0.3983 \cdot 0.9374 \cdot 0.0066 \cdot 0.4923] \approx 0.999. \quad (9)$$

The total probability of car failure was 99.9%, which significantly exceeds the critical level of 0.5. This fact emphasizes the need for immediate technical intervention, including major repairs or decommissioning of the car.

Based on the presented calculations and analysis of the failure probabilities, the technical condition of the units and the total costs, the following decision to decommission the car was made based on the optimal decision-making graph (Figure 1), since the

total probability of failure is 99.9%, which significantly exceeds the critical level of 0.5. This means that the car is in a state of high accident rate and its further operation is impossible without significant interventions, and the main unit requiring repair - the body, has a critically high probability of failure (0.9934). This indicates its high wear, which makes restoration extremely ineffective, since the cost of replacing the body is actually approaching the cost of a new car.

It is not economically feasible to carry out a major overhaul of the car in the case if:

- the total cost of the repair is 169.22 Euro, but this does not include the replacement of the body, which is the main problem.
- after the repair, there is a high probability of new failures, which will lead to additional costs in the future.
- the car downtime during the repair increases operational losses, reducing the economic efficiency of the restoration.

According to the decision-making column, if the probability of failure exceeds the permissible level and a major overhaul is not economically viable, the car is subject to writing-off.

Based on the above, as well as on the analysis of the technical condition and economic efficiency, the optimal decision is to write-off the car, since further operation is impossible without significant costs, and a major overhaul does not justify the invested funds.

5 Results and discussion

Thus, the analysis confirms that the car body is the most vulnerable unit that requires careful monitoring and timely repair. Automatic coupling units on the contrary show the lowest failure rate, which makes them the most reliable.

Having analyzed possible scenarios of operation and failure of freight cars, there can be drawn the following conclusions:

- The greatest number of failures occurs in the body, which requires development of new approaches to its maintenance and repair.
- It is economically advantageous to pay attention to the restoration of automatic coupling units, since their probability of failure is minimal.
- The probability of failure-free operation of brake equipment and wheel sets is at the level of

about 87-88%, which requires regular preventive maintenance.

The use of this algorithm for making decisions on the operation of freight cars allows minimizing the financial costs for maintenance and repair, ensuring the maximization of profits and operational reliability of the rolling stock. Based on the data provided, the probability of profit is 1496.78 Euro. This approach takes into account the probability of failure-free operation of units, minimizes costs and helps to make an informed decision for the efficient operation of wagons.

Based on the analysis and calculations of the failure rate, failure probabilities and failure-free operation of freight car units, the following data were obtained (presented in Figures 6-8).

The highest probability of failures is for the car body (0.9934), which indicates the significant wear or high load on this unit. For automatic brake equipment, other

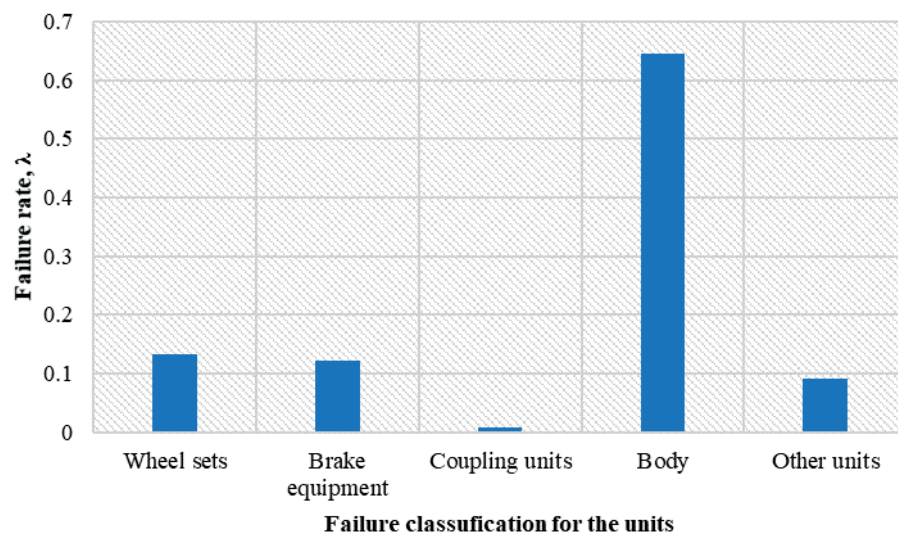


Figure 6 Failure rate of freight car units on the Karaganda branch of the railway for 2023

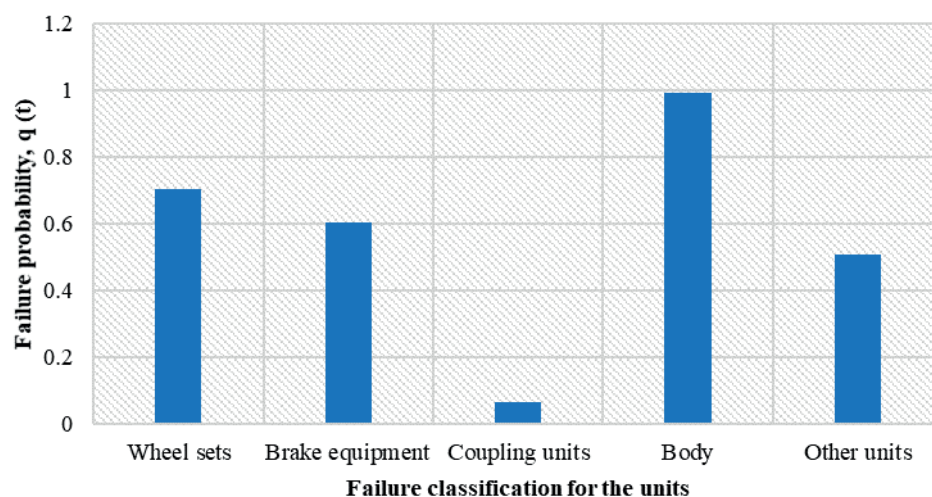


Figure 7 Probability of failure of freight car units on the Karaganda branch of the road for 2023

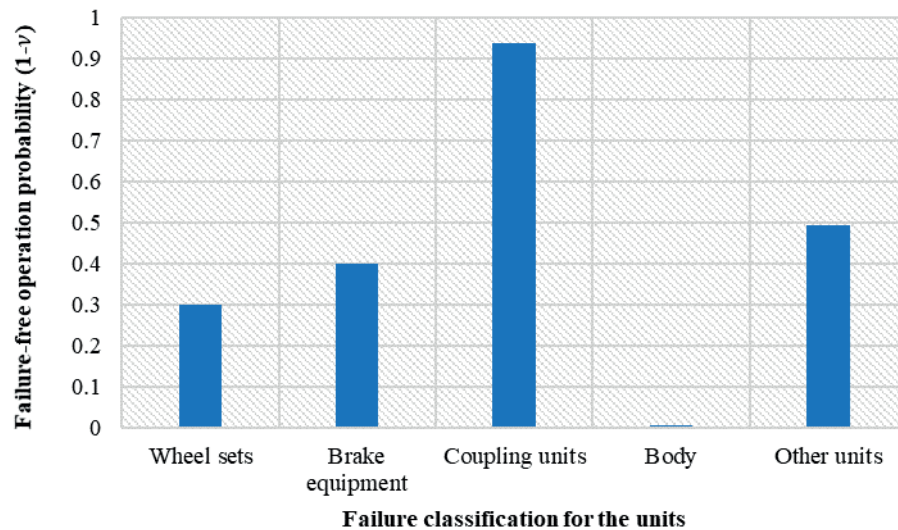


Figure 8 Probability of failure-free operation of freight car units on the Karaganda branch of the road for 2023

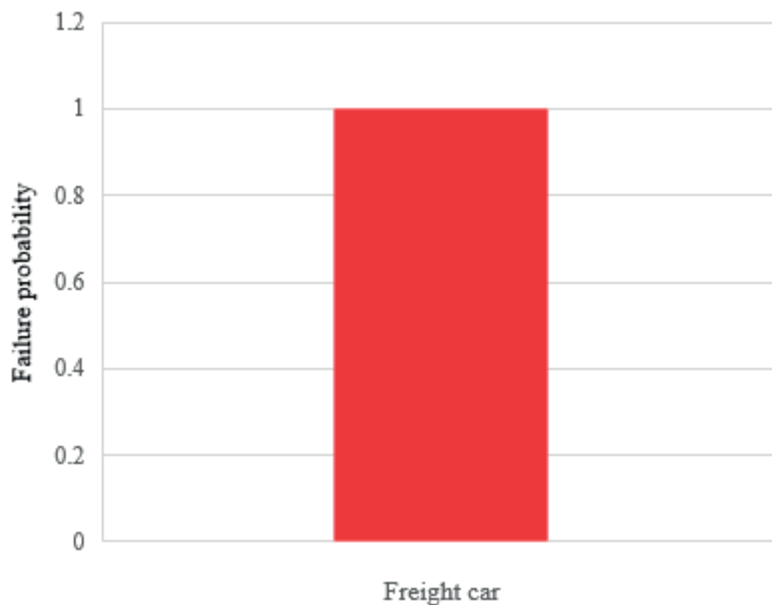


Figure 9 Total probability of the freight car failure

units and wheel pairs, the probability of failures is lower (from 0.0626 to 0.7022, respectively), which indicates a lower intensity of their failures. Automatic coupling devices showed the minimum probability of failures (0.008), which indicates their high reliability.

Automatic coupling devices demonstrate the highest probability of failure-free operation (0.9374), followed by the other components (0.4923) and automatic brake equipment (0.3983). Wheel sets have the failure-free operation probability of 0.2978, and the body has the lowest indicator (0.0066).

Figure 9 shows the total probability of freight car failures, which is 99.9%. This figure significantly exceeds the critical level of 50% and indicates an unacceptable level of risk for further operation of the cars. With the total probability of failure above 0.5, operation

of the cars becomes economically inexpedient and potentially unsafe, so it is recommended to immediately carry out major repairs or to consider writing off the cars.

6 Conclusion

The study confirmed that the application of the decision-making algorithm for operation of the freight cars according to the developed graph allows significant reducing of the costs and increasing the efficiency of the resource use.

The study allows drawing the following conclusions and coming to the following algorithm for selecting the optimal decision regarding the operation of freight

cars based on the optimality criterion, i.e. the profit maximization:

- assessing the current technical condition of the cars;
- analyzing the costs for all scenarios;
- assessing the profitability of continued operation;
- making a decision on the repairing of units and parts, and/or replacing the components, and/or writing-off the car, which maximizes the profit and takes into account the resource of units and parts.

Regardless of the country, engineering and rail transport follow the same patterns. The working conditions of railway transport and the patterns of wear do not depend on the country in which it is used. Therefore, the proposed algorithm for making the optimal decision for the further operation of freight cars can be used in the other countries, as well.

Implementation of this approach helps to free up the financial resources that can be directed to modernizing the infrastructure and improving the quality of service. This makes the car operation management system more flexible and resilient to changes in the market conditions, and applicable in the other industries.

The application of the developed methodology reduces the risks associated with the inefficient use of the rolling stock. The results of the study provide

railway companies with effective tools for optimizing the processes of technical maintenance, repair and decommissioning of the cars, which ultimately allows for a significant reduction in costs and increasing the profitability of transportation.

Thus, the versatility of the proposed method makes it applicable not only in the railway industry but also in the other areas where the management of operational resources plays the key role. This emphasizes the relevance of the study and its significance for a wide range of specialists.

Acknowledgements

The authors received no financial support for the research, authorship and/or publication of this article.

Conflicts of interest

The authors declare that they have no known competing financial interests or personal relationships that could have appeared to influence the work reported in this paper.

References

- [1] Freight wagons market size and share analysis - growth trends and forecasts (2025 - 2030) - Mordor Intelligence [online]. Available from: <https://www.mordorintelligence.com/industry-reports/freight-wagons-market>
- [2] KADYROVA, I. A., MINDUBAYEVA, F. A., GRJIBOVSKI, A. M. Prediction of outcomes after stroke: a systematic review. *Ekologiya cheloveka / Human Ecology* [online]. 2015, **22**(10), p. 55-64. ISSN 1728-0869, eISSN 2949-1444. Available from: <https://doi.org/10.17816/humeco16983>
- [3] 2024 report on combined transport in Europe [online]. Available from: https://uic.org/IMG/pdf/uic_uirr_report_2024-2.pdf
- [4] MOLOKOVITCH, A., DIONORI, F. *Logistics and transport competitiveness in Kazakhstan*. Geneva: Economic Commission for Europe, United Nations Geneva, 2019. ISBN 978-92-1-004220-8.
- [5] Integrated annual report of the joint-stock company "National company Kazakhstan Temir Zholy" for 2023 (in Russian) [online]. Available from: https://kase.kz/files/emitters/TMJL/tmjlp_2023_rus.pdf
- [6] DIZO, J., BLATNICKY, M., MOLNAR, D., FALENDYSH, A. Calculation of basic indicators of running safety on the example of a freight wagon with the Y25 bogie. *Communications - Scientific Letters of the University of Zilina* [online]. 2022, **24**(3), p. B259-B266. ISSN 1335-4205, eISSN 2585-7878. Available from: <https://doi.org/10.26552/com.C.2022.3.B259-B266>
- [7] ZVOLENSKY, P., STUCHLY, V., GRENCIK, J., POPROCKY, R. Evolution of maintenance systems of passenger and freight wagons from the ECM certification point of view. *Communications - Scientific Letters of the University of Zilina* [online]. 2014, **16**(11), p. 40-47. ISSN 1335-4205, eISSN 2585-7878. Available from: <https://doi.org/10.26552/com.C.2014.3A.40-47>
- [8] Technical regulation of the Customs Union On the safety of railway rolling stock approved by the Decision of the Customs Union Commission dated July 15, 2011. No. 710. TR CU 001/2011. EAC, 2011.
- [9] Regulation on the maintenance and repair system for freight wagons authorized for operation on public railway infrastructure in international transport (in Russian) [online]. 2012. Available from: https://online.zakon.kz/Document/?doc_id=31396597&pos=6;-106#pos=6;-106
- [10] Instructions on technical maintenance of wagons in service (manual for wagon inspectors). Council for Railway Transport of the Member States of the Commonwealth of Independent States (CIS), 2013.
- [11] TSUNASHIMA, H. Railway condition monitoring, present and application for regional railways. In: Transportation and Logistics Conference: proceedings [online]. 2017. eISSN 2424-3175. Available from: <https://doi.org/10.1299/jsmetld.2017.26.CL>

- [12] PANCHENKO, S., GERLICI, J., LOVSKA, A., RAVLYUK, V. The service life prediction for brake pads of freight wagons. *Communications - Scientific Letters of the University of Zilina* [online]. 2024, **26**(2), p. B80-B89. ISSN 1335-4205, eISSN 2585-7878. Available from: <https://doi.org/10.26552/com.C.2024.017>
- [13] SCHNEIDHOFER, CH., DUBEK, K., DORR, N. Robust sensors enabling condition-based maintenance of lubricated components in locomotives and wagons. *Transportation Research Procedia* [online]. 2023, **72**, p. 3236-3243. ISSN 2352-1457, eISSN 2352-1465. Available from: <https://doi.org/10.1016/j.trpro.2023.11.866>
- [14] LI, C., LUO, S., COLE, C., SPIRYAGIN, M. An overview: modern techniques for railway vehicle on-board health monitoring systems. *Vehicle System Dynamics* [online]. 2017, **55**(7), p. 1045-1070. ISSN 0042-3114, eISSN 1744-5159. Available from: <https://doi.org/10.1080/00423114.2017.1296963>
- [15] STRANO, S., TERZO, M. Review on model-based methods for on-board condition monitoring in railway vehicle dynamics. *Advances in Mechanical Engineering* [online]. 2019, **11**(2). ISSN 1687-8132, eISSN 1687-8140. Available from: <https://doi.org/10.1177/1687814019826795>
- [16] JANSSON, E., OLSSON, N. O. E., FROIDH, O. Trackside sensors in unattended train mainline systems - a case study of alarm logs from Sweden. *Transportation Research Procedia* [online]. 2024, **78**, p. 151-157. ISSN 2352-1457, eISSN 2352-1465. Available from: <https://doi.org/10.1016/j.trpro.2024.02.020>
- [17] ARMSTRONG, J. S. Evaluating forecasting methods [online]. In: *Principles of forecasting. A handbook for researchers and practitioners. International series in operations research and management science. Volume 30.* ARMSTRONG, J. S. (Ed.). Boston, MA.: Springer, 2001. ISBN 978-0-7923-7401-5, eISBN 978-0-306-47630-3. Available from: https://doi.org/10.1007/978-0-306-47630-3_20
- [18] CALLEJA-SANZ, G., OLIVELLA-NADAL, J., SOLE-PARELLADA, F. Technology forecasting: recent trends and new methods [online]. In: *Research methodology in management and industrial engineering. Management and industrial engineering.* MACHADO, C., DAVIM, J. P. (Eds.). Cham: Springer, 2020. ISBN 978-3-030-40895-4, eISBN 978-3-030-40896-1, p. 45-69. Available from: https://doi.org/10.1007/978-3-030-40896-1_3
- [19] ZUO, J., DONG, L., DING, J., WANG, X., DIAO, P., YU, J. Design and validation of a self-powered device for wireless electronically controlled pneumatic brake and onboard monitoring in freight wagons. *Energy Conversion and Management* [online]. 2021, **239**, 114229. ISSN 0196-8904, eISSN 1879-2277. Available from: <https://doi.org/10.1016/j.enconman.2021.114229>
- [19] PISLARU, C., BALL, A., GU, F. Modern techniques for condition monitoring of railway vehicle dynamics. *Journal of Physics: Conference Series* [online]. 2012, **364**, 012016. ISSN 1742-6596. Available from: <https://doi.org/10.1088/1742-6596/364/1/012016>
- [20] The 8 most common types of rail cars for freight shipping - Seminole Gulf Railway [online]. 2022. Available from: <https://www.floridairail.com/news/the-8-most-common-types-of-railcars-for-freight-shipping/>
- [21] PAPAELIAS, M., AMINI, A., HUANG, Z., VALLELY, P., DIAS, D. C., KERKYRAS, S. Online condition monitoring of rolling stock wheels and axle bearings. *Proceedings of the Institution of Mechanical Engineers, Part F: Journal of Rail and Rapid Transit* [online]. 2014, **230**(3), p. 709-723. ISSN 0954-4097, eISSN 2041-3017. Available from: <https://doi.org/10.1177/0954409714559758>
- [22] BOSSO, N., GUGLIOTTA, A., ZAMPIERI, N. Design and testing of an innovative monitoring system for railway vehicles. *Proceedings of the Institution of Mechanical Engineers, Part F: Journal of Rail and Rapid Transit* [online]. 2016, **232**(2), p. 445-460. ISSN 0954-4097, eISSN 2041-3017. Available from: <https://doi.org/10.1177/0954409716675005>
- [23] Numbered record book of availability and repair of defective freight wagons form VU-31. Karaganda Station, Karaganda Railway Division, Republic of Kazakhstan, 2024.
- [24] Establishment of sectoral indicators, data sources, and record-keeping procedures in railway transport. Almaty: Association of National Freight Forwarders of the Republic of Kazakhstan (ANEF), 2022.
- [25] Distribution of the main faults of freight cars by the reasons for their occurrence (in Russian) [online]. Available from: https://online.zakon.kz/Document/?doc_id=30840092
- [26] Amendments and additions to the Regulation on the conventional numbers for marking railway rolling stock and its components approved at the 61st meeting of the Council, in terms of passenger cars (in Russian) [online]. Available from: https://online.zakon.kz/Document/?doc_id=37416245
- [27] About 54 million tons of coal were delivered via the KTZh network for Kazakhstan consumers (in Russian) [online] Available from: <https://rail-news.kz/ru/cargo-transportation/19727-okolo-54-mln-tonn-uglia-dostavleno-po-seti-ktz-dlia-kazaxstanskix-potrebitelei.html>
- [28] GOST 34056-2017 Railway transport. Rolling stock composition. Terms and definitions. Interstate standard (in Russian) [online]. 2017. Available from: <https://www.tdesant.ru/info/item/295>
- [29] Manual on technical servicing of wagons in use (instructions for wagon inspectors) (in Russian) [online]. Available from: https://online.zakon.kz/Document/?doc_id=31501231

Appendix A - Reference 2653 Information of the last executed repair

REPORT 2653. THURSDAY FEBRUARY 22, 2024 13:44

(AFTER THE CAR NUMBER THERE CAN BE SET THE NUMBER OF THE REPAIRS (3 BY DEFAULT))

REPORT ON THE REPAIRS MADE ON CAR 28807352 ON 22.02.24 13:44:18.4

NO REPAIR TYPEOE DATE ROAD REPAIR DEPOT

```

-----
1  RUN-1      DECEMBER 15, 2012  68 KAZAKHSTAN R/W 4048 the depot car part
(DCP)DCP-34 CDC BOROVOYE
(220 - SLIDER CLEARANCE INCOMPLIANCE)
2  RUN-1      APRIL 13, 2014    68 KAZAKHSTAN R/W 4042 DCP-19 KOSTANAI
(212 - CAP SLIDER CRACK)
3  RUN-2      MAY 25, 2014     80 SOUTH-URAL RAILWAY 4102 SECTION TOP ST.
MAGNITOGORSK CDCE-5 KARTALY OF THE Joint-stock Company Russian Railways (hereafter
RR JSC)
(117 - IRREGULAR RUNNING ON THE CIRCLE RIDING ABOVE THE NORM)
4  DEP.      -- ----- Y. 68 KAZAKHSTAN R/W 4154 DCP-24
(570 - DEPOT MAINTENANCE CALENDAR SCHEDULE EXPIRED)
5  DEP.      OCTOBER 29, 2014  68 KAZAKHSTAN R/W 745 Ust-Kamenogorsk Car
repair depot (hereafter CRD)
(7600 - PLANNED REPAIR WITH STENCIL PLACING)
(3108 - MOUNTING DURABLE TROLLEYS MODEL 18-100 )
(2158 - MODIFICATION OF THE FIXATION UNIT, BRAKE SHOE)
(1213 - MODERNIZING THE LOCK OF THE COVERED CARS DOORS)
6  INSPECTION DECEMBER 04, 2016  92 EAST-SIBERIAN R/W 4126 DCP-13 TAISHET RR
JSC
(102 - THIN RIB)
(107 - SHELLING OF THE DRIVING WHEEL)
7  INSPECTION JANUARY 07, 2017  92 EAST-SIBERIAN R/W 4126 DCP-13 TAISHET RR
JSC
(574 - ADVANCED DELIVERY TO DEPOT REPAIR DUE TO TECHNICAL CONDITION)
8  INSPECTION FEBRUARY 09, 2017  92 EAST-SIBERIAN R/W 4126 DCP-13 TAISHET RR
JSC
(107 - SHELLING OF THE DRIVING WHEEL)
(219 - RAISING/LOWING THE FRICTION WEDGE RELATIVE TO SUPPORTING
SURFACE)
9  INSPECTION FEBRUARY 17, 2017  92 EAST-SIBERIAN R/W 4126 DCP-13 TAISHET RR
JSC
(574 - ADVANCED DELIVERY TO DEPOT REPAIR DUE TO TECHNICAL CONDITION)
10 RUN-2      FEBRUARY 17, 2017  92 EAST-SIBERIAN R/W 4126 DCP-13 TAISHET RR
JSC
(107 - SHELLING OF THE DRIVING WHEEL)
11 RUN-2      SEPTEMBER 14, 2017  61 VOLGA R/W 4129 DCP-10 ASTRAKHAN
R/W
(211 - CAP SLIDER CRACK)
12 DEP.      -- ----- 68 KAZAKHSTAN R/W 4035 DCP-3 UTALSK
(570 - EXPIRED CALENDAR SCHEDULE)
13 DEP.      OCTOBER 27, 2017  68 KAZAKHSTAN R/W/ 684 DCP URALSK -
KAZNEMIRTRANS JSC BRANCH
(7600 - PLANNED REPAIR WITH STENCUL PLACING)
(3108 - MOUNTING DURABLE TROLLEYS MODEL 18-100 )
14 RUN-2      OCTOBER 05, 2018  85 CRIMEAN R/W 1507 DCP JANKOI R/W
(214 - SPRING DAMAGE )
(912 - COMPLAINTS OF THE QUALITY OF THE DEPOT REPAIR )
15 RUN-1      -- ----- Y. 68 KAZAKHSTAN R/W 4046 DCP-30 ARYS
(214 - SPRING DAMAGE )
16 RUN-1      MAY 27,2019 68 KAZAKHSTAN R/W 4281 ARYSSHPALZAVOD LLP
17 RUN-1      SEPTEMBER 19, 2019 68 KAZAKHSTAN R/W 4047 DCP-26
(539 - DAMAGE TO THE HATCH COVER AND HINGES)
18 INSPECTION OCTOBER 08, 2020 68 KAZAKHSTAN R/W 4045 DCP-27 JAMBYL
(214 - SPRING DAMAGE )
19 DEP.      -- ----- Y. 68 KAZAKHSTAN R/W 613 DCP-8 ASTANA

```


(570 - EXPIRED CALENDAR SCHEDULE)
 20 DEP. OCTOBER 16, 2020 68 KAZAKHSTAN R/W 608 DCP BURABAI CRD
 (7600 - PLANNED REPAIR WITH STENCUL PLACING)
 (3108 - MOUNTING DURABLE TROLLEYS MODEL 18-100)
 21 RUN-2 DECEMBER 23, 2022 28 NORTH R/W 4120 DCP-7 LOSTA R/W
 OJSC
 (107 - SHELLING OF THE DRIVING WHEEL)
 (537 - DOOR LOCK FAILURE)
 (912 - COMPLAINTS OF THE QUALITY OF THE DEPOT REPAIR)
 22 INSPECTION SEPTEMBER 05, 2023 68 KAZAKHSTAN R/W 4045 DCP-27 JAMBYL
 (537 - DOOR LOCK FAILURE)
 23 RUN-1 SEPTEMBER 06, 2023 68 KAZAKHSTAN R/W 4045 DCP-27 JAMBYL
 (537 - DOOR LOCK FAILURE)
 (411 - FAILURE OF THE AUTO PRESS BEAM OR EE MOUNTING)
 24 INSPECTION OCTOBER 03, 2023 68 KAZAKHSTAN R/W 1019 DCP-13 KARAGANDA
 (537 - GOOR LOCK FAILURE)
 25 DEP. -- ----- 68 KAZAKHSTAN R/W 1019 DCP-13 KARAGANDA
 (570 - EXPIRED CALENDAR SCHEDULE OF THE DEPOT REPAIR)
 26 DEP. OCTOBER 06, 2023 68 KAZAKHSTAN R/W 612 KAMKOR WAGON CRD
 BRANCH
 (3108 - MOUNTING DURABLE TROLLEYS MODEL 18-100)
 (7600 - PLANNED REPAIR WITH STENCUL PLACING)

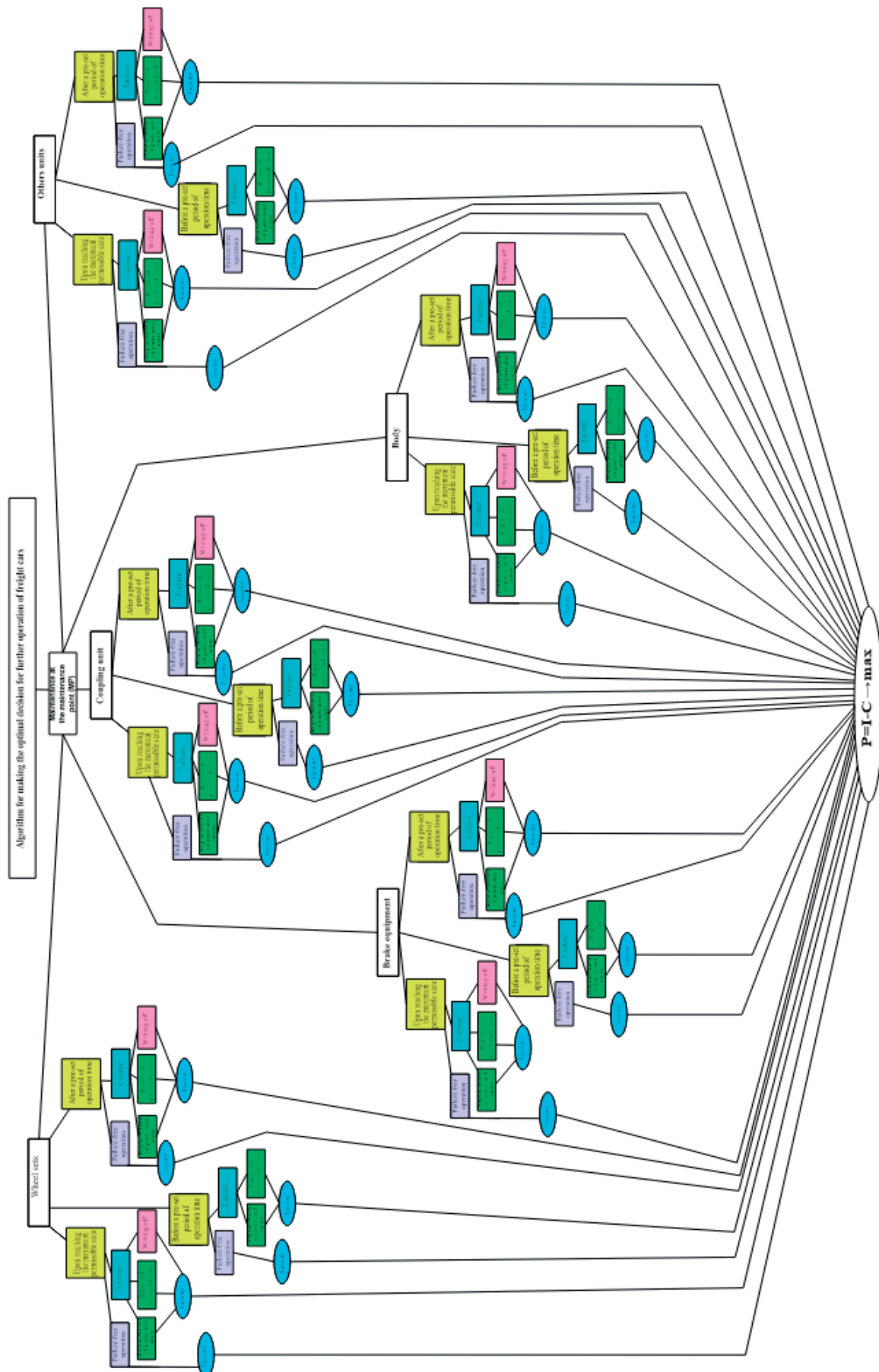
 INFORMATION OF THE LAST REPAIRS OF CAR NO 28807352
 *** REPAIR 26 *** 06.10.23 19:10 ** LAST *****
 C A R NO 28807352
 DATE OF COMMISSIONING OCTOBER 06, 2023 16:11
 OWNER 27 KAZAKHSTAN
 ROAD 68 KAZAKHSTAN R/W
 REPAIR DEPOT 0612 KAMKOR WAGON CRD BRANCH
 TROUBLES --
 PLANNED REPAIR WAS ASSIGNED BY THE 1 DEPOT ON OCTOBER 16, 2023
 TYPE OF THE REPAIR MADE 1 DEPOT
 EXCHANGE STATION VU-23 --
 NOTIFICATION NUMBER VU-23 --
 DATE-TIME OF TROUBLESHOOT --
 REPAIR START OCTOBER 06, 2023 08:00 EMPTY RUNNING 33329 KM
 REPAIR END OCTOBER 06, 2023 19:10 LOADED RUNNING 65910 KM
 NOTIFICATION NUMBER VU-36 22 f68 (44 6813 8)00
 MODERNIZATIONS 3108 MOUNTING DURABLE TROLLEYS MODEL 18-100
 7600 PLANNED REPAIR WITH STENCUL PLACING

REPORT 1353 IS ABSENT
 *** REPAIR 25 *** 03.10.23 10:42 ** NEAREST TO LAST *****
 C A R NO 28807352
 DATE OF COMMISSIONING OCTOBER 03, 2023 07:43
 OWNER 27 KAZAKHSTAN
 ROAD 68 KAZAKHSTAN R/W
 REPAIR DEPOT 1019 CDC-13 KARAGANDA
 TROUBLES 570 EXPIRED CALENDAR SCHEDULE OF THE DEPOT REPAIR
 TYPE OF REPAIR 1 DEPOT
 EXCHANGE STATION VU-23 67307
 NOTIFICATION NUMBER VU-23 30 F68 (44 6813 8)00
 DATE/TIME OF TROUBLE OCTOBER 03, 2023 10:42
 REPAIR START --
 REPAIR COMPLETION --
 NOTIFICATION NUMBER VU-36 --
 NO MODERNIZATIONS

REPORT 1354 IS ABSENT
 *** REPAIR 24 *** 03.10.23 10:39 *****
 C A R NO 28807352
 DATE OF COMMISSIONING OCTOBER 03, 2023 07:40
 OWNER 27 KAZAKHSTAN
 ROAD 68 KAZAKHSTAN R/W
 REPAIR DEPOT 1019 CDC-13 KARAGANDA
 TROUBLES 537 DOOR LOCK DAMAGE
 TYPE OF REPAIR 9 INSPECTION
 EXCHANGE STATION VU-23 67386
 NOTIFICATION NUMBER VU-23 1 F68 (44 6813 8)07

DATE-TINE OF TROUBLE OCTOBER 01, 2023 17:49
REPAIR START OCTOBER 03, 2023 10:38 EMPTY RUNNING 33329 KM
REPAIR END OCTOBER 03, 2023 10:39 LOADD RUNNING 65910 KM
NOTIFICATION NUMBER VU-36 0 F68 (44 6813 8)07
NO MODERNIAZATIONS
***** REPORT END *****

Appendix B - The decision-making algorithm for the further operation of the freight car



Dear colleagues,

Journal for sciences in transport Communications - Scientific Letters of the University of Žilina are a well-established open-access scientific transport journal aimed primarily at the topics connected with the field of transport. The main transport-related areas covered include Civil engineering, Electrical engineering, Management and informatics, Mechanical engineering, Operation and economics, Safety and security, Travel and tourism studies. Research in the field of education also falls under these categories. The full list of main topics and subtopics is available at: https://komunikacie.uniza.sk/artkey/inf-990000-0500_Topical-areas.php

Journal for sciences in transport Communications - Scientific Letters of the University of Žilina is currently indexed, abstracted and accepted by CEEOL, CLOCKSS, COPE (Committee on Publication Ethics), Crossref (DOI), digitálne pramene, DOAJ, EBSCO Host, Electronic Journals Library (EZB), ERIH Plus, Google Scholar, Index Copernicus International Journals Master list, iThenticate, JournalGuide, Jouroscope, Norwegian Register for Scientific Journals Series and Publishers, Portico, ROAD, ScienceGate, SCImago Journal & Country Rank, SciRev, SCOPUS, Web of Science database, WorldCat (OCLC).

Journal for sciences in transport Communications - Scientific Letters of the University of Žilina is preserved in CLOCKSS and Portico to guarantee long-term digital preservation and is archived in the national deposit digitálne pramene.

Authors can share their experiences with publishing in our journal on SciRev.

Journal for sciences in transport Communications - Scientific Letters of the University of Žilina has been selected for inclusion in the Web of Science™. Articles published after 2022, beginning with 24(1), will be included in the product Emerging Sources Citation Index (ESCI).

I would like to invite authors to submit their papers for consideration. We have an **open access policy under Creative Commons (CC BY) license** and Article Processing Charge (APC) is **400 Euro** (price excluding VAT). The price of one additional page of the submitted article beyond the prescribed scope (15 pages) is **50 Euro** (price excluding VAT). Print edition fee is **100 Euro** per one piece (price excluding VAT) including shipping costs. Our journal operates a standard single-anonymous peer-review process, the successful completion of which is a prerequisite for publication of articles.

Our journal is issued four times a year (in January, in April, in July and in October).

I would also like to offer you the opportunity of using already published articles from past issues as source of information for your research and publication activities. All papers are available at our webpage: <http://komunikacie.uniza.sk>, where you can browse through the individual volumes. Our journal offers access to its contents in the open access system on the principles of the license Creative Commons (CC BY 4.0).

For any questions regarding the Journal for sciences in transport Communications - Scientific Letters of the University of Žilina please contact us at: komunikacie@uniza.sk.

We look forward to future cooperation.

Sincerely



Branislav Hadzima
editor-in-chief



This is an open access article distributed under the terms of the Creative Commons Attribution 4.0 International License (CC BY 4.0), which permits use, distribution, and reproduction in any medium, provided the original publication is properly cited. No use, distribution or reproduction is permitted which does not comply with these terms.

EVALUATION OF SILICON CARBIDE MOSFET DRIVING CIRCUIT PERFORMANCE

Veronika Švárna, Michal Frivaldský*

Department of Mechatronics and Electronics, Faculty of Electrical Engineering and Information Technologies, University of Zilina, Zilina, Slovakia

*E-mail of corresponding author: michal.frivaldsky@uniza.sk

Michal Frivaldsky  0000-0001-6138-3103

Resume

The performances of different driving circuits configurations designed for silicon carbide MOSFET transistors are compared in this research. The simulation of the double-pulse test (DPT) was performed with the use of three driving circuit configurations. The SiC MOSFET NTH4L022N120M3S has great dynamic parameters, which made it suitable for the DPT simulation. It was performed with six different driving voltage ranges, all within the range between -10 V and 20 V. The results were taken across the wide range of driving resistances placed between the driver and the SiC MOSFET, where the switching losses were taken. Drawing from the observed measurements and derived plots, the optimal U_{GS} driving interval for managing the SiC MOSFET transistor is determined to be -10 V/20 V when using a circuit design that incorporates both turn-on and turn-off resistors and diodes.

Article info

Received 6 May 2025

Accepted 9 July 2025

Online 27 August 2025

Keywords:

silicon carbide
power transistor
driving circuit
double pulse test
energy losses

Available online: <https://doi.org/10.26552/com.C.2025.047>

ISSN 1335-4205 (print version)

ISSN 2585-7878 (online version)

1 Introduction

In this paper is discussed how the configuration of the driving circuit affects the switching performance and power losses of high-end SiC power transistors. To analyze the impact of gate drive topology, accurate, validated simulation models and the simulation-based methods were utilized. The results show that a well-designed driving circuit configuration can optimize power loss in the transistor, thereby improving the thermal performance of the power semiconductor converter.

Presently, the silicon-carbide MOSFET transistors are becoming increasingly popular, and, in many applications, they are taking over the role of the switching component instead of classic silicon MOSFET transistors, [1]. Although both devices are metal oxide semiconductor field effect transistors, intrinsic electrical properties of silicon-carbide material introduce the need for the driving circuits with the properties optimized for the new material. Silicon carbide (SiC) power devices offer high switching speeds that enhance efficiency, power density, and overall performance. However, their unique characteristics require careful gate driver design to ensure optimal switching behavior, [2].

With the improved properties and advantages come a few drawbacks that need to be taken into consideration. SiC-MOSFETs are well-suited for power converters due to their superior performance, but their fast switching can lead to surge voltages, spike currents, and EMI problems. Therefore, optimizing the gate drive circuit is essential to fully harness their capabilities while minimizing adverse effects, [3]. One of many interesting features of SiC MOSFETs is the ability of inverse conduction, [4]. However useful the feature is, consequently, it influences the efficiency of an application and power losses, [5]. The detailed examination of the gate drive requirements for SiC-MOSFETs is essential to mitigate the risk of undesirable events leading to unintended switching or excess switching losses, [6].

The complex design of a gate driver depends on whether it operates a high-side or low-side MOSFET, with low-side drivers being simpler due to their ground reference. High-side drivers require additional components to handle varying source potentials, [7]. Furthermore, the distinct characteristics of SiC MOSFETs demand tailored driver circuits to ensure the proper functionality and performance, [8].

In this work is explored how different gate driver

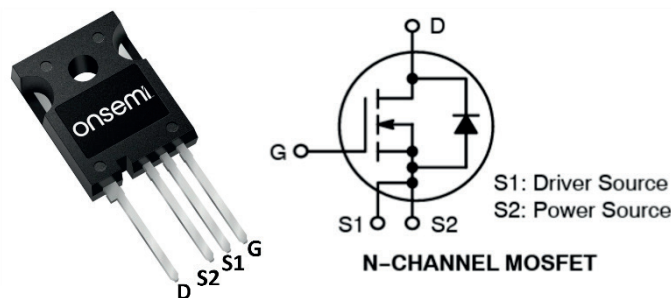


Figure 1 The silicon-carbide based MOSFET NTH4L022N120M3S from onsemi (left: real-life image, right: schematic symbol with description)

configurations affect the switching losses of a high-performance 1200 V SiC power transistor. The analysis relies on time-domain simulations using detailed non-linear SPICE models to ensure accuracy. Three distinct driver setups, along with variations in gate-source voltage amplitude, were evaluated to assess their impact on device performance.

2 The selection of the power MOSFET transistor

Due to the great thermal and electrical properties, the silicon-carbide MOSFET NTH4L022N120M3S from onsemi was selected. This transistor shown in Figure 1, represents the latest generation of the SiC power transistors with the planar manufacture technology aiming the best-in-class operational performance. Instead of that, a wide portfolio of the PSpice libraries is available for simulation purposes, while these models are exhibiting verified and accurate electro-thermal behavior. With the focus given on the simulation research methodology (saving time in relation to laboratory measurements) this was the key factor for the component selection.

This MOSFET has a breakdown voltage of 1200 V, and it is capable to withstand the maximum drain current of 89 A. The typical on-state resistance of the MOSFET is 22 m Ω at 18 V. The recommended operation driving voltage range is -3 V to 18 V and the absolute maximum voltage range allowed on the gate is from -10 V up to 22 V. It is suitable for high switching speeds because of its very low total gate charge of 137 nC, [9]. A key advantage of this MOSFET is its TO-247-4 package. This package provides excellent thermal performance, with $R_{JC} = 0.43$ $^{\circ}\text{C}/\text{W}$ and $R_{JA} = 40$ $^{\circ}\text{C}/\text{W}$. It also features a four-pin layout. The gate and Kelvin source pins are placed close together to reduce the loop inductance, [10].

3 Methodology - simulation approach

The ideal configuration of the double-pulse test is used for the purpose of simulation. In this configuration, shown in Figure 2, the selected MOSFET is used as

lower and upper transistor, while the lower one is the device under the test. The upper transistor is connected in diode configuration with the -3 V DC source connected between the gate and source of the MOSFET. This ensures that the transistor stays closed during the process, and after the first pulse, the current will flow only through the body diode of the upper MOSFET.

The V3 source is connected to the gate through resistors and other simple driving circuits. It was set up to deliver a pair of pulses to activate the gate of the lower MOSFET. The timing parameters, labeled T1 through T8, were fine-tuned for optimal performance. These adjustments ensured that the drain current reached a value of 50 A by the conclusion of the initial pulse.

The selected silicon-carbide MOSFETs are connected in a half-bridge configuration connected to the 400 V DC source. In parallel to this, the capacitor of 500 μF with series resistor of 1 m Ω . In parallel to the upper transistor, the inductor of 80 μH with series resistance of 80 m Ω is connected to upper transistor in diode configuration.

The first tested configuration is simple, one resistor driving circuit. This configuration was chosen due to the reduced size compared to the other driving circuits, and number of components. The major disadvantage of this configuration lies in the resistor alone. It controls both turn-on and turn-off process and all power in this section is dissipated via this single resistor. This may lead to reliability issues and reduced lifespan. Moreover, larger resistor values may lead to a partial gate discharge, increasing the chance of unintended turn-on and failing to adequately suppress oscillations, which makes them poorly suited for high-frequency use. Still, this configuration is preferred in the case of more affordable and simpler solutions if the performance can be neglected.

The second tested configuration, shown in Figure 3, is optimal for the high-frequency MOSFET control, as it allows separate turn-on and turn-off times, improving efficiency, reducing EMI and switching losses, and enhancing stability. Diodes ensure correct current direction but introduce voltage drop losses. Though the more complex and costly, with two resistors and two diodes, proper component selection is crucial.

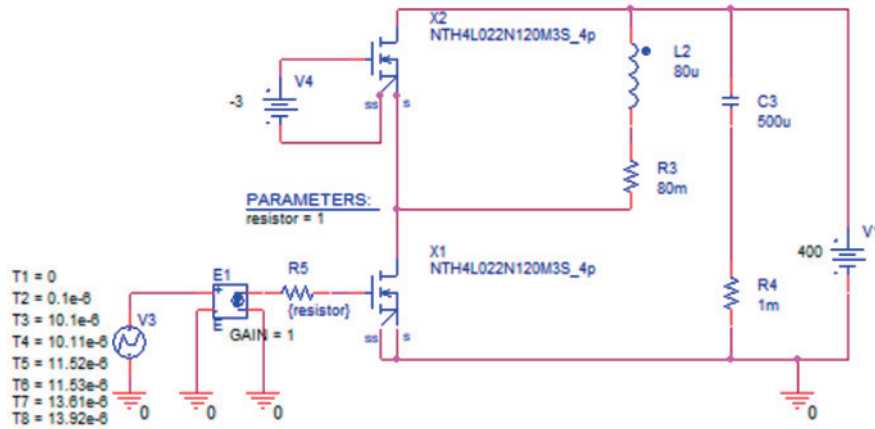


Figure 2 The double-pulse test schematics using the single resistor gate drive and SiC MOSFET NTH4L022N120M3S

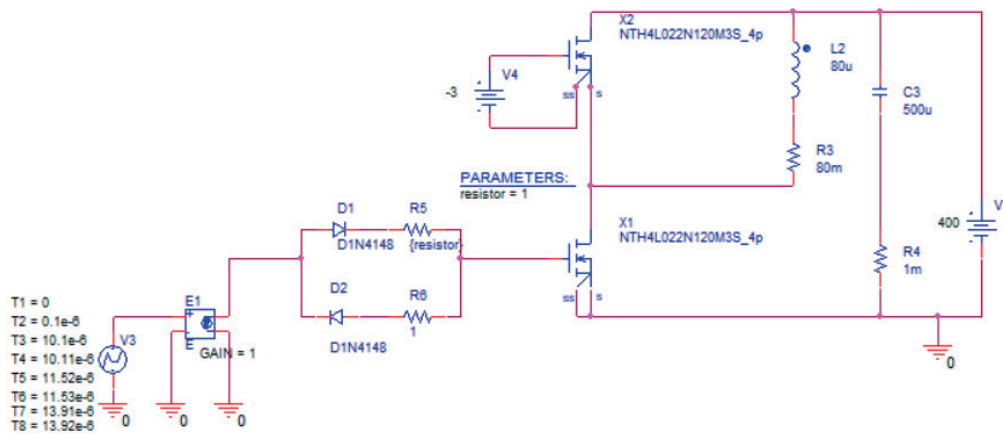


Figure 3 The double-pulse test schematics using the turn-on and turn-off resistors gate drive and SiC MOSFET NTH4L022N120M3S

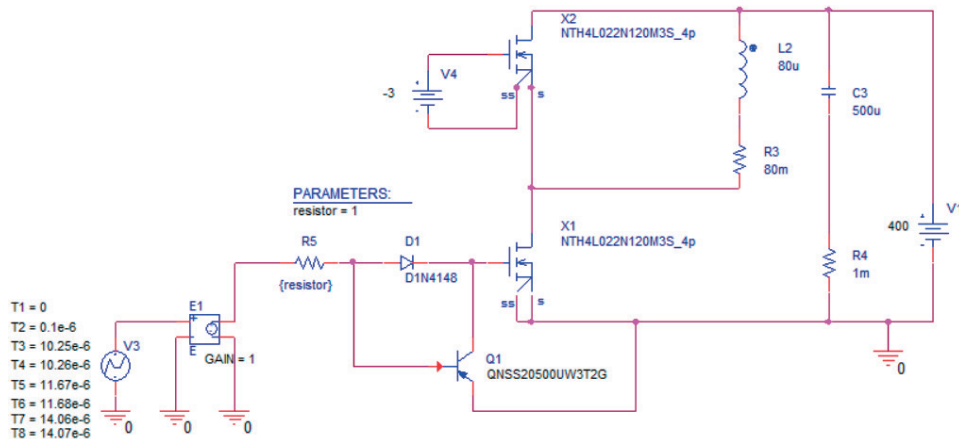


Figure 4 The double-pulse test schematics using the turn-on and turn-off resistors gate drive and SiC MOSFET NTH4L022N120M3S

Mismatched values can cause slow switching or high EMI. In this case, the turn-off resistor was fixed based on prior tests, while the turn-on resistor was adjusted within a chosen range.

The third tested configuration, shown in Figure 4, was adjusted to use onsemi PNP transistor NSS20500UW3T2G as a speed-up element. It is rated

20 V, 5 A which makes it sufficient for this application. Though it appears straightforward, this setup demands precise execution. Choosing unsuitable transistors or resistors can greatly impair functionality. Nevertheless, it remains the most common speed-up circuit used in real-world applications. It has several advantages such as easy implementation and control and simple

topology. The major advantage, however, is the element's direct connection to the source of the SiC MOSFET and its capability to discharge the gate of the MOSFET faster. Despite this, the speed-up element elevates the complexity of the driving circuit and overall energy losses which lead to lower efficiency. The design of this kind of driving circuit needs to be done properly. Improper design may lead to oscillations at the gate of MOSFET or high current spikes at high frequencies.

4 Results

The results were obtained from the simulation in OrCAD PSpice, which serves as a reliable platform for accurately modelling and analyzing electrical circuits under various conditions. The simulation focused on determining the total energy loss, which was extracted directly from the program's output data related to voltage, current, and power dissipation across transistor during the switching cycle, an example of which is shown in Figure 5. To ensure the theoretical consistency, the total energy loss was calculated using established equations for energy loss in Equation (1) and Equation (2) listed below. This dual approach - using both simulation data and analytical expressions - helps validate the accuracy and reliability of the findings.

$$E_{ON} = \int_{t_{ON1}}^{t_{ON2}} V_{DS} I_D dt, \quad (1)$$

$$E_{OFF} = \int_{t_{OFF1}}^{t_{OFF2}} V_{DS} I_D dt. \quad (2)$$

where: E_{ON} - turn-on energy loss, E_{OFF} - turn-off energy loss, t_{ON1} - initial time for turn-on process, t_{ON2} - ending time for turn-on process, t_{OFF1} - initial time for turn-off process, t_{OFF2} - ending time for turn-off process, V_{DS} - drain - source voltage of device, I_{DS} - drain current of device

To test the correct function of this circuit and verify the level of the I_D current at the end of the first pulse, a timing analysis of the circuit was performed in the range of 10 μ s and with a maximum simulation step of 1e-6. The details of the DPT waveform are shown in Figure 6.

The resulting graphs were split into two segments: one showing energy patterns for U_{GS} values up to 10 V, and the other extending to 20 V, to maintain readability and distinction. In the legend of each presented graph, the R represents the resistor which resistance was changed throughout the parametric simulation. In the case of turn-on and turn-off resistors, only turn-on resistor, was changing during the simulation. The turn-off resistor had a fixed value of 1 Ω . Figure 7 shows the graph of the turn-on energy losses in different driver circuit configurations across the range of resistor

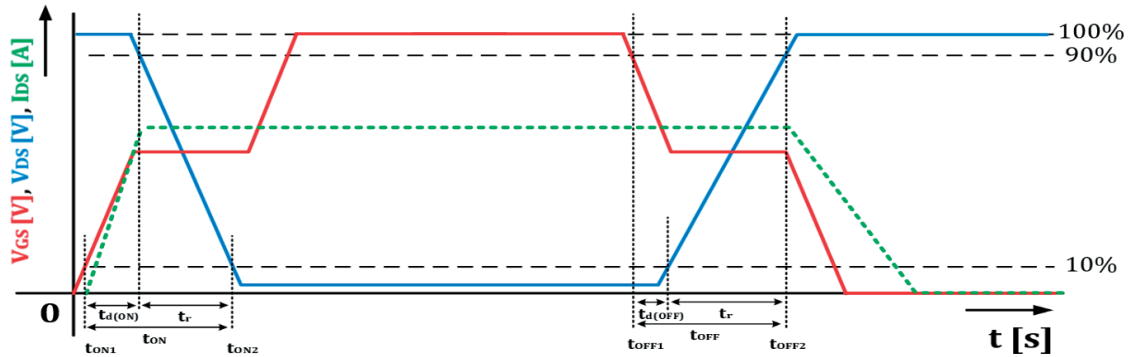


Figure 5 One switching cycle of SiC MOSFET transistor

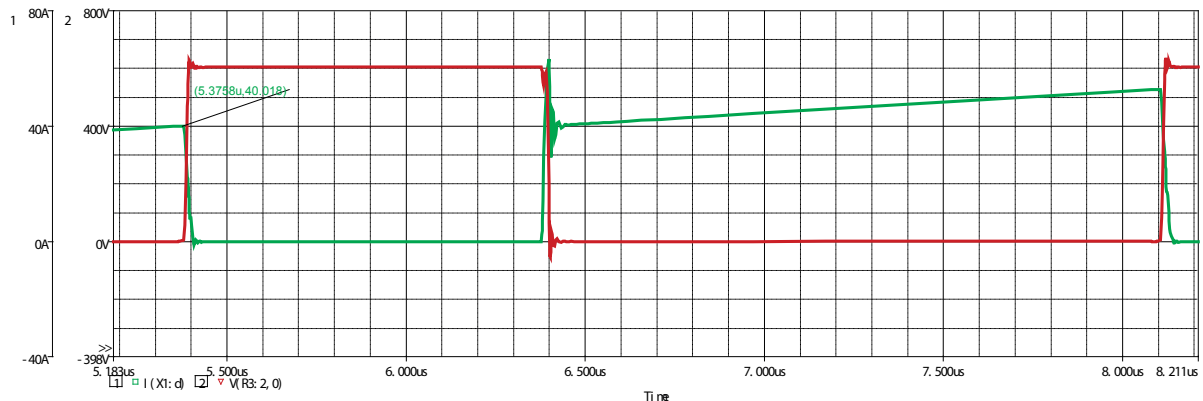


Figure 6 Example of the simulation DPT result for evaluation of the energy losses

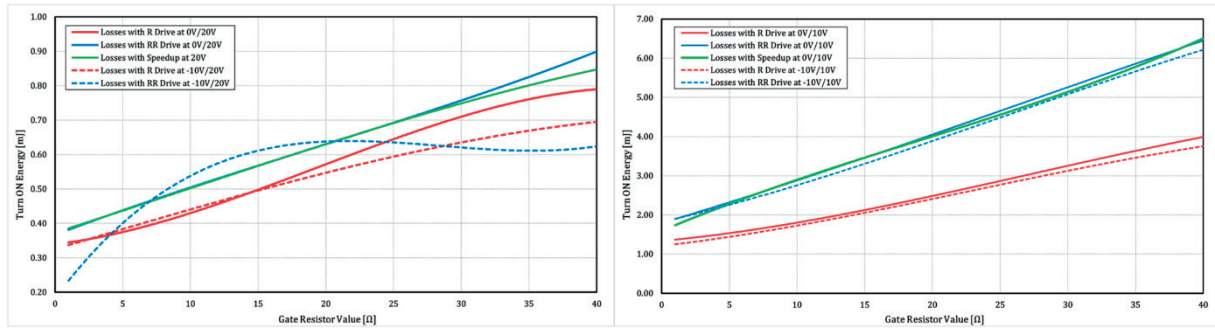


Figure 7 The turn-on energy losses obtained from the double-pulse test simulation

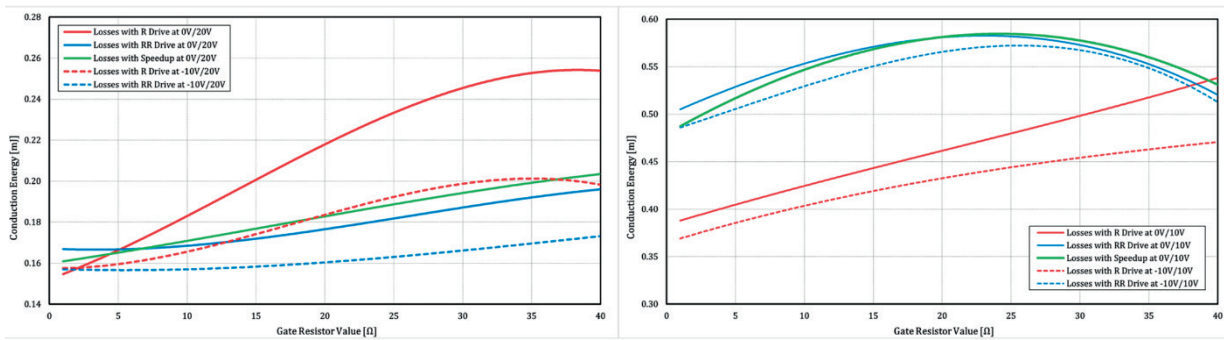


Figure 8 The conduction energy losses obtained from the double-pulse test simulation

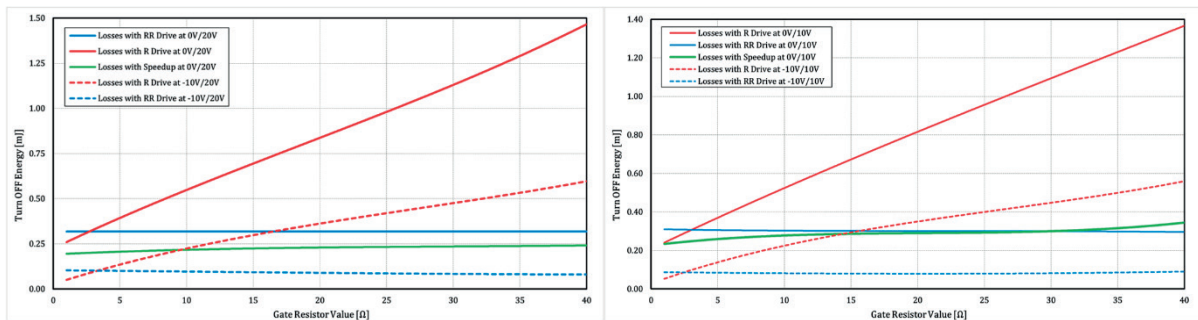


Figure 9 The turn-off energy losses obtained from the double-pulse test simulation

values. An analysis of both depicted graphs indicates that the most suitable configuration for the relatively low switching losses is the configuration with single resistor with the driving voltage range of -10 V/20 V in the whole range of selected resistor values. From the lower driving voltage ranges up to 10 V, the most suitable configurations seem to be the ones with turn-on and turn-off resistors within the whole range of selected resistor values. However, the switching loss values with the voltage ranges up to only 10 V were three times higher on average. This same is valid for the conductive, turn-off and consequently, total energy losses.

The graph of the conduction losses, shown in Figure 8, indicates that the most suitable configuration is the one with turn-on and turn-off resistors in the range of driving voltage from -10 V to 20 V. The lowest losses were achieved specifically at 1 Ω but the results show that the losses stayed very low within the whole range of selected resistor values.

The turn-off losses obtained with the driving voltage ranges up to only 10 V were three times higher than those obtained by the driving voltages up to 20 V despite the similarities observed in the graph in Figure 9. Moreover, the results show that similarly to the turn-on, the best option within the tested driver configurations is the one with turn-on and turn-off resistors with the driving voltage -10 V/20 V. The lowest energy loss achieved was recorded at 35 Ω .

The total energy losses (Figure 10) were evaluated and considered separately according to the driving voltage range, up to 10 V and up to 20 V ranges, due to the significant difference in the overall energy loss results. Observing the results in the driving voltage ranges -10 V/10 V, -5 V/10 V, and 0 V/10 V, it is possible to come to a conclusion that the worst configuration in this voltage range category is the one with speed up element, specifically with using 40 Ω resistor at 0 V/10 V driving voltage (7.363 mJ). Opposite to this, the best

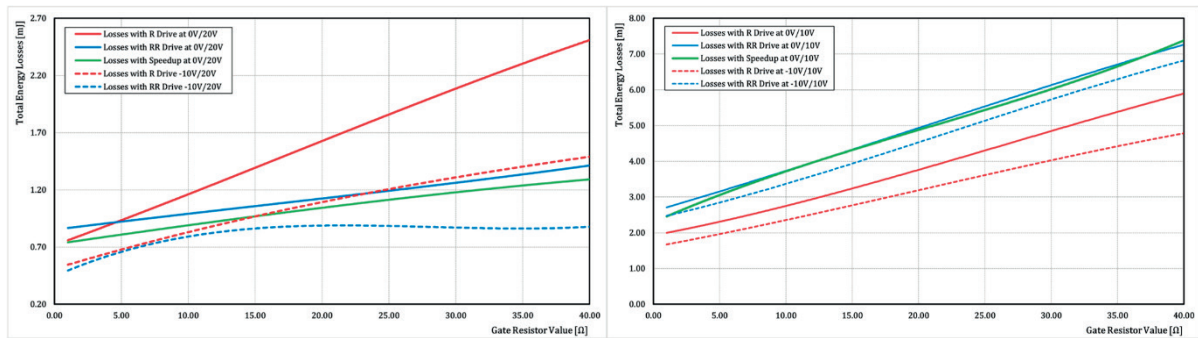


Figure 10 The total energy losses obtained from the double-pulse test simulation

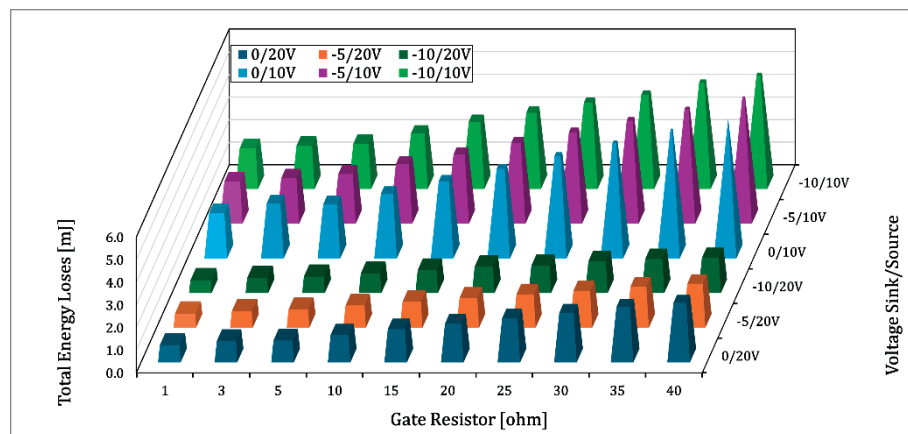


Figure 11 Total losses at different control voltage ranges in single resistor configurations

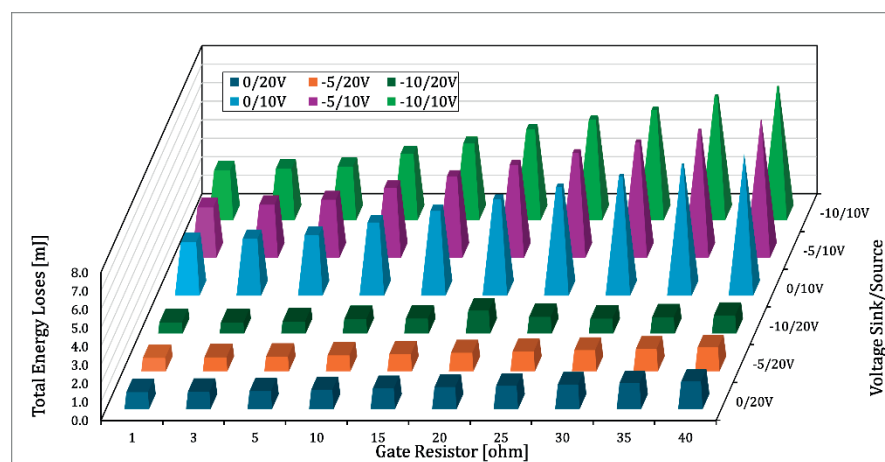


Figure 12 Total losses at different control voltage ranges in configurations with turn-on and turn-off resistors

option for tested configurations is the one with a single resistor at -10 V/10 V range (1.705 mJ). As mentioned earlier, the losses in this category are approximately three times higher than the losses in the voltage ranges 10 V/20 V, -5 V/20 V, and 0 V/20 V and therefore the results from this category were more interesting for the overall findings.

The highest losses were observed at the driving voltage 0 V/20 V whilst using at 30 Ω, 35 Ω, and 40 Ω resistors in single-resistor configuration. The best

results, in terms of low energy losses were observed in the configuration with turn-on and turn-off resistors at the driving voltage range of -10 V/20 V across the whole range of selected resistors.

The presented results, graphs in Figure 11, Figure 12 and Figure 13, show that the most suitable configuration for controlling the selected MOSFET transistor NTH4L022N120M3S is the one with two resistors using a control voltage from -10 V to 20 V. On the contrary, the worst results were achieved by the

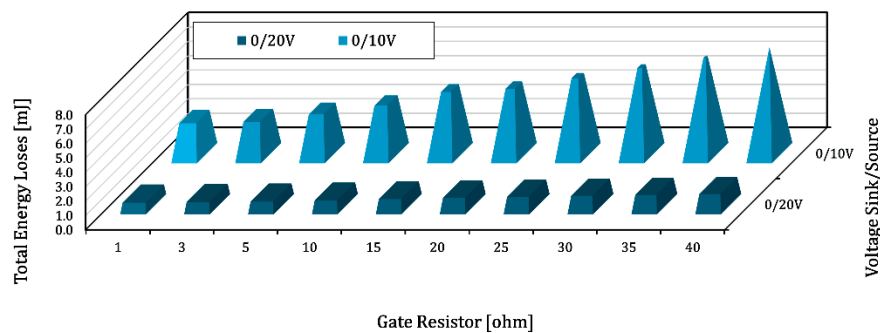


Figure 13 Total losses at two control voltage ranges in configurations with an accelerating element

configuration with an accelerating transistor in both control voltage ranges that were simulated, which can be seen in Figure 12.

In general, it is not recommended to use positive voltages lower than 13 V to drive the silicon carbide MOSFETs. This fact results from the physical properties of the structure. This was observed in the high losses at the control voltage ranges of -10 V/10 V, -5 V/10 V and 0 V/10 V in the tables and graphs. With such control, there is a risk of thermal leakage due to high losses and there is also a high risk of false switching due to slower turn-off and a wavy voltage waveform at turn-off.

5 Conclusion

The analysis confirmed the critical importance of proper gate drive voltage selection for SiC MOSFETs, specifically the NTH4L022N120M3S, in power electronics applications. Expanding on this in relation to the current state of technology, SiC MOSFETs are increasingly favored over traditional silicon-based devices due to their superior efficiency, high switching speeds, and thermal robustness. However, their unique physical properties also demand careful optimization of the gate drive circuits. In recent advancements, industry trends continue to reinforce the recommendation of avoiding positive gate drive voltages below 13 V. This aligns with ongoing efforts to improve power efficiency while mitigating risks such as thermal runaway and unintended turn-on. The latter issue, often exacerbated

by slow turn-off dynamics and voltage oscillations, has led to further research into innovative gate driver designs. Modern solutions include active gate control techniques that dynamically adjust gate drive parameters to minimize energy losses and improve switching reliability. Additionally, the emphasis on turn-on and turn-off resistors in gate drive configurations remains relevant as engineers strive to refine these circuits for applications in electric vehicles, renewable energy converters, and industrial power supplies. Optimized driving methodologies are being explored to balance the switching speed, EMI suppression, and thermal management, ensuring that SiC MOSFETs can deliver their maximum potential without reliability concerns.

Acknowledgment

The authors would like to thank the National grant agency APVV for project funding APVV-21-0462 and to national grant agency Vega for project funding 1/0274/24.

Conflicts of interest

The authors declare that they have no known competing financial interests or personal relationships that could have appeared to influence the work reported in this paper.

References

- [1] HAIHONG, Q., CEYU, M., DAN, W., HAOTIAN, X., ZIYUE, Z., KEFENG, X., SHISHAN, W. An overview of SiC MOSFET gate drivers. In: 2017 12th IEEE Conference on Industrial Electronics and Applications (ICIEA): proceedings [online]. IEEE. 2017. eISSN 2158-2297, eISBN 978-1-5090-6161-7, p. 25-30. Available from: <https://doi.org/10.1109/ICIEA.2017.8282808>
- [2] onsemi, application note AND90204/D, onsemi EliteSiC Gen 2 1200V SiC MOSFET M3S Series [online] [accessed 2025-4-19]. Available from: <https://www.onsemi.com/download/application-notes/pdf/and90204-d.pdf?isLicenseAgreementAccepted=true>

- [3] ANURAG, A., ACHARYA, S., BHATTACHARYA, S. Gate drivers for high-frequency application of silicon-carbide MOSFETs: design considerations for faster growth of LV and MV applications. *IEEE Power Electronics Magazine* [online]. 2019, **6**(3), p. 18-31. ISSN 2329-9207, eISSN 2329-9215. Available from: <https://doi.org/10.1109/MPEL.2019.2925238>
- [4] SUN, N., HUANG, K., SUN, M., ZHANG, J., GAO, Z., CUI, C., WANG, T. A SiC MOSFET low switching loss strategy based on a reverse conduction. *IEICE Electronics Express* [online]. 2025, **22**(7), 20250050. eISSN 1349-2543. Available from: <https://doi.org/10.1587/elex.22.20250050>
- [5] PRAZENICA, M., KASCAK, S., RESUTIK, P. Power losses investigation in direct 3×5 matrix converter using MATLAB simulink. *Applied Sciences* [online]. 2023, **13**(6), 4049. eISSN 2076-3417. Available from: <https://doi.org/https://doi.org/10.3390/app13064049>
- [6] ALVES, L. F. S., LEFRANC, P., JEANNIN, P. -O., SARRAZIN, B. Review on SiC-MOSFET devices and associated gate drivers. In: 2018 IEEE International Conference on Industrial Technology ICIT: proceedings [online]. IEEE. 2018. eISBN 978-1-5090-5949-2, p. 824-829, Available from: <https://doi.org/10.1109/ICIT.2018.8352284>
- [7] SIMCAK, J., FRIVALDSKY, M., RESUTIK, P., KINDL, V., SKALA B., ZAVREL, M. Evaluation of the efficiency performance of 3-phase and 6-phase voltage source inverter. In: 2024 ELEKTRO (ELEKTRO): proceedings [online]. 2024. eISSN 2691-0616, eISBN 979-8-3503-7235-9, p. 1-4. Available from: <https://doi.org/10.1109/ELEKTRO60337.2024.10556894>
- [8] GHORBAL, M. J. B., NAOUAR, M. W. A systematic design methodology for power MOSFET gate drivers [online]. In: 2022 IEEE International Conference on Electrical Sciences and Technologies in Maghreb CISTEM: proceedings [online]. IEEE. 2022. eISBN 978-1-6654-5168-0. Available from: <https://doi.org/10.1109/CISTEM55808.2022.10044019>
- [9] onsemi, datasheet of NTH4L022N120M3S [online] [accessed 2025-4-19]. Available from: <https://www.onsemi.com/download/data-sheet/pdf/nth4l022n120m3s-d.pdf>
- [10] MANDAL, M., ROY, S., BASU, K. Analytical switching transient model of TO-247-4 packaged SiC MOSFETs and comparison with TO-247-3 devices [online]. In: 2022 IEEE Energy Conversion Congress and Exposition (ECCE): proceedings [online]. IEEE. 2022. eISSN 2329-3748, eISBN 978-1-7281-9387-8, p. 1-8. Available from: <https://doi.org/10.1109/ECCE50734.2022.9947557>



This is an open access article distributed under the terms of the Creative Commons Attribution 4.0 International License (CC BY 4.0), which permits use, distribution, and reproduction in any medium, provided the original publication is properly cited. No use, distribution or reproduction is permitted which does not comply with these terms.

DETECTION OF SELECTED REGULATORY TRAFFIC SIGNS USING COMMON DASHBOARD CAMERA

Dušan Koniar*, Libor Hargaš, Matúš Danko

Department of Mechatronics and Electronics, Faculty of Electrical Engineering and Information Technology, University of Zilina, Zilina, Slovakia

*E-mail of corresponding author: dusan.koniar@uniza.sk

Dušan Koniar 0000-0003-3029-3193,
Matúš Danko 0000-0002-2828-5189

Libor Hargaš 0000-0001-8716-0944,

Resume

Nowadays, many modern vehicles contain a lot of systems for autonomous functions or driver assistance systems (traffic sign recognition). Modern vehicles contain many embedded systems and control units (also for signal and image processing), so implementation of deep learning or AI-based algorithms is possible. In older vehicles, mentioned systems missing or they are limited. In this paper is presented a design of algorithm for detection of selected regulatory traffic signs to extend the selected autonomous or intelligent functions of older vehicles. Algorithm is based on shape and color detection of key features of selected regulatory traffic signs (amplification of specified color pixels and Generalized Hough Transformation). This algorithm can be easily implemented or used in many other applications, such as for driving mobile or robotic platforms. Detection efficiency of algorithm is also evaluated in this paper.

Article info

Received 19 June 2025

Accepted 14 August 2025

Online 29 September 2025

Keywords:

traffic sign recognition
color features
shape features
optical character recognition

Available online: <https://doi.org/10.26552/com.C.2025.051>

ISSN 1335-4205 (print version)

ISSN 2585-7878 (online version)

1 Introduction

Traffic sign recognition is an important part of autonomous driving, advanced driver-assistance systems (ADAS), and smart transportation systems. Traffic signs are important to ensure safe driving and efficient traffic flow. With the development of car assistance systems, the requirements for automated traffic sign detection are also increasing [1]. Traffic sign detection is often realized based on images taken from the dashboard cameras. Compared to other items like automobiles and trees, traffic signs are often smaller in images [2]. Usually, they take up less than 5% of the entire image. Extracting the necessary elements from photos of traffic signs is quite difficult because of their small size.

There are several methods used for traffic sign recognition, often involving machine learning, deep learning, and computer vision techniques. One of the most used computer vision techniques is color-based segmentation. Color-based segmentation is a fundamental technique in traffic sign recognition that uses distinctive colors (e.g., red, blue, yellow) of traffic signs to detect and classify them effectively. This

technique uses only color information. As mentioned in [3], Gaussian distributions are used to model each color for detection. Another technique used is color space extraction from various color models, e.g., HSL (Hue, Saturation, Value) [4-5], and consecutive creation of binary images that isolate objects of specific colors. The HSL color space is most effective for this purpose [6].

Segmentation techniques, based on the shape detection, are very useful for searching circular, triangular, or rectangular shapes [7]. These algorithms often use the Hough Transform, which can identify traffic signs based on their geometric shapes.

Hybrid methods combine traditional computer vision and deep learning techniques for improved recognition. These methods are used to speed up the detection of objects through preprocessing procedures. While the deep learning approaches handle classification, methods such as color segmentation or the Histogram of Oriented Gradients (HOG) technique reduce the number of searched features [8].

Presented algorithm is developed mainly for older vehicles to create basic or extend intelligent or autonomous functions. Detection of selected traffic signs

is important, especially in the cities where the traffic infrastructure is very complex and can negatively affect the driver's attention. In this paper is given an approach to the speed limit traffic signs, but the algorithm can be easily extended for other shapes and colors of traffic signs. The algorithm is divided into two steps: detection of traffic sign and reading the textual information from speed limiting sign. Information about speed limit can be used like a single information for driver (e.g., information on head-up display) or serve as input for adaptive cruise control.

2 Materials, methods, algorithms

The main goal of the proposed algorithm was to create a non-expensive and computationally simple system for detecting regulatory traffic signs (especially speed limits) using a car dashboard camera. Common dashboard cameras store video data using codecs (e.g., H.264). Reducing the memory storage demands usually results in worse image quality and color fidelity, or strong block effects [9]. Lower image quality is always a big challenge for vision algorithms focused on object detection in images.

On the other side, for the detection of specific regulatory traffic signs (speed limits), several typical features are assumed, which facilitate the detection process: selected regulatory signs have regular shape and expressive color to be in contrast with surroundings (typically circle with red rim, triangle with red rim...). From this point of view, one can focus on partial algorithms that search for or amplify image regions with specific colors or search for regular shapes.

In this work, several variants of possible algorithms are used and compared and selected the most effective and successful one. The algorithms were primarily tested offline on selected video sequences and static images from a real dashboard camera (MiVue C570).

For the evaluation of algorithm efficiency, the standard metrics based on computing precision and recall, was used.

First detection was based on Pattern Matching or Geometric Matching algorithm [10-13] running on an 8-bit grayscale version of the camera image. This pilot experiment was inspired by work [5]. In this study, the mentioned detection techniques were used for ideal (synthetic) images of traffic signs, except those with textual information (e.g., speed limits). We updated this work with this kind of traffic sign and real input images obtained from a dashboard camera. Pattern Matching is based on normalized cross-correlation between the inspected image and the defined template. Due to possible color variations of traffic signs, depending on weather conditions (rainy, sunny, misty, dark), only the intensity character of detected objects is assumed and classic Pattern Matching is preferred over the Color Pattern Matching. Assuming the geometrical features of traffic signs, we used Geometric Matching [10-13], also running on an 8-bit grayscale image from a camera.

Unfortunately, a real complex scene from a dashboard camera (containing buildings, trees, other traffic infrastructure, image noises and distortions) produces many image gradients (many false edges), which can be counterproductive using e.g., Geometric Matching. The accuracy or recall metrics reached approximately 20-30% in most cases. From this point of view, another version of the algorithm was proposed.

2.1 Algorithm - part 1: detection of traffic signs in input image

In our proposed final variant of the algorithm, we combined the color detection (represented by amplifying the given color channel) and shape detection provided by Generalized Hough Transformation (GHT) [14-15] for searching regular shapes (ellipses), followed by

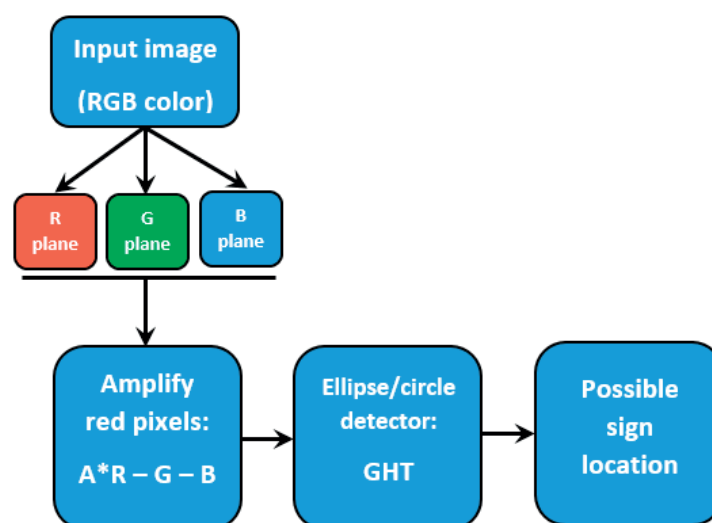


Figure 1 Detecting the traffic sign in entire dashboard image - block diagram

reading the textual content by an OCR algorithm. This pilot research was focused on circular signs with a red rim. Generalized Hough Transformations allow for the detection of other shapes: triangles, squares, hexagons. The first part of the detection algorithm is shown in Figure 1.

When using the NI LabVIEW environment for developing and debugging the algorithm, the Generalized Hough Transformation is built in a function called Shape Detection. The shape was set to an ellipse just from a practical point of view: the traffic sign in a real dashboard camera image is often an ellipse due to the strong variability of projection (when a car passes the traffic sign in a road bend, the circle changes to an ellipse). The detailed overview of the Shape Detection function is given in [11]. Using this function, users can modify several parameters for shape detection and its acceleration (searching for edges/gradients in the image and filtering of edges based on strength and length, setting the range for minor and major radius of the ellipse, setting the match score for the ellipse).

To simplify the input for the Shape Detection function, a preprocessed version was created of the input color image and amplified the red pixels (when detecting the signs with red rims). The resulting monochromatic

image I_r after the red amplification, is given by the formula:

$$I_r = A * R - G - B, \quad (1)$$

where A is the amplification constant for the red channel R, G is the green channel, and B is the blue channel of the input color image. Constant A is set empirically to 1.5 - 2.5. For further enhancement of the proposed algorithm, this constant can be computed based on the global mean value of the input image. The mean value of the input image strongly corresponds with weather conditions and illumination of the scene. The resulting amplified image I_r is set to 8-bit resolution using the saturation method.

Figure 2 shows the detection of a circular traffic sign in the input dashboard camera image.

In many cases, the traffic sign is detected twice (inner and outer edge of red rim), duplicities are removed by a simple algorithm using comparison of detected center points. Immediately after this step, the bounding boxes (Figure 3) are computed, and detected signs are extracted from the original input images. If the traffic sign detection is done upon the inner edge, the given ellipse major radius is increased by 10%, for

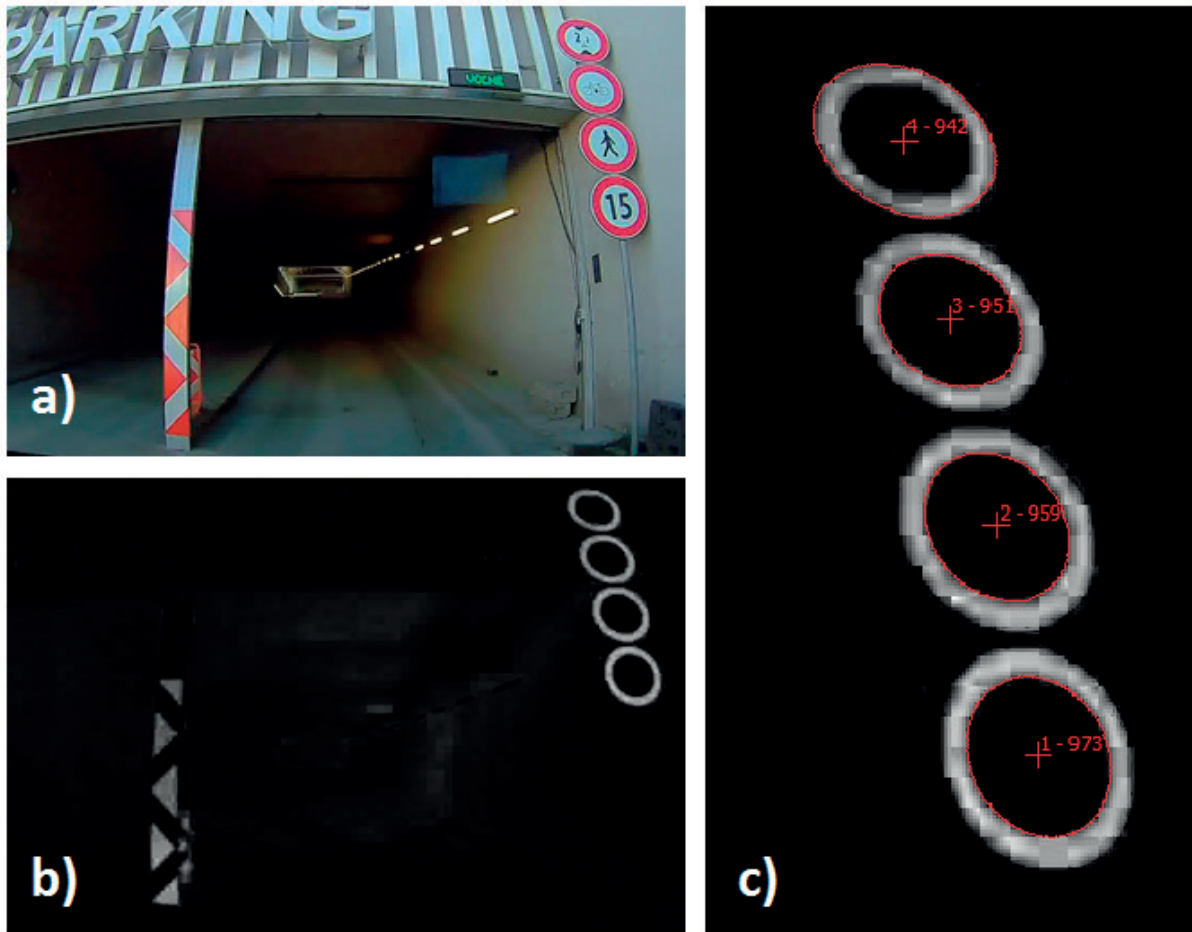


Figure 2 Detection of ellipses in input image: original color image (a); monochromatic image I_r after amplification of red pixels (b); output from Shape Detection function with highlighted center, radius and matching score (c)

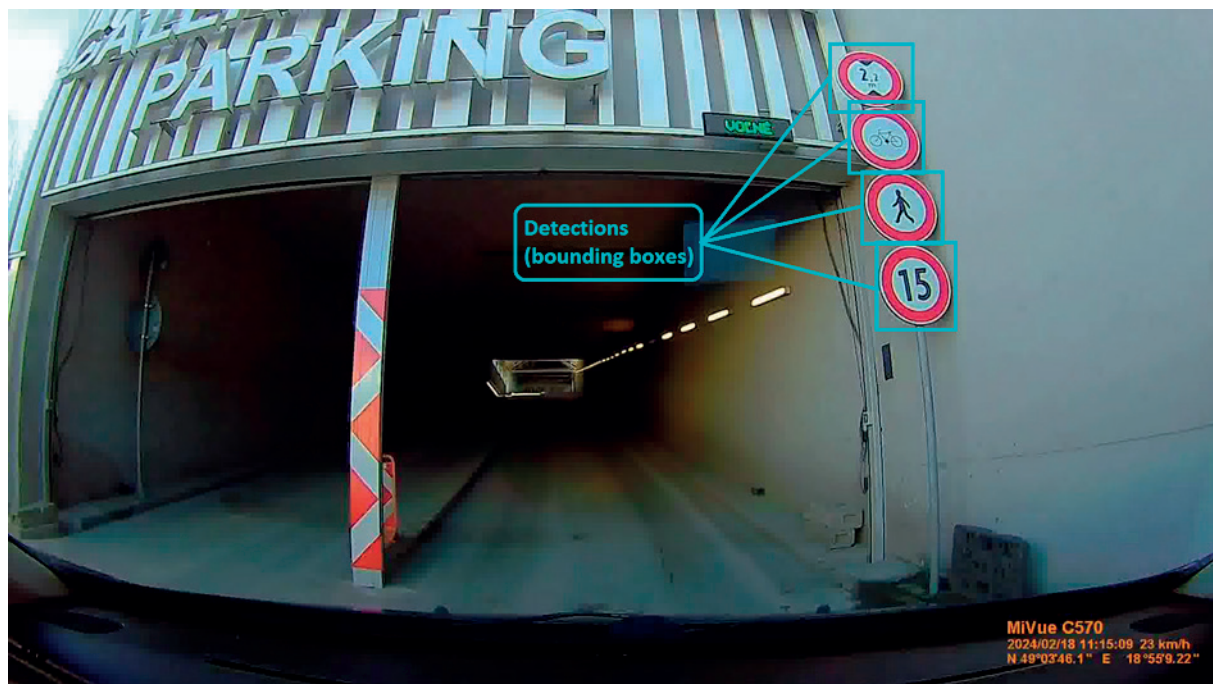


Figure 3 Construction of bounding boxes to detected circular traffic signs

example. This ensures that the traffic sign is extracted completely from the original image. Extracted image regions are then sent to the OCR algorithm for reading textual information about the speed limit.

2.2 Algorithm - part 2: preparation to OCR

The optical character recognition is a process that converts an image of text into a machine-readable text. The OCR is not a universal algorithm, but the main engine of this process is based on the classification of image patterns into classes representing numbers or

characters. In work [16] one can see that classification of image patterns can be provided by conventional methods of classification (e.g., k-Nearest Neighbor algorithm) or by using neural networks. In our implementation, the OCR algorithm was based on the k-Nearest Neighbor algorithm. In this approach, each image pattern, representing an alphanumerical character is binarized, then described by selected features (the feature vector is created). In the last step, the selected distance (Manhattan, Euclidean...) of the current feature vector is computed from each feature vector in the training set. From k minimal distances, the classification class is selected by the majority affiliation to the trained class.

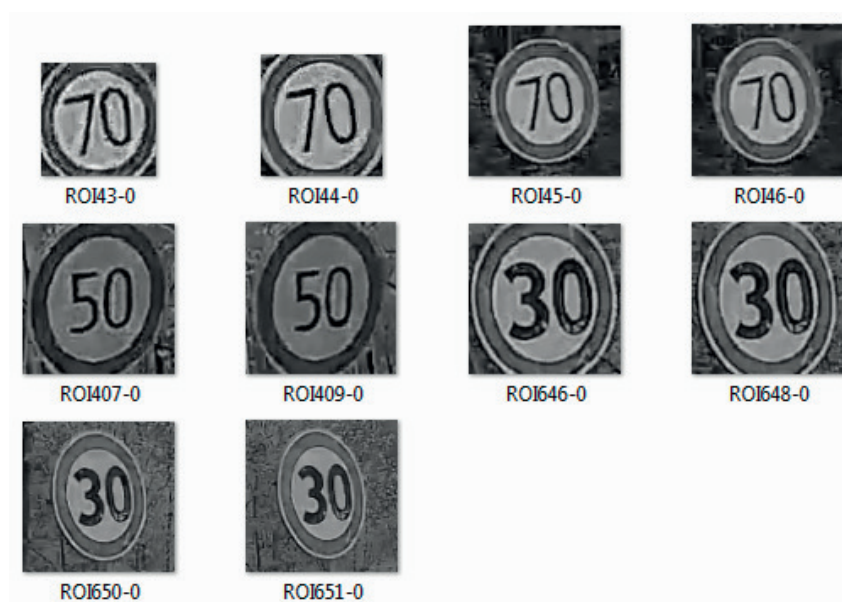


Figure 4 Several samples in OCR training dataset

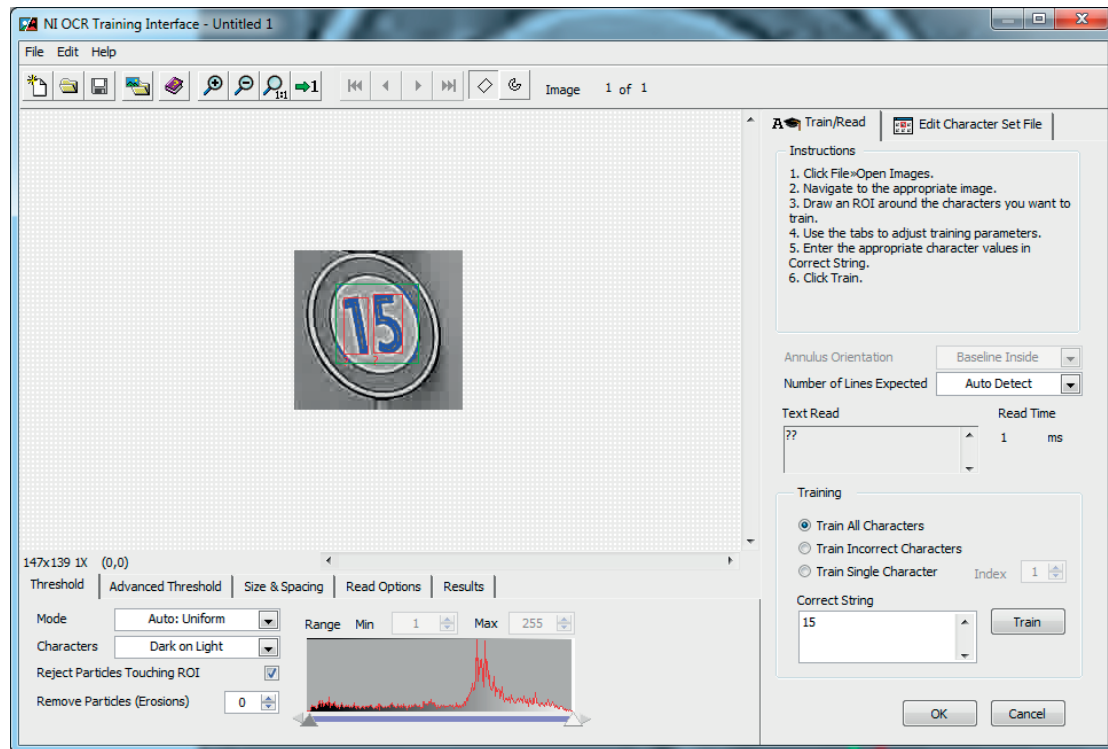


Figure 5 NI OCR Training interface

Based on [11], the features of binarized image patterns, representing text elements, must be scale and rotation-invariant: circularity, elongation, convexity, analysis of holes, spread, and slenderness.

The first part of the classification process is building the training dataset. When focusing on speed limit traffic signs, we created a dataset from numerical symbols only. In our dataset, each symbol, from 0 to 9, was used in at least 50 samples. Several samples of OCR

training datasets are shown in Figure 4. The dataset was created by combining the extracted traffic signs from the dashboard camera using a previously described algorithm, or using images taken from Google Street View. All the outliers (damaged signs, distorted signs) were removed from the training process.

After the training dataset was collected, the training process of OCR was provided in LabVIEW using the function NI OCR Training Interface (Figure 5).

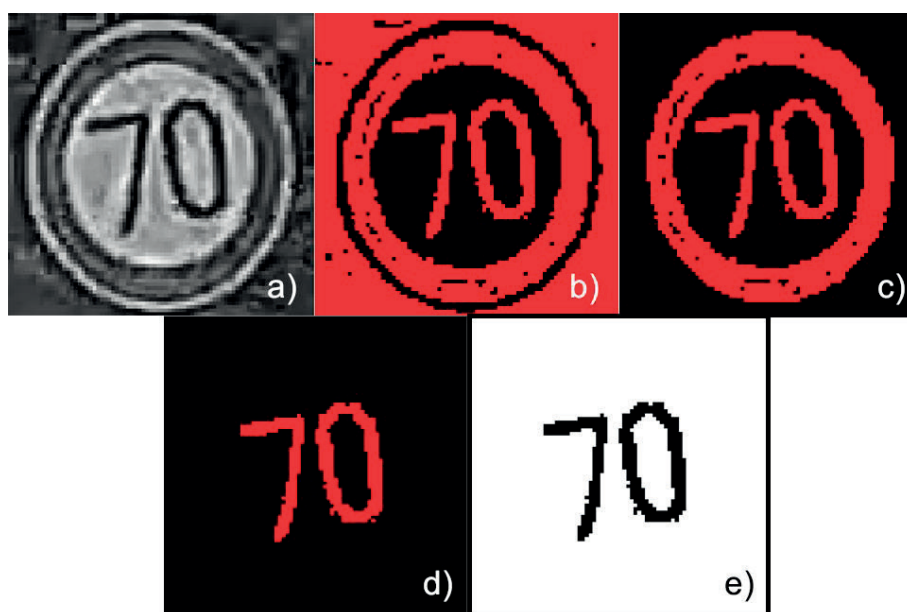


Figure 6 Morphological cleaning of extracted traffic sign before OCR: original of extracted traffic sign in 8-bit intensity mode (a); thresholding by Entropy method (b); removing border objects (c); filtering the objects lying outside of defined surroundings of image center point (d); binarized characters in black and white scale - dark objects on bright background (e)

2.3 Algorithm - part 3: Classification by OCR

To increase the efficiency of the classification process of a trained OCR system, a morphological clean-up algorithm was proposed. The OCR running directly on extracted traffic signs from the original image, and converted to an 8-bit intensity image, had worse results than OCR running on images after the morphological cleaning (Figure 6). The morphological algorithm consists of:

- binarization (Automatic threshold, Entropy method [11]);
- removing objects touching the image edge;
- keeping objects with center of mass lying in the given surroundings from the image center.

After this morphological cleaning, the OCR focuses mainly on proper binary patterns representing numerical symbols.

In this algorithm, other types of circular traffic signs with red rim can be detected and extracted from the input image (see Figure 2 or Figure 3). If any other symbol except numerical one appears in the sign content, the OCR function returns symbol “?” and this sign is ignored. If there is a requirement for classification of other types of traffic signs, NI Vision Particle Classification Training module serves as extension of OCR for any binary symbol.

3 Experimental results

To verify the efficiency and accuracy of the proposed algorithm, 10 video sequences were selected. From each video sequence, we extracted 100-200 frames where

the traffic signs - selected speed limits - had a critical radius (at least 30 pixels for minor or major radius). Video sequences were captured by the dashboard camera MI Vue C570 using the built-in codec H.264 (MP4 container). Different illumination and scene conditions were contained in video sequences (sunny, night, rain, traffic signs in shadow, traffic signs in front of buildings, trees, etc.). The entire algorithm was implemented into the NI LabVIEW interface (and later tested during driving - Figure 7). To amplify red pixels, we used a gain constant $A = 1.75$.

The detection performance of the entire process is evaluated in two steps. First, we measured the precision and recall for the detection of circular traffic signs (speed limit) from the input image. The accuracy of the OCR process was measured separately.

For evaluation of the traffic sign detection (the first step), the entire set of input images (a total of 1395 images) was manually annotated. True positive (TP), false positive (FP), and false negative (FN) states used for the computation of performance metrics are illustrated in Table 1.

The standard formulas for precision (P) and recall (R) computation were used:

$$P = \frac{TP}{TP + FP} \cdot 100\%, \quad (2)$$

$$R = \frac{TP}{TP + FN} \cdot 100\%. \quad (3)$$

Precision parameter expresses how many signs were detected in proper locations in images (the influence of false detections). Recall expresses how many signs were detected from the real number of traffic signs. In Table 2 one can see the precisions and

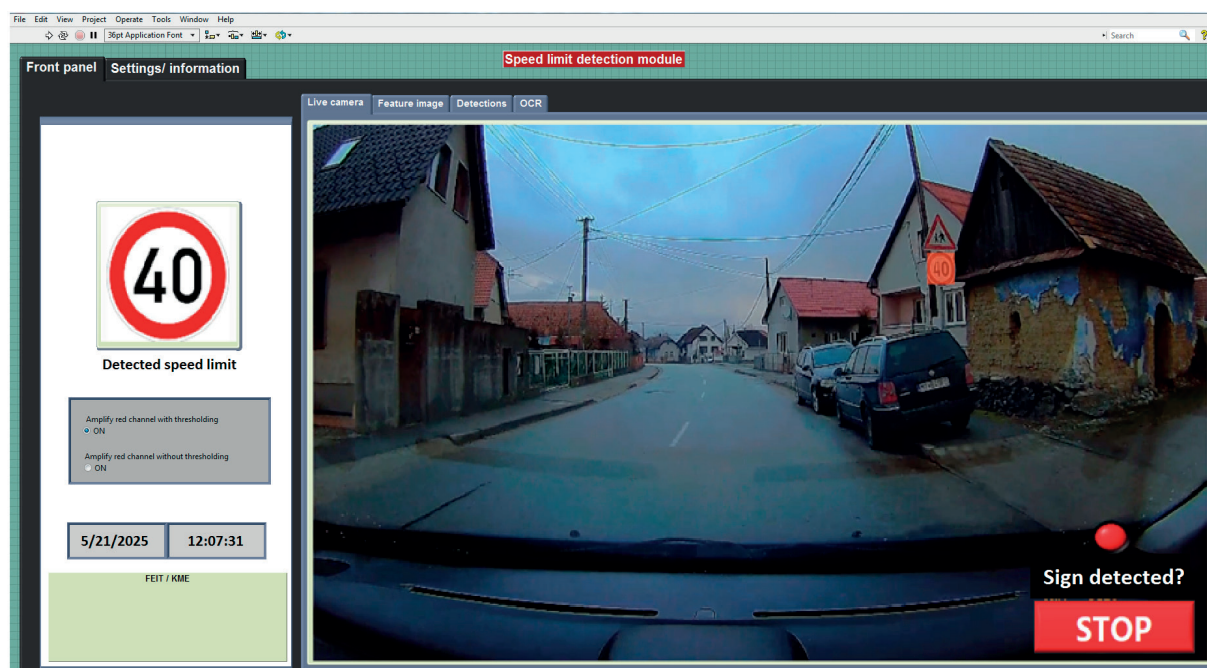


Figure 7 Algorithm implemented into LabVIEW and tested during car driving

recalls for each video sequence.

To measure the efficiency of the OCR algorithm, a set of images (real traffic signs contents) was prepared

with almost 500 characters. Number of each character, from 0 to 9, is shown in Table 3 along with success rate of correct reading in OCR.

Table 1 TP, FP and FN states in traffic sign detection




States	Sign detection	Images
True positive (TP)	Sign detected properly	
False positive (FP)	Sign detected in wrong location	
False negative (FN)	Sign not detected	

Table 2 Evaluation of precision and recall for speed limit sign detection

Sequence #	Weather / conditions	Precision [%]	Recall [%]
1	Sunny, field	95.37	92.66
2	Sunny, city	91.67	89.37
3	Sunny, combined backgrounds	96.74	91.67
4	Sunny, sun directly into the camera	25.14	24.35
5	Cloudy, city	89.37	87.36
6	Sunny, city - shadows	88.73	87.98
7	Rain, city	79.67	71.42
8	Rain, field	85.67	80.35
9	Night, car reflectors	80.29	63.19
10	Night, street lighting	73.98	45.78

Table 3 Evaluation of OCR conversion process

Single character			
Character	Number of characters	Correctly read	Success rate
0	89	76	85.39%
1	43	39	90.69%
2	50	41	82%
3	56	48	85.71%
4	45	35	77.77%
5	33	28	84.84%
6	42	37	88.10%
7	40	36	90%
8	45	38	84.44%
9	33	18	75%
All characters			
Number of characters		Correctly read	Success rate
476		396	83.19%

4 Discussion and conclusion

In this paper is presented an algorithm for detection and reading of selected regulatory traffic signs (especially speed limit signs, circular with red rim and textual-numerical content). Algorithm is based on traditional methods for color and shape detection following by OCR based on kNN classification of binarized numerical characters.

As one can see, the detection power of algorithm must be evaluated in two steps: accuracy of traffic sign localization from input image and accuracy of OCR reading process. The accuracy of localization and extraction of traffic sign from entire input image varies depending on the weather (scene illumination) conditions. The best results are achieved generally during the day, except in situations where the sun directly shines into the camera. The worse results were obtained during the rain and night. Success rate of OCR process varies from 75% to almost 91%. The most affecting reason for the process accuracy decreasing is usage of dashboard camera with serious image quality degradation and extreme weather conditions. In the future, many values set empirically, could be computed adaptively (e.g., the red channel amplifying constant A could be computed from global image illumination characteristics).

On the other side, precisions and recalls in Table 2 are computed from a set of independent images and they seem not to be so high. During the real driving,

however, a particular road sign is in the camera field for several seconds. The detection system often obtains several dozen images from it. In this case, for example, 80% recall is sufficient to confirm that a particular sign is correctly detected. Providing such experiments, the “global” recall can reach 95-100%.

Due to relatively simple partial algorithms, this solution can be easily implemented into older vehicles to extend intelligent or autonomous functions. Any other types of traffic signs can be easily added by the same process (reading other colors and shapes, training general binary patterns for traffic sign contents).

Acknowledgment

The results in this project were supported by grant VEGA 1/0563/23: Research and development of visual inspection algorithms for manufacturing process quality increasing of power semiconductor modules.

Conflicts of interest

The authors declare that they have no known competing financial interests or personal relationships that could have appeared to influence the work reported in this paper.

References

- [1] KHALID, S., SHAH, J. H., SHARIF, M., DAHAN, F., SALEEM, R., MASOOD, A. A Robust intelligent system for text-based traffic signs detection and recognition in challenging weather conditions. *IEEE Access* [online]. 2024, **12**, p. 78261-78274 [accessed 2025-04-30]. ISSN 2169-3536. Available from: <https://doi.org/10.1109/ACCESS.2024.3401044>
- [2] ZENG, G., HUANG, W., WANG, Y., WANG, X., E, W. Transformer fusion and residual learning group classifier loss for long-tailed traffic sign detection. *IEEE Sensors Journal* [online]. 2024, **24**(7), p. 10551-10560 [accessed 2025-04-30]. ISSN 1558-1748. Available from: <https://doi.org/10.1109/JSEN.2024.3360408>
- [3] LOPEZ, L. D., FUENTES, O. Color-based road sign detection and tracking [online]. In: *Image analysis and recognition (ICIAR 2007). Part of the book series: Lecture notes in computer science, Vol. 4633*. KAMEL, M., CAMPILHO, A. (Eds.). Berlin: Springer Heidelberg, 2007. ISSN 0302-9743, p. 1138-1147. Available from: https://doi.org/10.1007/978-3-540-74260-9_101
- [4] FLEYEH, H. Color detection and segmentation for road and traffic signs. In: *IEEE Conference on Cybernetics and Intelligent Systems: proceedings* [online]. IEEE. 2004. ISBN 0-7803-8643-4, p. 809-814. Available from: <https://doi.org/10.1109/ICCIS.2004.1460692>
- [5] PANOIU, M., RAT, C. L., PANOIU, C. Study on road sign recognition in LabVIEW. *IOP Conference Series: Materials Science and Engineering* [online]. 2016, **106**, 012009. ISSN 1757-899X. Available from: <https://doi.org/10.1088/1757-899X/106/1/012009>
- [6] WANG, Q., LIU, X. Traffic sign segmentation in natural scenes based on color and shape features. In: *2014 IEEE Workshop on Advanced Research and Technology in Industry Applications WARTIA: proceedings* [online]. IEEE. 2014. ISBN 9781479969890, p. 374-377. Available from: <https://doi.org/10.1109/WARTIA.2014.6976273>
- [7] HORAK, K., CIP, P., DAVIDEK, D. Automatic traffic sign detection and recognition using colour segmentation and shape identification. In: *2016 3rd International Conference of Industrial Engineering and Applications ICEA 2016: proceedings* [online]. 2016. ISSN 2261-236X. Available from: <https://doi.org/10.13140/RG.2.1.2292.6961>

- [8] YOUSSEF, A., ALBANI, D., NARDI, D., BLOISI D. D. Fast traffic sign recognition using color segmentation and deep convolutional networks [online]. In: *Advanced Concepts for Intelligent Vision Systems ACIVS 2016. Part of the book series: Lecture Notes in Computer Science. Vol. 10016*. BLANC-TALON, J., DISTANTE, C., PHILIPS, W., POPESCU, D., SCHEUNDERS, P. (Eds.). Cham: Springer, 2016. ISBN 9783319486796, p. 205-216. Available from: https://doi.org/10.1007/978-3-319-48680-2_19
- [9] UNTERWEGER, A. Compression artifacts in modern video coding and state-of-the-art means of compensation [online]. In: *Multimedia networking and coding*. FARRUGIA, E. A., DEBONO, C. J. (Eds.). IGI Global Scientific Publishing, 2013. ISBN 9781466626607, eISBN 9781466626911. Available from: <https://doi.org/10.4018/978-1-4666-2660-7.ch002>
- [10] CHEN, C. H. *Handbook of pattern recognition and computer vision* [online]. 6. ed. World Scientific Publishing, 2020. ISBN 978-981-12-1106-5, eISBN 978-981-12-1108-9. Available from: <https://doi.org/10.1142/11573>
- [11] IMAQ vision concepts manual [online] [accessed 2025-05-20]. Available from: <https://download.ni.com/support/manuals/322916b.pdf>
- [12] SAGA, M., BULEJ, V., CUBONOVA, N., KURIC, I., VIRGALA, I., EBERTH, M. Case study: performance analysis and development of robotized screwing application with integrated vision sensing system for automotive industry. *International Journal of Advanced Robotic Systems* [online]. 2020, **17**(3), p. 1-23 [accessed 2025-04-28]. ISSN 1729-8806, eISSN 1729-8814. Available from: <https://doi.org/10.1177/1729881420923997>
- [13] VERYKOKOU, S., IOANNIDIS, C. Image matching: a comprehensive overview of conventional and learning-based methods. *Encyclopedia* [online]. 2025, **5**(1), 4 [accessed 2025-05-22]. eISSN 2673-8392. Available from: <https://doi.org/10.3390/encyclopedia5010004>
- [14] BALLARD, D. H. Generalizing the Hough transform to detect arbitrary shapes. *Pattern Recognition* [online]. 1981, **13**(2), p. 111-122 [accessed 2025-05-17]. ISSN 0031-3203, eISSN 1873-5142. Available from: [https://doi.org/10.1016/0031-3203\(81\)90009-1](https://doi.org/10.1016/0031-3203(81)90009-1)
- [15] JAULIN, L., BAZEILLE, S. Image shape extraction using interval methods. *IFAC Proceedings Volumes* [online]. 2009, **42**(10), p. 378-383. ISSN 1474-6670. Available from: <https://doi.org/10.3182/20090706-3-FR-2004.00062>
- [16] TOMAR, S., KISHORE, A. A review: optical character recognition. *International Journal of Engineering Sciences and Research Technology* [online]. 2018, **7**(4), p. 233-238 [accessed 2025-05-30]. ISSN 2277-9655. Available from: <https://zenodo.org/records/1213078>



This is an open access article distributed under the terms of the Creative Commons Attribution 4.0 International License (CC BY 4.0), which permits use, distribution, and reproduction in any medium, provided the original publication is properly cited. No use, distribution or reproduction is permitted which does not comply with these terms.

MODELLING OF DYNAMIC STATES OF FIVE-PHASE INDUCTION MOTOR

Pavel Záskalický*, Daniela Perduková, Jan Kaňuch

Faculty of Electrical Engineering and Informatics, Technical University of Kosice, Kosice, Slovakia

*E-mail of corresponding author: pavel.zaskalicky@tuke.sk

Pavel Záskalický 0000-0001-7335-8458,
Jan Kaňuch 0000-0001-5723-0198

Daniela Perduková 0000-0002-2856-2027,

Resume

In this paper is presented a mathematical model of a five-phase induction motor with a cage rotor and a stator coils connected to a star. In constructing the mathematical model, It is assumed that the motor is fed from a five-phase frequency converter with an ideal harmonic waveform of the output supply voltage. It is considered that the motor operates in an open control loop with the ability to control the frequency and amplitude of the supply voltage.

The basic voltage equations in a two-phase coordinate system coupled to a stator are derived, as well as the relation for the electromagnetic moment. Based on the parameters measured on a real motor, a dynamic model was implemented in Matlab-Simulink environment. Using the dynamic model, various motor operating states were simulated, such as frequency ramp-up, speed reversal, or operation at super-nominal frequencies.

Article info

Received 19 June 2025

Accepted 18 September 2025

Online 7 October 2025

Keywords:

induction motor
mathematical model
five-phase motor
MATLAB Simulink
dynamic states

Available online: <https://doi.org/10.26552/com.C.2025.053>

ISSN 1335-4205 (print version)

ISSN 2585-7878 (online version)

1 Introduction

With the evolution of power semiconductor converters, multiphase motors have gained increasing importance - most commonly five- or six-phase machines. Among them the five-phase motors offer significantly more advantages than their three- or six-phase counterparts.

A key benefit is the reduction of stator current for the same power output. This results in a decreased current load on the converter's semiconductor components as well as lower Joule losses in the stator windings. This advantage becomes particularly important in high-power motor applications [1].

The five-phase motors are also known for their quiet operation, making them suitable for installations in residential buildings, hospitals, and hotels where the low noise levels are critical. Another benefit is their fault-tolerant capability: they can continue operating even if one supply phase is lost. By appropriate phase-shifting the remaining supply voltages, a rotating magnetic field can still be produced. Although the motor operates with reduced power, functionality is preserved. In contrast,

a power loss in one phase of a three-phase motor typically leads to total failure. This makes the five-phase motors ideal for applications such as elevator drives in high-rise or medical buildings, where unexpected stoppages can cause serious disruption.

An additional important advantage is their higher efficiency compared to similarly rated three-phase motors [2-5].

Increasing the number of supply phases also increases electromagnetic torque for a motor of the same physical volume. This necessitates the development of appropriate mathematical methods to assess the performance benefits of five-phase machines [6-9].

Typically, the five-phase motors are powered by a five-phase voltage source inverter using pulse-width modulation (PWM) of the output voltage. When the modulation frequency is sufficiently high, the output voltage and current waveforms of the inverter can be considered harmonic in nature [3, 10-11].

The inverter circuit supplying five-phase motors consists of five legs, each made up of series-connected transistors with anti-parallel freewheeling diodes, as shown in Figure 1.

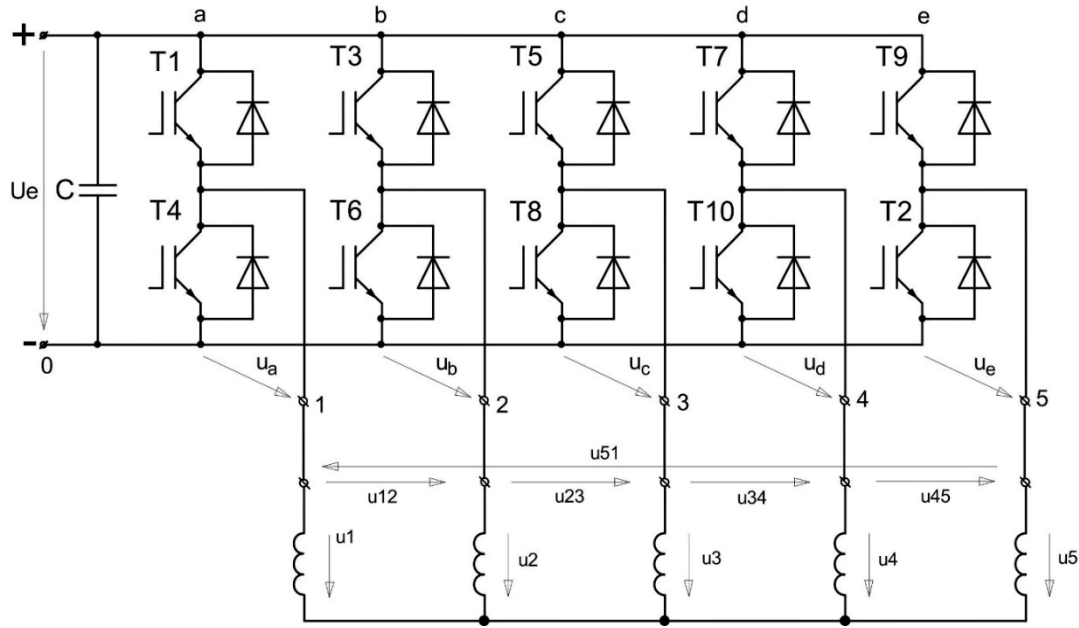


Figure 1 Five-phase voltage source inverter

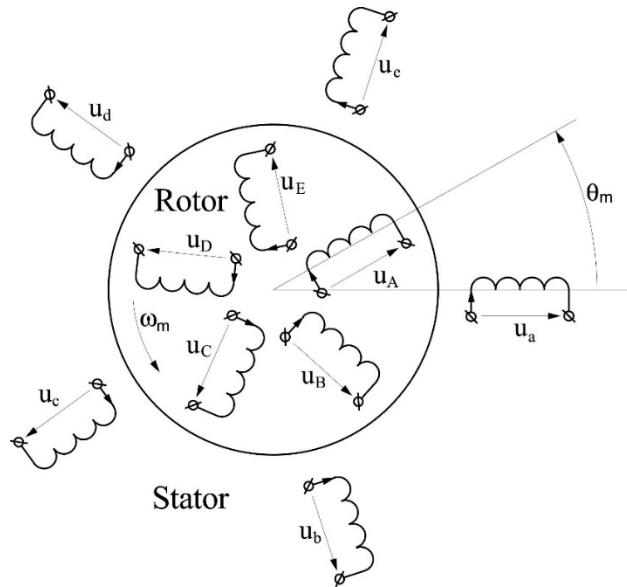


Figure 2 Windings of a five-phase machine

2 Mathematical model of a five-phase IM

When building the mathematical model of a motor, one starts from the two-pole version and assumes a motor with a wound armature, as shown in Figure 2. [12-14], where: $u_a, u_b, u_c, u_d,$ and u_e are the stator supply voltages. u_A, u_B, u_C, u_D and u_E are the rotor supply voltages.

The following voltage equations are valid for the motor stator coils:

$$\begin{aligned} u_a &= R_a i_a + \frac{d\psi_a}{dt}; u_b = R_b i_b + \frac{d\psi_b}{dt}; \\ u_c &= R_c i_c + \frac{d\psi_c}{dt}; u_d = R_d i_d + \frac{d\psi_d}{dt}; \\ u_e &= R_e i_e + \frac{d\psi_e}{dt}. \end{aligned} \quad (1)$$

Similarly, for the rotor windings:

$$\begin{aligned} u_A &= R_A i_A + \frac{d\psi_A}{dt}; u_B = R_B i_B + \frac{d\psi_B}{dt}; \\ u_C &= R_C i_C + \frac{d\psi_C}{dt}; u_D = R_D i_D + \frac{d\psi_D}{dt}; \\ u_E &= R_E i_E + \frac{d\psi_E}{dt}. \end{aligned} \quad (2)$$

where: R_{abcde} and R_{ABCDE} are the resistances of the stator and rotor coils, respectively;

i_{abcde} are the currents of the stator coils and i_{ABCDE} of the rotor coils, respectively;

ψ_{abcde} are the linkage fluxes of the stator coils and ψ_{ABCDE} of the rotor coils, respectively.

It is assumed that both the stator and rotor winding coils are symmetrical, so the coil resistances will be identical:

$$R_a = R_b = R_c = R_d = R_e = R_s; R_A = R_B = R_C = R_D = R_E = R_R.$$

The voltage Equations (1) and (2) can be expressed in the matrix form:

$$\begin{aligned} [u_{abcde}] &= R_s[i_{abcde}] + \frac{d}{dt}[\psi_{abcde}], \\ [u_{ABCDE}] &= R_R[i_{ABCDE}] + \frac{d}{dt}[\psi_{ABCDE}]. \end{aligned} \quad (3)$$

All the matrices in Equations (3) are column matrices.

For the linkage fluxes the following matrix equations are valid:

$$\begin{aligned} [\psi_{abcde}] &= [L_s][i_{abcde}] + [L_{SR}][i_{ABCDE}] \\ [\psi_{ABCDE}] &= [L_{SR}][i_{abcde}] + [L_R][i_{ABCDE}]. \end{aligned} \quad (4)$$

where, $[L_s]$ is stator, $[L_R]$ rotor and $[L_{SR}]$ stator-rotor matrix of inductances.

Matrix of stator inductances takes a form:

$$[L_s] = \begin{bmatrix} L_a & L_{ab} & L_{ab} & L_{ab} & L_{ab} \\ L_{ab} & L_a & L_{ab} & L_{ab} & L_{ab} \\ L_{ab} & L_{ab} & L_a & L_{ab} & L_{ab} \\ L_{ab} & L_{ab} & L_{ab} & L_a & L_{ab} \\ L_{ab} & L_{ab} & L_{ab} & L_{ab} & L_a \end{bmatrix} \quad (5)$$

where, L_a is a self-inductance and L_{ab} is a mutual inductance of stator windings.

Matrix of rotor inductances can be written as:

$$[L_R] = \begin{bmatrix} L_A & L_{AB} & L_{AB} & L_{AB} & L_{AB} \\ L_{AB} & L_A & L_{AB} & L_{AB} & L_{AB} \\ L_{AB} & L_{AB} & L_A & L_{AB} & L_{AB} \\ L_{AB} & L_{AB} & L_{AB} & L_A & L_{AB} \\ L_{AB} & L_{AB} & L_{AB} & L_{AB} & L_A \end{bmatrix} \quad (6)$$

where, L_A is a self-inductance and L_{AB} is a mutual inductance of rotor windings.

Matrix of stator-rotor mutual inductances depends on the rotor position:

$$[L_{SR}] = L_{aA} \begin{bmatrix} \cos \theta_m & \cos(\theta_m - \frac{2\pi}{5}) & \cos(\theta_m - \frac{4\pi}{5}) & \cos(\theta_m - \frac{4\pi}{5}) & \cos(\theta_m - \frac{2\pi}{5}) \\ \cos(\theta_m - \frac{2\pi}{5}) & \cos \theta_m & \cos(\theta_m - \frac{2\pi}{5}) & \cos(\theta_m - \frac{4\pi}{5}) & \cos(\theta_m - \frac{4\pi}{5}) \\ \cos(\theta_m - \frac{4\pi}{5}) & \cos(\theta_m - \frac{2\pi}{5}) & \cos \theta_m & \cos(\theta_m - \frac{2\pi}{5}) & \cos(\theta_m - \frac{4\pi}{5}) \\ \cos(\theta_m - \frac{4\pi}{5}) & \cos(\theta_m - \frac{4\pi}{5}) & \cos(\theta_m - \frac{2\pi}{5}) & \cos \theta_m & \cos(\theta_m - \frac{2\pi}{5}) \\ \cos(\theta_m - \frac{2\pi}{5}) & \cos(\theta_m - \frac{4\pi}{5}) & \cos(\theta_m - \frac{4\pi}{5}) & \cos(\theta_m - \frac{2\pi}{5}) & \cos \theta_m \end{bmatrix} = L_{aA}[C], \quad (7)$$

where $[C]$ is a matrix of cyclic rotor position and L_{aA} is a mutual inductance between the stator and rotor windings.

Finally, one can write the matrix equations for the stator and rotor linkage fluxes

$$\begin{aligned} [\psi_{abcde}] &= [L_s][i_{abcde}] + L_{aA}[C][i_{ABCDE}] \\ [\psi_{ABCDE}] &= L_{aA}[C]^t[i_{abcde}] + [L_R][\psi_{ABCDE}]. \end{aligned} \quad (8)$$

3 Voltages equations transformation

The transformation of the five-phase stator quantities into a two-phase system ($\alpha\beta xy0$) is realized using the transformation matrix $[A_s]$:

$$[A_s] = \begin{bmatrix} \cos(0) & \cos(\frac{2\pi}{5}) & \cos(\frac{4\pi}{5}) & \cos(\frac{6\pi}{5}) & \cos(\frac{8\pi}{5}) \\ \sin(0) & \sin(\frac{2\pi}{5}) & \sin(\frac{4\pi}{5}) & \sin(\frac{6\pi}{5}) & \sin(\frac{8\pi}{5}) \\ \cos(0) & \cos(\frac{6\pi}{5}) & \cos(\frac{12\pi}{5}) & \cos(\frac{18\pi}{5}) & \cos(\frac{24\pi}{5}) \\ \sin(0) & \sin(\frac{6\pi}{5}) & \sin(\frac{12\pi}{5}) & \sin(\frac{18\pi}{5}) & \sin(\frac{24\pi}{5}) \\ \frac{1}{2} & \frac{1}{2} & \frac{1}{2} & \frac{1}{2} & \frac{1}{2} \end{bmatrix}. \quad (9)$$

The transformation of the stator voltage Equations (3) is realized by multiplying them by the transformation matrix in Equation (9) from the left as follows:

$$[A_s][u_{abcde}] = R_s[A_s][i_{abcde}] + [A_s]\frac{d}{dt}[\psi_{abcde}], \quad (10)$$

where:

$$\begin{aligned} [A_s][u_{abcde}] &= [u_{\alpha\beta xy0}] \\ [A_s][i_{abcde}] &= [i_{\alpha\beta xy0}] \\ [A_s]\frac{d}{dt}[\psi_{abcde}] &= \frac{d}{dt}[\psi_{\alpha\beta xy0}]. \end{aligned}$$

For a symmetrical five-phase supply voltages system the following applies:

$$u_x = u_y = u_0 = 0.$$

Then, the stator voltages equations in the system ($\alpha\beta xy0$) take a form:

$$u_{\alpha s} = R_s i_{\alpha s} + \frac{d\psi_{\alpha s}}{dt}, u_{\beta s} = R_s i_{\beta s} + \frac{d\psi_{\beta s}}{dt}. \quad (11)$$

Transforming matrix for rotor quantities $[A_R]$ depends on the rotor position and takes a form:

$$[A_R] = \begin{bmatrix} \cos(\theta) & \cos\left(\theta_m - \frac{2\pi}{5}\right) & \cos\left(\theta_m - \frac{4\pi}{5}\right) & \cos\left(\theta_m - \frac{6\pi}{5}\right) & \cos\left(\theta_m - \frac{8\pi}{5}\right) \\ \sin(\theta_m) & \sin\left(\theta_m - \frac{2\pi}{5}\right) & \sin\left(\theta_m - \frac{4\pi}{5}\right) & \sin\left(\theta_m - \frac{6\pi}{5}\right) & \sin\left(\theta_m - \frac{8\pi}{5}\right) \\ \cos(\theta_m) & \cos\left(\theta_m - \frac{6\pi}{5}\right) & \cos\left(\theta_m - \frac{12\pi}{5}\right) & \cos\left(\theta_m - \frac{18\pi}{5}\right) & \cos\left(\theta_m - \frac{24\pi}{5}\right) \\ \sin(\theta_m) & \sin\left(\theta_m - \frac{6\pi}{5}\right) & \sin\left(\theta_m - \frac{12\pi}{5}\right) & \sin\left(\theta_m - \frac{18\pi}{5}\right) & \sin\left(\theta_m - \frac{24\pi}{5}\right) \\ \frac{1}{2} & \frac{1}{2} & \frac{1}{2} & \frac{1}{2} & \frac{1}{2} \end{bmatrix}. \quad (12)$$

Similarly, by multiplying the rotor voltage matrix equation by the transformation matrix $[A_S]$ and adjustment, one obtains the rotor voltage equations in the system $(\alpha\beta\gamma 0)$:

$$\begin{aligned} u_{ar} &= R_R i_{ar} + \frac{d\psi_{ar}}{dt} + \omega_m \psi_{\beta r} \\ u_{\beta sr} &= R_S i_{\beta r} + \frac{d\psi_{\beta r}}{dt} + \omega_m \psi_{ar}. \end{aligned} \quad (13)$$

4 Transformation of linkage magnetic fluxes

To transform the stator matrix equation of the linkage magnetic fluxes in Equation (8) one needs to multiply by the transformation matrix $[A_S]$ from the left as follow:

$$[A_S][\psi_{abcde}] = [A_S][L_S][i_{abcde}] + L_{aA}[A_S][C][i_{ABCDE}]. \quad (14)$$

After the solving, one obtains:

$$\begin{aligned} \psi_{as} &= L_s i_{as} + L_{sr} i_{ar} \\ \psi_{\beta s} &= L_s i_{\beta s} + L_{sr} i_{\beta r} \\ \psi_{xs} &= L_{xs} i_{xs} \\ \psi_{ys} &= L_{ys} i_{ys} \\ \psi_{0s} &= L_{0s} i_{0s}, \end{aligned} \quad (15)$$

where:

$$\begin{aligned} L_s &= L_a - L_{ab} \\ L_{0s} &= L_a + 2L_{ab} \\ L_{xs} &= L_a + 3L_{ab} \\ L_{ys} &= L_a + 3L_{ab} \\ L_{sr} &= \frac{5}{2}L_{aA}. \end{aligned}$$

The transformation of the rotor matrix equation is performed in the same way. One needs to again multiply the rotor matrix equation of the linkage magnetic fluxes in Equation (8) by the transformation matrix $[A_R]$ from the left:

$$\begin{aligned} [A_R][\psi_{ABCDE}] &= L_{aA}[A_R][C][i_{abcde}] + \\ &+ [A_R][L_R][i_{ABCDE}]. \end{aligned} \quad (16)$$

After the solving, one obtains:

$$\begin{aligned} \psi_{ar} &= L_R i_{ar} + L_{sr} i_{as} \\ \psi_{\beta r} &= L_R i_{\beta r} + L_{sr} i_{\beta s} \\ \psi_{xr} &= L_{xr} i_{xr} \\ \psi_{yr} &= L_{yr} i_{yr} \\ \psi_{0r} &= L_{0r} i_{0r}, \end{aligned} \quad (17)$$

where:

$$\begin{aligned} L_R &= L_A - L_{AB} \\ L_{0r} &= L_A + 2L_{AB} \\ L_{xr} &= L_A + 3L_{AB} \\ L_{yr} &= L_A + 3L_{AB} \\ L_{sr} &= \frac{5}{2}L_{aA}. \end{aligned}$$

Since in a symmetrical voltage supply system the following is valid: $i_{xs} = i_{ys} = i_{0s} = i_{xr} = i_{yr} = i_{0r} = 0$,

So even: $\psi_{xs} = \psi_{ys} = \psi_{0s} = \psi_{xr} = \psi_{yr} = \psi_{0r} = 0$.

For the linkage magnetic fluxes one can write the following matrix equations:

$$\begin{bmatrix} \psi_{as} \\ \psi_{ar} \end{bmatrix} = \begin{bmatrix} L_s & L_{sr} \\ L_{sr} & L_r \end{bmatrix} \begin{bmatrix} i_{as} \\ i_{ar} \end{bmatrix} \quad (18)$$

$$\begin{bmatrix} \psi_{\beta s} \\ \psi_{\beta r} \end{bmatrix} = \begin{bmatrix} L_s & L_{sr} \\ L_{sr} & L_r \end{bmatrix} \begin{bmatrix} i_{\beta s} \\ i_{\beta r} \end{bmatrix}, \quad (19)$$

5 Electromagnetic torque equation

The equation for the electromagnetic torque of a five-phase motor can be derived from the power in the air gap:

$$M = \frac{5}{2}pL_{sr}(i_{\beta s}i_{ar} - i_{as}i_{\beta r}). \quad (20)$$

To build a dynamic model of the motor, one also needs a mechanical equation:

$$M - M_p = J \frac{d\omega_m}{dt}, \quad (21)$$

where: J is the inertia moment recalculated on the motor shaft, M_p is the load torque.

6 Control of the induction motor (IM)

To control the IM, classical scalar method in an open control loop was used. At the scalar method, the induction motor speed is controlled by setting the voltage and frequency of the stator, so that the magnetic field in the gap is maintained at the desired value. To maintain a constant magnetic field in the gap, U/f ratio must be constant at different motor speeds, [14].

At low speed, it is necessary to compensate the voltage drop across the stator resistance, therefore, the U/f ratio at low speed is set higher than the rated value. For the simulation purposes, the ratio was replaced by a parabolic waveform (Figure 3).

The parabolic waveform can be expressed, using the frequency range (-50,50) Hz and the minimum voltage U_{\min} , according to the relation:

$$u = \frac{46f}{500} + U_{\min} \quad (22)$$

7 Induction motor model in Matlab

To investigate the dynamic properties of the motor, a dynamic model was created in the Matlab-Simulink environment. A block diagram of the drive with a five-phase induction motor is shown in Figure 4. The model was developed based on real measured values on a real

two-pole five-phase motor. The following data were used in the structure of the dynamic model, [11, 15]:

$$\begin{aligned} P_n &= 1.95 \text{ kW}; U_n = 200 \text{ V}/50 \text{ Hz}; p = 1; \\ n_n &= 2910 \text{ rev/min}; R_1 = 3.778 \Omega; R'_2 = 2.498 \Omega; \\ L_m &= 0.436 \text{ H}; L_{1\sigma} = 6.83 \text{ mH}; L'_{2\sigma} = 11.88 \text{ mH}; \\ J &= 0.01 \text{ kgm/s}^2. \end{aligned}$$

The stator linkage magnetic fluxes are calculated based on Equations (11). However before doing that, one needs to transform the five-phase supply voltages into a two-phase system (α, β) in block expressed as 5/2:

$$\begin{aligned} \psi_{\alpha s} &= \int (u_{\alpha s} - R_s i_{\alpha s}) dt \\ \psi_{\beta s} &= \int (u_{\beta s} - R_s i_{\beta s}) dt. \end{aligned} \quad (23)$$

The rotor linkage magnetic fluxes are calculated based on Equations (13) (block Psr), for a motor with a squirrel-cage rotor, $u_{ar} = u_{\beta r} = 0$.

$$\begin{aligned} \psi_{ar} &= \int (-R_r i_{ar} - \omega_m \psi_{\beta r}) dt \\ \psi_{\beta r} &= \int (-R_r i_{\beta r} - \omega_m \psi_{ar}) dt \end{aligned} \quad (24)$$

The stator and rotor currents components are calculated from matrix Equations (19):

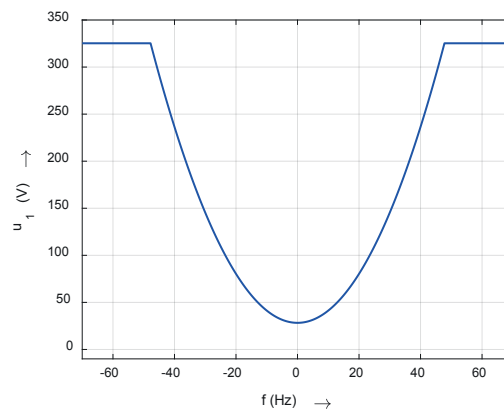


Figure 3 Voltage versus frequency

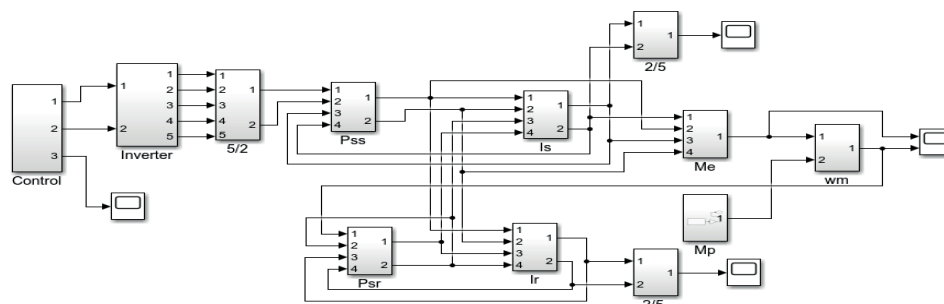


Figure 4 Block diagram of the five-phase IM drive

$$\begin{aligned} i_{as} &= \frac{L_r}{L_s L_r - L_{sf}^2} \psi_{as} - \frac{L_{sf}}{L_s L_r - L_{sf}^2} \psi_{ar} \\ i_s &= \frac{L_r}{L_s L_r - L_{sf}^2} \psi_{\beta s} - \frac{L_{sf}}{L_s L_r - L_{sf}^2} \psi_{\beta r}, \end{aligned} \quad (25)$$

$$\begin{aligned} i_{ar} &= \frac{L_r}{L_s L_r - L_{sf}^2} \psi_{ar} - \frac{L_{sf}}{L_s L_r - L_{sf}^2} \psi_{as} \\ i_r &= \frac{L_r}{L_s L_r - L_{sf}^2} \psi_{\beta r} - \frac{L_{sf}}{L_s L_r - L_{sf}^2} \psi_{\beta s}, \end{aligned} \quad (26)$$

The electromagnetic torque of the motor is calculated based on the Equation (20).

The motor speed is calculated by integrating the Equation (21):

$$\omega_m = \frac{1}{J} \int (M - M_p) dt. \quad (27)$$

8 Simulation results

Using the MATLAB simulation model of a five-phase induction motor, some dynamic states of the drive were simulated. The motor works in an open control loop with control of the voltage-frequency ratio.

Figure 5 shows the waveform of an electromagnetic torque and speed of the motor under frequency start-up and load change. The frequency of the supply voltage during start-up increases linearly from zero to a value of $f = 50$ Hz for $t = 1$ s. The motor is not loaded during a start-up. After the start-up the motor is loaded with a torque equal to the nominal value of the machine ($m_p = 6.5$ Nm). Subsequently, the load torque is reduced to the value of $m_p = 3$ Nm. The corresponding stator and rotor current waveforms are shown in Figure 6. The rotor current value is recalculated to stator.

Figure 7 shows the frequency run-up of a motor

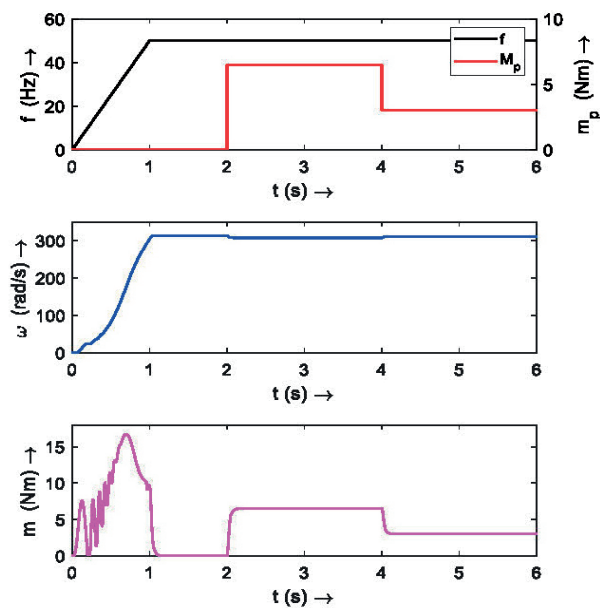


Figure 5 Not loaded motor frequency start-up

loaded with a constant torque of 3 Nm at a frequency of 50 Hz. During the start-up, the ratio U/f is kept constant (Figure 3). Subsequently, the motor is started at a frequency of 80 Hz. In this region, the supply voltage is already independent of frequency and is equal to the nominal value. In Figure 8, the corresponding values of the stator and rotor currents are shown.

Figure 9 shows the simulation results of the frequency reversal drive. The motor is started with a load of 3 Nm at a frequency of 50 Hz. After the start-up, the supply frequency is linearly changed to -50 Hz. During the reversal, the ratio U/f is kept constant. Figure 10 shows the stator and rotor current waveforms during motor reversal, respectively.

9 Conclusion

In the research presented in this paper, a mathematical model of a five-phase induction motor with a squirrel-cage rotor and star-connected stator winding is developed. However, the derived equations are also applicable to pentagonal and pentagram connection systems.

Several typical dynamic states of the motor are demonstrated using the proposed model. The machine's transient behavior is illustrated through the waveforms of stator and rotor phase currents, electromagnetic torque, and speed under various loading conditions.

The motor's characteristics during the frequency ramp-up, reversal, and sudden load application, in the regions of constant torque and constant power operation, are presented.

By comparing the simulation results to waveforms measured on a real five-phase motor drive - previously

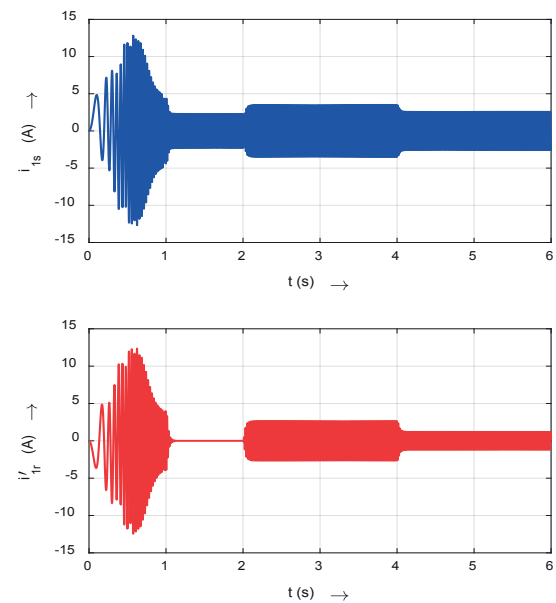


Figure 6 Stator and rotor phase-current

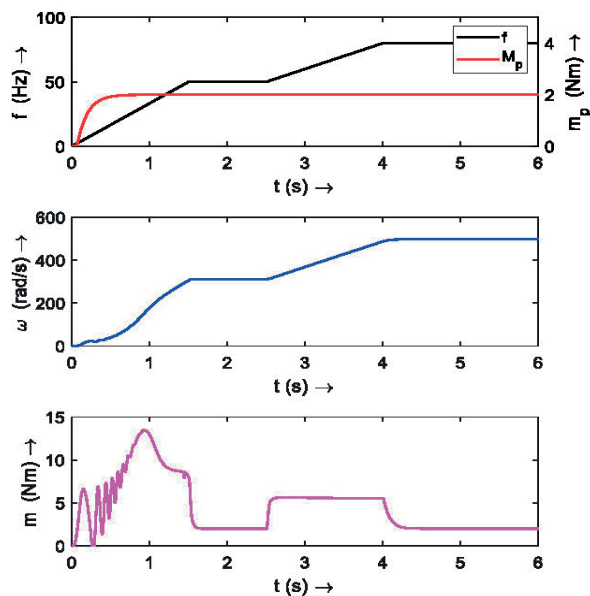


Figure 7 Loaded motor frequency start-up

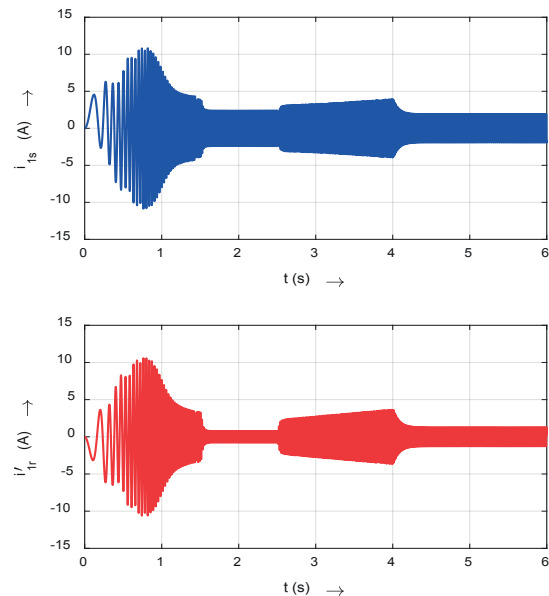


Figure 8 Stator and rotor phase-current

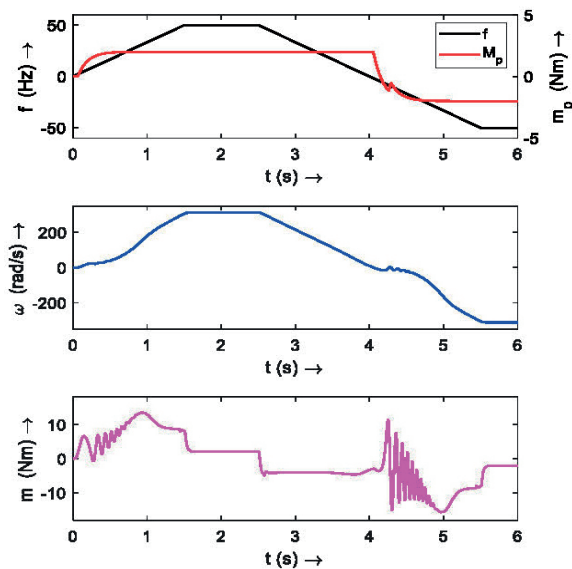


Figure 9 Motor frequency reversal

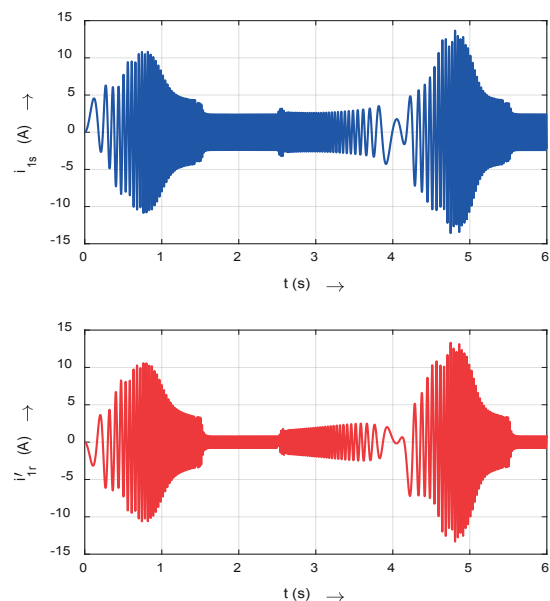


Figure 10 Stator and rotor phase-current

published in [11] - it is concluded that the model is sufficiently accurate and suitable for investigating various dynamic states of the machine. Thus, the proposed model may be accepted as a simulation model, capable of replicating the different operating conditions of an actual motor operating in an industrial environment.

The presented computer simulation model is effective for transient analysis of the five-phase induction motor. Using the SIMULINK software, each block of the model may be connected and modified easily. Some limit conditions, such as saturation of magnetic circuit and stator current limit, may be easily inserted in the function blocks.

Acknowledgment

This work was supported by project APVV-19-0210, project VEGA 1/0363/23 and by the EU Next Generation EU through the Recovery and Resilience Plan for Slovakia under the project No. 09I05-03-V02-00018.

Conflicts of interest

The authors declare that they have no known competing financial interests or personal relationships that could have appeared to influence the work reported in this paper.

References

- [1] SPANIK, P., DOBRUCKY, B., FRIVALDSKY, M., DRGONA, P. Measurement of switching losses in power transistor structure. *Elektronika ir Elektrotechnika / Electronics and Electrical Engineering*. 2008, **2**, p. 75-78. ISSN 1392-1215.
- [2] KELLNER, J., PRAZENICA, M. Research into the possibility of improving the efficiency and torque ripple of a drive with a five-phase induction motor by changing the control in a fault state. In: 2022 International Symposium on Power Electronics, Electrical Drives, Automation and Motion SPEEDAM 2022: proceedings. 2022. p. 663-670.
- [3] KELLNER, J., KASCAK, S., FERKOVA, Z. Investigation of the properties of a five phase induction motor in the introduction of new fault-tolerant control. *Applied Sciences* [online]. 2022, **12**(4), 2249. eISSN 2076-3417. Available from: <https://doi.org/10.3390/app12042249>
- [4] CHOMAT, M., SCHREIER, L. Investigation of induction machine with rotor-bar faults. In: International Conference on Electrical Drives and Power Electronics: proceedings [online]. IEEE. 2019. eISBN 978-1-7281-0389-1, eISSN 1339-3944, p. 12-17. Available from: <https://doi.org/10.1109/EDPE.2019.8883888>
- [5] HOLY, T. Mathematical models of multiphase machines based on symmetrical components decomposition in relation to space harmonics. In: 24-th International Scientific Conference on Electric Power Engineering, EPE 2024: proceedings. 2024.
- [6] CHOMAT, M., SCHREIER, L. Effect of stator winding configuration on operation of converter fed five-phase induction machine. In: Electric Drives and Power Electronics EDPE: proceedings [online]. IEEE. 2015. eISBN 978-1-4673-7376-0, eISSN 1339-3944. Available from: <https://doi.org/10.1109/EDPE.2015.7325343>
- [7] TIAN, B., LU, R., HU, J. Single line/phase open fault-tolerant decoupling control of a five-phase permanent magnet synchronous motor under different stator connections. *Energies* [online]. 2022, **15**(9), 3366. eISSN 1996-1073. Available from: <https://doi.org/10.3390/en15093366>
- [8] FAN, S., MENG, D., AI, M. Comparison and analysis of the performance of five-phase induction motors with different stator winding connections under open-circuit conditions. *Diangong Jishu Xuebao / Transactions of China Electrotechnical Society* [online]. 2022, **37**(7), p. 1679-1688. ISSN 1000-6753. Available from: <https://doi.org/10.19595/j.cnki.1000-6753.tces.201643>
- [9] KUCZMANN, M., HORVATH, K. Design of feedback linearization controllers for induction motor drives by using stator reference frame models. In: 2021 IEEE 19th International Power Electronics and Motion Control Conference PEMC 2021: proceedings. 2021. p. 766-773.
- [10] DOBRUCKY, B., KASCAK, S., PRAZENICA, M., RESUTIK, P. Direct controlled [3x5] matrix converter supplying 5-phase pentacle IM. In: 13th International Conference ELEKTRO 2020: proceedings [online]. 2020. eISBN 978-1-7281-7542-3. Available from: <https://doi.org/10.1109/ELEKTRO49696.2020.9130228>
- [11] KYSLAN, K., LACKO, M., FERKOVA, Z., ZASKALICKY, P. V/f control of five phase induction machine implemented of DSP using Simulink coder. In: 13th, International Conference ELECTRO 2020: proceedings [online]. 2020. eISBN 978-1-7281-7542-3. Available from: <https://doi.org/10.1109/ELEKTRO49696.2020.9130358>
- [12] CHATELAIN, J. *Electrical machines* (in French). Vol. X. University of Lausanne: Romandy Polytechnic Presses, 1983. ISBN 9782604000020.
- [13] SAIKUMAR, V. V., SATHIVANY, B., SURESH, J. Mathematical modeling of five-phase and three-phase induction motor and their result comparison. *IOP Conference Series: Materials Science and Engineering* [online]. 2020, **981**, 042059. ISSN 1757-899X. Available from: <https://doi.org/10.1088/1757-899X/981/4/042059>
- [14] ZHAO, P., LIPO, T. A. Space vector PWM control of dual-phase induction machine using vector space decomposition. *IEEE Transactions on Industry Applications* [online]. 1995, **31**(5), p. 1100-1109. ISSN 0093-9994, eISSN 1939-9367. Available from: <https://doi.org/10.1109/28.464525>
- [15] ZASKALICKY, P., KANUCH, J. Dynamic model of five-phase induction motor. In: 2023 International Conference on Electrical Drives and Power Electronics EDPE 2023: proceedings [online]. IEEE. 2023. eISBN 979-8-3503-2275-0, eISSN 2770-7652. Available from: <https://doi.org/10.1109/EDPE58625.2023.10274057>



This is an open access article distributed under the terms of the Creative Commons Attribution 4.0 International License (CC BY 4.0), which permits use, distribution, and reproduction in any medium, provided the original publication is properly cited. No use, distribution or reproduction is permitted which does not comply with these terms.

MODELLING THE EQUIVALENCY FACTOR OF E-RICKSHAW UNDER HETEROGENEOUS TRAFFIC CONDITIONS

Amir Ali Khan*, Sachin Dass

Deenbandhu Chhotu Ram University of Science and Technology, Murthal, Sonapat, Haryana, India

*E-mail of corresponding author: amirm640@gmail.com

Amir Ali Khan 0000-0002-3309-9831,

Sachin Dass 0000-0003-1015-4807

Resume

E-rickshaws, as emerging transport modes, notably affect mixed traffic flow on urban roadways. To evaluate their influence relative to other vehicle types, this study aim was to determine the Passenger Car Unit (PCU) value for e-rickshaws, as the Indian Roads Congress has yet to assign one. Three analytical methods were used: Chandra's method, the homogeneous coefficient method, and multiple linear regression. Data were gathered via three-hour video recordings at three different locations, each in Hapur and Sonapat. Using VLC media player, vehicle speeds and counts were extracted for analysis. The data were then processed in SPSS and Excel to derive equivalency values and assess influencing factors. Results indicate that the e-rickshaw's PCU value increases with rising traffic speed, but decreases with higher e-rickshaw concentration. Additionally, when the traffic volume increases, but composition remains unchanged, the PCU value for e-rickshaws shows a declining trend. These findings can help to refine the traffic flow modelling in heterogeneous conditions.

Article info

Received 29 January 2025

Accepted 9 July 2025

Online 25 July 2025

Keywords:

e-rickshaw
equivalency factor
Chandra's method
homogeneous coefficient method
speed-based modelling

Available online: <https://doi.org/10.26552/com.C.2025.046>

ISSN 1335-4205 (print version)
ISSN 2585-7878 (online version)

1 Introduction

E-rickshaws are the three-wheeled electric vehicles that can carry up to four passengers. They are becoming increasingly popular as a mode of transport in urban areas due to their low operating costs and environmental friendliness. The PCU (Passenger Car Unit) or PCE (Passenger Car Equivalency) or equivalency factor is a comparative weightage factor implemented to the volume of traffic of individual vehicle types to cope with variability in a mixed flow environment [1]. For analyzing various traffic factors, it is critical to compute equivalency factors. The precision of the equivalency factor for e-rickshaw is extremely important in traffic flow analysis due to its diverse uses. Even though there are a large number of e-rickshaws running on urban streets, the equivalency factor of an e-rickshaw is not available [2]. This research aim was to derive the equivalency factor of an e-rickshaw and the impact of various parameters on its value. It could aid the traffic planners in adequately coping with mixed traffic scenarios

The speed of traffic and the proportion of vehicle types in the stream significantly impact the equivalency factors of vehicle types. Many researchers [3-4] conducted studies to determine this impact on heavy vehicles, but there is no available significant research in the case of slow-moving vehicles. This study aim was to check this effect on the equivalency factor of e-rickshaw (slow-moving vehicle).

This research had the following purpose:

- To calculate the traffic speed.
- To calculate the equivalency factor of e-rickshaw.
- To check the impact of traffic speed on the equivalency factor of e-rickshaw.
- To check the impact of the composition of e-rickshaw on the equivalency factor of e-rickshaw.
- To check the effect of traffic volume on the equivalency factor of e-rickshaw.

This research results could be valuable for traffic planners and engineers as there is currently a lack of substantial research on the equivalency factor of e-rickshaws, and would aid them in effectively addressing this issue.

2 Literature review

2.1 Methods of equivalency factor estimation

Several methods are available for PCU estimations. However, different methods are used for different traffic and roadway conditions. Various methods published in reputed journals are (i) Chandra's method- proposed by [5], (ii) Homogeneous Coefficient method, (iii) Headway method- used by [6], (iv) Multiple linear regression- used by [7-8], (v) Speed based modelling - used by [9], (vi) Density method- used by [10], (vii) Huber's method- proposed by [11]. Among these methods, the Chandra's method, homogeneous coefficient method, multiple linear regression, and speed-based modelling are commonly used methods for heterogeneous or mixed traffic conditions, and the rest are used primarily for homogeneous conditions.

2.2 Factors affecting passenger car unit

The PCU or PCE of a vehicle is influenced by many traffic and geometric parameters. Some of the important factors mentioned in the reputed journals are described below: (i) Traffic speed, (ii) Traffic volume, (iii) Traffic composition, (iv) Carriageway width, (v) Shoulder width, (vi) Gradient of the road, (vii) Horizontal and vertical curvature of the road, (viii) Weather condition, (ix) Time, (x) Amount of rainfall, (xi) Type of terrain, (xii) Headway, (xiii) Level of service (LOS) and more.

2.3 Review of previous research papers

Passenger car unit for e-rickshaw was determined by Barman et al. (2025) on divided Indian urban roads. According to the study, the static PCU was 0.78 with a range of [0.53-1.80]. Additionally, when the traffic density increases, the PCU becomes less sensitive to the road's operating condition, according to a sensitivity analysis [12]. Khan and Dass (2025) estimated and compared PCU values using different methods of estimation and concluded that out of many methods, Chandra's method is best suited in mixed traffic conditions. The PCU of e-rickshaw was also calculated in this study, and it is smaller than 1 [13]. Kalogo and Costa (2024) accessed the PCU values due to change in width of roadway using speed based method and found out that the influence of a road's decreasing effective width on travel speed is substantial. Variations in travel speed have an impact on the comparable values for passenger cars [14]. Khan and Singh (2021) calculated the equivalency factor of an e-rickshaw on non-rural arterials in Sonipat, Haryana, using Chandra's approach and speed-based modelling. They found that the equivalency factor of e-rickshaw changes with varying traffic parameters. It was also concluded that there is no relationship

between the carriageway width and the PCU value of E-rickshaw [2]. Sharma and Biswas (2021) presented a review of the literature on approaches of equivalency factor estimation and their relevance to urban arterials. Among the different ways of computing the PCU value of vehicle types present in the flow, the speed-based method (Chandra's method) is extensively employed, particularly on metropolitan routes. The effect of different traffic and geometric parameters on the PCU values of different vehicles was also discussed [1]. Vijay and Khataavkar (2019) used the Chandra's approach to determine the influence of lane width, horizontal radius, and speed on PCU values of different vehicle kinds. They found that when the speed increased, PCU values increased as well. It was concluded that the increase in lane width and radius substantially caused an increase in PCU value [15]. Rao et al. (2017) reviewed equivalency factor studies in both mixed and non-mixed flow scenarios. The major purpose of this research was to examine and define data trends, as well as to identify areas for future research in order to improve PCU values. Their research revealed that traffic and geometric characteristics must be taken into account while developing a model for calculating the most acceptable PCU values of vehicles that may be applied universally [15]. Tullu et al. (2021) used the Chandra's method and regression analysis to determine Passenger Car Units for urban roads in Addis Ababa, Ethiopia. The impact of traffic volume and carriageway width on equivalency factors was studied, and it was observed that increasing the values of both factors increases the PCU value of vehicles [16]. Biswas et al. (2017) used a kriging-based system to illustrate the impacts of vehicular volume and composition on velocity and equivalency values for vehicles on an intercity roadway under a heterogeneous traffic mix [17]. Patkar and Dhamaniya (2020) demonstrated the impact of non-motorized vehicle types on the operating speed and potential of mixed road transport in urban arterial mid-block segments. In nations such as India, combining non-motorized vehicles with motorized automobiles without lane driving is very common. The existence of NMVs (non-motorized vehicles) is observed to markedly slow down the speed of motorized vehicles and, thus, the stream speed. The reduced stream speed decreases the capacity of city road sections significantly. The percentage of non-motorized vehicles in a stream of traffic determines this decline in capacity [18]. Sekhar et al. (2016) studied the assessment of free flow speeds on inter-urban roadways. This research is primarily concerned with a review of the alternate meanings of (FFS) Free Flow speed reported in the literature. Bases for evaluating the free flow speed (FFS) for the two-lane intercity highways were also studied [19]. Mondal et al. (2017) published a paper on the estimation of PCU values and to check variations due to changes in traffic composition and traffic volume using the Chandra's method and found that any change in traffic parameters leads to a change in PCU values [20]. Variation in PCU

values due to lane width, traffic volume, and composition using Chandra's method was studied by Mardani et al. (2015), and the result of the research shows that these parameters have a considerable impact on PCU values of vehicle types [21]. Dhananjaya et al. (2023) used Chandra's method to evaluate PCUs for midblock sections of Sri Lanka under mixed traffic situations. In the Colombo district of Sri Lanka, PCU values of ten vehicle classifications for four separate mid-block road sections were assessed. Field surveys were used to gather information about the two key variables in this method: category speed and vehicle area. The outcomes of the four-lane highways were integrated and contrasted with the currently present PCEs with the aim of recommending a revised set for general transport investigations in Sri Lanka [22].

3 Methodology

The methodology employed in this research is presented in Figure 1. Initially, the study area was chosen and data on traffic and geometry were collected and analyzed to determine the speed and equivalency factor. Subsequently, in this study was investigated the impact of traffic speed and the composition of e-rickshaws on the road and the traffic volume in the stream.

4 Study area and data collection

Three divided urban roads of Hapur city, Uttar Pradesh, and three divided urban roads of Sonipat city, Haryana, were considered as the study area. Both cities have similar kinds of traffic environments. The details of the selected roads is shown in Table 1 and maps displaying selected sites where traffic was measured are shown in Figures 2 and 3 for Hapur and Sonipat city, respectively. The criteria used to select the sites were that they must be divided roads and free of obstacles such as parking lots, crossroads, stoppages, etc. All the sites from both cities were in the urban environment. A section of a certain length on each road was marked for capturing the videos. The 3-hour long videos were captured on each site. Later, those videos were interpreted to determine the average speed and volume count of each vehicle type with the help of VLC Media Player. Speed and volume data were extracted in 15-minute intervals. A total of 12 intervals of 15 minutes were extracted from 3-hour-long videos. Using a VLC media player, captured videos were slowed down to note down the traffic volume and Frame-by-frame analysis was done to divide the video footage into separate frames so that the movements of vehicles could be precisely examined to help in determining the speed of vehicles. Dimensions of cars and e-rickshaws were

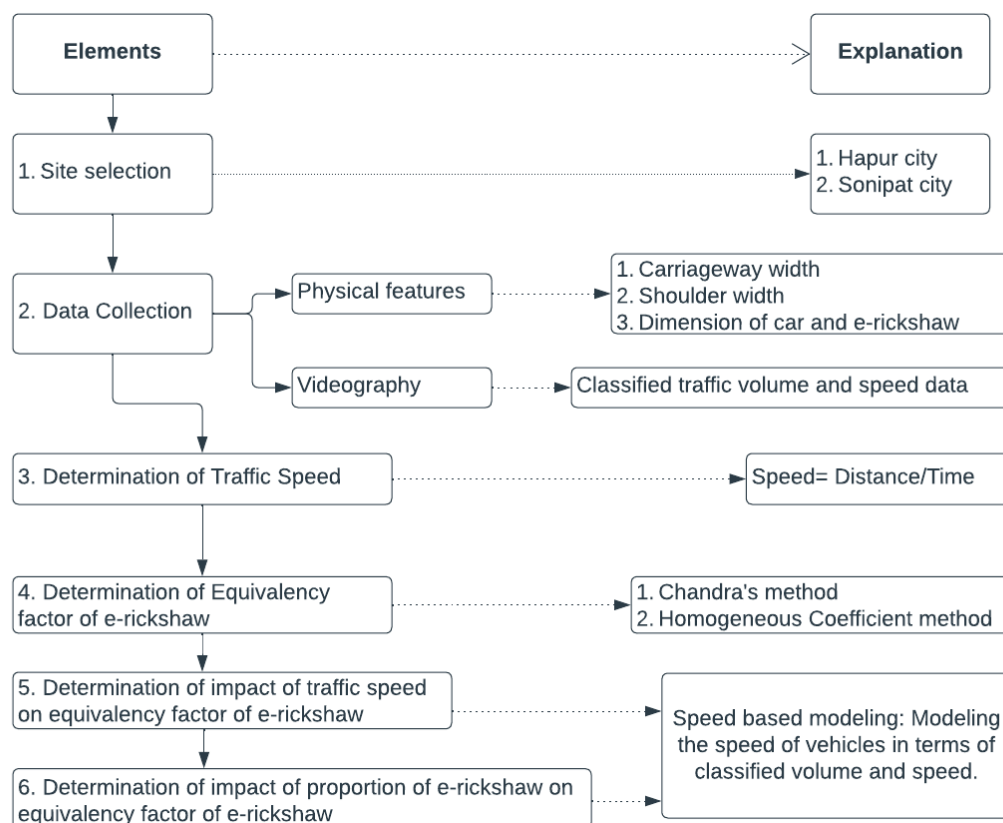


Figure 1 Adopted methodology

measured as well, as shown in Table 2. The average traffic composition and hourly volume obtained from the captured videos for Hapur City are presented in Figure 4 and for Sonipat City in Figure 5.

Table 1 Detail of selected roads

City	Site	Carriageway width (m)	Shoulder width (m)
Hapur City	Site 1	7.02	5.24
	Site 2	9.91	3.21
	Site 3	6.79	4.81
Sonipat City	Site 1	4.11	2.54
	Site 2	7.22	5.80
	Site 3	4.73	1.75

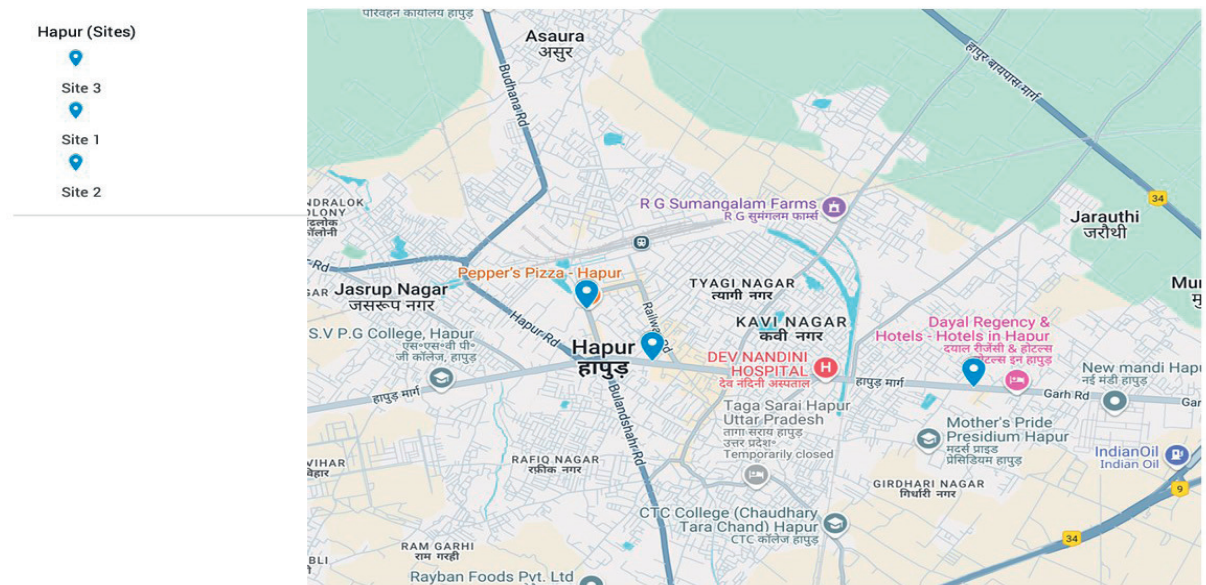


Figure 2 Map displaying selected sites of Hapur city

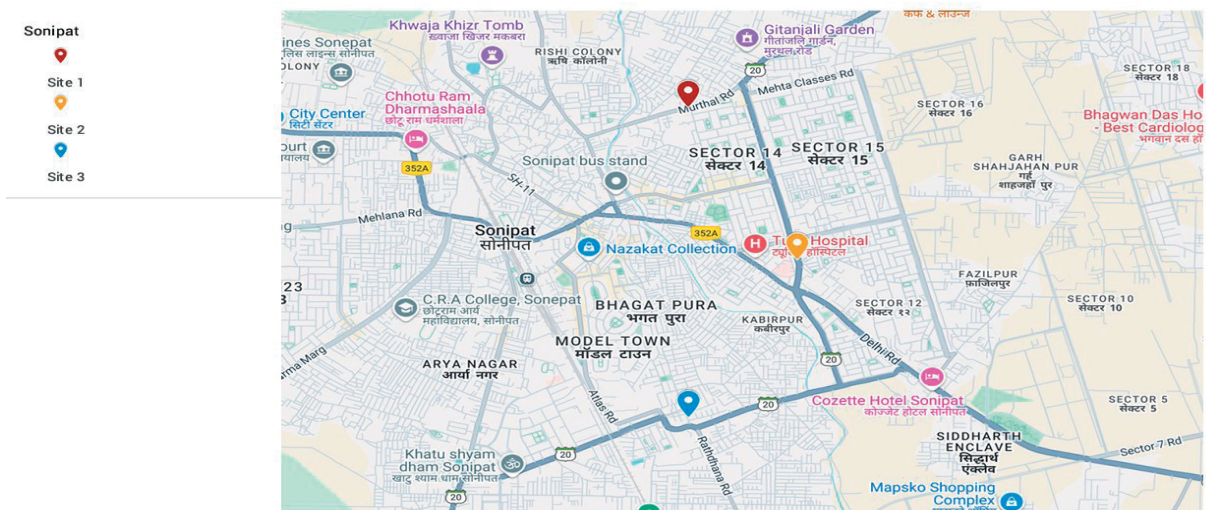


Figure 3 Map displaying selected sites of Sonipat city

Table 2 Observed area of car and E-rickshaw

Vehicles	Area (length * width) of the vehicle in m ²
Car	5.360
E-rickshaw	2.720

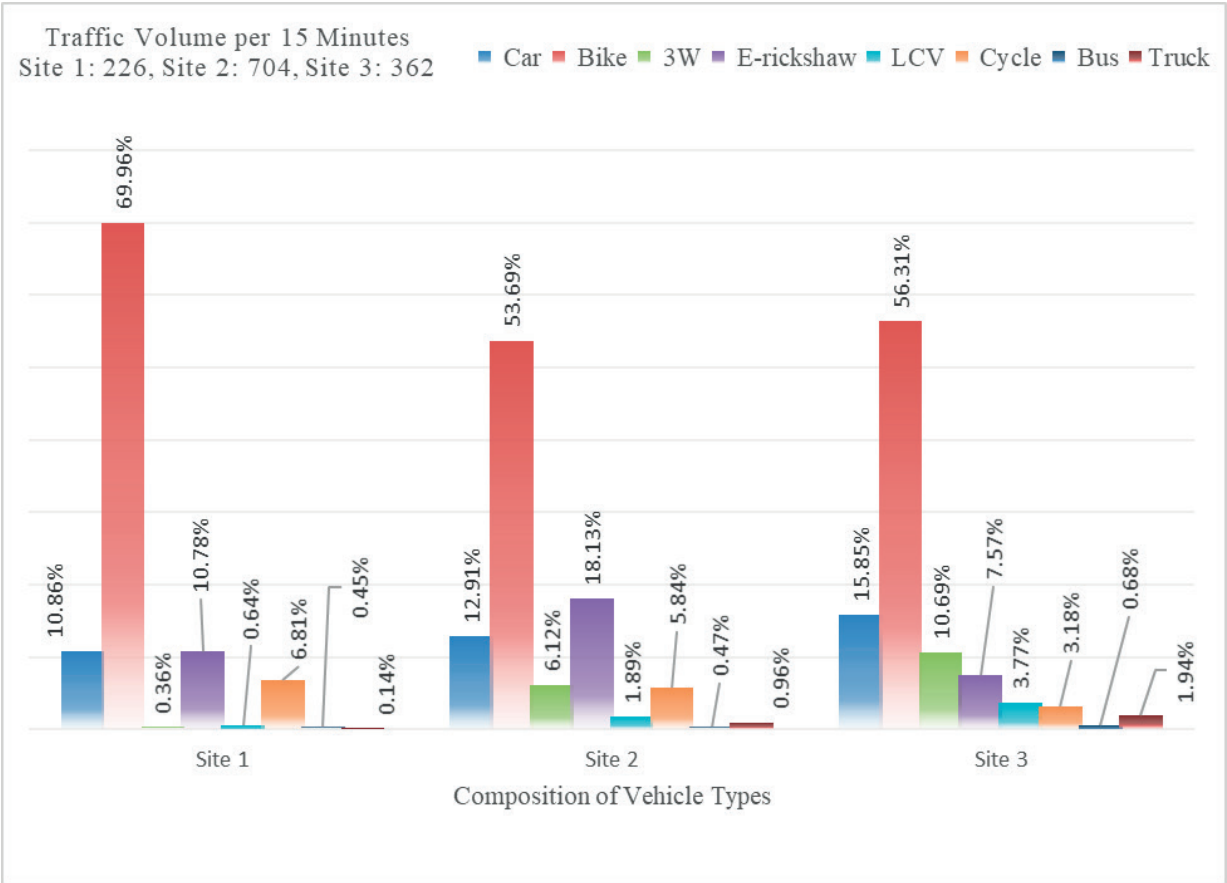


Figure 4 Traffic volume and composition obtained from three sites of Hapur City

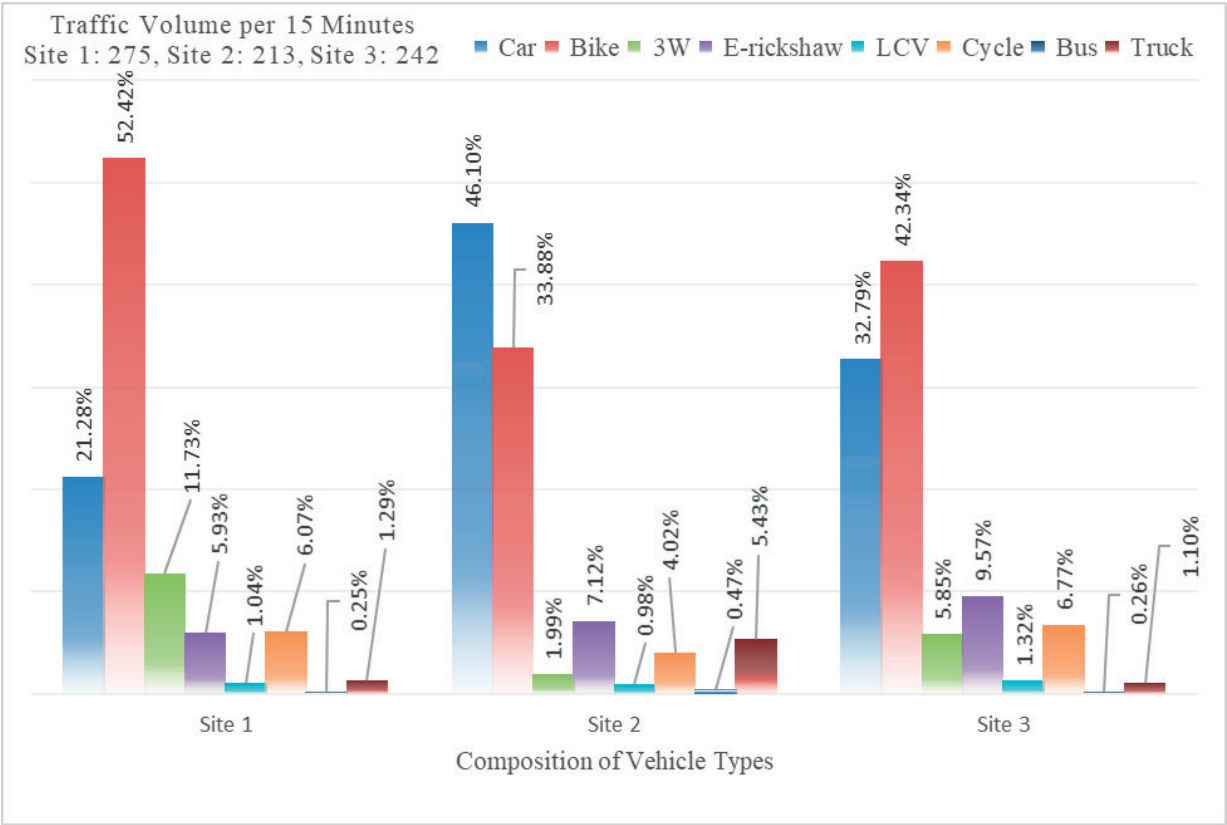


Figure 5 Traffic volume and composition obtained from three sites of Sonipat City

5 Determination of the traffic speed

Frame-by-frame analysis was used to extract the time required by individual vehicles to pass the designated section from the captured videos using a VLC media player. Time taken to cross the selected areas of a certain length by vehicle type was noted. The section of a certain length was marked on the road using masking tape so that entry and exit points are visible in the captured videos to help in determining the time required to cross that section by different vehicles. The length of section was measured manually by measuring tape and then the speed of each vehicle

category was estimated. The estimated speed of each vehicle category was then converted into space mean speed using Equation (1), and then the average speed of traffic was estimated. The mean speed of traffic in m/s for the roads of Hapur city and Sonipat city is shown in Figure 6. A descriptive analysis of traffic speed obtained from the selected sites is shown in Table 3. Space mean speed of car and e-rickshaw is shown in Table 4.

$$V_s = n / \left(\sum_{i=1}^n 1/V_i \right), \quad (1)$$

where V_s is space mean speed, n is the number of vehicles, and V_i is the vehicle category.

Table 3 Descriptive statistics (traffic speed in m/s)

City	Site	Mean	Median	Standard deviation	Minimum	Maximum
Hapur	Site 1	6.495	6.720	0.505	5.248	6.875
	Site 2	8.319	8.330	0.171	8.026	8.618
	Site 3	9.909	9.841	0.438	9.179	10.614
Sonipat	Site 1	8.801	8.509	1.054	8.173	12.014
	Site 2	9.329	9.407	0.258	8.799	9.662
	Site 3	9.955	9.965	0.280	9.514	10.328

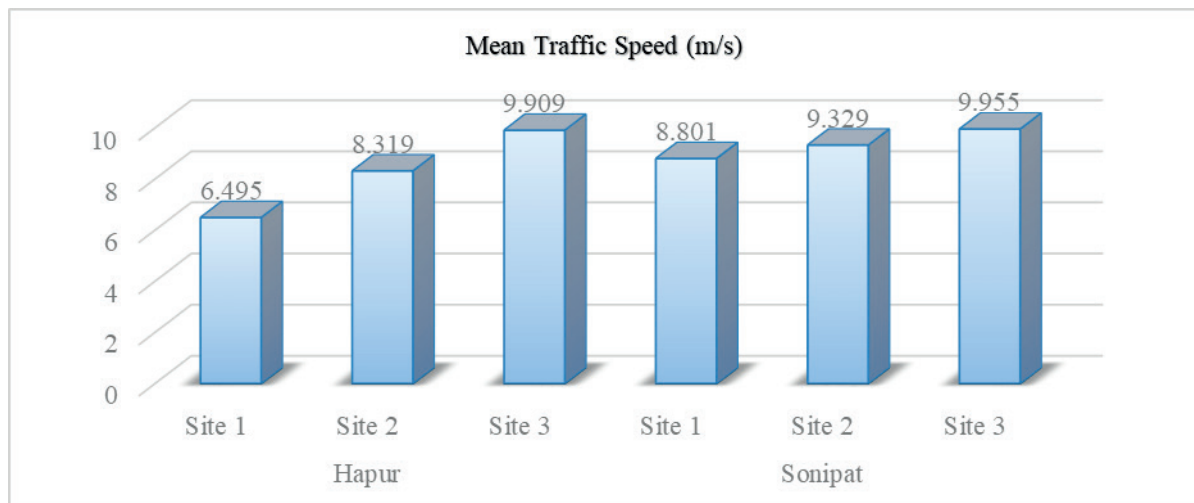


Figure 6 Traffic mean speed (m/s)

Table 4 Space mean speed of car and E-rickshaw in m/s

City	Site	Car	E-rickshaw
Hapur	Site 1	8.085	5.549
	Site 2	10.225	6.633
	Site 3	12.344	6.832
Sonipat	Site 1	10.374	6.992
	Site 2	11.560	7.713
	Site 3	11.815	8.489

6 Determination of equivalency factor of e-rickshaw

The equivalency factor of e-rickshaw was determined using the method based on the Chandra's approach and the homogeneous coefficient method and the multiple linear regression method. According to Chandra and Kumar (2003), the PCU or equivalency factor is a function of vehicle speed and area, and it may be computed as: [23].

$$PCU_e = \frac{V_c/V_{er}}{A_c/A_{er}}, \quad (2)$$

where V_c , V_{er} are the speed of car and e-rickshaw respectively, and A_c , A_{er} are the area of car and e-rickshaw respectively. Dasani et al. (2020) used the Homogeneous coefficient method for the PCU or equivalency factor determination. The equivalency factor, using the homogeneous coefficient method, can be calculated as [24].

$$PCU_e = \frac{V_c/V_{er}}{L_c/L_{er}}, \quad (3)$$

where L_c and L_{er} are the lengths of car and e-rickshaw, respectively. The only difference between the two methods is that area of a vehicle is considered in Chandra's method, and the length of the vehicle is considered in the case of the homogeneous coefficient method.

Multiple linear regression method is a direct method for estimating the PCU of a vehicle. The average speed of passenger cars is expressed based on classified traffic volumes in a form of multiple linear equation:

$$V_c = X_0 + \sum_{j=1}^n X_j N_j. \quad (4)$$

If a stream consists of eight different types of vehicles, then Equation (4) can be expanded as:

$$V_c = X_0 + X_c N_c + X_b N_b + X_{ar} N_{ar} + X_{er} N_{er} + X_l N_l + X_{cy} N_{cy} + X_{bs} N_{bs} + X_{tr} N_{tr}, \quad (5)$$

where V_c = average speed of passenger cars, N_j = volume of vehicle category "j", X_0 = intercept, X_c , X_b , X_{ar} , X_{er} , X_l ,

X_{cy} , X_{bs} , X_{tr} are the regression coefficients for car, bike, auto-rickshaw, e-rickshaw, light commercial vehicle, cycle, bus, truck, respectively; N_c , N_b , N_{ar} , N_{er} , N_l , N_{cy} , N_{bs} , N_{tr} are the volume of car, bike, auto-rickshaw, e-rickshaw, LCV, cycle, bus, truck respectively in the stream; n = number of vehicle categories. Coefficients are determined exercising regression technique. The PCU of a vehicle category "j" (PCU_j) is estimated as:

$$(PCU)_j = \frac{x_j}{x_1}, \quad (6)$$

where x_1 is the weightage factor for the standard vehicle (car).

To utilize multiple linear regression method, the mean speed of car was regressed based on classified traffic volume for selected sites consist of car, bike, auto-rickshaw, e-rickshaw, bus, truck, cycle and LCV with the help of SPSS (Statistical Package for the Social Sciences) software. Obtained coefficients for site 1 of Hapur site and site 1 of Sonipat city are listed in Table 5. Similar procedures were employed for other sites. After obtaining the coefficients, the PCU of e-rickshaw was developed which is listed in Table 6.

After analyzing the collected data, equivalency factors of e-rickshaw, using Equations (2), (3), (5) and (6), were developed for Hapur and Sonipat cities, which are shown in Table 6. From Table 6, it is clear that multiple linear regression method does not provide accurate result as there is a significant disparity in the obtained result. On the other hand, values obtained by Chandra's method and homogeneous coefficient method are accurate comparatively. Out of all three methods, Chandra's method is the most reliable.

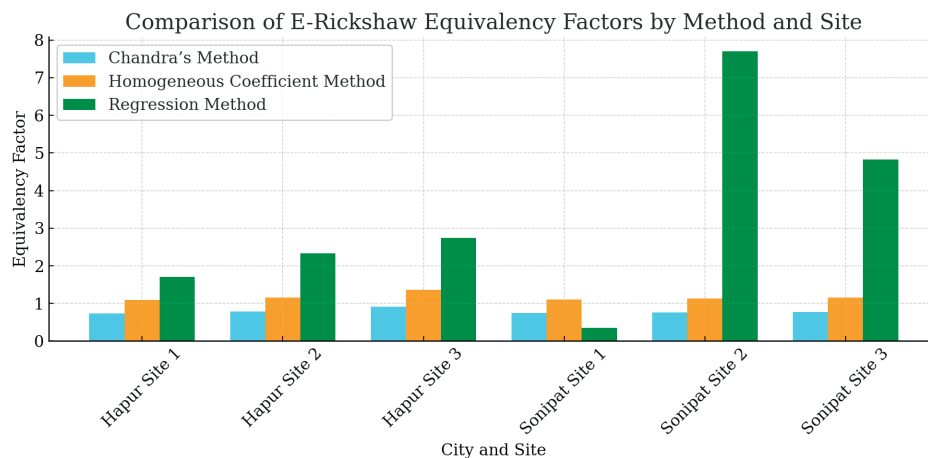
A comparative analysis of the three methodologies employed is shown in Figure 7. Among the three methodologies evaluated, the Chandra's method consistently produced the lowest and most stable PCU values for e-rickshaws across all selected sites, with values ranging from 0.739 to 0.917. This suggests that, under this approach, e-rickshaws are perceived as occupying relatively less road space and operating at lower speeds compared to standard vehicles. The Homogeneous Coefficient Method yielded the PCU estimates within a range of 1.093 to 1.355. In contrast, the Multiple Linear Regression Method demonstrated

Table 5 Obtained coefficient for Equation (5)

Hapur City:	X_0	11.075	Sonipat City:	X_0	7.124
Site 1	X_c	-.047	Site 1	X_c	.056
	X_b	.005		X_b	-.007
	X_{ar}	.074		X_{ar}	.019
	X_{er}	-.080		X_{er}	.020
	X_l	-.025		X_l	.041
	X_{cy}	-.027		X_{cy}	-.063
	X_{bs}	-.220		X_b	.176
	X_{tr}	-.090		X_{tr}	.297

Table 6 Developed Equivalency Factor of E-rickshaw

City	Site	Chandra's method	Homogeneous coefficient method	Multiple linear regression method
Hapur	Site 1	0.739	1.093	1.702
	Site 2	0.782	1.156	2.333
	Site 3	0.917	1.355	2.736
Sonipat	Site 1	0.752	1.111	0.357
	Site 2	0.761	1.127	7.703
	Site 3	0.772	1.152	4.830

**Figure 7** Comparative analysis of developed PCU values of e-rickshaw**Table 7** Impact of traffic speed on equivalency factor of E-rickshaw

City	Site	Traffic Speed (m/s)	Equivalency Factor of E-rickshaw	
			Chandra's method	Homogeneous Coefficient Method
Hapur	Site 1	6.495	0.739	1.093
	Site 2	8.319	0.782	1.156
	Site 3	9.909	0.917	1.355
Sonipat	Site 1	8.801	0.752	1.111
	Site 2	9.329	0.761	1.127
	Site 3	9.955	0.772	1.152

the greatest variability in PCU values, with estimates spanning from as low as 0.357 (Sonipat Site 1) to as high as 7.703 (Sonipat Site 2). This wide fluctuation highlights the method's high sensitivity to site-specific traffic dynamics, making it particularly responsive to local variations in flow patterns, vehicle interactions, and operational characteristics.

7 Impact of traffic speed on equivalency factor of e-rickshaw

To check the impact of traffic speed on the equivalency factor of e-rickshaw, the traffic speed and equivalency factor of e-rickshaw, as shown in Figure 6

and Table 7, respectively, were correlated, as shown in Table 7.

The obtained relationship between the equivalency factor of e-rickshaw and the mean traffic speed for Hapur and Sonipat cities is shown in Figures 8 and 9, respectively. The equivalency factor of e-rickshaw estimated using both approaches (Chandra's method and Homogeneous Coefficient method) is high for the site having a higher mean traffic speed. After analyzing the results, the models obtained between the traffic speed and equivalency factor of e-rickshaw are shown in Table 8, along with the r squared value. As the relationship between the equivalency factor and traffic speed is exponential, the equivalency factor of e-rickshaw is exponentially correlated with the traffic speed for both

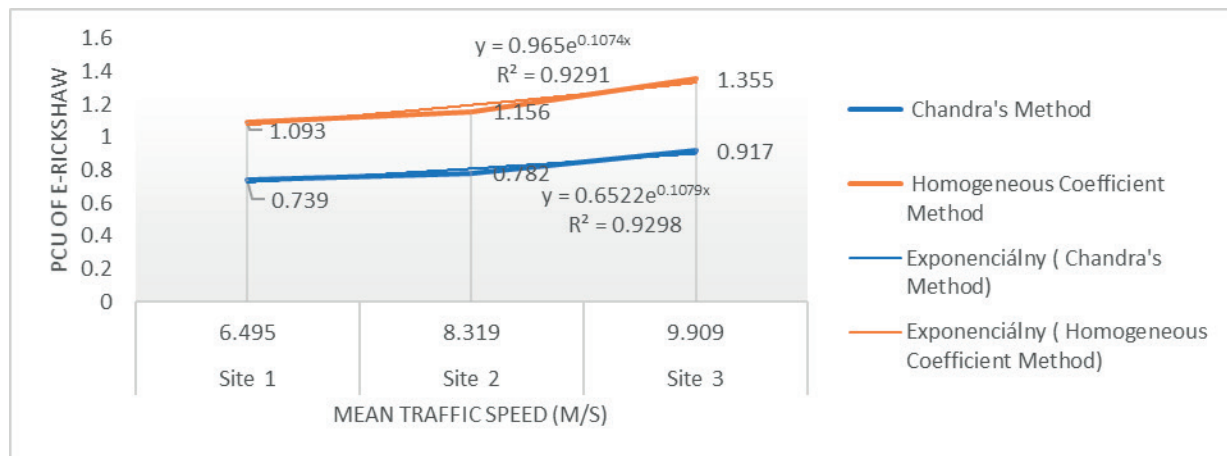


Figure 8 Relationship between the equivalency factor of E-rickshaw and average traffic speed (m/s) for Hapur City



Figure 9 Relationship between equivalency factor of E-rickshaw and mean traffic speed (m/s) for Sonipat City

Table 8 Obtained model for impact of traffic speed on equivalency factor of E-rickshaw

City	Method	Obtained Model	R squared value
Hapur	Chandra's method	$y = 0.6522e^{0.1079x}$	$R^2 = 0.9345$
	Homogeneous Coefficient method	$y = 0.965e^{0.1074x}$	$R^2 = 0.9338$
Sonipat	Chandra's method	$y = 0.7419e^{0.0131x}$	$R^2 = 0.9971$
	Homogeneous Coefficient method	$y = 1.0897e^{0.0181x}$	$R^2 = 0.9855$

Abbreviations: y= equivalency factor of e-rickshaw, x= mean traffic speed (m/s)

Hapur and Sonipat cities. After analyzing the results, the models obtained between the traffic speed and equivalency factor of e-rickshaw have r squared value greater than 0.90 for each case.

8 Relation between equivalency factor of e-rickshaw and composition of e-rickshaw

Speed-based modelling was used to check the impact of the proportion of e-rickshaw ([2, 25]). According to this modelling, the speed of different vehicles can be modelled in terms of volume and speed of vehicle types as Equations (7) and (8). Later, the modelled

speed can be used in Chandra's, and Homogeneous coefficient method to estimate the equivalency factor of the e-rickshaw.

$$V_c = a_{0-c} + a_{1-c}(n_c/V_c) + a_{2-c}(n_b/V_b) + a_{3-c}(n_{ar}/V_{ar}) + a_{4-c}(n_{er}/V_{er}) + a_{5-c}(n_l/V_l) + a_{6-c}(n_{cy}/V_{cy}) + a_{7-c}(n_{bs}/V_{bs}) + a_{8-c}(n_{tr}/V_{tr}), \quad (7)$$

$$V_{er} = a_{0-er} + a_{1-er}(n_c/V_c) + a_{2-er}(n_b/V_b) + a_{3-er}(n_{ar}/V_{ar}) + a_{4-er}(n_{er}/V_{er}) + a_{5-er}(n_l/V_l) + a_{6-er}(n_{cy}/V_{cy}) + a_{7-er}(n_{bs}/V_{bs}) + a_{8-er}(n_{tr}/V_{tr}), \quad (8)$$

Volume and speed of vehicle types for 15-minute intervals were interpreted from the captured videos of sites of Hapur city and used in Equations (7) and (8) for speed-based modelling to check the impact. These equations were regressed using the SPSS software, and Microsoft excel to find out the speed of cars and e-rickshaws, and then the equivalency factor of e-rickshaw was estimated. Multiple linear regression was employed in the SPSS software to model the speeds. For modelling the speed of the car, the dependent variable is the speed of the car and the independent variables are the ratio of volume and the speed of

available vehicle categories respectively. Similarly, the speed of the e-rickshaw was modelled with the speed of the e-rickshaw being the dependent variable. Later, the composition of the e-rickshaw was increased and decreased, keeping the proportion of other vehicle types constant to check its impact on the equivalency factor of e-rickshaw. The observed composition of e-rickshaw on site 1, site 2, and site 3 are 11%, 18%, and 8%, respectively.

Notation: V_c and V_{er} are the modelled speed of cars and e-rickshaw, respectively; (n/V) is the ratio of volume and speed of respective vehicles, where c

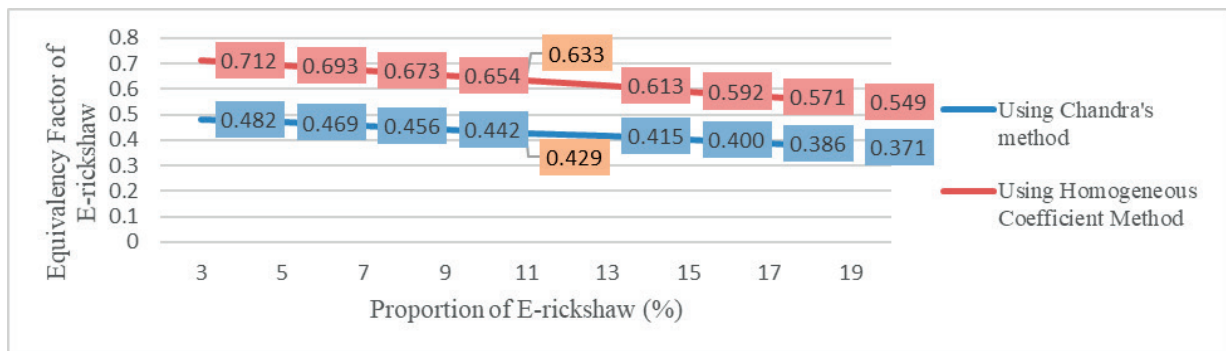


Figure 10 Impact of proportion of e-rickshaw on equivalency factor of e-rickshaw for Site 1

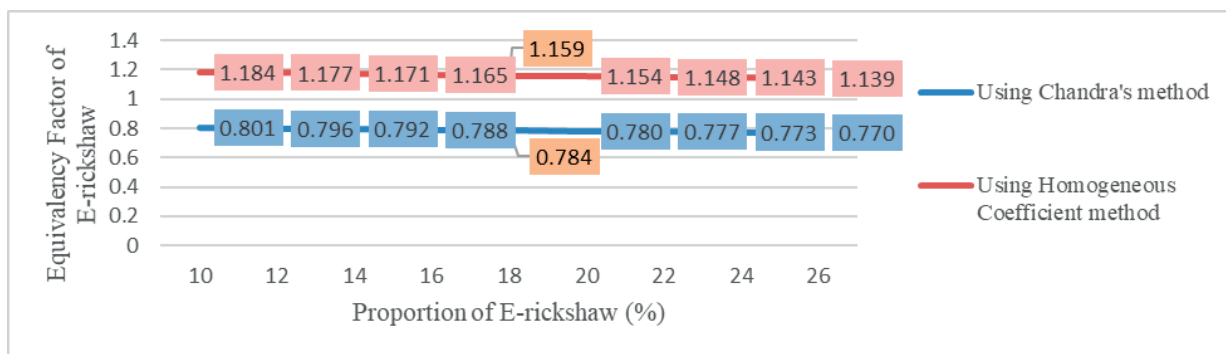


Figure 11 Impact of proportion of e-rickshaw on equivalency factor of e-rickshaw for Site 2

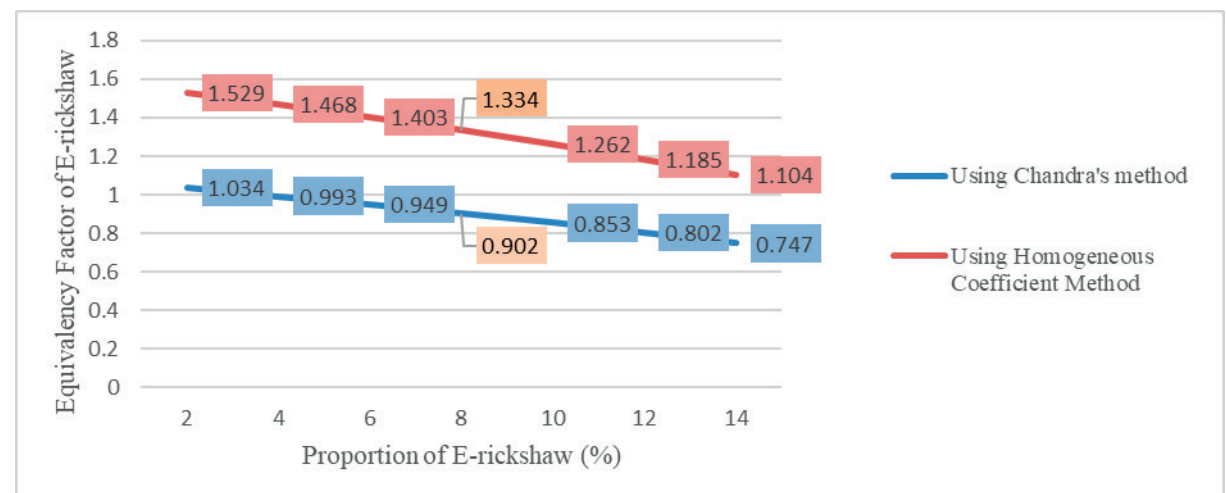


Figure 12 Impact of proportion of e-rickshaw on equivalency factor of e-rickshaw for Site 3

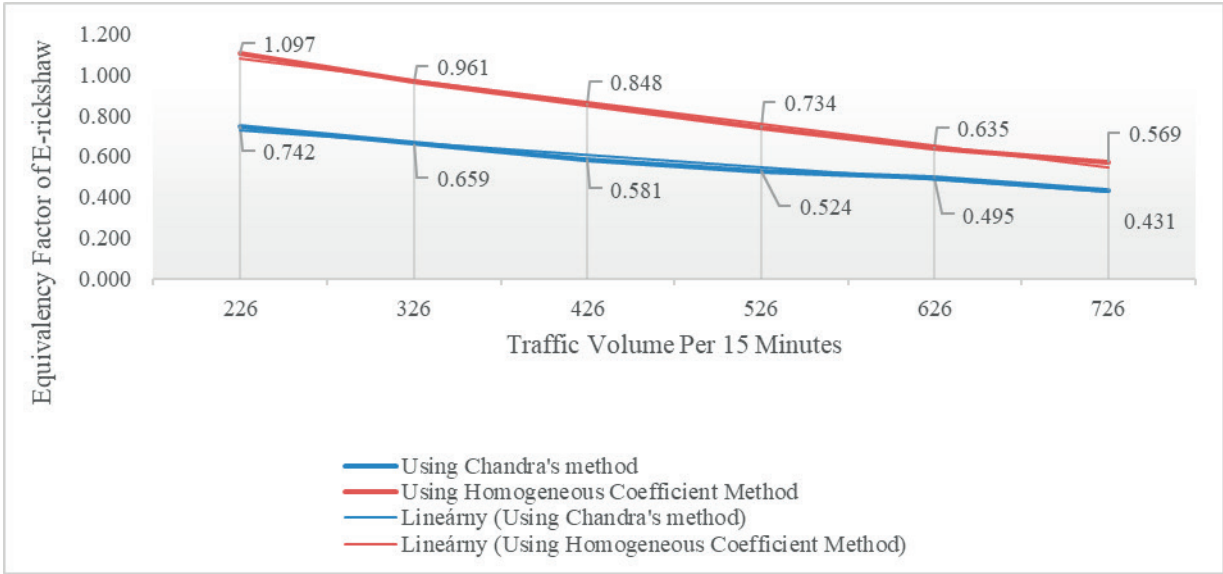


Figure 13 Impact of traffic volume on equivalency factor of e-rickshaw for site 1 of Hapur City

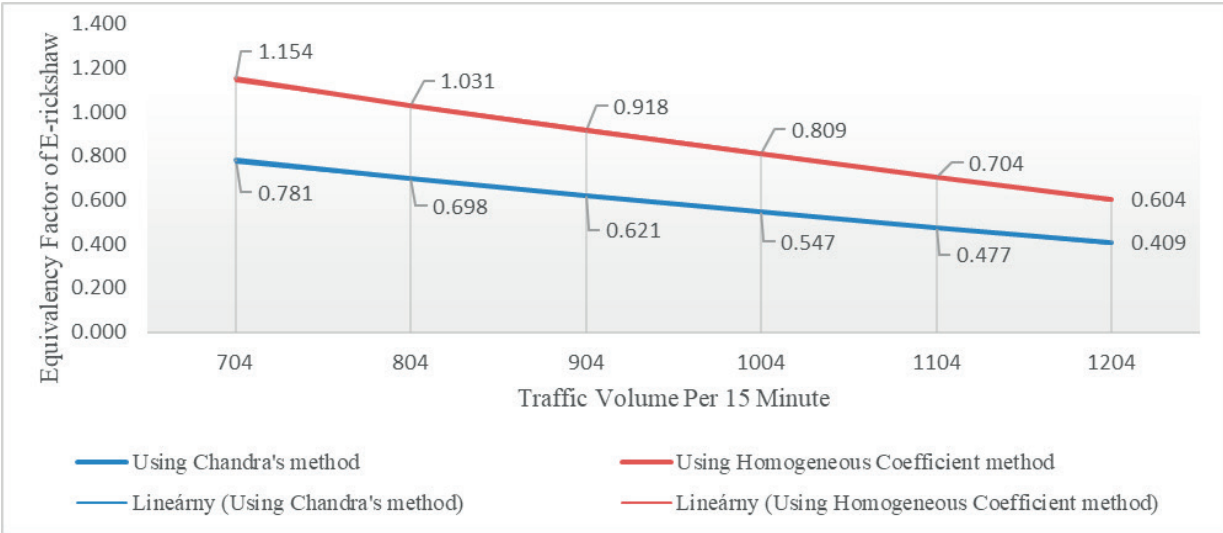


Figure 14 Impact of traffic volume on equivalency factor of e-rickshaw for site 2 of Hapur City

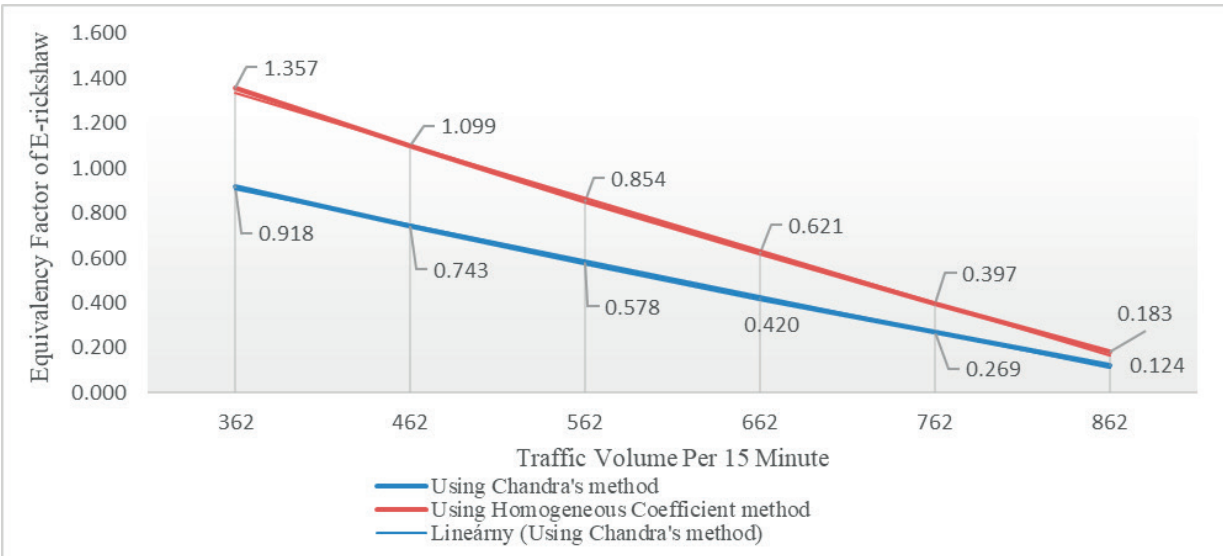


Figure 15 Impact of traffic volume on equivalency factor of e-rickshaw for site 3 of Hapur City

is for car, b is for bike, a_r is for autorickshaw, er is for e-rickshaw, l is for LCV, cy is for cycle, bs is for bus, and tr is for Truck. And a₀, a₁,, a₈ are the coefficients.

Figures 10, 11, and 12 show the impact of the composition of E-rickshaw on the equivalency factor of e-rickshaw, and it can be concluded that on increasing and decreasing the proportion of e-rickshaw keeping the proportion of other vehicles' types as constant, the equivalency factor of e-rickshaw decreases and increases respectively.

9 Impact of traffic volume on equivalency factor of e-rickshaw

To check the impact of traffic volume on equivalency factor of e-rickshaw, Equations (7) and (8) were regressed using the SPSS software and Microsoft excel. For site 1 of Hapur city, the traffic volume was increased by 100 vehicles per 15 minutes at a time from 226 vehicles per 15 minutes to 336 vehicle per 15 minutes to check the impact then from 336 to 446 vehicles per 15 minutes while keeping the composition of vehicle types' constant. Overall traffic volume was increased from 226 vehicles per 15 minutes to 726 vehicles per 15 minutes with an interval of 100 vehicles per 15 minutes in each step. Similar process was employed for site 2 and site 3. From Figures 13, 14 and 15, it is clear that when the traffic volume increases in the stream, equivalency factor of e-rickshaw decreases.

10 Conclusions and discussion

The country's traffic is of a mixed nature. To effectively analyze this mixed traffic, the concept of PCU was developed to assess various types of vehicles on a common basis. Thus, the Equivalency factor or PCE or PCU is an important parameter considered to assess a mixed traffic stream [26]. Estimating the PCE values is crucial for traffic capacity assessments, level of service measurements, signal design and synchronization, determining saturation flow rates, and creating traffic flow models. The precision of PCE values is thought to have a big impact on traffic flow analysis because of the large number of applications.

Significant research is not available for determination of the equivalency factor of e-rickshaw as e-rickshaws are a new vehicle type. In this study, equivalency factors of E-rickshaw were estimated using two methods, namely the Chandra's method and the Homogeneous coefficient method, with the help of data from three sites each from two cities, Hapur city, and Sonipat city. The videography method was employed to collect the classified traffic volume and speed data. After analyzing the data, it was found that the equivalency factor of e-rickshaw is less than 1 when estimated using

the Chandra's method and is greater than 1 in the case of the homogeneous coefficient method.

The impact of traffic speed on the equivalency factor of e-rickshaw was also checked in this study, and it was found that the equivalency factor of e-rickshaw is higher on the sites having greater mean traffic speed. This effect was also checked using six sites, three sites each from Hapur city and Sonipat city. The developed models between the equivalency factor and traffic speed show that the relationship between the equivalency factor and traffic speed is exponential, i.e., the equivalency factor of e-rickshaw is exponentially correlated with the traffic speed for both Hapur and Sonipat cities. After analyzing the results, the models obtained between traffic speed and equivalency factor of e-rickshaw have r squared value greater than 0.90 for each case.

A study was conducted to analyze the impact of the composition of e-rickshaws on the speed of traffic in Hapur city. The analysis was carried out using a speed-based modelling approach. The volume and speed of each vehicle type in the traffic stream were modelled using SPSS software and Microsoft Excel. Equivalency factors for e-rickshaws were developed based on the modelled speed. The proportion of e-rickshaws was varied, while keeping the volume count of other vehicle types constant. The results showed that as the proportion of e-rickshaws increased, the value of the equivalency factor decreased, and as the proportion decreased, the value of equivalency factor increased.

A study on impact of traffic volume on equivalency factor was also conducted for sites of Hapur city. This study was also carried out using the speed-based modelling approach. To check the impact, traffic volume in the stream was increased in an interval of 100 vehicles per 15 minutes keeping the composition of different vehicle types constant. Then, the speed based equations were solved. it was found that on increasing the traffic volume, equivalency factor decreases.

11 Practical implications and recommendations

The findings of this study have several practical applications in the field of traffic engineering and urban planning. By establishing a more accurate equivalency factor for e-rickshaws, the traffic flow models can better represent their impact on road capacity and congestion levels. This is especially important in cities where the e-rickshaws form a significant part of the vehicle mix and traditional passenger car unit (PCU) values fail to capture their unique operating characteristics.

Transportation planners can use the derived equivalency factors to design the more realistic traffic simulations, optimize signal timings, and improve intersection performance. The policymakers and city authorities can also refer to these findings when formulating regulations or infrastructure plans that involve the integration or control of e-rickshaw traffic.

12 Limitations and future scope of the study

While this study sheds light on how the e-rickshaws interact with mixed traffic and how their equivalency factor can be modelled, there are a few limitations worth noting.

Data collection was confined to specific locations and time frames, which might not fully reflect the wide variability in traffic patterns. The localized traffic behaviour could have introduced some level of bias, potentially influencing the accuracy of the results. It would also be valuable to conduct similar studies in different cities, especially those with unique traffic compositions or infrastructure. Using the traffic simulations or real-time data analytics could further improve the precision of equivalency factor of e-rickshaw and help to adapt the findings to changing traffic scenarios.

To deepen the analysis, future research could make

use of advanced statistical methods-like sensitivity analysis-to better understand how different factors affect the equivalency factor of e-rickshaw calculated in the study.

Acknowledgements

The authors received no financial support for the research, authorship and/or publication of this article.

Conflicts of interest

The authors declare that they have no known competing financial interests or personal relationships that could have appeared to influence the work reported in this paper.

References

- [1] SHARMA, M., BISWAS, S. Estimation of passenger car unit on urban roads: a literature review. *International Journal of Transportation Science and Technology* [online]. 2021, **10**(3), p. 2383-298. ISSN 2046-0430, eISSN 2046-0449. Available from: <https://doi.org/10.1016/j.ijtst.2020.07.002>
- [2] KHAN, A. A., SINGH, G. Development of PCU value of e-rickshaw on urban roads. In: *Advances in Water Resources and Transportation Engineering. Lecture Notes in Civil Engineering, vol 149*. MEHTA, Y. A., CARNACINA, I., KUMAR, D. N., RAO, K. R., KUMARI, M. (Eds.) [online]. Singapore: Springer, 2021. ISBN 978-981-16-1302-9, eISBN 978-981-16-1303-6. Available from: https://doi.org/10.1007/978-981-16-1303-6_10
- [3] SRINIVASA RAO, R., GUPTA, V. S. S. R., NITESH, Y., RAO, G. V. Review on passenger car unit studies in homogeneous and heterogeneous traffic flow-a perspective. *International Journal of Civil Engineering and Technology*. 2017, **8**(8), p. 1279-1289. ISSN 0976-6308, eISSN 0976-6316.
- [4] DHAMANIYA, A., BARI, C. S., PATKAR, M. Capacity analysis of urban arterial midblock sections under mixed traffic conditions. *International Journal of Intelligent Transportation Systems Research* [online]. 2022, **20**(2), p. 409-421. ISSN 1348-8503, eISSN 1868-8659. Available from: <https://doi.org/10.1007/s13177-022-00298-1>
- [5] CHANDRA, S., KUMAR, V., SIKDAR, P. K. Dynamic PCU and estimation of capacity of urban roads. *Indian Highways*. 1995, **23**(4), p. 17-28. ISSN 0376-7256.
- [6] WERNER, A., MORRALL, J. F. Passenger car equivalencies of trucks, buses, and recreational vehicles for two-lane rural highways. *Transportation Research Record*. 1977, **615**, p. 10-17. ISSN 0361-1981, eISSN 2169-4052.
- [7] MINH, CH. C., MAI, T. T., BINH, T. H., SANO, K. The delay estimation under heterogeneous traffic conditions. *Journal of the Eastern Asia Society for Transportation Studies*. 2010, **8**, p. 1583-1595. eISSN 1881-1124. Available from: <https://doi.org/10.11175/easts.6.1496>
- [8] ADAMS, C. A., ABDUL, M. ZAMBANG, M., BOAHEN, R. O. Effects of motorcycles on saturation flow rates of mixed traffic at signalized intersections in Ghana. *International Journal of Traffic and Transportation Engineering* [online]. 2015, **4**(3), p. 94-101. ISSN 2325-0062, eISSN 2325-0070. Available from: <https://doi.org/10.5923/j.ijtte.20150403.03>
- [9] RAO, R. S., YADAV, N. Determination and comparison of PCU on urban roads under mixed traffic conditions - a case study. In: *Conference Urbanization Challenges in Emerging Economies: proceedings* [online]. 2018. Available from: <https://doi.org/10.1061/9780784482025.064>
- [10] TIWARI, G., FAZIO, J., PAVITRAVAS, S. Passenger car units for heterogeneous traffic using a modified density method. In: *4th International Symposium on Highway Capacity: proceedings*. 2000. p. 246-257.
- [11] HUBER, M. J. Estimation of passenger - car equivalents of trucks in traffic stream. *Transportation Research Record*. 1982, **869**, p. 60-70. ISSN 0361-1981, eISSN 2169-4052.
- [12] BARMAN, S., DEVI, N. S., BISWAS, S. Determining passenger car unit for e rickshaw on divided Indian urban roads. *Journal of The Institution of Engineers (India): Series A* [online]. 2025. ISSN 2250-2149, eISSN 2250-2157. Available from: <https://doi.org/10.1007/s40030-025-00890-0>

- [13] KHAN, A. A., DASS, S. Revisiting PCU values of various vehicles in mixed traffic conditions: estimation and comparison. *Communications - Scientific Letters of the University of Zilina* [online]. 2025, **27**(2), p. D76-D89. ISSN 1335-4205, eISSN 2585-7878. Available from: <https://doi.org/10.26552/com.C.2025.025>
- [14] KALOGO, E., COSTA, D. G. N. Determining of appropriate passenger car unit values due to a change in effective width of roadway. *Engineering and Technology Journal* [online]. 2024, **09**(05), p. 4172-4178. eISSN 2456-3358. Available from: <https://doi.org/10.47191/etj/v9i05.38>
- [15] VIJAY, B. G., RAJENDRAKHATAVKAR Comparative study of methods used for a capacity estimation on two lane undivided national highways. *Journal of Traffic and Transportation Engineering* [online]. 2019, **7**(1). ISSN 2325-0062, eISSN 2325-0070. Available from: <https://doi.org/10.17265/2328-2142/2019.01.004>
- [16] HORDOFA TULLU, H., TUCAY QUEZON, E. Determination of passenger car unit for urban roads: a case study in Addis Ababa. *American Journal of Construction and Building Materials* [online]. 2021, **5**(2), p. 57-63. ISSN 2640-0022, eISSN 2640-0057. Available from: <https://doi.org/10.11648/j.ajcbm.20210502.13>
- [17] BISWAS, S. CHAKRABORTY, S. CHANDRA, S., GHOSH, I. Kriging-based approach for estimation of vehicular speed and passenger car units on an urban arterial. *Journal of Transportation Engineering, Part A: Systems* [online]. 2017, **143**(3). ISSN 2473-2907, eISSN 2473-2893. Available from: <https://doi.org/10.1061/JTEPBS.0000031>
- [18] PATKAR, M., DHAMANIYA, A. Influence of nonmotorized vehicles on speed characteristics and capacity of mixed motorized traffic of urban arterial midblock sections. *Journal of Transportation Engineering, Part A: Systems* [online]. 2020, **146**(4). ISSN 2473-2907, eISSN 2473-2893. Available from: <https://doi.org/10.1061/JTEPBS.0000325>
- [19] SEKHAR, C. R., NATARAJU, J., VELMURUGAN, S., KUMAR, P., SITARAMANJANEYULU, K. Free flow speed analysis of two lane inter urban highways. *Transportation Research Procedia* [online]. 2016, **17**, p. 664-673. ISSN 2352-1457, eISSN 2352-1465. Available from: <https://doi.org/10.1016/j.trpro.2016.11.121>
- [20] MONDAL, S. CHAKRABORTY, S., ROY, S. K., GUPTA, A. Estimation of passenger car unit for heterogeneous traffic stream of urban arterials: case study of Kolkata. *Transportation Letters* [online]. 2017, **15**(10), p. 1276-1288. ISSN 1942-7867, eISSN 1942-7875. Available from: <https://doi.org/10.1080/19427867.2017.1293313>
- [21] MARDANI, N. M., CHANDRA, S., GHOSH, I. Passenger car unit of vehicles on undivided intercity roads in India. *Procedia Computer Science* [online]. 2015, **52**, p. 926-931. eISSN 1877-0509. Available from: <https://doi.org/10.1016/j.procs.2015.05.167>
- [22] PAPER, O. S., LANKA, S., OPTIMIZATION, L., LANKA, S. Passenger car units for different midblock sections in Sri Lanka under mixed traffic condition. *Journal of Applied Engineering Science* [online]. 2023, **21**(2), p. 375-383. ISSN 1451-4117. Available from: <https://doi.org/10.5937/jaes0-36600>
- [23] CHANDRA, S., KUMAR, U. Effect of lane width on capacity under mixed traffic conditions in India. *Journal of Transportation Engineering* [online]. 2003, **129**(2), p. 155-160. ISSN 2473-2907, eISSN 2473-2893. Available from: [https://doi.org/10.1061/\(ASCE\)0733-947X\(2003\)129:2\(155\)](https://doi.org/10.1061/(ASCE)0733-947X(2003)129:2(155))
- [24] DASANI, Y. R., VALA, M., PATEL, B. Estimation of dynamic equivalency factor under heterogeneous traffic condition on urban arterial road - a case study of Porbandar city. In *Transportation Research. Lecture Notes in Civil Engineering*, vol 45. MATHEW, T., JOSHI, G., VELAGA, N., ARKATKAR, S. (Eds.) [online]. Singapore: Springer, 2020. ISBN 978-981-32-9041-9, eISBN 978-981-32-9042-6, p. 465-474. Available from: https://doi.org/10.1007/978-981-32-9042-6_37
- [25] DHAMANIYA, A., CHANDRA, S. Conceptual approach for estimating dynamic passenger car units on urban arterial roads by using simultaneous equations. *Transportation Research Record: Journal of the Transportation Research Board* [online]. 2016, **2553**(1), p. 108-116. ISSN 0361-1981, eISSN 2169-4052. Available from: <https://doi.org/10.3141/2553-12>
- [26] METKARI, M., BUDHKAR, A., KUMAR MAURYA, A. A Review of passenger car equivalence for Indian conditions. *Conference on Emerging Frontiers in Technology For Rural Area EFITRA 2012: proceedings*. 2012.



This is an open access article distributed under the terms of the Creative Commons Attribution 4.0 International License (CC BY 4.0), which permits use, distribution, and reproduction in any medium, provided the original publication is properly cited. No use, distribution or reproduction is permitted which does not comply with these terms.

GEOLOCATION OF DEVICES IN LOW-POWER WIDE-AREA LORA NETWORK

Ladislav Zemko*, Daniel Hroš, Alexander Valach, Marek Galinski, Pavel Čičák

Institute of Computer Engineering and Applied Informatics, Faculty of Informatics and Information Technologies, Slovak University of Technology, Bratislava, Slovakia

*E-mail of corresponding author: ladislav.zemko@stuba.sk

Ladislav Zemko 0000-0002-5635-265X,
Alexander Valach 0000-0001-8299-0914,
Pavel Čičák 0000-0002-3021-1971

Daniel Hroš 0009-0002-7850-7509,
Marek Galinski 0000-0001-6622-526X,

Resume

This article is focused on the geolocation possibilities in low-power deployments. A novel Logarithmic Distance Path Loss Model with a Memory (LDPL-M) algorithm is proposed to enhance the accuracy of determining the location of end devices. The proposed solution, utilizing the RSSI-based trilateration, proved more accurate by 24.54% compared to the conventional Logarithmic Distance Path Loss Model (LDPL). Compared to the Global Positioning System (GPS), the power consumption was 48.8% lower. These findings make it suitable for energy-harvesting deployments, environments with limited power supply, or generally hard-to-reach areas, covering various logistics, transportation, or asset tracking scenarios. Overall, in this article, a valuable insight into the geolocation, focusing on the accuracy and efficiency, is provided.

Article info

Received 19 May 2025

Accepted 6 August 2025

Online 19 September 2025

Keywords:

LoRa
LoRaWAN
geolocation
IoT
LPWAN
RSSI
trilateration

Available online: <https://doi.org/10.26552/com.C.2025.050>

ISSN 1335-4205 (print version)

ISSN 2585-7878 (online version)

1 Introduction

LoRa technology belongs to the field of Low-Power Wide-Area Networks (LPWANs). It enables the connection of end devices that send small data volumes over long distances several times a day with minimal energy consumption. They last 5 to 10 years on a single charge and can be placed even in hard-to-reach places without access to electricity.

New opportunities for the geolocation of end devices are presented by the Internet of Things (IoT) environment. Position can be traditionally determined by the Global Navigation Satellite Systems (GNSS), including the Global Positioning System (GPS), via a constellation of multiple satellites orbiting the Earth. Navigation messages are continuously transmitted by the satellites to the end devices, allowing their position to be calculated. The GPS-independent systems are currently being considered a promising research area. An uninterrupted connection between the receiver and the satellite is required by GNSS, which affects the power consumption. The signals sent can be blocked by

obstacles and weather changes, resulting in a certain error. Therefore, such systems are not suitable for the indoor use [1].

The LPWANs' properties have the potential to enable the device geolocation, while maintaining low power consumption [2-5]. LoRa is a wireless technology promoted by the LoRa Alliance. It is based on a proprietary Chirp Spread Spectrum (CSS) modulation, which means a regular change in signal frequency, increasing or decreasing over time, operating on the physical layer of the Open Systems Interconnection (OSI) model [3, 6]. It uses the freely available Industrial Scientific and Medical (ISM) band for data transmission, so observing the so-called duty cycle (DC) is necessary. The DC limits the time a device can transmit. In our use case, this is 1% of time, which equals 36 seconds per hour [7-8].

Above the LoRa physical modulation operates the LoRaWAN protocol, ensuring bi-directional communication. LoRaWAN is standardized by the LoRa Alliance and has the possibility of roaming, but with the costs of higher energy consumption, compared to

other protocols, e.g., LoRa@FIIT [7, 9-11]. A typical implementation of a LoRaWAN network consists of end devices (simple battery-powered sensors), gateways, a network server, and an application server. In most applications, end devices are autonomous, connected in a star¹ topology, sending the collected data via LoRa technology to all the gateways within their range. After the gateway receives a message, it immediately adds metadata to it: timestamp, Received Signal Strength Indicator (RSSI), Signal to Noise Ratio (SNR), and others, which are crucial for the geolocation in wireless networks [9].

Unlike the GNSS, geolocation use cases in LoRaWAN network are specific to the standardized roaming architecture, allowing end devices to use the gateways of different networks and therefore to send messages between different LoRaWAN operators. As the uplink communication is not bound to a specific gateway, it improves the coverage and capacity, which has the potential to reduce the costs and energy consumption [6, 12]. The main problem with the GPS-equipped devices is the power consumption of around 30-50 mA. A typical power consumption of a LoRaWAN device is about 2.8 mA in the active state, 38.9 mA during uplink transmission, and 14.2 mA during downlink reception [13].

The research was focused on the LoRaWAN protocol and the LoRa technology, which belong to the category of LPWANs. The findings are not limited to this specific technology but are generally applicable to wireless communication technologies. The geolocation accuracy in LoRa networks depends on types of devices and communication parameters, as well as the method used, i.e., triangulation, trilateration, and multilateration. A novel Logarithmic Distance Path Loss Model with Memory (LDPL-M) algorithm is proposed, considering not only the actual end device's location, but the previous locations, as well. The geolocation is determined by the RSSI-based trilateration. Compared to the standard methods using GNSS, LPWANs allow the location of end devices to be determined over a wide area with minimal power consumption. Results have shown that this modification improves the overall geolocation accuracy for both the stationary and mobile devices. The benefit of this solution is that no additional communication overhead is required.

The main contribution of this article lies in the following:

- Research in the field of LPWANs and suitable geolocation methods: LPWANs with the focus on the LoRa technology are described, and an overview of the methods applicable in LoRa network with low power consumption in mind is provided throughout the research.
- Proposal of the LDPL-M algorithm: The LDPL-M algorithm for the geolocation of the end devices based on the trilateration using RSSI is proposed.

¹ star-of-stars

Compared to the existing solutions, it computes the end device's position using not only the current location, but considers n previously determined locations, which improves the overall accuracy. The accuracy, or the error, of the proposed algorithm is also measured and compared to other methods, including the GPS sensor data.

The article is organized as follows: in Section 2, related work and the geolocation techniques applicable in LPWANs are described. In Section 3, a private LoRaWAN network and its components are described, and the methodology of data collection and processing in both the private and public provider networks is explained. A method for estimating the initial position is also described, and the LDPL-M algorithm is proposed to improve geolocation accuracy. The web interface for displaying the end device's position on the map and the software architecture of the solution are also described in this section. The dataset gathered is described in Section 4. In Section 5, the achieved results are discussed, and the accuracy of geolocation is compared. Additionally, the impact of utilizing the GPS sensor on power consumption is assessed. In Section 6, the limitations of the solution and potential future research directions are discussed. Finally, the article is concluded in Section 7.

2 Related work

Geolocation of LoRa end devices is an active research area, with several proposed methods and algorithms to enhance the overall accuracy. Recent studies have demonstrated that machine learning algorithms and hybrid methods combining different techniques offer promising results [6]. Furthermore, the proper deployment and positioning of LoRa gateways can significantly influence geolocation accuracy, so further research is still required to optimize the gateway placement in different environments. Several studies have examined the deployment and type of LoRa gateways and their influence on geolocation accuracy, including a study by Podevijn et al. [14] that examined the impact on geolocation accuracy in an urban environment.

Although the considerable research has been done on geolocation in LoRa networks, there is a need for more publicly available data on this topic in Bratislava, Slovakia. This study aim was to examine the accuracy and feasibility of geolocation in a real-world environment and provide insights into the factors that could impact the precision.

The three most common geolocation techniques used in the wireless networks are multilateration, trilateration, and triangulation, which require knowledge of the location of reference points (gateways). The choice of the appropriate technique depends on the use case and the available information about the end device [13].

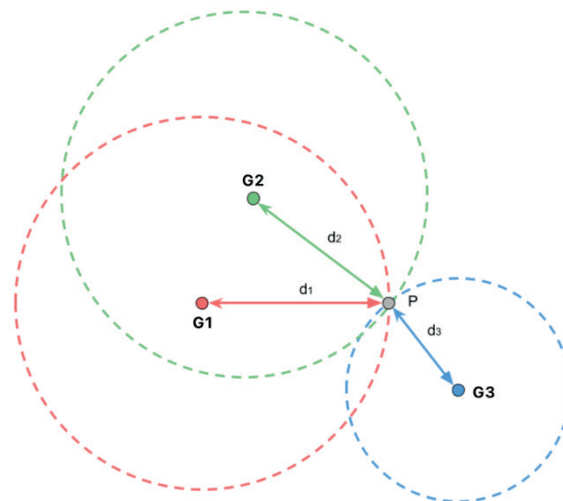


Figure 1 Position calculation using trilateration [15]

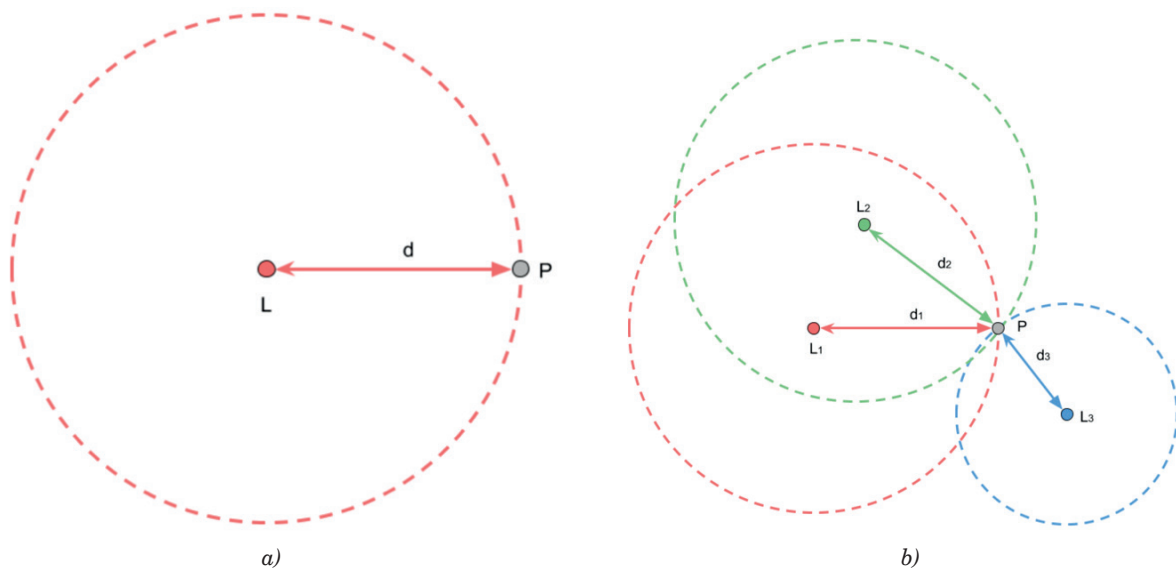


Figure 2 Representation of distance from (a) single reference point and (b) multiple reference points [15]

The trilateration uses the distance between the transmitting device and each reference point in its calculation, as shown in Figure 1. The distance between devices can be calculated in two ways:

- Based on the Time of Arrival (ToA),
- Based on the RSSI value.

For the correct calculation of the distance in the ToA method, it is essential to correctly determine the transmission time between devices. The proper determination requires time synchronization between the end device and all the reference points in the network. Time synchronization on end devices requires additional communication and thus can increase power consumption. Trilateration using ToA for determining the end device's location is therefore unsuitable for LPWANs [13, 16].

The multilateration does not require knowledge of the device's distance from each reference point, but only the difference of distances from each reference

point to the device. The Time Difference of Arrival (TDoA) between the end device and the reference points is used to calculate the distance difference. Thus, this method requires time synchronization only between the reference points [13]. Even a small error in the time synchronization (1 μ s) can cause a significant error in determining the position of the end device (300 m) [1].

The triangulation uses the geometry of a triangle defined by the two angles of the signal Angle of Arrival (AoA) for calculation. However, AoA measurements are not suitable for geolocation in the LoRa network due to the accumulating angle error with increasing distance from the reference points [13].

In LPWANs, the multilateration (TDoA values can be determined) and trilateration (RSSI value available in LoRaWAN packet) can be used to calculate the position of the end device. Studies show better accuracy of TDoA over RSSI [13, 17]. As the gateway clocks are synchronized using the Network Time Protocol (NTP),

only the precision at milliseconds is achieved, which is not sufficient for the TDoA-based geolocation.

The trilateration can be used to estimate location using RSSI. To simplify the calculations, the intersection of circles is in the Cartesian plane. Referring to Figure 2, the device's P location is intended to be determined using a reference point L whose location is known. Based on a single reference point, the location of the device P cannot be determined; it is possible to estimate the distance d between P and L using the RSSI-based techniques, as shown in Figure 2a. Each point is a potential candidate for P at this distance. For the correct determination of P , at least three circles whose intersection is at a single point are required. This point represents the actual location of the device, shown in Figure 2b. Multiple circles using various reference points are created, each at a known location L_i . For each reference point, it is possible to determine the distance d_i from P [15].

The equation for a circle in a plane:

$$(x - c_x)^2 + (y - c_y)^2 = d^2, \quad (1)$$

where the point (x, y) on the Cartesian plane lies on a circle of radius d centered on (c_x, c_y) . From Equation (1), it is possible to derive the equations for the circles generated by the reference points. Each reference point has a known location expressed by latitude and longitude coordinates (ϕ, λ) . The intersection of the circles can be obtained by solving the system of three linear equations, thereby determining the location of the point $P = (\phi, \lambda)$ [15, 18]:

$$\begin{aligned} (\phi - \phi_1)^2 + (\lambda - \lambda_1)^2 &= d_1^2, \\ (\phi - \phi_2)^2 + (\lambda - \lambda_2)^2 &= d_2^2, \\ (\phi - \phi_3)^2 + (\lambda - \lambda_3)^2 &= d_3^2. \end{aligned} \quad (2)$$

This method is mathematically correct, however, several problems were encountered that make it impractical. In the real world, a set of equations may not have a solution, as the circles may not intersect at a single point due to measurement error. For example, in [19], the authors tried to create a prototype of a wireless network in a coal mine to navigate miners out of the mine in case of an emergency. The geolocation proved to be unsuccessful due to the significant environmental interference, which caused errors in the measurement of the distance of the end devices from the reference points. In the same way, the measurements from more than three reference points cannot be used in the analytical approach. Therefore, this problem is approached more like an optimization problem by searching for a point $X = (\phi_x, \lambda_x)$ that provides the best approximation to P . Using the Mean Squared Error (MSE) calculation, it can be verified how well the point X replaces the point P [19]:

$$\frac{\sum_{i=1}^n [d_i - \text{dist}(X, L_i)]^2}{n}, \quad (3)$$

where $\text{dist}(X, L_i)$ is a distance between point X and reference point L_i .

If this distance coincides with the corresponding distance d_i , it contributes minimal error to the total error, or none at all (it is assumed that X is indeed P). The use of squares eliminates the mutual subtraction of positive and negative errors. The optimization algorithm should be able to converge to a reasonable result. Providing an estimate of the initial position of X can speed up its execution. The advantage is the possibility to use any number of reference points [15].

3 Proposed solution

A novel LDPL-M algorithm for determining the end devices' location is described in this section, including architecture, data collection and processing, initial position estimation, the LDPL-M algorithm itself, and results achieved for the stationary and mobile devices. The requirements for the proposed technique and its evaluation were the following:

1. The geolocation of end devices powered by a limited power source. The location of end devices is determined by the RSSI-based trilateration in a LoRaWAN network.
2. Comparison of the accuracy of existing geolocation methods within the trilateration. To compare the accuracy of individual geolocation techniques, a graph of the Cumulative Distribution Function (CDF) and a table of error rates of particular methods are used in each percentile. At the same time, using different methods, depending on specific use cases, may require different levels of accuracy.
3. Verification of the LDPL-M accuracy. An external GPS sensor is utilized to provide a reference value for the actual location of the end device, with an accuracy of 15mm.
4. Visualization of the end devices' location on the map. As a part of the research, a web interface that displays the last recorded location of the end device, along with information about the time of the most recent location update, was created.
5. Contribution to future research and community. The creation of a publicly available dataset contributes to the field of LPWANs and geolocation.

This research is focused exclusively on the geolocation by the RSSI-based trilateration, due to the hardware limitations. The basic principle of determining the end device's location based on the RSSI consists of associating the path loss with the distance between the transmitted and received signal. Path loss represents the loss of signal strength that occurs during the transmission through a communication medium and obstacles, such as air or a wall. Path loss can be calculated using the link budget, which includes all signal gains and losses during transmission from the

transmitter to the receiver. This budget is defined by [20-21]:

$$P_{Rx} = P_{Tx} + G_{Rx} + G_{Tx} - L_{PL}, \quad (4)$$

where: P_{Rx} is a signal strength at the receiver,
 P_{Tx} is a signal strength at the transmitter,
 G_{Rx} is a gain of the antenna used by the receiver,
 G_{Tx} is a gain of the antenna used by the transmitter,
 L_{PL} is a path loss.

The path loss is calculated by substituting the RSSI value into P_{Rx} in Equation (4). The path loss can be subsequently associated with the distance the signal has traveled through several models:

Free-space Path Loss Model (FSPL): The main idea is that the strength of a received wireless signal passing through free space decreases quadratically with increasing distance from the sender [22]:

$$P_{Rx}(d) = \frac{P_{Tx} G_{Tx} G_{Rx} \lambda^2}{(4\pi d)^2}, \quad (5)$$

where: $P_{Rx}(d)$ is a signal strength at receiver at a distance d ,
 λ is a wavelength,
 d is a distance between receiver and sender.

A more appropriate notation of the model is in units of decibels (dB):

$$FSPL(d) = 20 \log_{10}(d) + 20 \log_{10}(f) + 20 \log_{10}\left(\frac{4\pi}{c}\right), \quad (6)$$

where: $FSPL(d)$ is a path loss at a distance d ,
 d is a distance between receiver and sender,
 f is a carrier frequency,
 c is a speed of light.

Logarithmic Distance Path Loss Model (LDPL): In reality, most signals are received in an environment without direct visibility of devices (Non-Line of Sight, NLoS), which results in interference, especially in built-up areas. Interference is caused by reflections from buildings, weather, and other variables, considering the utilization of FSPL is more of an idealization. Based on empirical evidence, it is more appropriate to estimate the distance according to the LDPL formula [16, 21]:

$$L_{PL}(d) = L_{PL}(d_0) + 10\beta \log\left(\frac{d}{d_0}\right) + X_\sigma \quad (7)$$

where: $L_{PL}(d)$ is a path loss at a distance d in dB,
 $L_{PL}(d_0)$ is a path loss at a reference distance d_0 in dB,
 β is a path loss exponent - an empirical constant dependent on the environment,

X_σ is a path loss random variable from the shading factor with zero Gaussian mean value and standard deviation σ in dB.

By substituting L_{PL} from Equation (4) into Equation (7), the distance d can be estimated if the values of the parameters β and $L_{PL}(d_0)$ are available. These values can be obtained by performing empirical measurements - machine learning methods by fitting a logarithmic curve are used to describe the best the data obtained by the measurements. The values of the parameters β and $L_{PL}(d_0)$ depend on the environment [23].

In addition to the mentioned models, there are other models, such as Okumura-Hata, Cost 231, or IMT-2000 [21].

To improve the results of the RSSI-based geolocation, the RSSI can be substituted with the Estimated Signal Power (ESP) with the environmental interference considered. ESP is beneficial due to the characteristics of LoRa networks, in which a relatively noisy signal can be received (in practice, the gateway manages to decode even frames with the RSSI of approximately -120 dBm) [24]. The ESP equation can be written in the logarithmic form [21, 25]:

$$ESP_{(dBm)} = RSSI_{(dBm)} + SNR_{(dB)} - 10 \log_{10}(1 + 10^{0.1 SNR_{(dB)}}). \quad (8)$$

The ESP can be processed the same way as the RSSI, and therefore substituted into P_{Rx} in Equation (4), and then used to calculate the distance between the end device and the gateway using Equation (7). For most of the previous works, which determined the position of the RSSI device, determining the position in a smaller area or sparsely built-up areas with minimal environmental interference was specific. Any environmental obstacle seriously affects the geolocation accuracy [21]. It can therefore be concluded that such device geolocation is more suitable for a smaller area and environments with direct visibility of devices (Direct Line of Sight, DLoS).

3.1 Architecture

In this section, the primary focus is on the architecture of the private LoRaWAN network. Unfortunately, during the research, it was not possible to access the architecture of the public provider network, so it cannot be discussed in more detail. Figure 3 shows the locations of gateways within the private network. All gateways were strategically placed to form a polygon and maintain DLoS with the end device. The highlighted polygon illustrates the area in which the end device was able to move during the data collection. The network consisted of the following components:

- End device: Development Kit LilyGo TTGO ESP32 with SX1276 LoRa Chip and built-in NEO-6M GPS

module. The device was programmed to periodically transmit uplink (from the end device to the network server) messages at 868 MHz frequency band. The LMIC-node library [26] was used.

- **Network server:** Messages sent from end devices received by gateways were sent over the Internet to the ChirpStack network server. This open-source implementation provided a web interface to manage gateways, end devices, and applications [27]. Using the ChirpStack network server, all the measured
- **Gateways:** During the data collection phase, 8 Raspberry Pi microcomputers were utilized as gateways within the network. These microcomputers were attached a compatible backplane connecting the Raspberry Pi to an iC880A LoRaWAN concentrator with an 868 MHz antenna. Each gateway was running the Raspberry Pi OS operating system. One of the key advantages of using Raspberry Pi

data was downloaded and processed in JavaScript Object Notation (JSON) format.

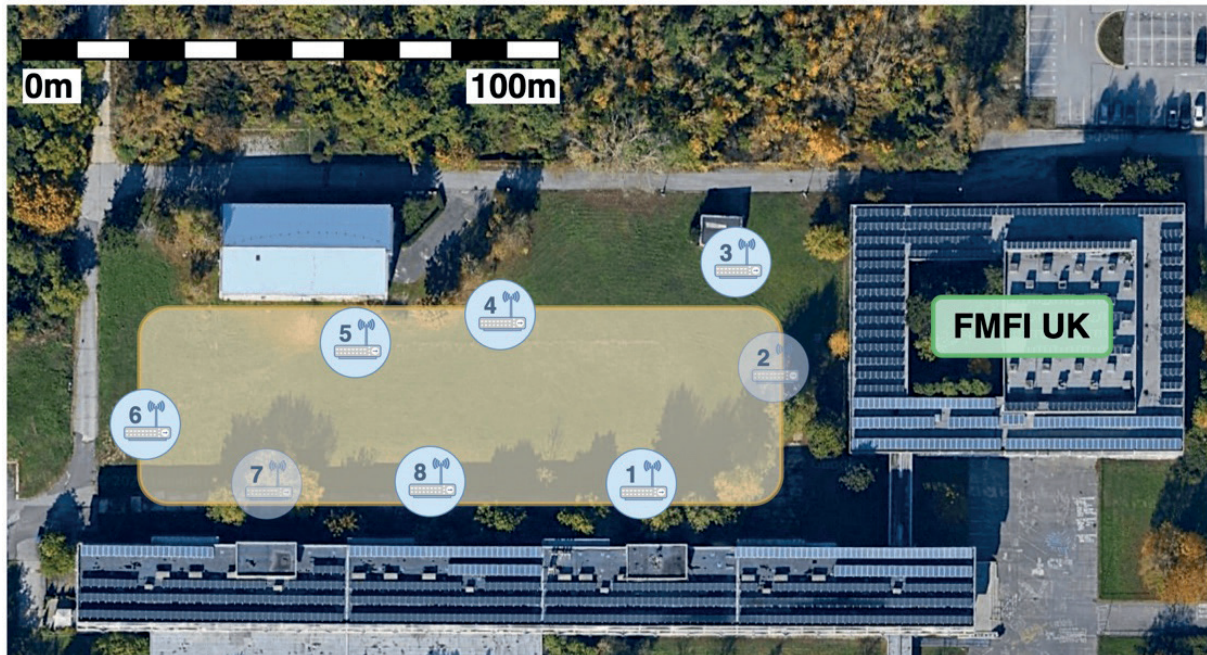


Figure 3 Gateways position - Google Maps data

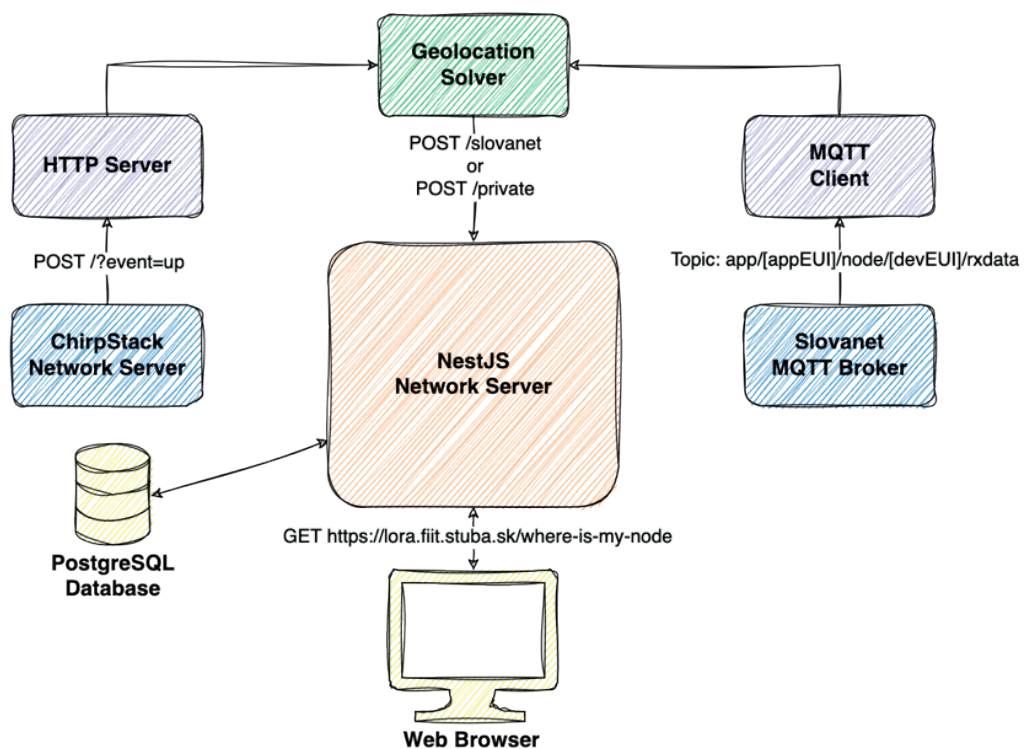


Figure 4 Software architecture

gateways was their mobility, as they can be powered by power banks.

During the data collection and experiments, a microservice architecture, shown in Figure 4, was used, which consisted of the following services:

- **Hypertext Transfer Protocol (HTTP) Server:** A minimalist HTTP server programmed in Python. The ChirpStack network server allows the captured uplink messages from the end device to be sent to any Internet Protocol (IP) address in real time using the HTTP protocol. The task of the HTTP server is to capture messages from the ChirpStack network server and then forward them via the HTTP protocol to a Geolocation Solver service.
- **Message Queuing Telemetry Transport (MQTT) Client:** A simple MQTT subscriber. The public provider sends the real-time uplink messages from the end device to this topic. When implementing the subscriber, it is suggested to use the *paho.mqtt* Python module. The task of this service is similar to the previous case, i.e., to forward uplink messages to the Geolocation Solver.
- **Geolocation Solver:** This service estimates the end devices' position in both networks separately. It uses the LDPL-M algorithm further described in the following sections. This service is implemented using a Python *http* module. After calculating the end device's position, the coordinates are sent to the NestJS web server via HTTP.
- **NestJS Web server:** A simple web server storing information about the end devices' location in the database (for each device in both networks separately). This service also contains the "Where is my node?" user interface described in Section 4.8 in more detail.

3.2 Initial position estimation

Algorithms that determine the location of end devices typically need an initial estimate of the starting position. The accuracy can be slightly lower, as the algorithms should eventually converge to more accurate results. The Weighted Centroid (WC) of the gateways that received the signal from the end device was used for the initial estimate. The path loss for the given gateway determined the weight. The inspiration for this idea came from a solution proposed by Bissett [21] - weight was linked to the ToA. It was assumed that a lower path loss value indicates a gateway closer to the end device and vice versa. Based on this assumption, the weight for each gateway was calculated as follows:

$$w = \frac{L_{PL_n} - L_{PL_i}}{L_{PL_n}} + \frac{c}{n}, \quad (9)$$

where: w_i is a weight of the i^{th} gateway's influence on the gravity center calculation,

L_{PL_i} is a path loss of the i^{th} gateway of the given transmission,

L_{PL_n} is the largest path loss of the given transmission,

c is a constant adding minimum weight for each gateway,

n is a number of gateways that received the uplink message.

The resulting formula for calculating the estimated initial value is as follows:

$$\begin{pmatrix} \hat{x} \\ \hat{y} \end{pmatrix} = \sum_{i=1}^n \hat{w}_i \begin{pmatrix} x_i \\ y_i \end{pmatrix}, \quad (10)$$

where: $\begin{pmatrix} \hat{x} \\ \hat{y} \end{pmatrix}$ is a weighted centroid of gateways' gravity, i.e., the estimated starting position of the end device.

In addition to estimating the initial position, the weighted centroid was used as one of the techniques to determine the actual position.

3.3 Map projection

Coordinates define the location on the ground. There are two coordinate systems: the Geographic Coordinate System (GCS) and the Projected Coordinate System (PCS). The GCS defines the position in angles based on latitude and longitude from the center of the Earth [28]. The PCS, or Cartesian Coordinate Systems (CCS), represents the three-dimensional GCS in two dimensions by projecting and leveling the Earth's surface onto a plane. During the projection, distortions occur (shape, area, distance, or direction). No kind of projection preserves all four geographic features at the same time. Each projection tries to preserve some geographical feature, but with the knowledge of compromising other features. For this reason, many different projections are divided into three main projection systems: cylindrical, conical, and planar. The main focus is on the cylindrical projection, as with this type of projection, the lines of latitude and longitude remain parallel to the x and y axes [21, 28].

Figure 5a shows the Mercator projection, one of the most popular and used cylindrical projections. It is used in most map applications, such as Google Maps or OpenStreetMap. However, this type of projection distorts areas further from the equator. The Equidistant projection, shown in Figure 5b, maintains constant distances along both lines of latitude and longitude, and thus is more suitable for experimental geolocation using the RSSI-based trilateration. In Equidistant projection, it is possible to directly assign the displayed pixel on the map to the corresponding geographic location on the Earth.

By a simple calculation, the GCS can be converted to the PCS, i.e., the latitude and longitude (λ, ϕ) can be converted to coordinates (x, y) in the Cartesian plane [21, 28-29]:

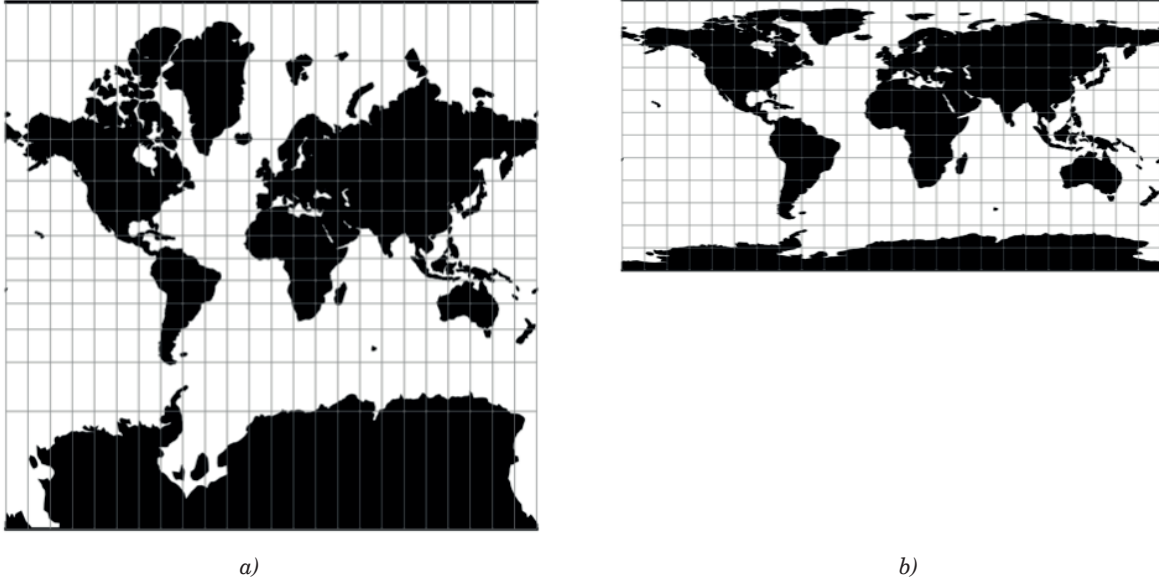


Figure 5 Cylindrical (a) Mercator and (b) Equidistant projections [29]

$$\begin{aligned} x &= R(\lambda - \lambda_0) \cos \phi_1, \\ y &= R(\phi - \phi_1), \end{aligned} \quad (11)$$

where: x is a horizontal coordinate on projected map,
 y is a vertical coordinate on projected map,
 R is an Earth radius in meters,
 λ is a projected longitude,
 λ_0 is a central map parallel,
 ϕ is a projected latitude,
 ϕ_1 is a standard parallel.

3.4 Accuracy evaluation

The distance between the two points must be calculated to evaluate the accuracy or error of the location determined by the techniques described in this

article. On a small scale, it can be assumed that the observed surface is flat without the curvature of the Earth. The distance D between the point $P = (\lambda_p, \phi_p)$ and $Q = (\lambda_q, \phi_q)$, can be thus calculated using the simple Euclidean distance [30]:

$$D = R \sqrt{\Delta \phi^2 + (\cos \phi_m \Delta \lambda)^2}, \quad (12)$$

where: R is the radius of the Earth,

$$\Delta \phi = |\phi_2 - \phi_1|,$$

$$\Delta \lambda = |\lambda_2 - \lambda_1|,$$

$$\phi_m = \frac{\phi_1 + \phi_2}{2}.$$

The Euclidean distance only approximates the distance between the two geographic points if they are relatively close to each other. Since the Earth is not flat, the so-called great-circle distance must be calculated. This distance can be imagined as the length of the shortest rope laid on the Earth surface, which connects the two points, as shown in Figure 6 [30]:

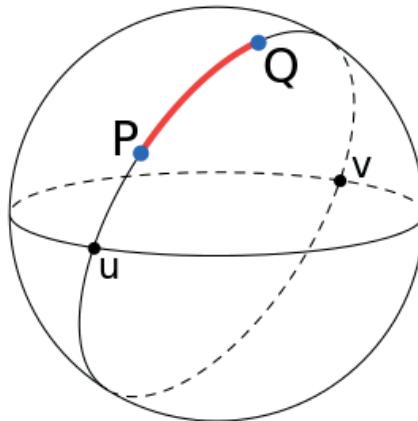


Figure 6 Great-circle distance [30]

$$D = R \tan^{-1} \left(\frac{\sqrt{(\cos \phi_2 \sin \Delta \lambda)^2 + (\cos \phi_1 \sin \phi_2 - \sin \phi_1 \cos \phi_2 \cos \Delta \lambda)^2}}{\sin \phi_1 \sin \phi_2 + \cos \phi_2 \Delta \lambda} \right) \quad (13)$$

Using this technique, it is assumed that the Earth is a perfect sphere. However, the Earth is an irregular ellipsoid. When calculating the distance between the two points, the error is never more significant than 0.5% [31]. Using Equation (13), it is possible to calculate the distance between the two points and thus verify the error rate of the geolocation methods.

3.5 Methodology of data collection and processing

Slovanet provided an end device from the manufacturer Ursalink, which periodically communicated with gateways connected to the public provider LoRaWAN network. In the private LoRaWAN network, the end device described in Section 3.1 was used during the experiments. The process of data collection was similar in both networks. To accurately record the real-time position of the end device, an external ublox GPS sensor with a precision of 15 mm placed next to the end devices was utilized during measurements, recording the position twice per second. The GPS sensor was also used to position the gateways. It is worth noting that the coordinates of the end device were processed not at the time of transmission but at the time of reception at the network server. The processing of measured data consisted of several steps:

Assignment of the recorded position by the external GPS sensor to uplink messages based on timestamps.

1. Transformation of latitude and longitude into x and y coordinates using the local cylindrical equidistant projection.
2. Determination of parameter values ($L_{PL}(d0)$ and β)

for individual gateways.

3. Evaluation of the geolocation accuracy.

The data collected from both networks are visualized in Figures 7a and 7b.

During the first step the end device's location was assigned to uplink messages based on the timestamps. Since the external GPS sensor recorded its position twice per second, it often happened that the time of message reception at the network server was not precisely the same as that of the external GPS sensor. In such a case, the location was selected at the time closest to the message reception time. The difference never exceeded 500 ms.

The second step consisted of transforming the latitude and longitude coordinates into x and y coordinates using the local cylindrical equidistant projection. To transform the coordinates while preserving the actual scale, it was first necessary to determine ϕ_1 and λ_0 . To verify the correctness of the so-called true scale equidistant cylindrical projection, the distance between the two most distant points in the dataset was compared using the Euclidean distance in the Cartesian two-dimensional plane and the great-circle distance. The maximum possible distance error between the two points using the Euclidean distance versus the great-circle distance was 0.000019 mm (0.0000000084%) at a length of 228.77 m. The margin of error is small enough that it is possible to continue working with the x and y coordinates in the Cartesian plane and using the Euclidean distance.

The next step was to determine the values of the parameters ($L_{PL}(d0)$ and β) for individual gateways, laying the logarithmic curve so that it best describes the relationship between the distance and path loss. It is observed that the theoretical FSPL model, compared to the LDPL model, is highly underestimated and unsuitable for determining the location of the end device. Based on the results, it is concluded that even a tiny obstacle between the gateway and the end device results in large fluctuations in the path loss, thus significantly affecting the geolocation accuracy. After

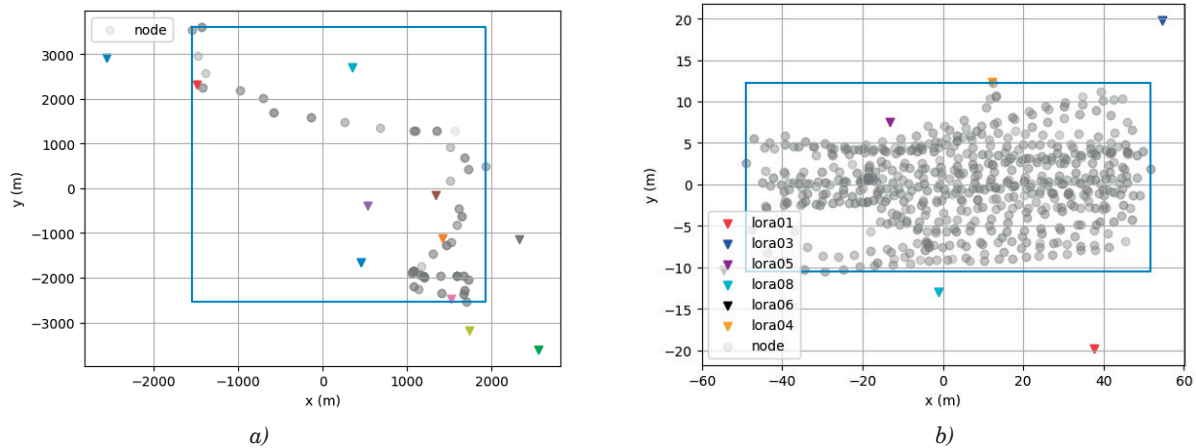


Figure 7 Visualization of measured data in (a) public provider and (b) private network using equidistant cylindrical projection

that, the distance of the end device from the gateway using the path loss was calculated.

The penultimate step was to perform the filtering of the unsuitable uplink messages - 132 of the original 233 messages could be used for the geolocation.

In the last step the accuracy of the geolocation techniques was evaluated.

3.6 LDPL-M algorithm

To determine the location of the end device, the use of the trilateration method was proposed, i.e., to associate the distance of the end device from individual gateways based on the value of the signal loss during propagation. The reason for using this method is the insufficient time synchronization between the gateways caused by the hardware limitations. This fact does not allow to determine the position using the multilateration method.

The collected dataset has a characteristic feature - since the end device sends uplink messages regularly in a certain period, the overall geolocation accuracy can be potentially improved by incorporating the previous locations into the calculation. The condition for this approach is to know the real location of the end device at the time of sending the first message. This data can be obtained either by one of the geolocation methods or by using GPS. It is also necessary to determine how far the device will most likely move until the next message reception. The distance the device can potentially travel can be determined in two ways:

Calculate all the distances between individual uplink transmissions based on empirical measurements and then determine the largest distance that the device

has traveled in 90% of cases.

Determine how fast the device usually moves and associate the distance traveled with the device's speed and the periodicity of the uplink transmission.

After defining the distance the device will most likely travel, it is proposed to use the previous location of the device as the location of an additional virtual gateway in the next transmission. The location of this virtual gateway will represent the center of a circle with a radius equal to the defined distance that the device will most likely travel. Adding the virtual gateway has the potential to improve the geolocation of the end device using the trilateration method, virtually increasing the number of gateways that have captured the message. The limitation of this method lies in the assumption that the device moves constantly, or its speed is part of movement data, i.e., known in advance, or is a part of the data payload.

In the case of a stationary device, the algorithm would worsen the measured results, since it assumes the device is in motion. Furthermore, this algorithm is not suitable for use cases where the speed of the end device changes significantly. The LDPL-M algorithm is thus proposed, its accuracy is experimentally verified on real data, and it is compared to the common trilateration methods described in previous sections. In the previous geolocation techniques, it was assumed that the end device was mobile. However, in the real-world scenarios, the situations where the end devices are stationary are often encountered. In the context of computing the end devices' location within the LoRaWAN network, this observation was leveraged to enhance the accuracy of the proposed model. To do this, a set of messages from the private LoRaWAN network was gathered, all close to each other (within a 2m range). By doing this, a scenario

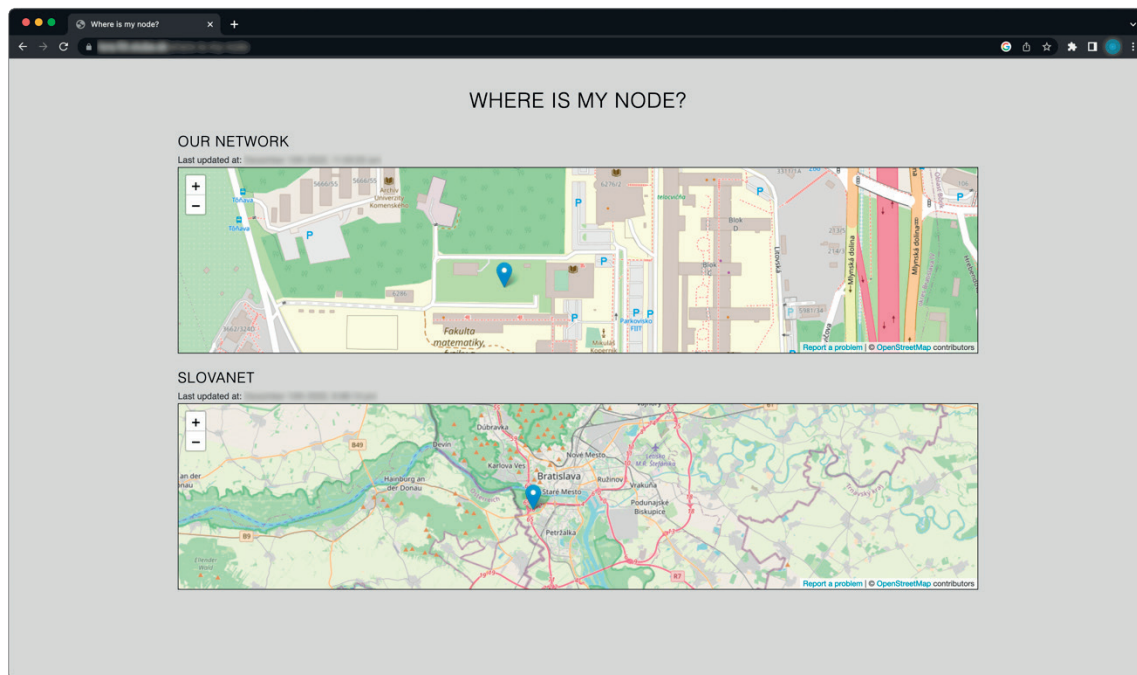


Figure 8 User interface

mimicking a stationary device was effectively created. In determining the stationary end device's location, the current estimation and the previous results were incorporated into the calculation. This was achieved by averaging the current estimated location with the results obtained from prior computations. To ensure stability and mitigate significant variations in the RSSI due to environmental factors, the averaging process was limited to the last N previously estimated end device's locations. This approach averages the location estimate to smooth abrupt RSSI value changes, potentially refining the geolocation accuracy for stationary end devices. It is important to note that the two different methods of averaging location exist:

1. The first way is to figure out the current location and then find the average of the locations determined before.
2. The second way is to figure out the current location and then find the average of earlier locations that had already been treated the same way (averaged). The second method provided better results.

3.7 "Where is my node ?"

The web application visualizing the end device's location is called "Where is my node ?" It is fully containerized using the Docker platform. A location update occurs every time an uplink message is received

from the end device. The user interface is shown in Figure 8. It displays the timestamp of the last location update. The page overviews the geolocation from both the public provider and private LoRaWAN networks.

4 Dataset

During the measurements, a dataset from both the private and the Slovanet public provider networks was created. The ublox external GPS sensor was used to gather the precise location data, shown in Figure 9c, as a reference. The format of messages received in the public provider network slightly differs from those captured in a private network. Therefore, it was necessary to reflect this fact during the implementation of the custom parser, which combines geographical data from the external GPS sensor and uplink message based on the timestamps. The dataset is publicly available for the community at the link <https://data.ail.sk/dataset-geolora/>.

In the private network a LilyGo TTGO ESP32 end device, equipped with an SX1276 LoRa chip and built-in NEO-6M GPS module, was utilized. The end device is shown in Figure 9a. The external GPS sensor near the end device serves as a ground truth for the proposed solution verification. The data from the end devices were processed by the ChirpStack network server and forwarded in JSON format to the external application

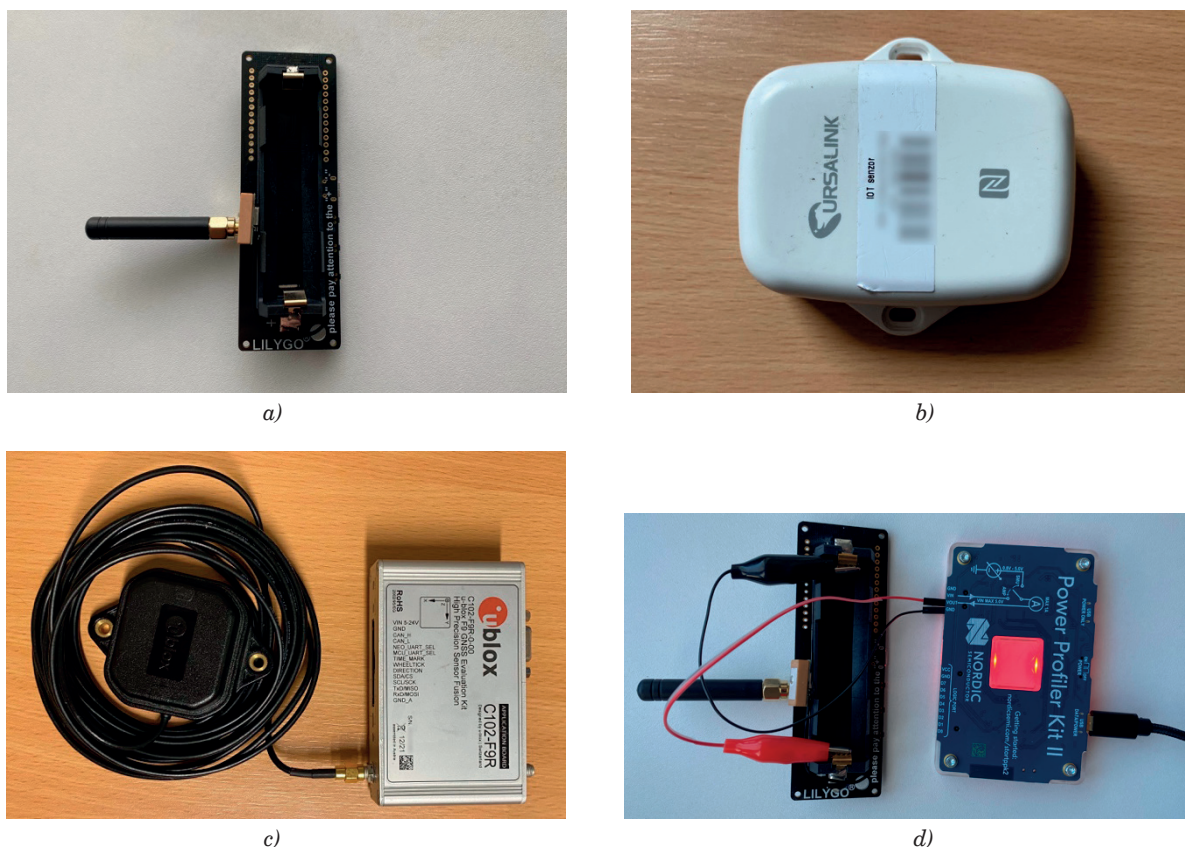


Figure 9 Hardware used during experimental setup - (a) LilyGo TTGO end device, (b) Ursalink end device, (c) ublox GPS sensor and (d) Power profiler kit II connected to the end device

server (HTTP) via an integration functionality. The server then extracted the message reception timestamp and appended a new line to the Comma-Separated Values (CSV) file. After the extraction, the output file was combined with the GPS sensor data using a custom parser. Finally, the static information about the locations of individual gateways was appended.

In the public provider network, the end device from the manufacturer Ursalink was used, shown in Fig. 9b. Access to the data was possible during the message reception or by obtaining historical data stored in the cache. The cache stored messages for 30 days and could be downloaded via the Representational State Transfer Application Programming Interface (REST API) in JSON format at most once a day. On the other hand, the MQTT protocol allowed the subscription to the topic of interest and thus provided access during packet reception. The data was collected using the MQTT client. The uplink messages were sent by a provider with a 5-minute periodicity, and the interval could not be further modified.

The only difference worth noting, compared to the private network, was encountered when filtering messages unsuitable for geolocation. As it was not possible to access the physical topology, the packet data in the public provider network contained the location of the gateways. Not every gateway had information regarding its location available. Therefore, it was necessary to remove such gateways and then evaluate whether at least three gateways with known positions received the message to be able to apply the trilateration.

5 Results and discussion

When determining the location of the end devices, the techniques discussed in this article - FSPL, LDPL,

WC, and the proposed LDPL-M - were compared to each other and the GPS data. In all cases working with the path loss, the RSSI was substituted with the ESP.

The detailed results of the error rate in the private LoRaWAN network with DLoS are shown in Figure 10 and Table 1. These results clearly show that the most accurate way to determine the location is to use the GPS sensor, which is located directly on the top of the end device but at the expense of increased power consumption. A similar average error is observed for all the discussed techniques. The difference in accuracy between the LDPL model with and without memory is more significant. The LDPL-M method improves the geolocation accuracy over the conventional LDPL model by 24.54% in 90% of cases. The WC results in a similar accuracy, but this method is only applicable for the geolocation within the polygon formed by the gateways. The disadvantage is that the nature of the device must be known in advance, i.e., the speed at which the device moves. This limits the possibilities of using the technique. However, the end device can also send the measured or estimated speed inside the LoRaWAN packet payload.

The detailed error results for the public provider LoRaWAN network without DLoS are shown in Figure 11 and Table 2. During this test, the device was moved around Bratislava by walking rather than staying in the reserved area defined by spread gateways. The results show that the absence of DLoS and densely built regions significantly impacted the geolocation accuracy. Depending solely on the RSSI without DLoS is unreliable. While our proposed model has improved the overall accuracy, the error rate is still high for majority of use cases.

Substituting the RSSI with the ESP proved to have a significant impact on the geolocation accuracy in the public provider network. In 90% of cases, the error rate

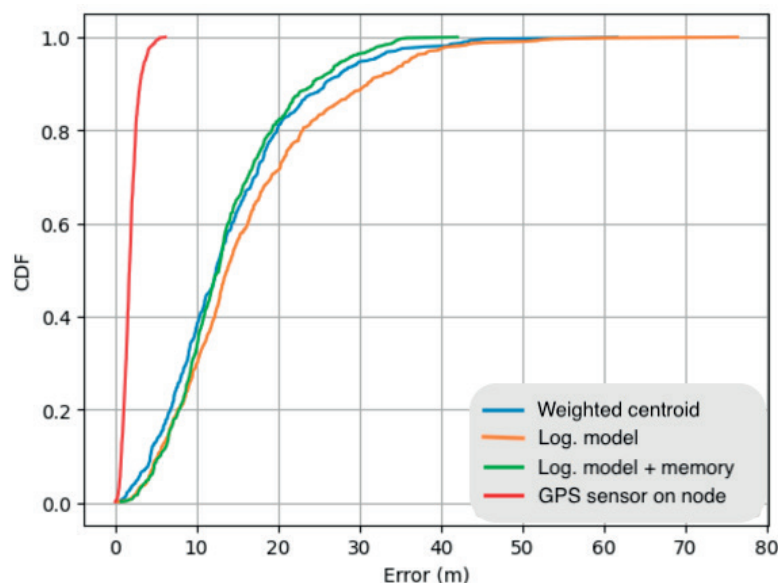
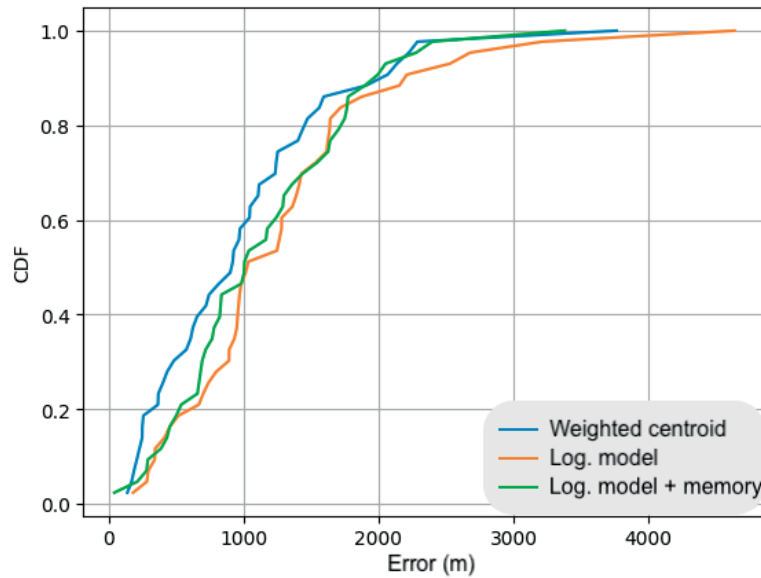


Figure 10 Accuracy comparison in private network

Table 1 Error rate comparison in private network (DLoS)

Method	90 percentile error (m)	50 percentile error (m)
GPS Sensor	3.11	1.78
LDPL-M	24.33	12.76
WC	25.80	12.43
LDPL	31.01	13.83

**Figure 11** Accuracy comparison in public provider network**Table 2** Error rate comparison in public provider network (no DLoS)

Method	90 percentile error (m)	50 percentile error (m)
LDPL-M	1974.99	1006.42
WC	2034.64	919.51
LDPL	2197.53	1035

using the RSSI to calculate the path loss in the LDPL model was less than or equal to 2478.31m, while using the ESP value it was 2197.53m. Therefore, a significant improvement in determining the location by 11.35% was observed. The impact of using the ESP decreases when the device is located closer to the gateway or with DLoS, because the ESP partially considers the environmental influence on the final RSSI.

In the case of an environment with DLoS, the ESP differs minimally from the RSSI, which could be observed in the data collected in the private network. It is still advisable to use the ESP instead of the RSSI.

Regarding the modification proposed for stationary devices, Tables 3 and 4 contain the comparison of error rate between the original and modified geolocation techniques for the stationary end device. The graphs of CDF curves for individual measurements are shown in Figures 12a and 12b.

The outcomes indicate that the modified methods enhance the geolocation accuracy. The results of the

previous $N = 10$ calculated locations were incorporated when averaging.

The precision of the LDPL-M algorithm increased from the initial 27.20m to 7.56m in 90% of cases. Thus, it is evident that determining the location of a stationary end device is significantly more accurate than determining the position of a mobile device.

The energy consumption between scenarios with and without the active GPS module during the message transmission and reception was compared, as well. To measure the power consumption, the Power Profiler Kit II from Nordic Semiconductor [32] was utilized, connected in sequence with the end device's battery pins, shown in Figure 9d. Bundled software recorded fluctuations in current over time.

The detailed results are shown in Table 5. The measurements showed the end device's power consumption significantly increased (by an average of 48.8%) when the GPS module was active. This finding underscores that utilization of the GPS module for the

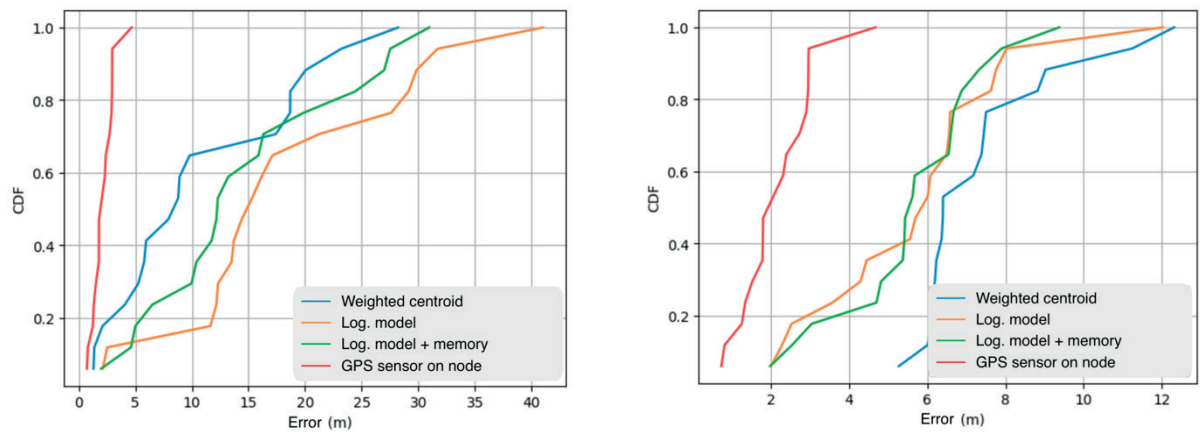


Figure 12 Accuracy comparison of (a) original and (b) modified methods for the stationary device

Table 3 Error rate for stationary device using original methods in private network

Method	90 percentile error (m)	50 percentile error (m)
LDPL-M	27.20	12.29
WC	21.31	8.79
LDPL	30.59	15.31

Table 4 Error rate for the stationary device using original methods in private network

Method	90 percentile error (m)	50 percentile error (m)
LDPL-M	7.56	5.62
WC	9.92	6.40
LDPL	7.87	6.01

Table 5 GPS module power consumption measurements

GPS module	Average (mA)	Transmission (mA)	RX window opened (mA)
Off	86	140	102
On	128	165	141

geolocation yields notably enhanced accuracy compared to the trilateration, but at the expense of a significantly higher power consumption.

6 Limitations and future work

Although the GPS-independent geolocation is a promising research area and the proposed solution provided reasonable results, the RSSI-based geolocation is commonly known to have its limitations.

In this section, firstly, the limitations encountered during the research are discussed. Secondly, the portability options are examined, and finally, the potential future work is described.

Limitations of the RSSI-based geolocation are tightly connected to the wireless nature of the underlying technology. The overall accuracy is affected by even more factors:

1. RSSI non-linearity or lack of DLoS. The DLoS between the gateways and the end device is important for a proper and accurate geolocation using the RSSI. Even a small obstacle results in a large path loss fluctuation, which affects the overall accuracy. Signals often reflect from the surfaces, creating multiple paths to the receiver, which also causes variations in the RSSI. Substituting the RSSI with the ESP had a significant impact on the accuracy, as it partially considers the environmental influence. This was more significant in the Slovanet public LoRaWAN network.
2. Gateway placement and density. The gateway placement and density are both crucial factors impacting the accuracy and reliability of the RSSI-based geolocation. Every end device should be placed within the range of multiple gateways, for the purposes of trilateration, at least three. The interference and multipath effect can be minimized

by placing the gateways in areas without reflective surfaces or electromagnetic noise. In addition, the overlap in coverage ensures reliability and accounts for the end device mobility. Despite the data collection process in the public provider network being very similar to the data collection in the private network, several public gateways did not provide information about their location. As access to the public infrastructure was not possible, the only option was to rely on the location data contained in the payload. Such gateways, missing the location data, had to be removed from the calculations.

3. Reliance on historical data. A standard LDPL model does not rely on historical data. On the other hand, the LDPL-M algorithm considers historical data during the calculation. The algorithm converged gradually and achieved higher accuracy with the increasing volume of collected data. The disadvantage of this approach is that if the gateway moves, the entire data collection must be repeated, and therefore, the previously collected data is unusable. Additionally, the uplink transmission periodicity can influence the accuracy.
4. Precise time synchronization. The research presented in the article was exclusively focused on the RSSI-based techniques instead of the TDoA due to the lack of precise time synchronization. Several studies show better accuracy of the TDoA over the RSSI [13, 17]. The applicability of the TDoA was limited by the hardware capabilities. The TDoA multilateration could potentially achieve higher precision; it would require the modification of the gateway hardware, as the time synchronization using the NTP proved to be insufficient for this use case.

In terms of portability, the proposed solution relies solely on the RSSI, which is contained within the LoRaWAN messages provided by the ChirpStack network server for the further operation at the application layer, and the known location of individual gateways. As long as these two prerequisites are met, the solution is independent of the underlying technology. It is still necessary to consider the above-mentioned limitations, especially the DLoS, proper placement and density of gateways, as well as the transmission periodicity.

The subject of the future work could be developing the geolocation method based on multilateration using the TDoA. This method requires modifying the gateway hardware, which must be equipped with an additional module to ensure a high degree of time synchronization between the individual gateways - in this case, the use of GPS may be appropriate, since the gateway usually has the permanent power supply, and therefore low power consumption is not as crucial as in the case of the energy-harvesting end devices.

The experiments confirmed that the geolocation using the RSSI-based trilateration is not suitable for

dense urban areas without DLoS. Instead, when certain conditions are met, the proposed solution achieves better results than commonly used algorithms. The advantage is that all the calculations are performed on the server, so the solution does not negatively impact the end device's power consumption. On the other hand, the disadvantage is that the end device still has no knowledge about its location.

7 Conclusion

Geolocation of the end devices in LPWANs, while maintaining the low power consumption over a relatively large area, is a promising research area that opens up many use cases. Choosing the proper technique requires a thorough evaluation of advantages and disadvantages, especially in terms of overall efficiency.

This research was focused on the comparison of the existing techniques in both the private and public LoRaWAN networks. Next, the process of data collection and processing was described. A novel LDPL-M algorithm utilizing the end device's previous locations was proposed to enhance the geolocation accuracy, while also concerning the low power consumption. Compared to the existing techniques, the LDPL-M also considers the end device's previous locations. To assess the accuracy, the location of the end device was determined using an external GPS sensor and matched with the collected uplink messages. Part of the research was dedicated to the estimation of the end device's starting position as an input to the discussed geolocation methods. A significant environmental influence on the RSSI value was observed during the experiments. The measurements confirmed that the geolocation of end devices in the LoRaWAN network using the trilateration is possible; however, it is not suitable for densely built-up areas without DLoS. During experiments, the LDPL-M achieved better results than commonly used techniques. The impact of the GPS module on the end device's power consumption was assessed. Results revealed a notable increase with GPS enabled by an average of 48.8%, which indicates using a GPS module is significantly more accurate than the trilateration technique in LPWANs, but at the cost of higher power consumption. At the same time, a significantly lower error rate for the geolocation of a stationary end device was observed compared to a mobile device scenario. The main benefit is that the proposed solution does not require additional communication overhead, which implies it has no negative effect on the power consumption compared to the standard operation. Finally, a web application that displays the location of the end device in real time in both the private and public provider networks was implemented.

To our knowledge, there is currently no similar dataset that pairs the geographic data with uplink reports from Bratislava, Slovakia. The measurements

confirm that the environment significantly affects the RSSI. The experiments proved that the proposed LDPL-M algorithm achieves better results than the commonly used techniques under specific conditions.

Although the research was focused on the LoRa technology and the LoRaWAN protocol, the findings are not specific to the underlying technology but rather generally applicable to wireless communication technologies.

supported by APVV-23-0137 project “Legal and technical aspects of cybersecurity situational awareness”. The authors would like to thank for financial contribution from the STU Grant scheme for Support of Young Researchers. The authors would also like to express their gratitude to Slovanet, a.s. for granting access to the public provider network and borrowing the equipment necessary for the research.

Acknowledgements

Funded by the EU NextGenerationEU through the Recovery and Resilience Plan for Slovakia under the project No. 09I05-03-V02-00012. This project has been

Conflicts of interest

The authors declare that they have no known competing financial interests or personal relationships that could have appeared to influence the work reported in this article.

References

- [1] DAWOUD, S. GNSS principles and comparison [online] [accessed 2025-04-15]. Potsdam, Germany: Potsdam University, 2012. Available from: http://www.snet.tu-berlin.de/fileadmin/fg220/courses/WS1112/snetproject/gnss-principles-and-comparison_dawoud.pdf
- [2] SINHA, R., YIQIAO W., HWANG, S. A survey on LPWA technology: LoRa and NB-IoT. *ICT Express* [online]. 2017, **3**(1), p. 14-21 [accessed 2025-04-15]. eISSN 2405-9595. Available from: <https://doi.org/10.1016/j.ict.2017.03.004>
- [3] LINK LABS A comprehensive look at low power, wide area networks [online] [accessed 2025-04-15]. 2016. Available from: <https://www.link-labs.com/low-power-wide-area-networks-white-paper>
- [4] GARCHE, J., DYER, C. *Encyclopedia of electrochemical power sources*. Elsevier, 2009. ISBN 9780444520944.
- [5] CHENEBAULT, P., VALLIN, D., THEVENIN, J., WIART, R. Impedance analysis of the lithium discharge in Li-SOCl₂ cells: synergetic effect of SO₂ and LiAl(SO₃Cl)₄. *Journal of Applied Electrochemistry* [online]. 1989, **19**(3), p. 413-420 [accessed 2025-04-15]. ISSN 0021-891X, eISSN 1572-8838. Available from: <https://doi.org/10.1007/BF01015245>
- [6] ANJUM, M., KHAN, M. A., HASSAN, S. A., MAHMOOD, A., GIDLUND, M. Analysis of RSSI fingerprinting in LoRa networks. In: 2019 15th International Wireless Communications and Mobile Computing Conference IWCMC: proceedings [online]. 2019. ISBN 978-1-5386-7748-3, p. 1178-1183. Available from: <https://doi.org/10.1109/IWCMC.2019.8766468>
- [7] ARAS, E., RAMACHANDRAN, G. S., LAWRENCE, P., HUGHES, D. Exploring the security vulnerabilities of LoRa. In: 2017 3rd IEEE International Conference on Cybernetics CYBCONF: proceedings [online]. 2017. ISBN 978-1-5386-2201-8, p. 1-6. Available from: <https://doi.org/10.1109/CYBConf.2017.7985777>
- [8] LORA ALLIANCE LoRaWAN specification v1.1 [online] [accessed 2025-04-15]. 2017. Available from: https://lora-alliance.org/resource_hub/lorawan-specification-v1-1/
- [9] Semtech Corporation LoRa and LoRaWAN [online] [accessed 2025-04-15]. 2024. Available from: <https://www.semtech.com/uploads/technology/LoRa/lora-and-lorawan.pdf>
- [10] PERESINI, O., KRAJCOVIC, T. More efficient IoT communication through LoRa network with LoRa@FIIT and STIOT protocols. In: 2017 IEEE 11th International Conference on Application of Information and Communication Technologies AICT: proceedings [online]. 2017. ISBN 978-1-5386-0502-8, p. 1-6. Available from: <https://doi.org/10.1109/ICAICT.2017.8686837>
- [11] MONTAGNY, S. LoRa - LoRaWAN and internet of things for beginners [online] [accessed 2025-04-15]. University of Savoy Mont Blanc, 2021. Available from: <https://www.univ-smb.fr/lorawan/wp-content/uploads/2022/01/Book-LoRa-LoRaWAN-and-Internet-of-Things.pdf>
- [12] ANJUM, M., KHAN, M. A., HASSAN, S. A., MAHMOOD, A., QURESHI, H. K., GIDLUND, M. RSSI fingerprinting-based localization using machine learning in LoRa networks. *IEEE Internet of Things Magazine* [online]. 2020, **3**(4), p. 53-59 [accessed 2025-04-15]. ISSN 2576-3180, eISSN 2576-3199. Available from: <https://doi.org/10.1109/IOTM.0001.2000019>
- [13] FARGAS, B., PETERSEN, M. GPS-free geolocation using LoRa in low-power WANs. In: 2017 Global Internet of Things Summit GIoTS: proceedings [online]. 2017. ISBN 978-1-5090-5874-7, p. 1-6. Available from: <https://doi.org/10.1109/GIoTTS.2017.8016251>

- [14] PODEVIJN, N., PLETS, D., AERNOOTS, M., BERKVEN, R., MARTENS, L., WEYN, M., JOSEPH, W. Experimental TDoA localisation in real public LoRa networks. In: 10th International Conference on Indoor Positioning and Indoor Navigation IPIN 2019: proceedings [online] [accessed 2025-04-15]. 2019. p. 211-218. Available from: <https://ceur-ws.org/Vol-2498/short28.pdf>
- [15] ZUCCONI, A. Positioning and trilateration [online] [accessed 2025-04-15]. 2017. Available from: <https://www.alanzucconi.com/2017/03/13/positioning-and-trilateration/>
- [16] OGUEJIOFOR, O., ANIEDU, A. N., EJIOFOR, H. C., OKOLIBE, A. U. Trilateration based localization algorithm for wireless sensor network. *International Journal of Innovative Science and Modern Engineering (IJISME)* [online]. 2013, 1(10). p. 21-27 [accessed 2025-04-15]. ISSN 2319-6386. Available from: <https://www.ijisme.org/wp-content/uploads/papers/v1i10/J04470911013.pdf>
- [17] LESTABLE, T., LALAM, M., GRAU, M. Location-enabled LoRa IoT network: Geo-LoRa-ting your assets [online] [accessed 2025-04-15]. 2015. Available from: <https://www.slideshare.net/slideshow/io-t-sagemcom-m2minnovationworldgeotrackv08/52922413>
- [18] RUSLI, M., ALI, M., JAMIL, N., DIN, M. M. An improved indoor positioning algorithm based on RSSI-trilateration technique for internet of things (IOT). In: 2016 International Conference on Computer and Communication Engineering ICCCE: proceedings [online]. 2016. ISBN 978-1-5090-2428-5, p. 72-77. Available from: <https://doi.org/10.1109/ICCCE.2016.28>
- [19] YANG, Z., LIU, Y. Quality of trilateration: confidence based iterative localization. In: 2008 The 28th International Conference on Distributed Computing Systems: proceedings [online]. 2008. ISSN 1063-6927, p. 446-453. Available from: <https://doi.org/10.1109/ICDCS.2008.59>
- [20] Semtech Corporation AN1200.22 LoRa modulation basics [online] [accessed 2025-04-15]. 2015. Available from: <https://www.frugalprototype.com/wp-content/uploads/2016/08/an1200.22.pdf>
- [21] BISSET, D. Analysing TDoA localisation in LoRa Networks. Master's thesis [online] [accessed 2025-04-15]. Delft: TU Delft, Faculty of Electrical Engineering, Mathematics and Computer Science, 2018. Available from: <https://resolver.tudelft.nl/uuid:bea423b1-6f04-4708-8ed4-e8663dd51cde>
- [22] GARG, V. *Wireless communications and networking*. San Francisco, CA: Morgan Kaufmann Publishers, Inc. 2010. ISBN 9780080549071.
- [23] JORKE, P., BOCKER, S., LIEDMANN, F., WIETFELD, CH. Urban channel models for smart city IoT-networks based on empirical measurements of LoRa-links at 433 and 868 MHz. In: 2017 IEEE 28th Annual International Symposium on Personal, Indoor, and Mobile Radio Communications PIMRC: proceedings [online]. 2017. ISBN 978-1-5386-3532-2, p. 1-6. Available from: <https://doi.org/10.1109/PIMRC.2017.8292708>
- [24] VALACH, A., MACKO, D. Exploration of the LoRa technology utilization possibilities in healthcare IoT devices. In: 2018 16th International Conference on Emerging eLearning Technologies and Applications ICETA: proceedings. 2018. ISBN 978-1-5386-7915-9, p. 623-628.
- [25] RAHMADHANI, A. Performance evaluation of LoRaWAN: from small-scale to large-scale network. Master's thesis [online] [accessed 2025-04-15]. Delft: TU Delft, Faculty of Electrical Engineering, Mathematics and Computer Science. 2017. Available from: <https://resolver.tudelft.nl/uuid:b8acf9d3-9629-4439-9148-9e66aecbec1c>
- [26] PARENTE, L. LMIC-node - GitHub [online] [accessed 2025-04-15]. 2021. Available from: <https://github.com/lnlp/LMIC-node>
- [27] BROCAAR, O. ChirpStack, open-source LoRaWAN Network Server [online] [accessed 2025-04-15]. 2016. Available from: <https://www.chirpstack.io/>
- [28] SNYDER, J. Map projections: a working manual. Professional Paper 1395 [online] [accessed 2025-04-15]. 1987. Available from: <https://doi.org/10.3133/pp1395>
- [29] Proj Contributors Proj coordinate transformation software library - Open Source Geospatial Foundation [online] [accessed 2025-04-15]. 2025. Available from: <https://doi.org/10.5281/zenodo.5884394>
- [30] ZUCCONI, A. Understanding geographical coordinates [online] [accessed 2025-04-15]. 2017. Available from: <https://www.alanzucconi.com/2017/03/13/understanding-geographical-coordinates/>
- [31] Great Britain. Ministry of Defence (NAVY) *Admiralty manual of navigation*. The Stationery Office, 1987, 1(45). ISBN 9780117714687.
- [32] Nordic Semiconductor Power Profiler Kit II [online] [accessed 2025-04-15]. 2024. Available from: <https://www.nordicsemi.com/Products/Development-hardware/Power-Profiler-Kit-2>



Editor-in-chief:

Branislav HADZIMA - SK

Associate editor:

Jakub SOVIAR - SK

Scientific editorial board:

Otakar BOKUVKA - SK
Jan COREJ - SK (in memoriam)

Scientific editorial board:

Greg BAKER - NZ
Abdelhamid BOUCHAIR - FR
Pavel BRANDSTETTER - CZ
Mario CACCIATO - IT
Jan CELKO - SK
Andrew COLLINS - GB
Samo DROBNE - SI
Erdogan H. EKIZ - UZ
Michal FRIVALDSKY - SK
Gabriel GASPAR - SK
Juraj GERLICI - SK
Vladimir N. GLAZKOV - RU
Ivan GLESK - GB
Marian GRUPAC - SK
Mario GUAGLIANO - IT
Mohamed HAMD AOUI - FR
Andrzej CHUDZIKIEWICZ - PL
Jaroslav JANACEK - SK
Zdenek KALA - CZ
Antonin KAZDA - SK
Michal KOHANI - SK
Tomasz N. KOLTUNOWICZ - PL
Jozef KOMACKA - SK
Matyas KONIORCZYK - HU

Executive editorial board

Michal BALLAY - SK
Pavol BELANY - SK
Martin BOROS - SK
Marek BRUNA - SK
Roman BUDJAC - SK
Nikola CAJOVA KANTOVA - SK
Kristian CULIK - SK
Jan DIZO - SK
Lukas FALAT - SK
Filip GAGO - SK
Lubica GAJANOVA - SK
Patrik GRZNAR - SK
Marian HANDRIK - SK
Stefan HARDON - SK
Martin HOLUBCIK - SK
Maros JANOVEC - SK
Daniela JURASOVA - SK
Daniel KAJANEK - SK

Executive editor:

Sylvia DUNDEKOVA - SK

Language editors:

Ruzica NIKOLIC - SK
Marica MAZUREKOVA - SK

Milan DADO - SK
Pavel POLEDNAK - CZ

Matus KOVAC - SK
Gang LIU - CN
Tomas LOVECEK - SK
Frank MARKERT - DK
Pavlo MARUSCHAK - UK
Jaroslav MAZUREK - SK
Marica MAZUREKOVA - SK
Vladimir MOZER - CZ
Jorge Carvalho PAIS - PT
Peter POCTA - SK
Maria A. M. PRATS - ES
Pavol RAFAJDUS - SK
Giacomo SCELBA - IT
Martin SOLIK - SK
Blaza STOJANOVIC - RS
Che-Jen SU - TW
Eva SVENTEKOVA - SK
Eva TILLOVA - SK
Anna TOMOVA - SK
Audrius VAITKUS - LT
Neven VRCEK - HR
Yue XIAO - CN
Franco Bernelli ZAZZERA - IT

Matus KOZEL - SK
Lenka KUCHARIKOVA - SK
Richard LENHARD - SK
Michal LOMAN - SK
Matus MATERNA - SK
Eva NEDELIKOVA - SK
Radovan NOSEK - SK
Daniel PAPAN - SK
Filip PASTOREK - SK
Pavol PECHO - SK
Slavka PITONAKOVA - SK
Jozef PROKOP - SK
Michal SAJGALIK - SK
Anna SIEKELOVA - SK
Jakub SVEC - SK
Michal TITKO - SK
Milan VASKO - SK
Vladislav ZITRICKY - SK

Each paper was reviewed by at least two reviewers.

Individual issues of the journal can be found on: <http://komunikacie.uniza.sk>

The full author guidelines are available at: https://komunikacie.uniza.sk/artkey/inf-990000-0400_Author-guidelines.php

Published quarterly by University of Žilina in EDIS - Publishing House of the University of Žilina.

Journal for sciences in transport / Communications is currently indexed, abstracted and accepted by CEEOL, CLOCKSS, COPE (Committee on Publication Ethics), Crossref (DOI), digitálne pramene,

DOAJ, EBSCO Host, Electronic Journals Library (EZB), ERIH Plus, Google Scholar,

Index Copernicus International Journals Master list, iThenticate, JournalGuide, Jouroscope,

Norwegian Register for Scientific Journals Series and Publishers, Portico, ROAD,

ScienceGate, SCImago Journal & Country Rank, SciRev, SCOPUS,

Web of Science database, WorldCat (OCLC).

**Journal for sciences in transport Komunikácie - vedecké listy Žilinskej univerzity v Žiline /
Communications - Scientific Letters of the University of Žilina has been selected
for inclusion in the Web of Science™.**

Contact:

Komunikácie - vedecké listy Žilinskej univerzity v Žiline
Communications - Scientific Letters of the University of Žilina
University of Žilina, Univerzitná 8215/1
010 26 Žilina, Slovakia

E-mail: komunikacie@uniza.sk
Web: <https://komunikacie.uniza.sk>

ISSN (print version): 1335-4205
ISSN (online version): 2585-7878

Registered No. (print version): EV 3672/09
Registered No. (online version): EV 3/22/EPP

Publisher, owner and distribution:
University of Žilina, Univerzitná 8215/1,
010 26 Žilina, Slovakia

Company identification number IČO: 00 397 563
Frequency of publishing: four times a year
Circulation: 30 printed copies per issue
Print edition price: 100 Euro (price without VAT)
Article Processing Charge (APC): 400 Euro (price without VAT)

Publishing has been approved by:
Ministry of Culture, Slovak Republic
© University of Žilina, Žilina, Slovakia





UNIVERSITY
OF ŽILINA

In its over 70 years of successful existence, the University of Žilina (UNIZA) has become one of the top universities in Slovakia.

Scientific conferences organized by University of Žilina

Horizons of Railway Transport 2025

Date and venue: 7 - 9 October 2025, Jasná (SK)

Contact: fpedas-horizonty@uniza.sk

Web: <https://hzd.uniza.sk/>

28th International Scientific Conference Crisis situations solution in specific environment

Date and venue: 15 - 16 October 2025, Žilina (SK)

Contact: crisis@uniza.sk

Web: <https://www.fbi.uniza.sk/> , <https://fbi.uniza.sk/en/aktuality/28th-conference-crisis-situations-solution-in-specific-environment>

Globalization and its Socio-Economic Consequences

Date and venue: 8 - 9 October 2025, Ražejské Teplice (SK)

Contact: globalizacia@uniza.sk

Web: <https://globalizacia.com>

Existing Bridges 2025

Date and venue: 6 - 7 November 2025, Žilina (SK)

Contact: fstav-konf-kskm@uniza.sk

Web: <https://existingbridges.uniza.sk/en/>

MedIN 2025

Date and venue: 10 December 2025, Žilina (SK)

Contact: medin@fhv.uniza.sk

Web: <https://umkd.uniza.sk/medin/>



UNIVERSITY OF ŽILINA
Science & Research Department

Univerzitná 8215/1,
010 26 Žilina,
Slovakia

Ing. Janka Macurová
tel.: +421 41 513 5143
e-mail: janka.macurova@uniza.sk